Libraries and Learning Services

University of Auckland Research Repository, ResearchSpace

Copyright Statement

ELECTRO-OSMOSIS CONSOLIDATION OF SOILS

Milad Naghibi Neishabouri

A thesis submitted in fulfilment of the requirements for the degree of Doctor of Philosophy in Civil Engineering, the University of Auckland, 2019.

Thesis Consent Form

This thesis may be consulted for the purposes of research or private study provided that due acknowledgement is made where appropriate and that permission is obtained before any material from the thesis is published. Students who do not wish their work to be available for reasons such as pending patents, copyright agreements, or future publication should seek advice from the Graduate Centre as to restricted use or embargo.

Author of thesis	Milad Naghibi Neishabouri
Title of thesis	Electro-osmosis Consolidation of Soils
Name of degree	Doctor of Philosophy in Civil Engineering
Date Submitted	15/01/2019

Print Format (Tick the boxes that apply)

✓	I agree that the University of Auckland Library may make a copy of this thesis available for the collection of another library on request from that library.
✓	I agree to this thesis being copied for supply to any person in accordance with the provisions of Section 56 of the Copyright Act 1994.

Digital Format - PhD theses

I certify that a digital copy of my thesis deposited with the University is the same as the final print version of my thesis. Except in the circumstances set out below, no emendation of content has occurred and I recognise that minor variations in formatting may occur as a result of the conversion to digital format.

Access to my thesis may be limited for a period of time specified by me at the time of deposit. I understand that if my thesis is available online for public access it can be used for criticism, review, news reporting, research and private study.

Digital Format - Masters theses

I certify that a digital copy of my thesis deposited with the University is the same as the final print version of my thesis. Except in the circumstances set out below, no emendation of content has occurred and I recognise that minor variations in formatting may occur as a result of the conversion to digital format.

Access will normally only be available to authenticated members of the University of Auckland, but I may choose to allow public access under special circumstances. I understand that if my thesis is available online for public access it can be used for criticism, review, news reporting, research and private study.

Copyright (Digital Format Theses) (Tick **ONE box only**)

✓	I confirm that my thesis does not contain material for which the copyright belongs to a third party, **(or)** that the amounts copied fall within the limits permitted under the Copyright Act 1994.
☐	I confirm that for all third party copyright material in my thesis, I have obtained written permission to use the material and attach copies of each permission, **(or)** I have removed the material from the digital copy of the thesis, fully referenced the deleted materials and, where possible, provided links to electronic sources of the material.

Signature M. Nagh̲

Date 15/01/2019

Comments on access conditions

Faculty Student Centre / Graduate Centre only: Digital copy deposited ☐ Signature   Date

THE UNIVERSITY OF AUCKLAND
Te Whare Wānanga o Tāmaki Makaurau
NEW ZEALAND

ABSTRACT

Consolidation of problematic, soft-grained soils is a major concern in geotechnical engineering. Traditional hydraulic ground improvement methods, such as pre-loading and vacuum pressure, usually take a long time. In addition, using these methods is not applicable in all cases, particularly in slopes. These conventional method limitations draw engineers' attentions to the electro-osmosis (EO) consolidation technique. In fact, applying electrical potential gradient to the soil leads to fundamental changes in its electro-hydro-mechanical (EHM) behaviour. However, some uncontrolled EO-induced chemical processes could significantly affect the efficiency of the EO consolidation technique. Although a large number of experimental and theoretical studies have been conducted in this topic, the practical application of the EO consolidation in geotechnical engineering is limited due to lack of knowledge in the field of EMH behaviour of soils, and unavailability of an accurate method to predict the expected efficiency and cost of the EO system.

In this study, a laboratory-scale experimental programme along with an extensive numerical investigation is conducted to study the soil behaviour during EO consolidation and the efficiency of the process. As the electrical resistivity of soil controls the efficiency of EO process and distribution of voltage in the soil body, the experimental programme is initiated with electrical resistivity tests. The laboratory experiments are carried out in two main phases: (1) Electrical resistivity experiments; and (2) EO tests. In each phase, the required numerical investigations are carried out using FlexPDE™ software, which is based on the finite element technique (FEM).

In Phase (1), a new apparatus is developed and fully calibrated to consider the effect of boundary conditions and void ratio on the laboratory-measured electrical resistivity of the soil. To be able to extend the results to various specimen sizes and boundary conditions, a numerical model is developed and successfully verified by experimental data from this study.

In addition, to be able to capture the spectrum of real soil behaviour, the effects of pore water salinity and level of soil sensitivity (clay content) on the electrical resistivity of soil are investigated. To achieve this, various soil mixtures at different levels of salinity and clay contents are tested in the calibrated apparatus. Then the obtained data are used to verify a proposed physical-numerical model.

In Phase (2) of experiments, a new apparatus and a uniform testing framework is developed to carry out the load application and required EO parameter measurements simultaneously in a

single cell with the same dimension as that developed in Phase (1). Then the data obtained from this phase of experiment is analysed along with the soil electrical resistivity to investigate the EHM and chemical effects as well as EO efficiency and power consumption. Finally, considering those factors, a new technique is proposed to reduce the level of chemical effects at the soil-electrode vicinity, enhance the soil-electrode contact and increase the EO efficiency.

The results show that detailed investigation of electrical resistivity is necessary to design an EO consolidation scheme efficiently. It is concluded that the electrical resistivity depends on soil void ratio and clay surface conductivity. In a constant level of salinity, up to 30% increase in the electrical resistivity of the soil and consequently in the efficiency of EO consolidation is observed in New Zealand kaolin clay depending on the initial condition and volumetric strain of soil during the EO process. However, the electrical resistivity drops drastically by increasing the salinity level of the pore solution indicating very low EO efficiency at higher salinity.

Furthermore, implementation of uniformly measured EO parameters, such as EO permeability, varying electrical resistivity (up to 30% variation) and time-dependent potential loss due to electrolysis at soil-electrode vicinity (up to 50% variation) into the existing EO consolidation governing equation, improves the estimation of soil behaviour undergoing EO consolidation considerably. In addition, it is found that the coefficient of EO consolidation (C_{ve}) should be utilised rather than the coefficient of consolidation (C_v) to estimate the rate of consolidation. In addition, the proposed model is extended to the field successfully and is verified using a well-documented field experiment.

Finally, to evaluate the effectiveness of the proposed technique to decrease the level of potential loss at soil-electrode interface, a relatively large EO cell is designed, fabricated and tested. It is shown that, as the generated gas is removed from the proposed cathode vicinity, the efficiency of EO system increases noticeably.

This study is the first to establish a robust, calibrated and uniform framework to measure the effective parameters affecting EO consolidation namely permeability coefficients, time-dependent potential loss and variable electrical resistivity in the laboratory and incorporate them in a single model to estimate the behaviour of the soil undergoing EO consolidation in the field and laboratory, the efficiency of the process and the level of power consumption. Therefore, geotechnical engineers, researchers and scientists are able to adopt the developed framework from this study to design a more efficient EO scheme.

ACKNOWLEDGEMENTS

TABLE OF CONTENTS

LIST OF TABLES

LIST OF FIGURES

1 INTRODUCTION

1.1 Background

Soft, fine-grained soils cover many parts of the world, such as the marine clays of Australia and Korean coastal zones, the highly compressive clay of Bangkok (Thailand) and clays of Nebraska, Michigan and Texas (U.S.A.) (Kalinski and Kelly, 1994; Bergado et al., 2000; Mimic et al., 2000). In many cases, those soils need improvement for the purpose of slope stabilisation and structural support. The traditional preloading consolidation method is one of the effective ground improvement techniques; however, it is time-consuming and is not applicable in all cases, such as in sloping ground. Therefore, there is still a need to find a ground improvement method that overcomes most of the limitations of the conventional method.

Electro-osmosis (EO) is one of the efficient techniques in geotechnical engineering that could be used for this purpose. In addition, considering the increasing concerns about environmental issues, EO can be used as a low-impact and environmentally friendly improvement technique instead of other improvement techniques, especially preloading, to preserve the forested environment. Moreover, in many situations, it is the most cost-effective technique and a unique option for ground improvement purposes. Unfortunately, the following drawbacks in the field of EO ground improvement restricts the applicability of this technique in the real cases:

- Lack of knowledge in the field of electrical and electro-hydro-mechanical (EHM) behaviour of soils, such as electrically-induced pore water pressure, volumetric strain and water flow, EO permeability, etc.

- The experimental apparatus, which are utilised for electrical resistivity and EO parameter measurements, are not conventional laboratory apparatus. Therefore, the required laboratory apparatus should be properly designed and fabricated to measure all the required parameters; however, previous proposed apparatus are not able to measure them. In addition, in majority of these apparatus, the voltage and load application stages are carried out in multiple cells. In the latter case, removing the specimen from the cell, after conducting either mechanical or EO consolidation, leads to soil rebound, changes in the structure of soil and condition of the interconnected void system. This imposes errors to the laboratory results and further analysis.

- The EO case histories show that laboratory results in terms of efficiency, power consumption, electrical resistivity, etc. cannot be extended to the field-scale directly. In such cases, numerical techniques can provide the engineers with the perfect tool to extend the laboratory scale results to the field effectively.

- The accuracy of estimated project cost and post-treatment behaviour of the soil cannot be trusted in majority of previous research due to the simplifications adopted in terms of electrical resistivity measurements and the unavailability of an accurate method to estimate the EO efficiency and the level of power consumption.

Therefore, there is a need for a uniform numerical and experimental framework and apparatus to measure the soil electrical resistivity and the EO parameters to have an accurate estimate of EO efficiency, post-treated soil behaviour and successful extension of the laboratory results to the field-scale. This study is mainly directed to enhance the current state of knowledge in the measurement of electrical resistivity, EO efficiency and EHM behaviour of the soil and in numerical modelling of electrical resistivity and EO consolidation.

1.2 Statement of the problem

Although past research has been conducted to determine the parameter(s) affecting EO consolidation and efficient design of EO scheme, there are uncertainties in this field. To date, there are limited information on the effect of electrical resistivity of the soil on EO consolidation. In addition, the apparatus and technique in measuring the electrical resistivity in the laboratory should be chosen more cautiously (Atkins and Smith, 1961; Abu-Hassanein et al., 1996; McCarter and Desmazes, 1997; Burnotte et al., 2004; Mitchell and Soga, 2005;

Fourie et al. 2007; Jeyakanthan et al. 2011; Kibria and Hossain, 2012; Oh et al., 2014). In majority of EO research, the effect of electrical resistivity is neglected which leads to an overestimation of EO efficiency (Lo et al., 1991; Chew et al., 2004; Ou et al., 2009; Jones et al. 2011; Glendinning et al., 2007). In addition, a few investigations have assumed the electrical resistivity to be constant during the EO process (Bjerrum et al. 1967; Hamir et al. 2001). However, Hu et al. (2012) considered electrical resistivity as a parameter which varies with the void ratio during the EO process. In these cases, no experiment has been conducted to measure the electrical resistivity of the soil during the EO process. To address this issue, Bjerrum et al. (1967) conducted a laboratory test for electrical resistivity measurement during EO consolidation. However, in this case, the effects of boundary condition, specimen size, void ratio, etc. were neglected and a constant value was assumed for the electrical resistivity of the soil during EO consolidation. However, to estimate the EO efficiency, the evolution of the electrical resistivity of soil during the consolidation process and the possible effect of surface conductance of clay particles, pore solution salinity and void ratio should be determined under a robust and standardised framework. In addition, there is a genuine need for performing numerical estimation of the electrical resistivity of soil before conducting any field trial, in order to estimate the level of power consumption and economy of the project accurately.

Moreover, there are inconsistencies in the measurement techniques and in the obtained experimental results of important parameters affecting EO consolidation. In previous research, the required parameters are generally measured in multiple cells (Win et al., 2001; Mimic et al., 2001; Mohamedelhassan and Shang, 2001; Mohamedelhassan, 2009; Jeyakanthan et al., 2011). An electric potential gradient is applied in the electric cell and then the soil sample is removed and placed in a conventional laboratory apparatus to measure the required parameters (Mohamedelhassan, 2009; Jeyakanthan et al., 2011). Consequently, the soil can rebound which affects the chemical and hydraulic parameters and the processes when compared with the real case scenario. In addition, as the boundary conditions and specimen size are important in the laboratory results, all stages of electrical resistivity and EO tests should be done in similar cell in terms of size, boundaries, duration and initial condition of specimen (Hamir et al., 2001; Lefebvre and Burnotte, 2001). Therefore, there is a need for a systematic measurement technique to measure the parameters affecting EO consolidation more realistically.

Furthermore, the effect of electro-chemical processes, especially electrolysis, is mainly ignored or underestimated in previous investigations (Lo et al., 1991; Chew et al., 2004; Glendinning

et al., 2007; Ou et al., 2009; Jones et al. 2011; Jeyakanthan et al., 2011). Thus, the contribution of these parameters needs to be defined and implemented in EO consolidation theories. The majority of previous research is in agreement that a portion of applied electric potential is lost at the soil-electrode vicinities (Bjerrum et al. 1967; Mohamedelhassan and Shang, 2001; Mohamedelhassan, 2009; Jeyakanthan et al., 2011). The potential loss reduces the effectiveness of EO consolidation technique and at the same time, increases the level of power consumption of the EO project. Therefore, finding a more efficient method to reduce the electrical potential losses at the electrode-soil interfaces is crucial to improve the efficiency of EO ground improvement techniques and decrease the level of power consumption.

1.3 Objectives

This study focuses on understanding the EO efficiency and EHM behaviour of saturated clays and the associated electrical resistivity behaviour. As electrical resistivity is controlling the EO efficiency and the voltage distribution within the soil body, it should be closely monitored during electro-osmosis consolidation using an acceptable testing technique. Then the EO consolidation behaviour needs to be investigated under a robust experimental and numerical framework considering the important parameters, including electrical resistivity. Finally, as increasing the efficiency of EO process is crucial, a new method should be proposed to decrease the potential loss at the soil-electrode vicinity and increase the efficiency of the EO process.

The specific objectives of this study are:

1. To accurately measure the electrical resistivity of soils undergoing consolidation process;
2. To study the effect of soil mineralogy and pore water chemistry on the electrical resistivity of saturated soils;
3. To establish a consistent experimental framework to measure the hydraulic and EO consolidation parameters in the same cell to that used in electrical resistivity measurements;
4. To investigate the behaviour of saturated clay undergoing EO consolidation experimentally and numerically, considering:
    -   possible variation of hydraulic and EO permeabilities of soils before and after EO consolidation at different stress level and history;
    -   variation of electrolysis and potential loss at electrodes; and

- soil electrical resistivity;

5. To propose an efficient method to reduce the electrical potential losses at electrode-soil interface and to test the effectiveness of the proposed method using a relatively large, bench-scale electric oedometer cell.

1.4 Limitations of study

This study has several limitations. First is the sample size; as the tests were conducted in the laboratory, the specimen sizes were limited. Generally, specimen diameters from 60 mm to 250 mm were previously tested in the laboratory whereas cells with diameters of 76 mm and 150 mm were used in this study. In addition, the previous laboratory tests were conducted with voltage gradients from 0.1 to 12 V/cm (Casagrande, 1949; Morris et al., 1984; Win et al., 2001; Lefebvre and Burnotte, 2002; Jeyakanthan et al., 2011). However, in the current study voltage gradients of 2.1 and 0.67 V/cm were utilised. Thus, the results might be influenced by the specimen size and the results need to be cautiously extended to the field. However, attempts were made to minimise such effect through extensive numerical investigation. Another limitation was soil mineralogy; electrical resistivity and EHM investigations have been conducted by different researchers on different types of clay, namely China Clay (Li et al., 2012), Mont St-Hilaire Clay (Lefebvre and Burnotte, 2002; Burnotte et al., 2004), Viadana clay and Scanzano clay from Italy (Gabrieli et al., 2008), Norwegian quick clay (Bjerrum et al., 1967), Singapore marine clay (Chew et al., 2004; Win et al., 2001), Leda clay from Canada (Lo et al., 1991) and marine sediments from south-west coast of Korea (Mohamedelhassan and Shang, 2001). In this research, the EHM behaviour of New Zealand Kaolin clay was investigated under constant temperature of 20°C. Although the results were expected to show some differences in comparison with other clays, the methodology and proposed relationships can be expanded to other soil types and various levels of temperatures. Finally, during the EO process a number of less important, uncontrolled chemical processes, such as pH variation, formation of new minerals and electrode polarisation, take place that were not measured nor controlled during this research.

1.5 Outline of thesis

The thesis is broken down into 9 chapters. A brief background of EO consolidation, importance of this research, objectives and limitations are described in Chapter 1.

Chapter 2 presents the available electro-osmosis theories and reviews the effect of electrical potential gradient on soil behaviour. Then, information about electrical resistivity and potential losses at soil-electrodes interface are also summarised.

Chapter 3 explains the detail of an extensive numerical study, which is conducted to calibrate the effect of boundary condition on the laboratory-measured electrical resistivity of soil using the standardised 4-electrode Wenner method. The numerical model is verified by experimental results from this study. Finally, the electrical resistivity of tested materials is presented and discussed.

The estimation of the electrical resistivity of clays considering the surface conductivity and sensitivity of clays is presented in Chapter 4. To achieve this, a new physical-numerical model is initially proposed. Then the governing equations for electrical current are presented and solved numerically over the introduced boundaries using finite element method (FEM). Finally, the model is fully verified by experimental results from this study considering different soil mixtures and salinity levels.

Experimental evaluation of EO consolidation is described in Chapter 5. The parameters affecting EO consolidation, namely hydraulic and EO permeabilities, potential loss at electrodes, volume changes and coefficients of EO and hydraulic consolidation, are measured experimentally where a single cell has been employed for load and potential difference applications.

In Chapter 6, the EO consolidation is investigated numerically. The investigation is conducted in the light of a robust framework which considers varying parameters, electro-chemical processes at soil-electrode interfaces and varying soil electrical resistivity. For this purpose, the theory and governing equation of EO consolidation are presented and then, the experimentally-measured parameters from Chapter 5 are implemented in the model. Finally, the EO governing equation is solved in conjunction with the electrical resistivity governing equation over a boundary similar to that of the experimental programme. The model is then verified using experimental results obtained from this study and other published data.

The laboratory-scale numerical model is then extended to the field case in Chapter 7. The extended model is verified using a full set of field data in terms of EO-induced soil settlement and shear strength improvement. In addition, a comparison is made between the published results in the literature and those using the proposed model.

The efficiency of EO process is discussed in Chapter 8 and, to enhance the efficiency of an EO system, an innovative electrode is proposed to decrease the level of potential loss at the soil-electrode vicinity. The proposed electrode is tested experimentally in a bench-scale EO cell and its effectiveness is discussed.

Finally, a summary of the major conclusions of the preceding chapters is provided in Chapter 9, along with the recommendations for further research in this field.

2 LITERATURE REVIEW

2.1 Introduction

Application of electric potential difference to the soil body by means of conductive electrodes has a long history in engineering and science. In geotechnical engineering point of view, the developed net water flow under the influence of voltage application to the soil body holds a great importance and is widely known as electro-osmosis (EO). The application of this technique has been relatively limited due to uncertainties in the post-treated soil behaviour and, more importantly, cost of the project. In this chapter, the literature in the field of EO consolidation has been systematically reviewed in order to have a better understanding of the current state of knowledge in this field. In addition, an endeavour to address the current drawbacks of EO technique is conducted to reduce the level of uncertainties in the estimation of post-treated soil behaviour.

Initially an overview of electrically-induced processes (electro-kinetic) in the soil body is presented. Then, the application of EO in science, engineering and technology is discussed. As the applicability of EO technique in the field is controlled by the post-treated soil behaviour and the cost of the project, these factors are also reviewed. The available laboratory apparatus and test results and observations are then discussed. In addition, various EO consolidation models and previous numerical studies are presented. Finally, the important parameters affecting the project costs are investigated.

2.2 Electro-kinetic processes

Generally, electro-kinetic phenomena involve relative movement of soil particles and pore water. EO and streaming potential are described by the movement of water relative to the solid particles. Water movement due to external electrical gradients is termed as electro-osmosis whereas the generated electrical potential due to the movement of water relative to the solid particles, which is usually caused by an imposed hydraulic head difference, is defined as streaming potential. The movement of solid particles through the fluid is characterised by electro-phoresis and sedimentation potential. Electro-phoresis is the movement of solids through solution due to an external electrical potential whereas sedimentation potential involves generating an electrical potential by solid settlement under gravity (Mitchell and Soga, 2005). The electro-kinetic processes are shown schematically in Fig. 2.1.

Electro-kinetic processes can be employed to trigger the transport of water in the body of soils which mainly includes EO, as shown in Fig. 2.1 (a).
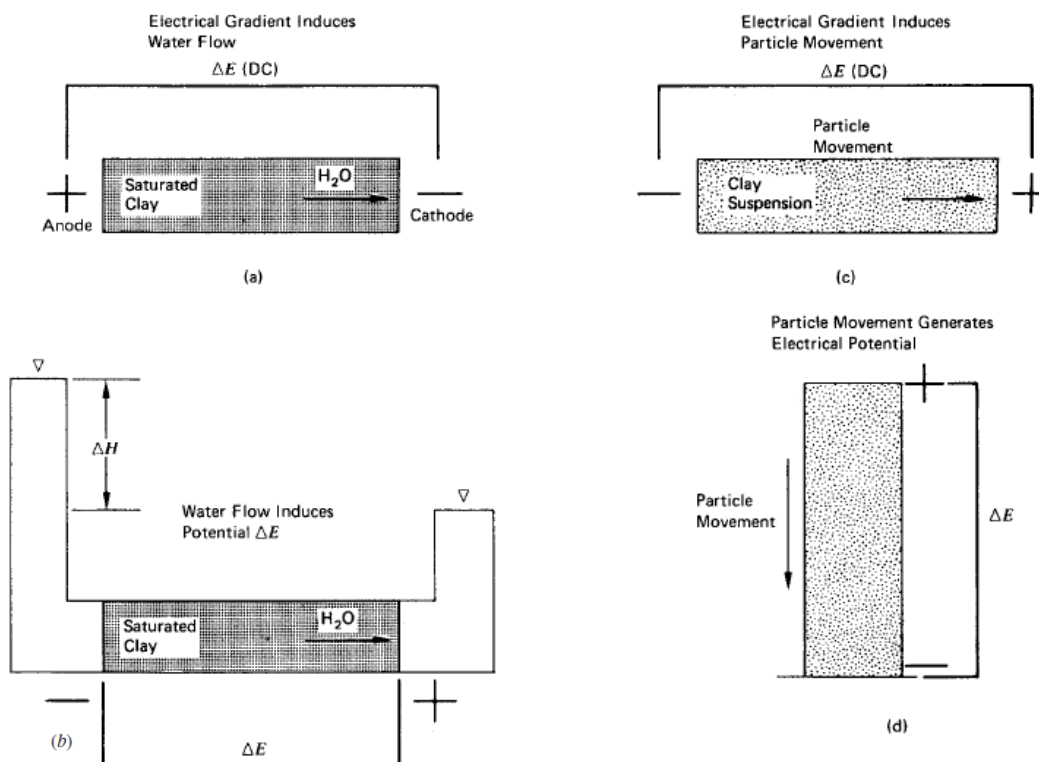
Fig. 2.1 Electro-kinetic phenomena: (a) electro-osmosis; (b) streaming potential; (c) electro-phoresis; (d) sedimentation potential (Mitchell and Soga 2005)

2.3 Electro-osmosis applications in soils

EO phenomenon is applied in many fields of science and engineering. The initial practical application of EO in geotechnical engineering is documented by Bjerrum et al. (1967). EO was applied to stabilise a railway embankment on Norwegian quick clay. The EO technique was identified then as a unique option for that case due to site and financial considerations. It was successfully employed to increase the soil shear strength to the required level and stabilise the soil at a railway site. Since then, the EO technique has been known as an environmentally-friendly and cost-effective ground improvement technique to consolidate the soil, enhancing the shear strength of fine-grained soils and stabilising slopes where load application is not practical. In addition, EO techniques have been successfully utilised to de-water and for volume reduction of hazardous materials, such as bio-solids and solid wastes, ground water recharge and mining applications (Glendinning et al., 2007; Fourie et al., 2007; Jones et al., 2011). In addition, the electrical vertical drains (EVD) offers a fast and reliable technique to consolidate the soil with no load application (Chew et al., 2004; Rittirong et al., 2008).

The effectiveness of EO consolidation technique is well defined and has been reported experimentally in the field and in laboratory scale by many researchers. In addition, as there is no conventional laboratory apparatus available for experimental investigation of EO consolidation, various researchers used different set-up for laboratory trials mainly by modifying the conventional laboratory apparatus, such as oedometer and triaxial cells. Therefore, the employed modified apparatus should be designed to capture all the required parameters from a single sample. Herein, the utilised apparatus from literature are investigated and the test results are discussed.

2.4 Experimental investigation of EO consolidation

The EO consolidation test is not a common experiment in the laboratory. Therefore, researchers adopted various apparatus to conduct EO consolidation tests in the laboratory. The properties of EO set-ups employed by various researchers are listed in the Appendix (Tables A.1).

2.4.1 Previously developed EO apparatus

The very first setup for EO test was proposed by Reuss (1809). In that set up, wires were used as electrodes and no load was applied to the soil and the water transport was observed

qualitatively. Casagrande (1949) used a simple apparatus where solid electrodes for voltage application were utilised. These two apparatus are shown in Fig. 2.2.

(a) Casagrande (1949)   (b) Reuss (1808)
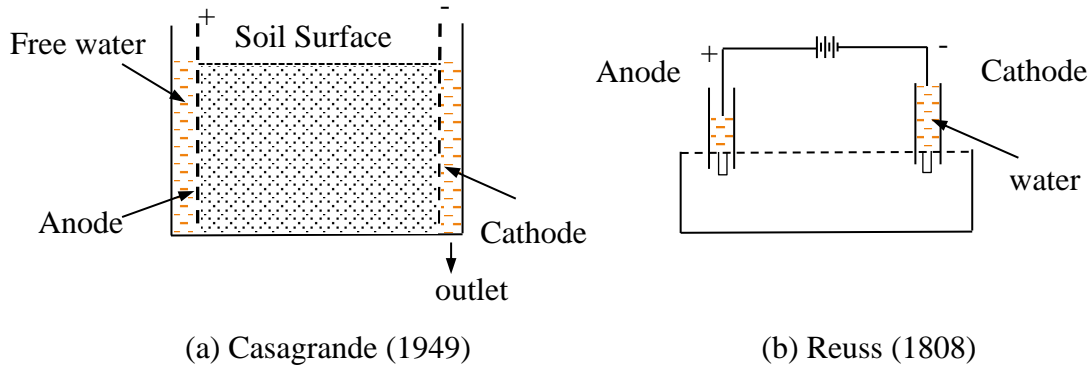
Fig. 2.2 Early apparatus for EO consolidation investigations

Casagrande (1949) proposed a popular relationship for estimation of water volume in the soil body under the effect of electrical potential gradient; however, no surcharge was applied to the specimen in his research. To apply the load, Morris (1984) used a column of clay which was placed between two horizontal electrodes, as shown in Fig. 2.3.
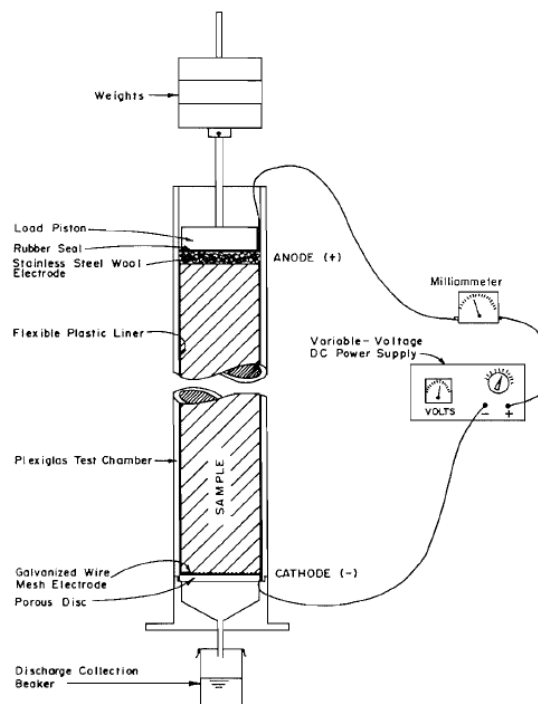
Fig. 2.3 Apparatus proposed by Morris (1984)

The specimen was loaded from the top of the sample and then the electrical potential gradient was applied. Finally, the soil was removed and tested in conventional oedometer and triaxial cells. Although the specimen was loaded initially, the level of stress was as low as 30 kPa. In addition, removing the specimen from the EO cell produces suction in the soil body. As the soil is open to drainage from the cathode side, water returns to the soil body due to that suction and consequently noticeable rebound is generated in the soil body which can affect the results. Therefore, the measurement of the required parameters and the application of load and electric potential gradient need to occur within the same cell for higher order of effective stress. Similar apparatus as that of Morris (1984) has been used by Wu et al. (2015) to verify the effect of electrode material and voltage distribution in the soil during EO consolidation. In addition, the apparatus had a camera which was used for image analysis to qualitatively examine the effect of EO consolidation at the soil-electrode interfaces, as shown in Fig. 2.4.
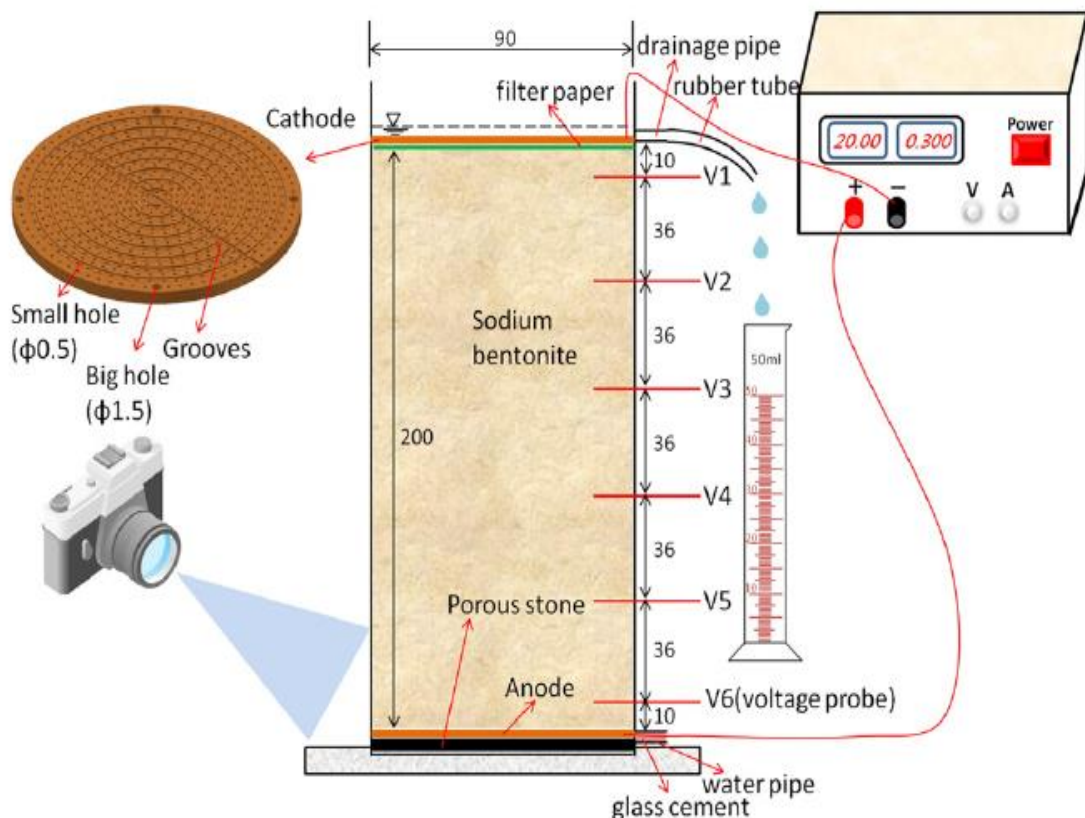
Fig. 2.4 Apparatus proposed by Wu et al. (2015)

Mimic et al. (2001) developed a 5.1 L EO consolidation tank as shown in Fig. 2.5. The electrical treatment and soil tests were conducted in same cell; however, the order of preconsolidation pressure was maintained to the same level as that of Morris (1984). A Similar EO tank as that of Mimic et al. (2001) was also employed by Mohamedelhassan and Shang (2001), Mohamedelhassan (2009) and Xue et al. (2015), as shown in Fig. 2.6. Win et al. (2001) and Jeyakanthan et al. (2011) modified the triaxial cell and tested the modified apparatus in the laboratory, as shown in Fig. 2.7. Although a wide range of effective stresses was applied to the soil in both studies, the pore water pressure could not be measured due to gas generation at the electrodes. In addition, the soil treatment and parameter measurements were conducted in separate cells.
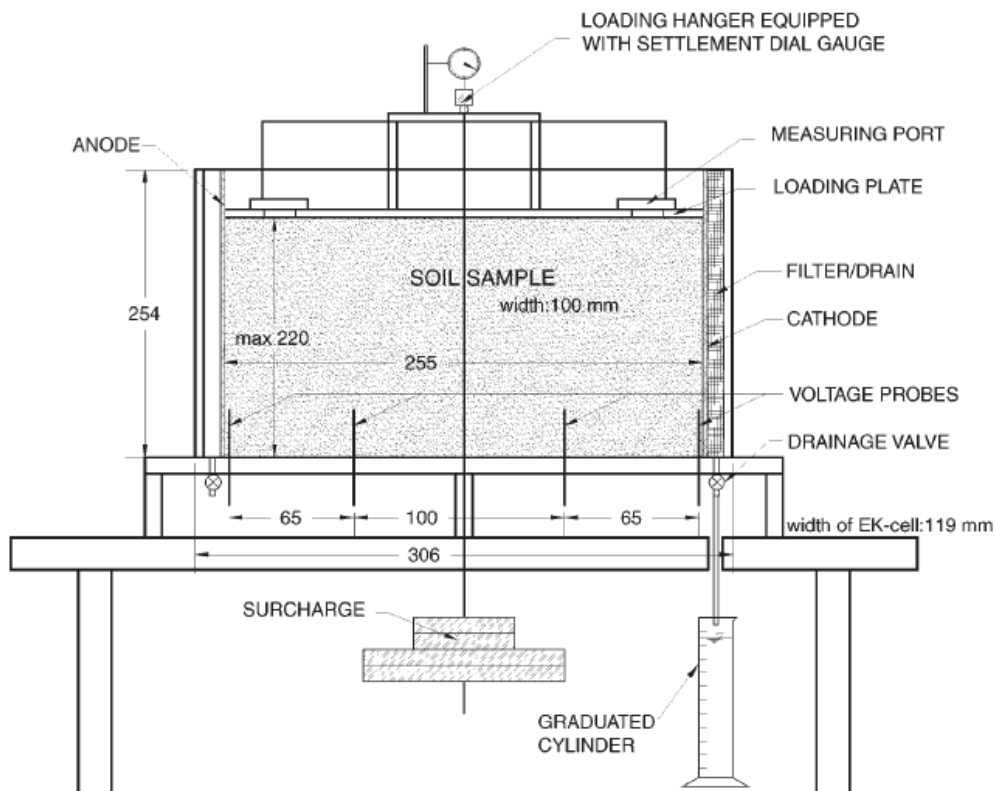
Fig. 2.5 Apparatus proposed by Mimic et al. (2001)

(a) Apparatus proposed by Mohamedelhassan and Shang (2001) and Mohamedelhassan (2009)

(b) Apparatus proposed by Xue et al. (2015)

Fig. 2.6 Other proposed apparatus

(a) Modified triaxial cell by Win et al. (2001)

(b) Modified triaxial cell by Jeyakanthan et al. (2011)

Fig. 2.7 Modified triaxial cells

Hamir et al. (2001) proposed an EO cell to apply higher orders of loads along with voltage gradient application and measured the pore water pressure, electrically-induced water flow rate and potential drop at soil-electrode interfaces in the same cell, as shown in Fig. 2.8. However, the soil electrical resistivity and potential drop at electrodes were not considered in their study.
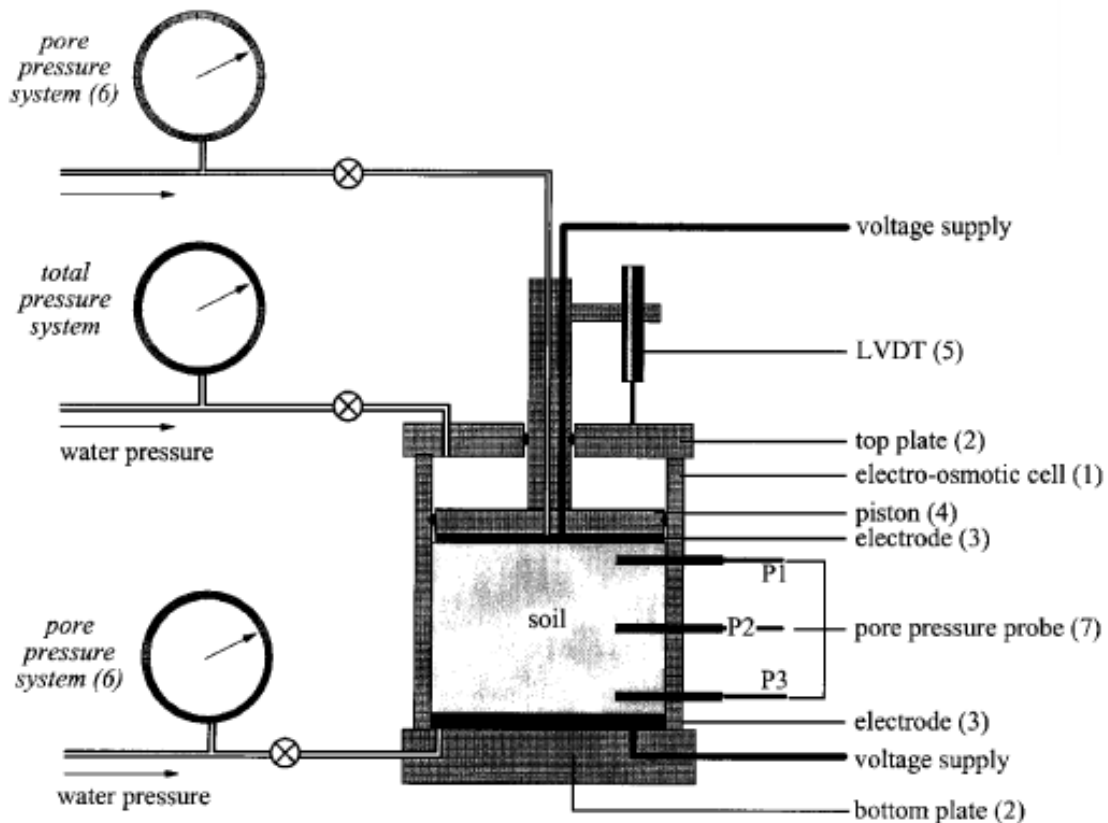
Fig. 2.8 Proposed apparatus by Hamir et al. (2001)

Using vertical electrodes and EVDs (electrical vertical drains) are also common in laboratory testing. Lefebvre and Burnotte (2002) and Chew et al. (2004) implemented steel tubes in a bench-scale oedometer cell, as shown in Fig. 2.9. In addition, a similar arrangement as that of Lefebvre and Burnotte (2002), with one set of anode and cathode, was used by Ou et al. (2009) to investigate the effect of saline solution injection on EO consolidation, as shown in Fig. 2.10.
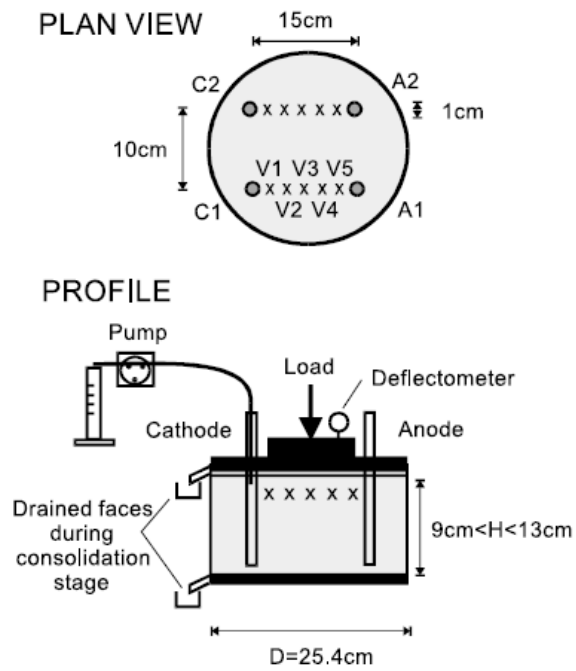
(a) Lefebvre and Burnotte (2002)
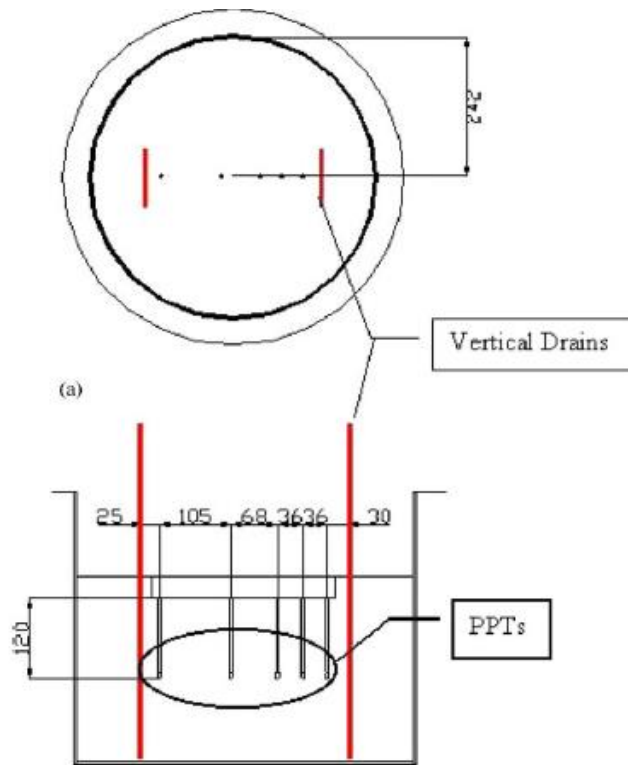
(b) Chew et al. (2004)

Fig. 2.9 Apparatus with vertical electrodes
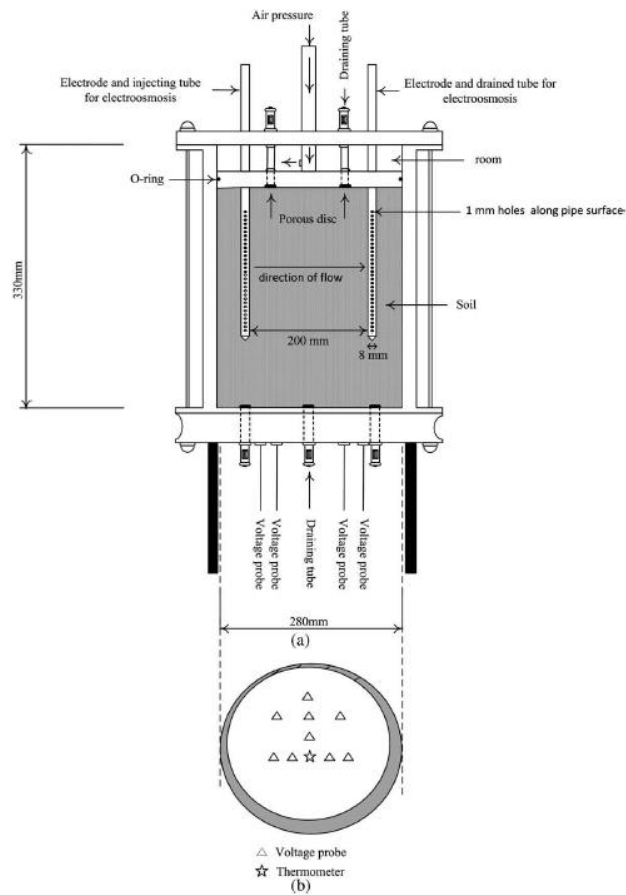
Fig. 2.10 Apparatus by Ou et al. (2009)

2.4.2 Comments on the developed EO laboratory apparatus

Basically, the drawbacks of the developed/modified apparatus for EO consolidation could be summarised as follows:

- In real cases, different levels of preconsolidation pressure can be observed in the field. Therefore, the developed apparatus should be designed with load application capability to induce the required level of preconsolidation stress, which is neglected in a number of previous investigations.

- As the electric current is highly sensitive to the interconnected voids in the soil body, the application of both loads and electrical potential difference should be applied within the same cell. In many testing apparatus, the electric potential difference is applied in an electric cell, after which the treated soil is moved to an oedometer or triaxial cell for experiments. Removing the treated soil from the electric cell will allow the soil to

rebound, which changes the status of the interconnected voids and affects the treated soil behaviour.

- Application of electric potential difference induces other types of processes in the soil body, such as chemical processes. In addition, the condition of the interconnected voids changes during the EO process which affects the electrical and geotechnical characteristics of the soil. Neglecting some of these processes and changes in soil properties impose a high level of error to the prediction of the post-treated soil behaviour. These parameters are time-dependent and depend on soil boundary conditions. Therefore, the suitable laboratory apparatus should be designed to address these issues and be able to measure the important parameters within a consistent and robust experimental framework.

To accurately investigate the EO consolidation, the design of a comprehensive laboratory apparatus and scheme is a crucial part. During the design of EO consolidation scheme, the drawbacks of the previously developed apparatus should be addressed and the important parameters which should be closely monitored during EO consolidation need to be identified. To achieve this, the behaviour and properties of the soil during EO consolidation as observed in previous research are thoroughly reviewed and discussed in the following section.

2.5 Behaviour and properties of electrically-treated soils

As the geotechnical behaviour and properties of electrically-treated (post-treated) soils and the cost of EO ground improvement technique are the controlling parameters in the applicability of EO technique, a review of previous experimental observations on EO consolidation is conducted considering these two groups of parameters.

2.5.1 Electro-osmosis permeability

The electro-osmotic permeability of soil (k_e) is defined as the velocity of hydraulic flow under the influence of a unit electric potential gradient. As k_e is a key parameter for the quantification of the EO flow rate, several theories were proposed to accurately estimate this parameter. Helmholtz-Smoluchowski (1879) assumed the soil as negatively-charged sheeted materials where cations from the pore water were absorbed by these negatively-charged soil particles to build a diffuse layer. By assuming a laminar flow regime in that area, the following relationship was proposed (cited in Mitchell and Soga, 2005):

$$k_e = \frac{\xi D}{\eta} n \qquad (2.1)$$

where ξ is the surface potential of diffuse layer of positive and negative charges adjacent to soil surface, D is dielectric constant, η is water viscosity and n is soil porosity. According to this theory, k_e is independent of pore sizes and this was questioned by a few researchers who proposed different relationships for k_e as a function of the pore sizes (Alshawbkeh and Acar, 1996; Mohamedelhassan and Shang, 2001). However, experimental results show that the Helmholtz-Smoluchowski's theory estimates k_e within an acceptable level for clays (Mitchell and Soga, 2005), but the parameters associated with this theory, specially the surface potential, ξ, are difficult to measure in the laboratory. To address this issue, Casagrande (1949) reported that k_e varies in a very limited range and proposed a constant value of $k_e = 5 \times 10^{-9}$ m^2/s·V for all soils based on a simple equation, which is similar to the Darcy's law:

$$k_e = \frac{Q_e L}{VA} \qquad (2.2)$$

where Q_e is the water discharge through the area, A and L are the area and height of the soil specimen, respectively, and V is the applied electric potential difference. In agreement with Casagrande (1949), Bjerrum et al. (1967) also stated that k_e is independent of the level of applied electric potential, implying that k_e varies for different types of soils. A constant value of 2×10^{-9} m^2/s·V was found for Norwegian quick clay. On the other hand, Win et al. (2001) showed that k_e varies with time during EO consolidation for Singapore marine clay. The value of k_e was determined to be in the narrow range of 1×10^{-9} to 1×10^{-8} m^2/s·V. Similarly, Burnotte et al. (2004) confirmed that k_e varies with time in the field within a narrow range similar to that proposed by Win et al. (2001). The average k_e value of 4×10^{-9} m^2/s·V was proposed for Mont St-Hilaire. In consistency with other researchers, Mitchell and Soga (2005) proposed that k_e varies in the range of 5×10^{-9} to 5×10^{-8} m^2/s·V for all soils and this range is widely accepted by other researchers (Win et al., 2001; Burnotte et al., 2004; Jeyakanthan et al., 2011).

In these cases, the effect of potential drop at the electrodes was neglected in the calculation of k_e. Jeyakanthan et al. (2011) concluded that k_e is independent of the stress level and only depends on the potential loss at soil-electrode vicinity. k_e was measured as 7.18×10^{-10} m^2/s·V in the laboratory and, considering a constant level of 60% electric potential gradient efficiency,

the value of 1.197×10^{-9} m^2/s·V was proposed. However, as the potential drop is a time-dependent factor, assuming a constant voltage drop is not realistic.

2.5.2 Hydraulic permeability

Based on the EO flow mechanism, the developed drag force directly depends on the coefficient of hydraulic permeability (k_h). When pore water can be freely transported within the soil body (high permeability), the developed drag force and, consequently, the developed negative pore water pressure decrease which can be estimated through coupled flow theory. The coupled flow theory is discussed in Section 2.6.2. In addition, k_h varies in the wide range of 1×10^{-3} to 1×10^{-11} m/s for various soil types depending on the mechanical and physico-chemical parameters, such as geometrical arrangement, tortuosity and individual flow channel sizes, which signify the sensitivity of electrically-developed pore water pressure to k_h (Mesri and Olsen, 1971; Mitchell and Soga 2005). In addition, for a specific type of soil, the variation in k_h occurs at different stress levels and void ratios. As void ratio varies during load and voltage application, k_h needs to be closely monitored. Finally, determining k_h after treatment is crucial in estimating the consolidation behaviour of post-treated soil, and this has received limited attention in available literature.

2.5.3 Electrically-induced pore water pressure

Considering EO flow mechanism, the development of negative pore water pressure during EO is expected. Based on the experimental results, the negative pore water pressure is developed up to a peak and then is dissipated progressively (Hamir et al., 2001; Chew et al., 2004). To date, the accurate measurement of pore water pressure during EO at the anode surface is not practical. As has been discussed, because of electrolysis during EO consolidation, oxygen and hydrogen gases will be generated in the electrode vicinity. The formation of these gases leads to disturbances in laboratory-measured pore water pressure and may lead to unexpected results especially in modified triaxial cells. Chew et al. (2004) installed 4 pore water pressure transducers inside a 500 mm diameter sample between two vertical electrodes. The pore water pressure far from the anode could be measured; however, the pore water pressure close to the anode showed large fluctuation after about 115 min. Although the results are not exactly at the anode surface, the trend for the pore water pressure has been confirmed by Hamir et al. (2001) who measured the negative pore water pressure using the apparatus shown in Fig. 2.8, close to

the anode medium. As shown in Fig. 2.11, the results of measurements by Hamir et al. (2001) and Chew et al. (2004) are in good agreement in terms of the trend in pore water pressure, apart from the unexpected fluctuations.
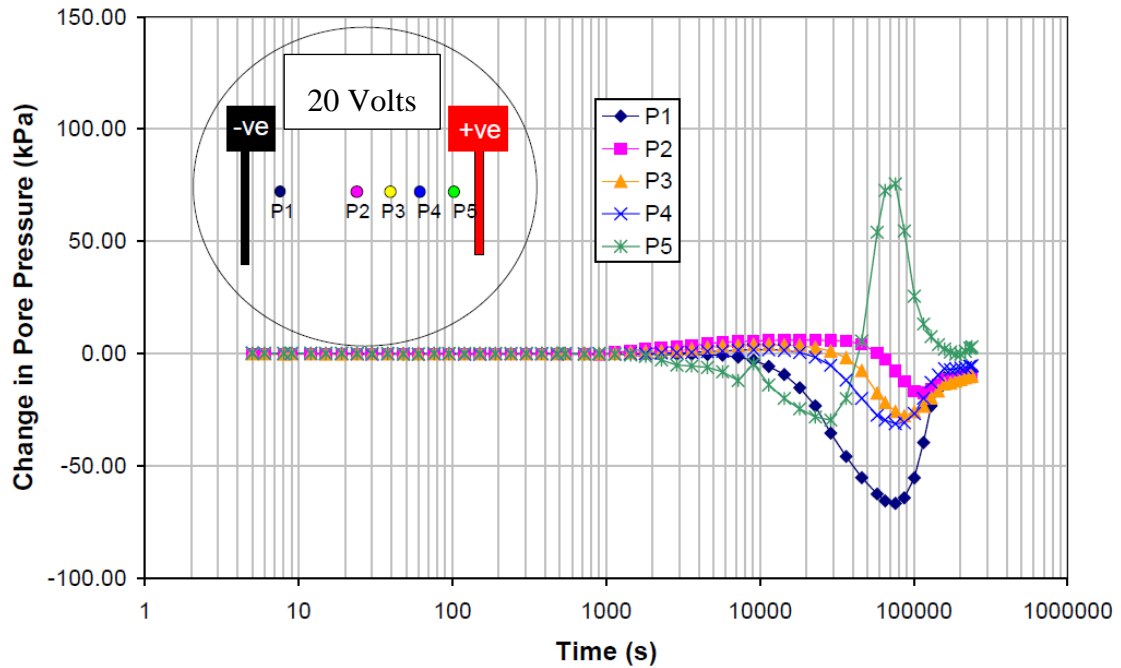
(a) Negative pore water pressure at various locations (Chew et al., 2004)
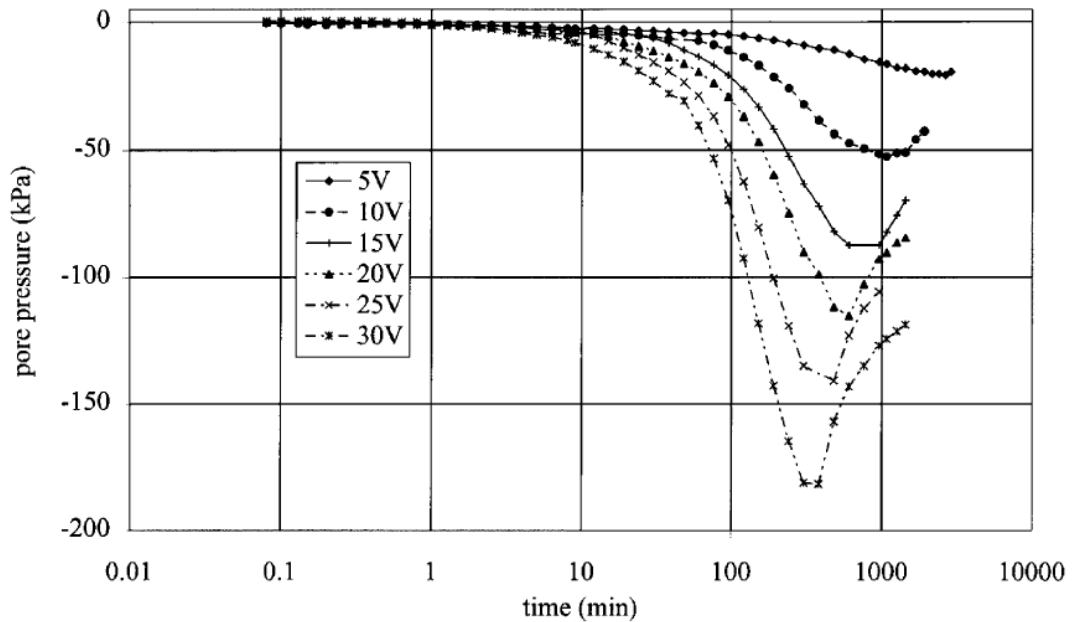
(b) Negative pore water pressure at anode (Hamir et al., 2001)

Fig. 2.11 Measured pore water pressure using oedometer cell

In addition, Win et al. (2001) attempted to measure the negative pore water pressure using the modified triaxial cell shown in Fig. 2.7 (a). Unreliable pore water pressure has been observed beyond the first 100 minutes due to gas generation at the anode and no conclusion has been made by Win et al. (2001) regarding pore water pressure. Similarly, system malfunction was reported by Jeyakanthan et al. (2011) in pore water pressure measurements using the apparatus shown in Fig. 2.7 (b).

Moreover, compared with results reported by Hamir et al. (2001) and Chew et al. (2004), the results from Jeyakanthan et al. (2011) showed negatively increasing pore water pressure only. Therefore, it cannot be extrapolated to full-scale pore water pressure. There is no data available for maximum developed pore water pressure as the returning point of pore water pressure (maximum negative pore water pressure) cannot be observed in the results. The measured pore water pressure by Jeyakanthan et al. (2011) is shown in Fig. 2.12, where E_1, E_2, and E_3 represent the tested specimens under horizontal effective stresses of 50, 100 and 150 kPa, respectively.
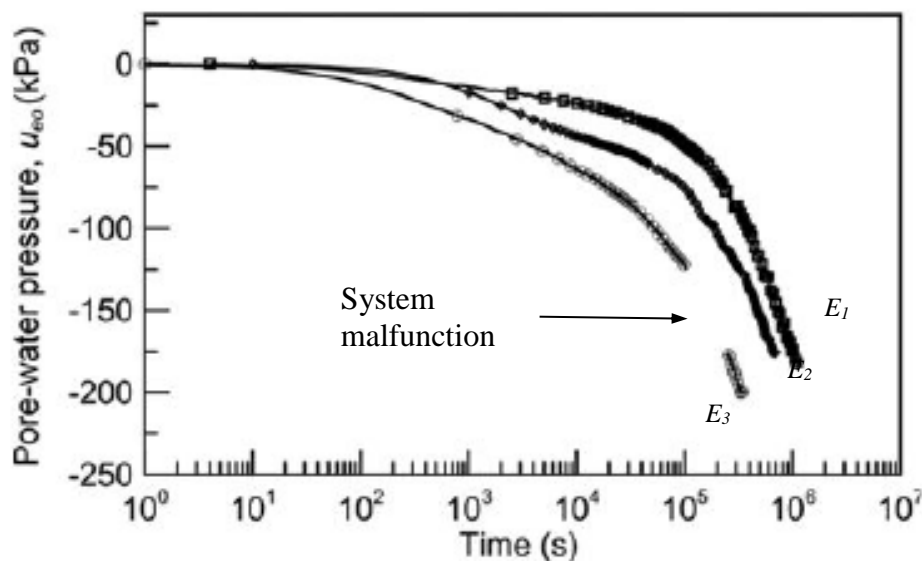
Fig. 2.12 Measured pore water pressure using modified triaxial cell (Jeyakanthan et al., 2011)

In addition to the experimental measurements, the maximum negative pore water pressure developed as a consequence of the application of an electric potential gradient is usually calculated by EO governing equation and numerical models. The EO governing equation in simplified form is known as the Esrig's theory. The EO governing equation, Esrig's theory and

numerical models will be discussed later in this chapter. Win et al. (2001) counter-checked the EO-induced preconsolidation pressure against Esrig's theory and reported that Esrig's theory slightly overestimated the developed pore water pressure and consequently achieved preconsolidation pressure. However, the effect of potential loss was neglected in the estimation of pore water pressure. Taking the electric potential loss at electrodes into account, Mohamedelhassan (2009) stated that the Esrig's theory estimates the developed negative pore water pressure during EO consolidation within an acceptable level.

2.5.4 Settlement and volumetric strain

The literature is consistent in terms of settlement and volumetric strain evolution in soil during the EO consolidation (Bjerrum, 1967; Lo et al., 1991; Win et al., 2001; Mimic et al., 2001; Burnotte et al., 2004; Mitchell and Soga, 2005; Rittirong et al., 2008; Jones et al., 2011; Jeyakanthan et al., 2011; Wu et al., 2015; Xue et al., 2015). As the water flows within the soil body and is drained at the cathode, soil consolidation occurs and consequently settlement is induced in the soil. Therefore, volumetric strain increases until the end of the EO consolidation process. The rate of settlement and volumetric strain depends on the maximum developed pore water pressure and the soil compressibility. The total settlement of the soil can be calculated as:

$$S_p = \frac{C_c H}{1 + e_0} \log(\frac{\sigma'_0 + \Delta\sigma'}{\sigma'_0})$$ (2.3)

where S_p is the final settlement, C_c is the compression index, H is the soil thickness, $\Delta\sigma'$ is the increase in the vertical effective stress and σ'_0 and e_0 are the initial vertical stress and initial void ratio of the soil, respectively. During EO consolidation, the increase in vertical effective stress is equal to the developed pore water pressure, which is given by Esrig's theory:

$$\Delta\sigma' = \frac{k_e}{k_h} \gamma_w V(y)$$ (2.4)

where $V(y)$ denotes the voltage at location y in the soil body, which is measured from the anode, as indicated in Fig. 2.13. Thus,

$$V(y) = \frac{Vy}{H}$$ (2.5)

which implies a triangular distribution over the soil body as shown in Fig. 2.13.
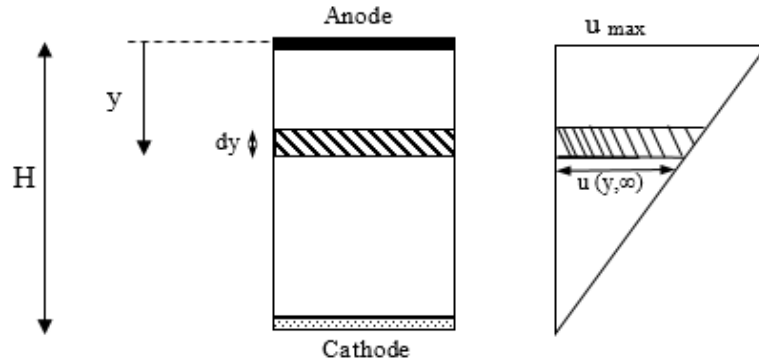
Fig. 2.13 Distribution of maximum pore water pressure in the soil body

Therefore:

$$dS_p = \frac{C_c}{1+e_0} \log \left[\frac{\sigma_0' + \frac{k_e}{k_h} \gamma_w \frac{V(y)}{H}}{\sigma_0'} \right] dy \qquad (2.6)$$

Finally, S_p can be calculated as:

$$S_p = \int_0^H \frac{C_c}{1+e_0} \log \left[\frac{\sigma_0' + \frac{k_e}{k_h} \gamma_w \frac{V(y)}{H}}{\sigma_0'} \right] dy \qquad (2.7)$$

In addition, the evolution of the compression index, C_c, and the initial condition of soil in terms of stress level and history should be considered.

Mimic et al. (2001) observed a maximum volumetric strain of 16% in Yulchon Korean clay with low preconsolidation pressure (15 kPa). However, Burnotte et al. (2004) observed about 4% volumetric strain in Mont St-Hilaire clay with the preconsolidation pressure of 175 kPa. The details of other experimental observations are listed in the Appendix (Table A.2). The observations indicate that although EO consolidation induces settlement in clays, the level of induced settlement depends on the coefficients of hydraulic and EO permeability, level of

applied electric potential gradient, preconsolidation pressure of the soil and initial void ratio of the soil.

2.5.5 Shear strength enhancement by EO consolidation

All the literature is in agreement that EO consolidation enhances the shear strength of the soil by dewatering the soil (Bjerrum, 1967; Lo et al., 1991; Win et al., 2001; Mimic et al., 2001; Burnotte et al., 2004; Mitchell and Soga, 2005; Rittirong et al., 2008; Jones et al., 2011; Jeyakanthan et al., 2011; Wu et al., 2015). In addition, as the water is transported from the anode to the cathode, the properties of the post-treated soil vary between the electrodes; however, a number of soil properties, such as shear strength and moisture content, have approximately linear behaviour between the anode and the cathode. Thus, the highest shear strength is observed at the anode vicinity where the lowest moisture content is reported, whereas the soil at the cathode medium shows minimal undrained shear strength very close to that of untreated soil. The average value of the shear strength between the anode and the cathode, which corresponds to the shear strength midway of the electrodes, is considered as the shear strength of the post-treated soil.

The shear strength improvement of post-treated soil is attributed to mechanical and chemical mechanisms. To consider the parameters affecting those mechanisms and consequently the level of improvement, various field and laboratory tests were collected from the literature as listed in Appendix A. It was concluded that the level of applied electric potential gradient, the water chemistry and geotechnical properties of the tested soils, including the soil types, sensitivity of tested soils, Atterberg limits and initial moisture contents, are affecting the mentioned mechanisms and consequently influencing the level of shear strength improvement. The effect of geotechnical properties of tested soils, including soil types, sensitivity of tested soils, Atterberg limits and initial moisture contents, is shown in Fig. 2.14.
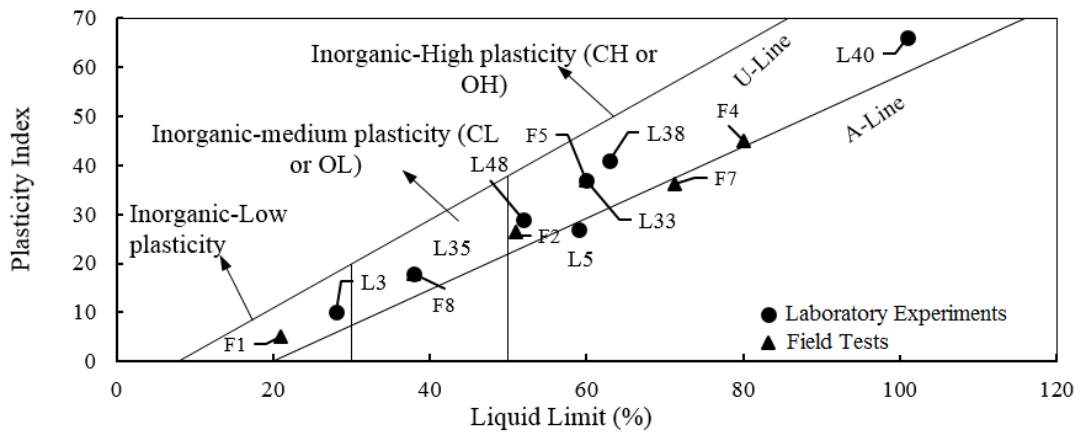
(a) Soil types
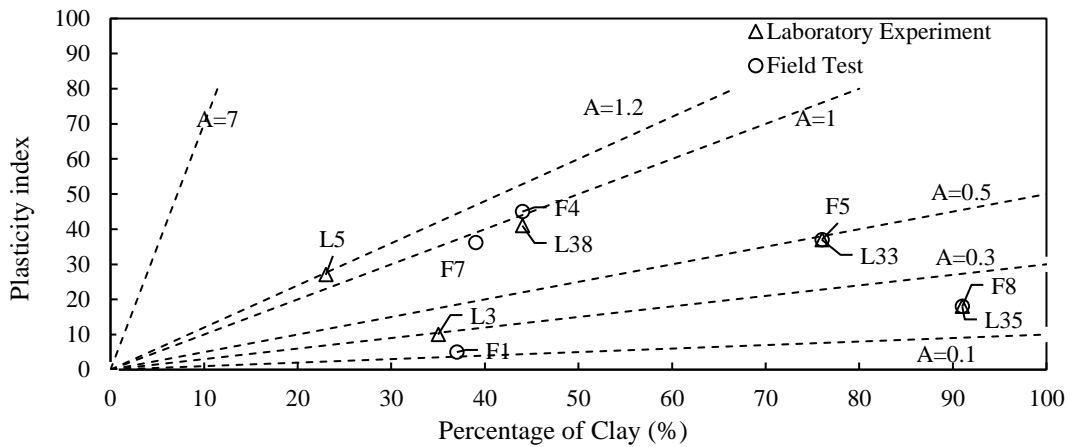
(b) Sensitivity of the soil (A is soil sensitivity)
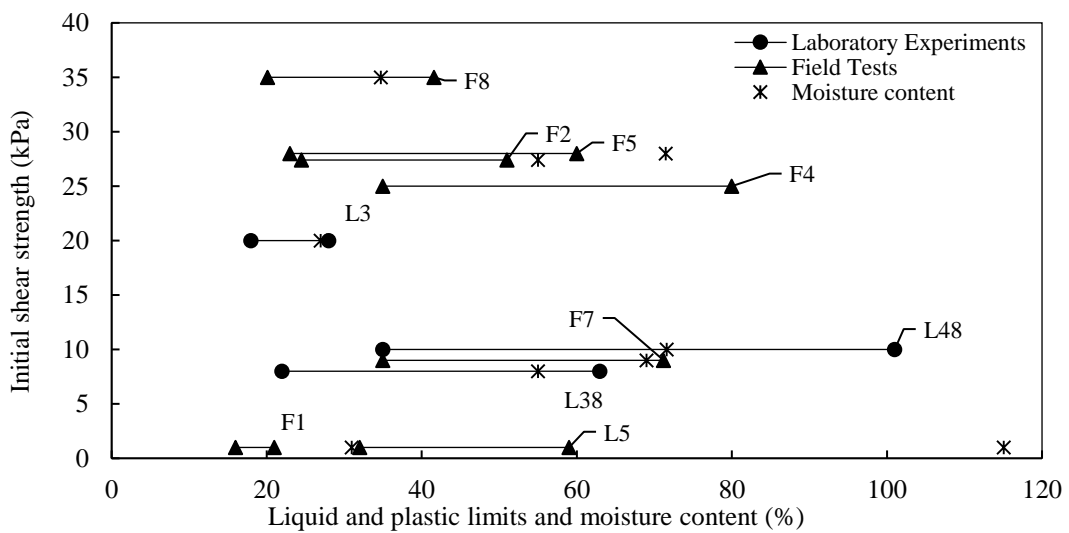
(c) Atterberg limits and moisture content (%)

Fig. 2.14 Geotechnical properties of tested soils from literature

The corresponding shear strength improvements are also shown in Fig. 2.15 together with the geotechnical properties of the soil and *USSR* (Undrained shear strength ratio) from field and laboratory tests (the details of the system properties of treatment are listed in Appendix A). The latter is defined as,

$$USSR = \frac{S_{u,post}}{S_{u,pre}} \tag{2.8}$$

where $S_{u,post}$ and $S_{u,pre}$ are the undrained shear strengths after and before treatment, respectively. It should be noted that the undrained shear strength of pre- and post-treated soils are estimated by vane shear test in the laboratory and in the field.

For a constant plasticity index, higher liquidity implies higher moisture content. Therefore, more free water will be available in the soil body. This means more water can be transported by the drag forces established during the EO process. Thus, larger volumes of water will be extracted from the soil body and higher *USSR* is expected. In addition, higher plasticity index indicates finer clayey mineral which leads to more negative charges in the diffuse double layer (DDL). Details of DDL are presented in Section 4.3.1.1. Therefore, free water can be better polarised and transported by drag forces.
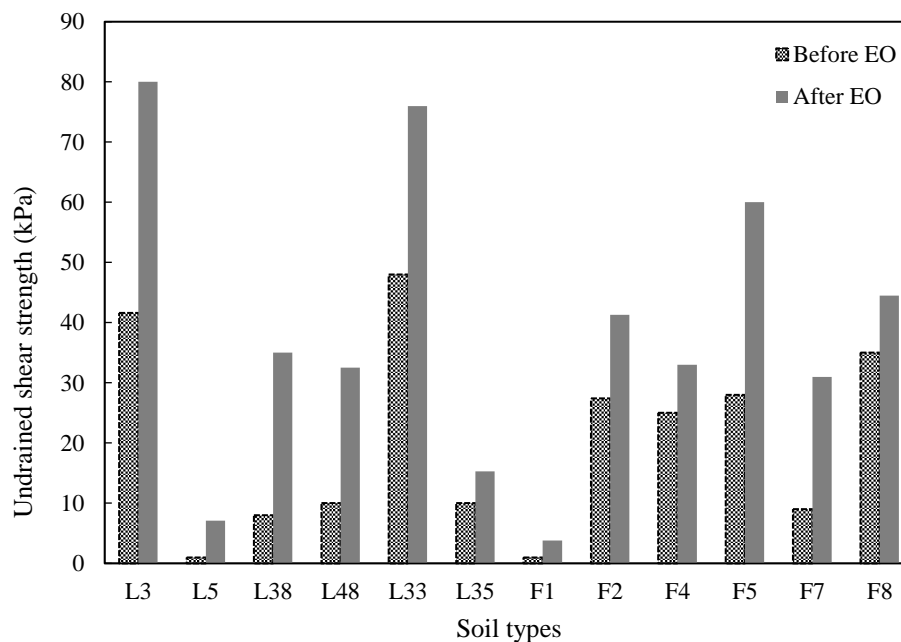
Fig. 2.15 Soil shear strength before and after the EO treatment

These behaviours are summarised in Fig. 2.15, albeit in various degrees of magnitudes. L5 soil, which is classified as high plasticity clay with liquidity index of 3, shows a *USSR* of 710%. With similar plasticity, liquidity decreases to 1 from L5 to L38 and *USSR* drops from 710% to 438%. From L38 to L48, with similar plasticity index, liquidity decreases and as a result, lower *USSR* is observed in L48. Form L5 to L3 the liquidity and plasticity of the soil decreases drastically and consequently, *USSR* decreases from 710% to 192%. These results signify the importance of soil minerology, pore water chemistry and initial condition of soil on post-treated soil behaviour.

In addition, the electric field intensity can also be an important factor affecting the shear strength enhancement of soils. F4 test was carried out with intensity of 0.12 V/cm while tests L3 and L48 were conducted under intensity of 0.45 and 0.8 V/cm, respectively. Apart from those, the electrical gradient intensities for majority of the laboratory and field tests listed in Appendix A were varied between 0.21 and 0.31 V/cm. However, a minimum value of 0.11 V/cm up to a maximum of 12 V/cm had been reported in different EO consolidation trials depending on soil types (Hamir et al. 2001).

Those observations signify that the level of applied electric field should be selected depending on the type of soil and the required level of improved shear strength, which is controlled by EO efficiency and time-dependent potential loss at electrodes.

2.5.6 Electrochemical processes

Once the electrical potential gradient is applied, in addition to oxidation and reduction, electrolysis occurs at soil-electrode interfaces as:

$$\text{Oxidation at anode:} \quad 2H_2O \rightarrow O_{2(g)} + 4H^+ + 4e^- \qquad (2.9)$$

$$\text{Reduction at cathode:} \quad 2H_2O + 2e^- \rightarrow 2OH^- + H_{2(g)} \qquad (2.10)$$
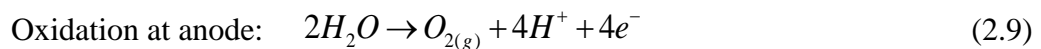
The oxygen and hydrogen gases are a part of the electrolysis products which accumulate in the vicinity of the soil-electrode interface. The accumulation of these gases forms a high-resistivity layer in those areas and, consequently, a noticeable portion of the applied electric potential gradient will be lost there (Bjerrum, 1967). Therefore, the applied potential difference (ΔV_{app}) can be given by:

$$\Delta V_{app} = (E_{cell} + \eta_a + \eta_c) + IR \qquad (2.11)$$

where η_a, η_c are the potential losses at anode and cathode, respectively, I is the current that passes through the soil, R is the ohmic resistance of soil body and E_{cell} is the generated voltage due to oxidation and reduction between the electrodes and the electrolyte which is the soil. The second term on the right-hand side of Eq. 2.11 shows the effective electrical potential gradient in the soil which is responsible for electro-osmosis consolidation. Thus, the effective electric potential gradient and potential drop, ΔV_{eff}, during the EO process can be determined by

$$IR = \Delta V_{eff} = \Delta V_{app} - \Delta V_{loss} \qquad (2.12)$$

where

$$\Delta V_{loss} = \eta_a + \eta_c + E_{cell} \qquad (2.13)$$

In an EO system, ΔV_{app} is a system property which is known. To determine the IR, all three other factors should be known. E_{cell} is independent of the electric potential application. However, η_a and η_c are present due to the voltage application and should be determined in each system in order to calculate the effective electric potential gradient.

In addition, depending on several factors, such as different behaviour of oxygen and hydrogen gases as electrolysis products and different anode and cathode materials, various levels of potential losses (η_a and η_c) are expected. Oxygen gas can react with many metallic anodes such as steel, copper and bronze and form a conductive metal oxide. Previous studies reported negligible potential loss in this case (Mohamedelhassan 2009; Jayakanthan et al. 2011). However, hydrogen gas is unable to react with the cathode and consequently a potential drop has been reported in majority of the studies (Win et al., 2001; Mimic et al., 2001; Burnotte et al., 2004; Mohamedelhassan 2009; Jeyakanthan et al. 2011).

Karunaratne (2011) observed that the level of the potential drop increases with time. Potential drops of approximately 10% to 60% were reported after 300 min and 823 min, respectively, in conductive geosynthetic electrodes. Therefore, the maximum potential drop can be expected at the end of EO consolidation, which is commonly considered as the potential drop of EO consolidation. In addition, the percentage of potential loss is independent of the level of applied voltage. Jeyakanthan et al. (2011) reported about 40% potential drop for various applied voltages ranging from 1.5 to 7.5 V, as shown in Fig. 2.16.
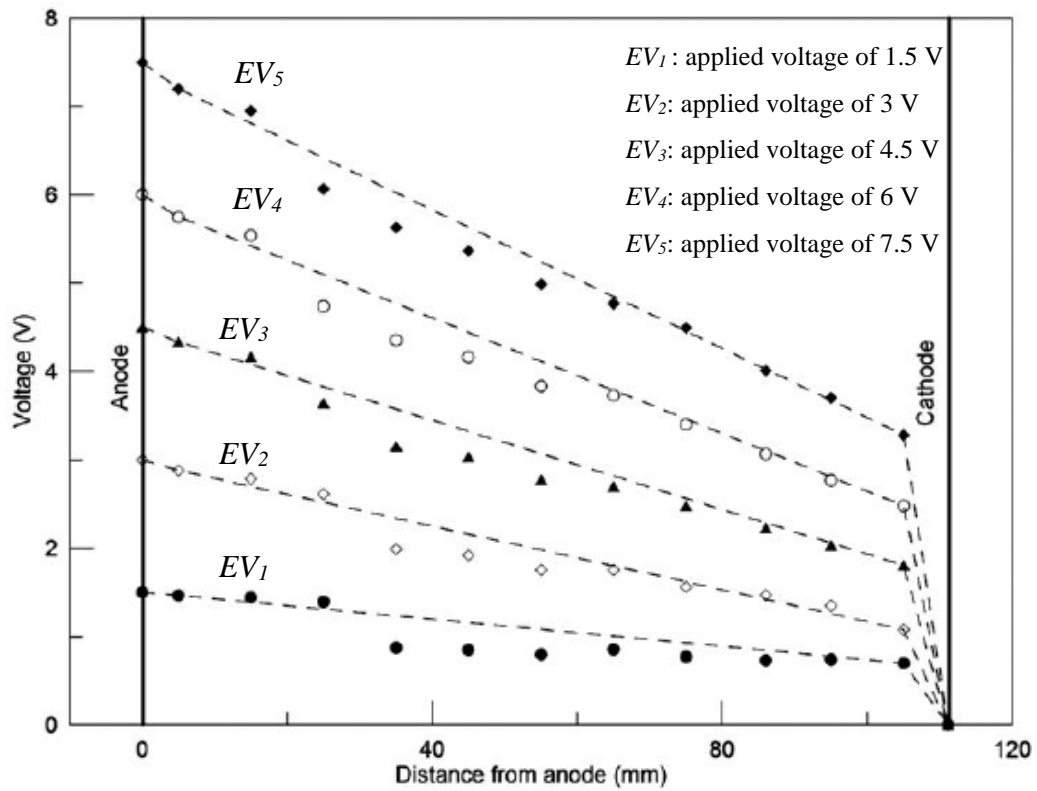
(a) Voltage drop near the copper electrodes (Jeyakanthan et al. 2011)
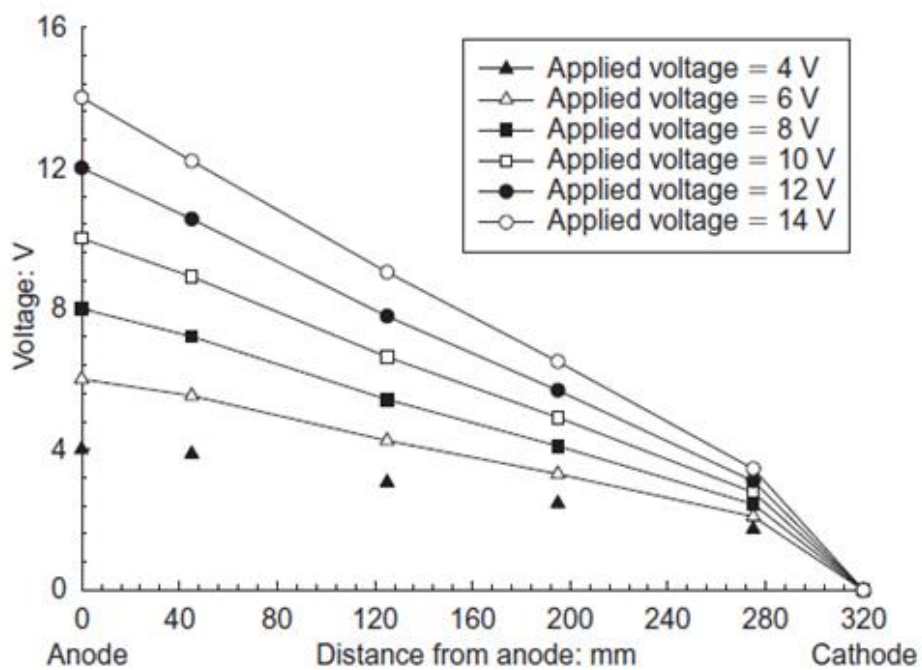
(b) Voltage drop near the steel electrodes (Mohamedelhassan 2009)

Fig. 2.16 Potential drop at the soil-electrode interfaces

On other hand, electrolysis at the electrode medium changes the pH regime in the soil body. Other electrolysis products, namely H^+ and OH^-, are in liquid phase and migrate throughout the soil towards the opposite terminal. In other words, the hydrogen produced at the anode migrates to the cathode medium and the hydroxide generated in the cathode will move to the anode. As the net flow is towards the cathode side, H^+ migrates easier than OH^- which leads to progressive acidification of the soil, as shown in Fig. 2.17.
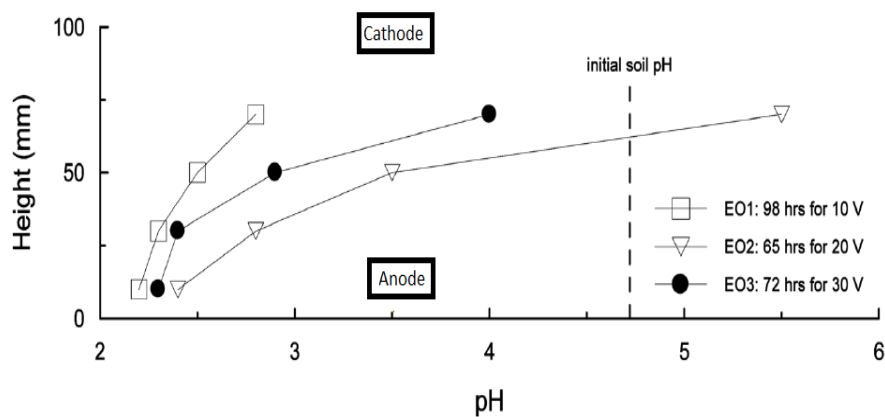
(a) Variation of pH with the height of specimen (Lee, 2007)
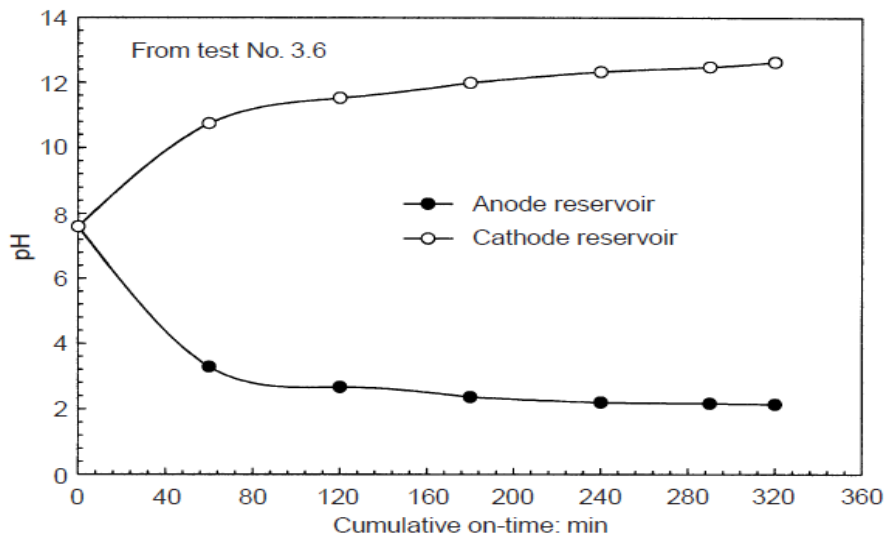
(b) Variation of pH with elapsed time (Mohamedelhassan and Shang, 2001)

Fig. 2.17 Acidification of the soil during EO consolidation

2.5.7 Summary of post-treated soil properties and behaviours

All of the reviewed literature consistently confirmed that EO consolidation could improve the geotechnical behaviour of fine-grained soils. In addition, the level of improvement in the behaviour of post-treated soils, including developed pore water pressure, induced settlement (volumetric/vertical strain) and shear strength, depends on the chemical and geotechnical properties of the soil, such as soil minerology, pore water chemistry, initial condition of tested soil and level of applied electric potential difference. To understand the relationship between these parameters and to identify the important parameters affecting EO consolidation, the governing theories and equations are developed, and these are reviewed in following section.

2.6 EO theories and governing equations

Basically, EO theories are based on the combination of hydraulic loading and electric potential gradient application. Each one triggers various flows within the soil body which can be coupled. To obtain the governing equation for EO consolidation, the conservation of mass law (for considering hydraulic loading) is combined with the electrically-induced flows under the framework of coupled flow theory considering special boundary conditions.

To understand the relationships between the parameters affecting EO consolidation, the flow mechanisms and the superposition of possible flows (coupled flow theory) are initially presented. Then the possible boundary conditions are discussed. Finally, the governing equation for EO consolidation is discussed using mass conservation law, coupled flow theory and suitable boundary conditions.

2.6.1 Electro-osmosis flow mechanism

Under the influence of a direct current (DC) electric potential gradient, the cations and anions in the pore water are drawn to the cathode and anode, respectively. In addition, ions carry their water of hydration and exert a viscous drag on the water around them. This type of soil behaviour subjected to DC electric potential gradient establishes a net water flow toward the cathode in fine-grained soils, which is known as direct EO water flow.

In addition to direct EO water flow, other types of secondary gradients, such as heat, hydraulic and chemical gradients, may develop because of electrical potential gradient application in the soil body. To study the effect of electrical gradient on soil and to quantify the total EO flow volume, the other types of generated gradients and the flows and interaction between those

flows should be considered. The direct and coupled effect of the applied electrical potential gradients on the soils can be studied under the framework of coupled flow theory.

2.6.2 Theory of coupled flow (transport phenomena)

Electricity, fluids, heat and chemicals flow through a porous media, such as soil, under the influence of special driving force. The flow rate of each of these is proportional to the driving force and the coefficient of that proportionality is a relatively constant number for a special type of soil (Mitchell and Soga, 2005). These flows are popularly called direct flows.

Moreover, once a driving force is applied to the soil body, in addition to direct flow, all other types of flow will develop simultaneously. These flows are called coupled flows. All direct and coupled flows are listed in Table 2.1.

The following general law can be written for coupled and direct flows:

$$\varphi_i = \Sigma L_{ij} X_j \qquad (2.14)$$

where L_{ij} are called coupling coefficients. φ_i is flow of type i and X_j is driving force of type j. Eq. 2.14 implies that each type of flow may be affected by the gradients of another type which is controlled by the coupling coefficient. However, detailed quantification of all types of driving gradients and flows is not an easy task and, in many cases, the coupling coefficient and developed gradient are very close to zero or can be neglected (Mitchell and Soga, 2005).

Table 2.1 Direct and coupled flow (Mitchell and Soga 2005)

	Gradient X			
Flow J	**Hydraulic Head**	**Temperature**	**Electrical**	**Chemical Concentration**
Fluid	Hydraulic conduction Darcy's law	Thermo-osmosis	Electro-osmosis	Chemical osmosis
Heat	Isothermal heat transfer or thermal filtration	Thermal conduction Fourier's law	Peltier effect	Dufour effect
Current	Streaming current	Thermo-electricity Seebeck or Thompson effect	Electric conduction Ohm's law	Diffusion and membrane potentials or sedimentation current
Ion	Streaming current ultrafiltration (also known as hyperfiltration)	Thermal diffusion of electrolyte or Soret effect	Electrophoresis	Diffusion Fick's law

2.6.3 Quantification of EO water transport and boundary conditions

Basically, in electro-osmosis flow, it is assumed that the chemical concentrations of pore water (salinity) and temperature of soil are constant throughout the process. However, pore water pressure will be developed in response to water transport from the anode to the cathode. This pore water pressure development implies a hydraulic gradient in the soil. The amount of pore water pressure and hydraulic gradient development due to the electrical gradient application depend on boundary conditions.

Fig. 2.18 illustrates the possible cases of boundary conditions along with the developed pore water pressure in each case. In the case of open anode and cathode (Case a in Fig. 2.18), the pore water flows from the anode to the cathode with no pore water pressure development. If water is supplied from the anode side, this flow will be in steady-state and the flow rate depends on the applied electric gradient between the anode and the cathode (Casagrande 1949).

However, because no pore water pressure has been developed in that case, the effective stress is maintained constant and no consolidation can be observed. Therefore, direct flow of water will take place and Eq. 2.14 can be rewritten as:

$$q_w = L_{eh} i_e \qquad (2.15)$$

where q_w is the water flow through the unit cross-section area of the soil, L_{eh} is the coupled flow coefficient and i_e is the potential gradient. When the cathode is open for drainage and the anode is sealed (Case b in Fig. 2.18), the pore water pressure can be dissipated in the cathode vicinity. In addition, due to the applied electrical potential, pore water will be transported from the anode to the cathode. This transport of water and the zero pressure in the cathode implies a negative pore pressure (vacuum) in the vicinity of the anode. As the total stress is maintained constant during the EO process, the effective stress will increase to compensate for the negative pressure. This increment in effective stress leads to the consolidation of the soil. Therefore, the application of electrical potential to the soil along with the special case of boundary condition develops hydraulic gradient in the soil body. In such case, the developed water flow in the soil depends on both the electrical and hydro-mechanical behaviour of the soil. Thus, Eq. 2.14 can be rewritten for water flow as:

$$q_w = L_{eh} i_e + L_{hh} i_h \qquad (2.16)$$

where L_{hh} is the coupled flow coefficient and i_h is the hydraulic gradient.

The latter two cases of boundary conditions (Cases c and d in Fig. 2.18) are sealed at the cathode and water accumulates in the cathode vicinity, causing swelling and no consolidation takes place. The combination of the mass balance equation and coupled flow theory in boundary conditions similar to Case b in Fig. 2.18, will lead to EO consolidation theory similar to Terzaghi's consolidation theory, which is widely accepted as an EO consolidation governing equation.
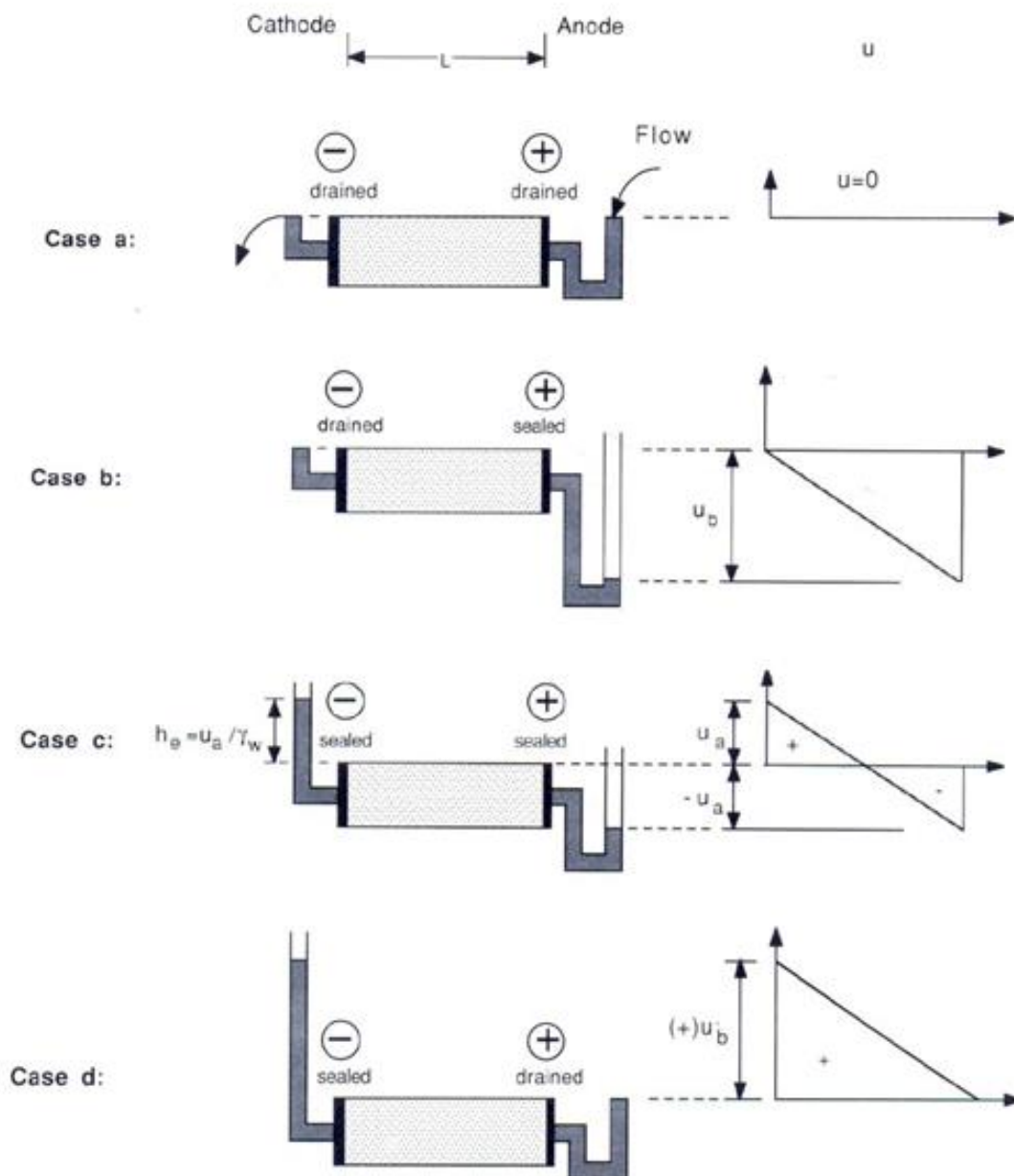
Fig. 2.18 Possible boundary conditions in electro-osmosis (Mitchell and Soga, 2005)

2.6.4 Governing equation of EO Consolidation

The governing equation of EO consolidation has been proposed based on the theory of mass balance and considering the following assumptions (Mitchell and Soga, 2005):

- The soil mass is homogeneous;

- The possible EO-induced soil chemistry changes are not considered;
- There are no electrical potential losses in the system;
- DC current is used for electrical consolidation of soil;
- No chemical processes happen at the electrodes;
- Electrically- and hydraulically-induced velocity may superimpose (coupled flow).

The volume change in a soil element is equal to the water flux through the element, as shown in Fig 2.19. Net water discharge through the element is equal to the velocity difference with time which is given by:

$$A\left[V_n(y+dy)-V_n(y)\right]=\frac{\partial\bar{v}}{\partial t} \qquad (2.17)$$
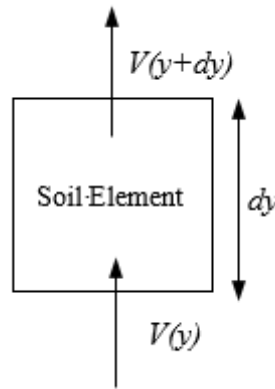
Fig. 2.19 Representative soil element under the influence of an electric potential gradient

where V_n denotes the induced water velocity during EO process. A and $\bar{v}$ are the cross-sectional area and volume of the soil element, respectively. Thus,

$$\frac{\partial\bar{v}}{\partial t}=\frac{\partial V_n}{\partial y}\bar{v} \qquad (2.18)$$

This relationship can be written based on the coefficient of volume compressibility (m_v) as:

$$\frac{\partial V_n}{\partial y}=-m_v\frac{\partial\sigma'}{\partial t} \qquad (2.19)$$

and

$$\frac{1}{\bar{v}}\frac{\partial \bar{v}}{\partial t} = -m_v \frac{\partial \sigma'}{\partial t}$$ (2.20)

where σ' is effective stress.

On the other hand, the total stress remains constant during the EO consolidation. Therefore,

$$\frac{\partial \sigma'}{\partial t} = -\frac{\partial u_e}{\partial t}$$ (2.21)

By substituting Eq. 2.19 into Eq. 2.21:

$$\frac{\partial V_n}{\partial y} = m_v \frac{\partial u_e}{\partial t}$$ (2.22)

In addition, the water velocity during EO consolidation can be computed based on coupled flow theory as outlined in Eq. 2.16. L_{eh} and L_{hh} are called the coefficients of electro-osmotic permeability and hydraulic permeability, respectively, and are popularly denoted as k_e and k_h, respectively. Therefore:

$$V_n = V_e + V_h$$ (2.23)

$$V_n = k_e \frac{\partial V}{\partial y} + \frac{k_h}{\gamma_w}\frac{\partial u_e}{\partial y}$$ (2.24)

where V is potential difference applied to the soil.

By combining Eq. 2.22 and Eq. 2.24, the following equation is obtained:

$$k_e \frac{\partial^2 V}{\partial y^2} + \frac{k_h}{\gamma_w}\frac{\partial^2 u_e}{\partial y^2} = m_v \frac{\partial u_e}{\partial t}$$ (2.25)

Using the coefficient of consolidation, C_v, defined as:

$$C_v = \frac{k_h}{m_v \gamma_w}$$ (2.26)

it follows that

$$\frac{\partial^2 u_e}{\partial y^2} + \frac{k_e \gamma_w}{k_h}\frac{\partial^2 V}{\partial y^2} = \frac{1}{C_v}\frac{\partial u_e}{\partial t}$$ (2.27)

Eq. 2.27 can be converted for radial flow as:

$$\frac{\partial^2 u_e}{\partial r^2} + \frac{k_e \gamma_w}{k_h} \frac{\partial^2 V}{\partial r^2} + \frac{1}{r}(\frac{\partial u_e}{\partial r} + \frac{k_e \gamma_w}{k_h} \frac{\partial V}{\partial r}) = \frac{1}{C_v} \frac{\partial u_e}{\partial t} \tag{2.28}$$

where r is the radial distance from the central axis of the central cathode to the central axis of the circumferentially arranged cathodes.

Esrig (1968) assumed completely linear distribution of voltage throughout the soil, neglected the electrical resistivity of the soil, and analytically solved Eq. 2.27 in one dimension. The dimensionless pore water pressure and degree of consolidation are shown in Fig. 2.20 versus time factor, T_v where

$$T_v = \frac{C_v t}{L^2} \tag{2.29}$$

In addition, when water is drawn from the anode to the cathode by applying electrical gradient, hydraulic gradient will be developed to balance the different amount of consolidation in the anode and cathode vicinity and will cause the water flow from the cathode to the anode. With time, the hydraulic gradient and counter-water flow increases until a balance occurs between the hydraulic and electro-osmosis flow. At that point, no flow occurs through the soil body and the electro-osmosis consolidation ceases. The pore water pressure in that situation is the maximum pore water pressure developed by EO consolidation. Therefore, based on Eq. 2.24:

$$k_e \frac{\partial V}{\partial y} + \frac{k_h}{\gamma_w} \frac{\partial u_{e\max}}{\partial y} = 0 \tag{2.30}$$

Solving Eq. 2.30 for du_{emax}:

$$du_{e\max} = -\frac{k_e \gamma_w}{k_h} dV \tag{2.31}$$

$$u_{e\max} = -\frac{k_e \gamma_w}{k_h} V + C \tag{2.32}$$

At the cathode vicinity, $V = 0$ and, because of drainage, $u_e = 0$. Finally:

$$u_{e\max} = -\frac{k_e \gamma_w}{k_h} V \tag{2.33}$$

It is widely known that k_e varies in a narrower range (1×10^{-8} to 1×10^{-9}) compared to k_h. Thus, the EO consolidation technique enables the development of pressure gradient more effectively in a soil with lower hydraulic permeability (fine-grained soils).
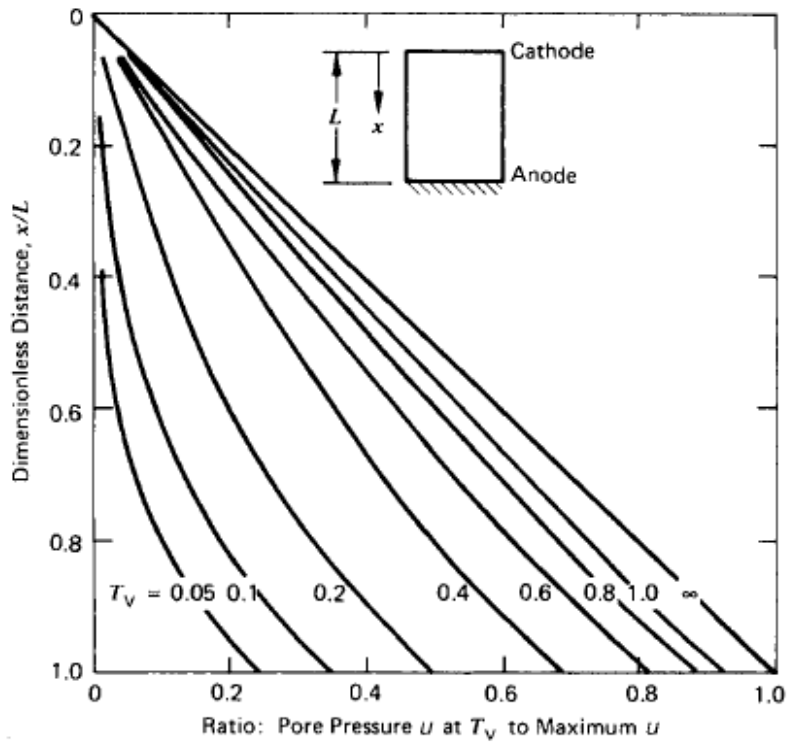
(a)
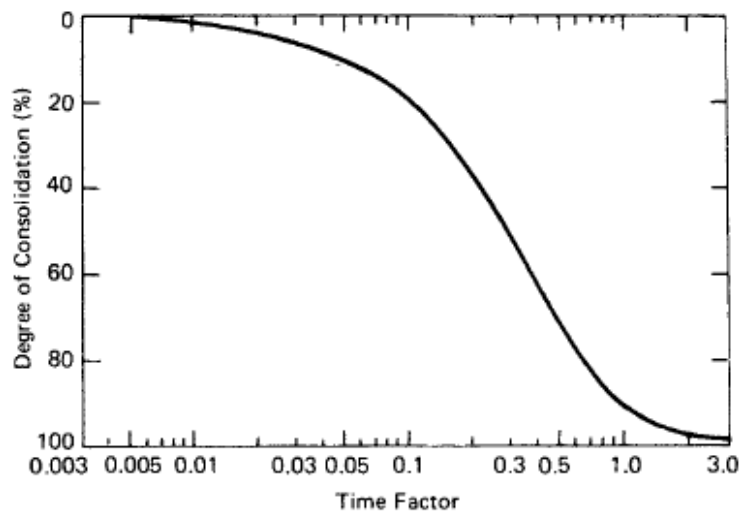
(b)

Fig. 2.20 (a) Dimensionless pore water pressure versus time factor during EO consolidation; (b) Average degree of consolidation versus time factor for EO consolidation (Esrig, 1968)

2.7 Cost of EO consolidation project

Basically, the cost of an EO project includes the fixed and power costs. Fixed costs are common between all EO projects, such as health and safety, project fencing and power supplier costs. However, power cost is variable and depends on the EO efficiency and the level of power consumption.

2.7.1 Electro-osmosis efficiency

One of the weaknesses of electro-osmosis ground improvement approach which restricts engineers from applying this method in the field is the lack of knowledge of the expected efficiency of the EO technique. One of the factors that control electro-osmosis efficiency is the soil electrical resistivity. By definition, the EO efficiency is the amount of transported water per unit charge that passed through the soil. Thus, if efficiency is denoted by η then:

$$Q = \eta I \tag{2.34}$$

where Q and I are the water discharge and the electrical current, respectively. Based on Casagrande's proposed relationship:

$$Q = k_e i_e A \tag{2.35}$$

where

$$i_e = \frac{V}{L} \tag{2.36}$$

and E and L are the electrical potential difference and the specimen height, respectively. Hence,

$$Q = k_e A \frac{V}{L} \tag{2.37}$$

By equating the discharge induced by the electric current from Eq. 2.36 and Eq. 2.37:

$$Q = k_e A \frac{V}{L} = \eta I \tag{2.38}$$

and after rearrangement:

$$\eta = k_e \frac{VA}{IL} \tag{2.39}$$

This can be simplified to

$$\eta = \rho k_e \qquad (2.40)$$

where ρ is soil electrical resistivity:

$$\rho = \frac{VA}{IL} \qquad (2.41)$$

As discussed earlier, in addition to EO efficiency, the electrical resistivity of the soil controls the distribution of the voltage in the soil body which needs to be accurately measured.

2.7.2 Comments on EO costs and theories

Although the governing equation for EO consolidation takes important factors into account, such as applied voltage and boundary conditions, and connects these parameters under acceptable frameworks, namely coupled flow theory and conservation of mass, many other soil properties and processes which occur concurrently with consolidation are ignored or highly simplified.

The effects of electrochemical processes, which mainly include gas generation and voltage loss, are ignored in the numerical modelling of the EO consolidation. In addition, for the sake of simplicity, the coefficient of consolidation during the hydraulic loading has been used in EO governing equation; however, the coefficient of consolidation during the EO consolidation should be measured and used in the EO governing equations. Furthermore, the distribution of voltage is assumed to be perfectly linear which cannot always satisfy the charge conservation law. The distribution and also the developed current in the soil body are controlled by the soil electrical resistivity. Finally, as discussed earlier, the electrical resistivity of soil governs the EO efficiency and consequently affects the cost of the EO project. Therefore, electrical resistivity of soil should be closely monitored during the EO consolidation tests.

2.8 Electrical resistivity of soil

2.8.1 Concept

The electrical resistivity is the capability of soil medium to ion transition. It is a fundamental property of materials and a measure of the material resistance against electrical current (Abu-

Hassanein et al., 1996). Electrical resistivity is related to the material and can be expressed in the Eq. (2.42).

$$R = \frac{\rho L}{A}$$ (2.42)

where R is the electrical resistance, V is the electrical potential difference, A is the cross-sectional area and L denotes the height of sample. The electrical resistivity is geometry-independent characteristic of the soil and it depends on the chemical and geotechnical properties of the soil.
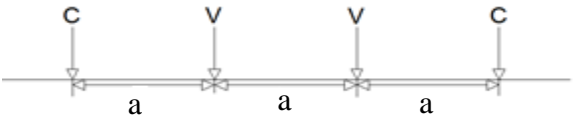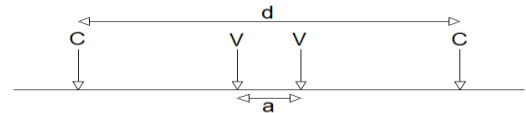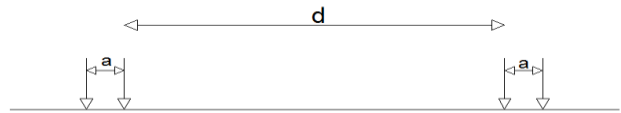
2.8.2 Electrical resistivity measurement

Soil electrical resistivity measurement usually involves the application of current to the soil and the measurement of voltage at various locations via multiple (two or more) electrodes. The measured voltage highly depends on the type of the applied current. In other words, soil electrical resistivity is a frequency-dependent parameter (Bordi et al., 2001; Cerato and Lin, 2012). Arulanandan and Smith (1973) stated that the soil electrical resistivity is frequency-dependent only in the range of 1 MHz to 100 MHz. Therefore, AC current can be used for electrical resistivity surveying in low frequencies (Abu-Hassanein et al., 1996). Nevertheless, Smith-Rose (1934) believed that the effective frequency range on electrical resistivity depends on the soil moisture content. Thus, to measure the actual electrical resistivity of soil, the frequency should be adjusted to the soil moisture content during the electrical resistivity surveying. In addition, Rinaldi and Cuestas (2002) observed that the electrical resistivity of soil with electrolyte concentration of more than 1% showed nonlinear behaviour under a frequency of 3 kHz. This type of behaviour was attributed to the electrode polarisation and a frequency of more than 3 kHz was recommended for electrical resistivity surveying in their research. Thus, to utilise AC current in electrical resistivity measurements, it is essential to perform calibration for the applied frequency in different moisture contents in parallel with other required calibrations.

In addition, the number of employed electrodes to measure the voltage and the current in soil body affects the calculated electrical resistivity of the soil. Based on this, electrical resistivity methods can be categorised into: (a) two electrode methods (2EM); and (b) four electrode methods (4EM). In 2EM, which is the most convenient method for electrical resistivity surveying, the current is applied via two electrodes to the soil and the voltage difference is

measured at the same electrodes (Fukue et al., 1999). However, in the 4EM, the current is given to the soil using the two electrodes and another pair of electrodes between the current electrodes is used to measure the potential difference. Rust (1952) applied 2EM and 4EM to measure the electrical resistivity of rock samples. A higher calculated electrical resistivity in 2EM was observed. The reason for this was the loose contact between the soil sample and the current electrodes in the separating surface. Thus, the air present in that area increases the resistivity locally, which considerably increases the soil electrical resistivity. It was concluded that the two electrodes method overestimates the electrical resistivity and is not as accurate as the four-electrode method. These findings are also supported by McCarter's (1984) results. The utilised 2EM apparatus in their experiments overestimated the clay electrical resistivity by more than 50% compared to the highest standard value of clay electrical resistivity proposed by other researchers (Palacky, 1987; Sheriff, 1973; Samouëlian et al., 2005). To tackle this problem, the 4EM has been widely used for electrical resistivity measurements (Abu-Hassanein et al., 1996; Campanella and Weemees, 1990; Kalinski and Kelly, 1994; 1993; Kim et al., 2011). Common 4EM configurations for electrical resistivity surveying are listed in Table 2.2.

Table 2.2 Common 4-electrode configurations

Arrangement	Geometry of arrangement	Formula
Wenner		$\rho = 2\pi a(\dfrac{V}{I})$
Schlumberger		$\rho = \pi \dfrac{(\dfrac{d}{2})^2 - (\dfrac{a}{2})^2}{a} \dfrac{V}{I}$
Dipole-Dipole		$\rho = \pi d(\dfrac{d}{a}+1)(\dfrac{d}{a}+2)\dfrac{V}{I}$

In the Wenner array, the potential electrodes are far apart from the current electrodes. Therefore, a larger voltage will be measured by the Wenner array compared to the other arrangements and reduce the errors in voltage measurements. In addition, the Wenner array is

less sensitive to noise and is a more reliable method in urban areas in comparison with other techniques. However, the length of cable used in the Wenner array is more than the Dipole-Dipole arrangement and, as a result, current leakage increases in the Wenner array. In addition, the Wenner array is slower than the Schlumberger method when applied in the field as all four electrodes need to be moved when testing different points. Thus, the Wenner array obtains more secure and reliable results but is slower in implementation in comparison with the other methods.

2.9 Summary

Generally, there are discrepancies in the literature in terms of the level of the effectiveness of EO consolidation on soil behaviour. This can be attributed to the underestimation or omission of several parameters affecting EO consolidation, such as electrical resistivity of the soil, potential loss at soil-electrode interfaces and coefficient of consolidation during EO process. On the one hand, the electrical resistivity of soil, which affects the estimation of EO efficiency, cost of project and potential distribution within the soil, cannot be measured during EO test using EO consolidation cell. Therefore, a separate test needs to be designed and conducted to accurately determine this parameter. In this case, a numerical electrical resistivity model can also be used as an effective tool to estimate the electrical resistivity of soil in various conditions, with a minimal number of experimental tests. On the other hand, laboratory apparatus used by various researchers to conduct EO consolidation tests and to identify important parameters, have several drawbacks which need to be addressed. Moreover, laboratory results cannot be directly extended to the field case due to scale effects. Therefore, a numerical framework is required to accurately estimate the post-treated soil behaviour in the field. Finally, as potential loss at soil-electrode interfaces noticeably reduces the effectiveness of EO consolidation, there is a need for a new technique to reduce the level of potential loss and enhance the effectiveness of EO consolidation.

3 DEVELOPMENT OF ELECTRICAL RESISTIVITY APPARATUS AND VALIDATION

3.1 Introduction

The electrical resistivity of soil is a controlling factor in EO consolidation process. As discussed in Chapter 2, the electrical resistivity governs the voltage distribution in the soil body and, consequently, the level of developed pore water pressure due to the electric potential gradient application. In addition, electrical resistivity controls the power consumption of the EO consolidation process. Therefore, accurate measurement of electrical resistivity of the soil is crucial in the estimation of the EHM behaviour of the soil and in the prediction of EO project cost. Large variety of experimental and modelling approaches have been proposed by various researchers based on various electrical principles to measure/predict the electrical resistivity of the soil. Among those, Wenner array is a method accepted by the ASTM standard which can be used in the field. In this research, the Wenner arrangement was adopted as basis in developing a laboratory apparatus to measure the electrical resistivity of the soil. Then the apparatus was fully calibrated and tested and the results were verified using experimentally obtained data.

3.2 Background

As discussed earlier, electrical resistivity is a fundamental property of soils. It is a function mainly of the moisture content and several other parameters, such as mineralogy, soil structure, texture, temperature, and salt content of the pore water (Archie, 1942; Rhoades et al., 1976; Revil et al., 1998; Mualem and Friedman, 1991; Seladji et al., 2010; Ekwue and Bartholomew, 2011; Cerato and Lin, 2012; Kibria and Hossain, 2012)

The electrical properties of saturated soft clays, such as electrical resistivity/conductivity, control the efficiency of EO consolidation method as it has a direct effect on the power consumption (Mitchell and Soga, 2005). As the electrical resistivity is a function of the void ratio of the consolidated soils, the evolution of the soil's electrical resistivity during the consolidation process, which involves decreasing void ratio, should be considered in the EO consolidation design process to assess the required change in EO efficiency and power consumption with time.

According to ASTM standard, Wenner four-electrode method is usually used to measure soil resistivity in the field. The method involves using four copper electrodes placed in equal separation, a (cm), in a straight line on the ground surface. A voltage is applied between the outer electrodes where the corresponding current, I, and the voltage drop between the inner electrodes, V, are measured (Wenner, 1915). AC or DC source of current can be used in electrical resistivity measurements (ASTM, 1995).

The electrical resistivity, ρ ($\Omega \cdot$m), was then determined as:

$$\rho = 2\pi a (\frac{V}{I})$$ (3.1)

It should be mentioned that the measured ρ by the Wenner four-electrode method represents the average resistivity of a hemisphere of soil of a radius approximately proportional, in homogenous medium, to the electrode separation, where the term ($2\pi a$) is a geometrical factor defined based on a semi-infinite boundary condition (half-space). In addition, in the laboratory-scale, the boundary conditions of the testing specimen generally do not comply with the boundary conditions of the Wenner method since the test cell does not provide the semi-infinite boundary condition required. Furthermore, the thickness of the test specimen (height of the cell) would not satisfy the hemisphere geometry requirement of the current flow.

Popular four-electrode testing apparatus have been proposed by Kalinski and Kelly (1993, 1994), Kim et al. (2011) and Choo et al. (2014), where an electrical resistivity probe was attached into the circumference of specimen and the bottom porous stone of a specially-designed oedometer, as shown in Fig. 3.1. As the electrical resistivity probe is small in size compared to the test specimen, the measured resistance value represents only that of a minimal fraction of the test specimen; therefore, it is not recommended for testing heterogeneous soils.
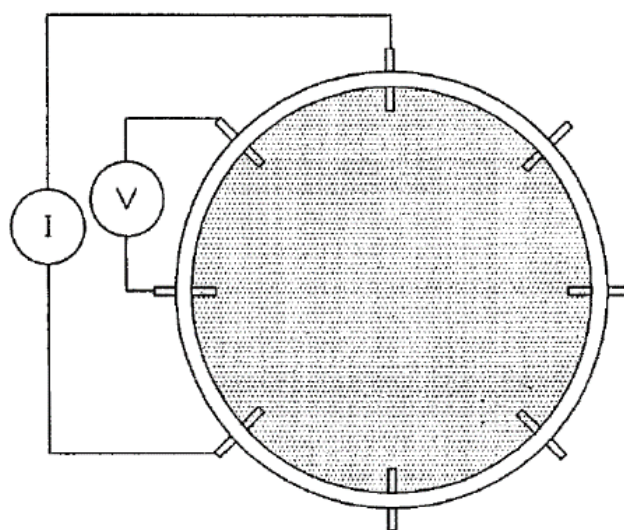
(a) Kalinski and Kelly (1993, 1994)
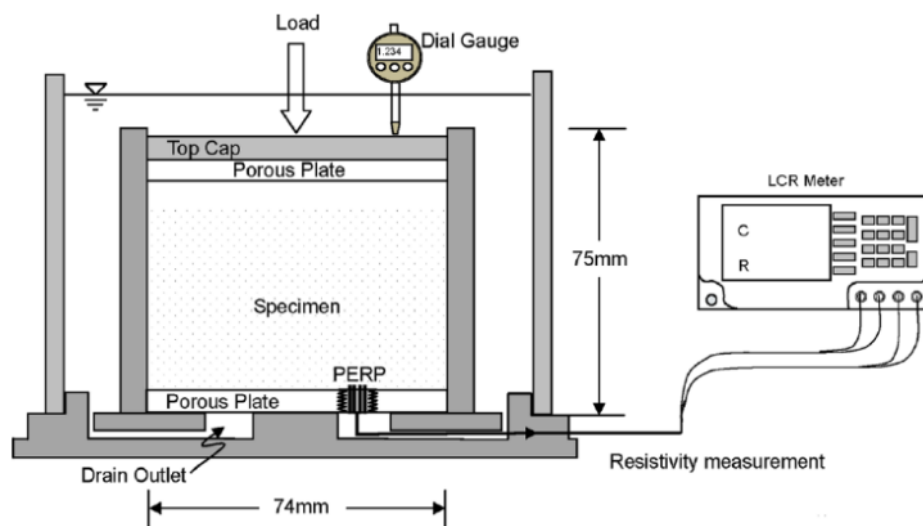
(b) Kim et al (2011) and Choo et al. (2014) (Note: PERP (Plane-type Electrical Resistivity Probe) consists of four electrodes installed based on Wenner array configuration)

Fig. 3.1 Electrical resistivity oedometer cells available in the literature

Furthermore, the effect of having bottom porous stone on the resistivity measurement should be assessed, as this boundary should be an electrical insulator in the Wenner method.

In this research, a modification of the conventional oedometer apparatus was proposed to measure the evolution of the electrical resistivity of saturated soils as the effective stress changes. To align with the ASTM standards (1995, 1999), DC source of current was used to measure the electrical resistivity of the soil. Furthermore, a robust calibration protocol for the possible effects of boundary conditions on the electrical resistivity measurements was introduced and validated.

3.3 Proposed modified electrical resistivity oedometer cell

Figure 3.2 shows the proposed modification to the conventional oedometer cell adopted in this research, where the specimen ring is made of PVC (Polyvinyl Chloride) and can accommodate a 76 mm diameter soil specimen with initial height of 20 mm. Four brass electrodes, equally spaced at 20 mm apart, are embedded into the PVC top cap to measure the electrical resistivity using the Wenner method. To allow for drainage during the consolidation process, a porous stone that rests on a PVC plate is used as the bottom boundary of the testing specimen. However, the geometric boundary conditions of the cell shown in Fig. 3.2 do not satisfy the assumptions of Eq. 3.1; therefore, a modified equation is required to reflect the effect of the proposed cell boundary conditions. A Rasor and Tinker^{TM} electrical resistivity meter model SR-2 was used in the tests. It is capable of measuring soil electrical resistance ranging from 0.1 Ω to 3.3 MΩ.
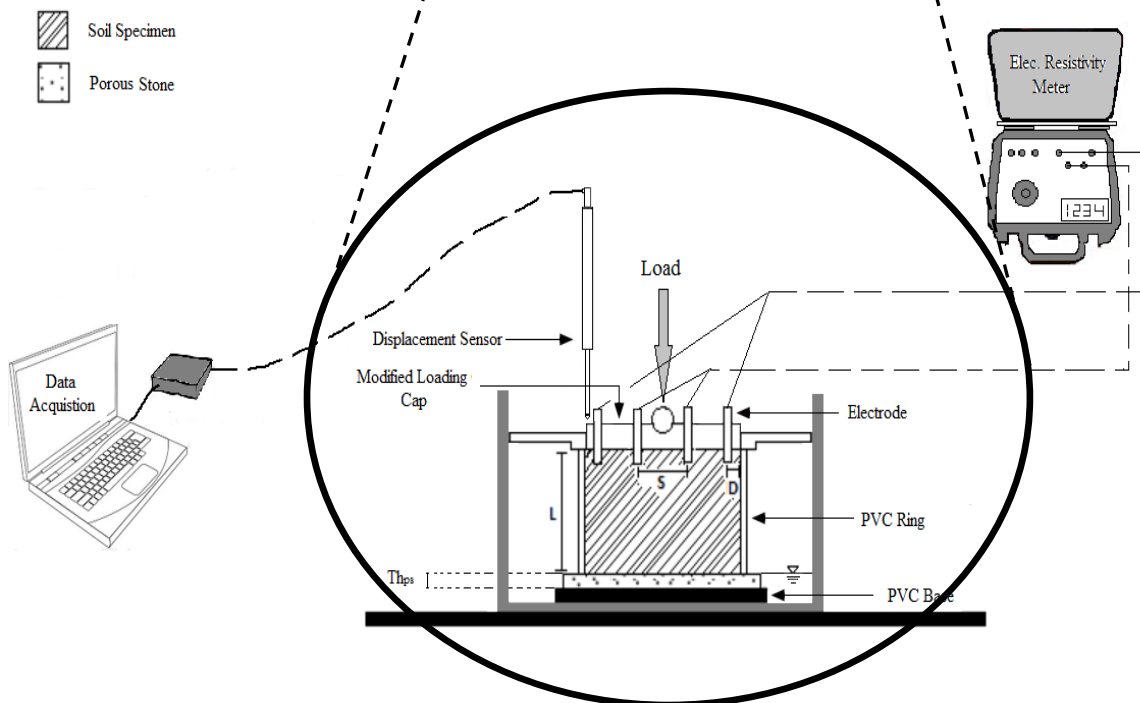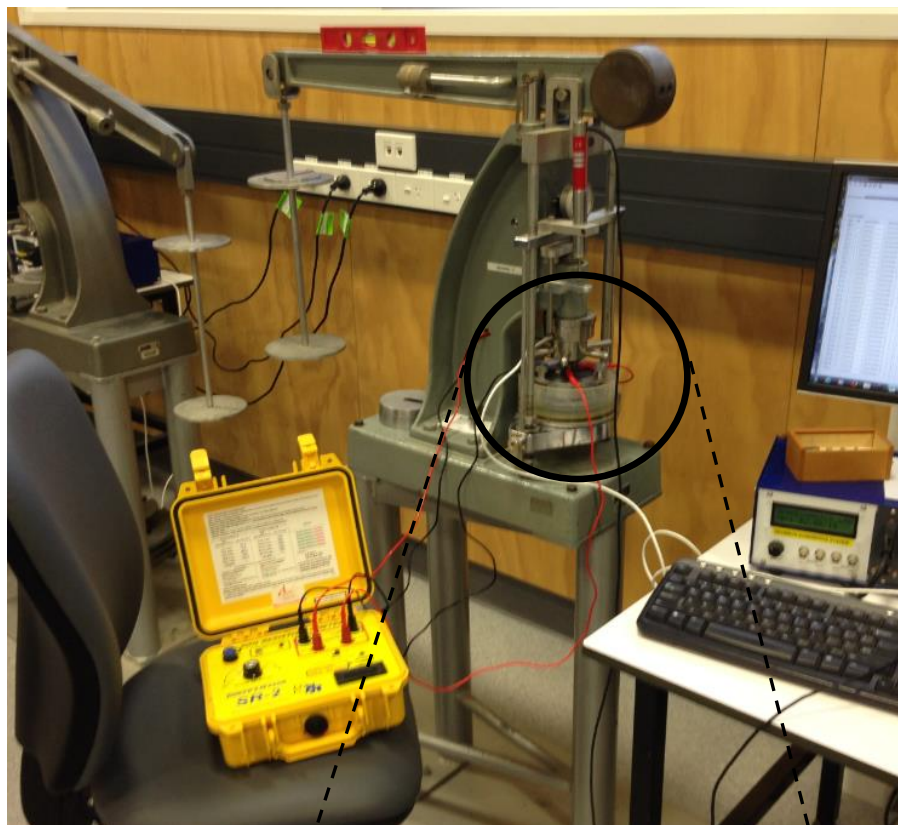
Fig. 3.2 Experimental measurement of electrical resistivity of soil

3.4 Boundary effects on measured electrical resistivity

The boundary conditions of the proposed cell that could affect the validity of Eq. 3.1 can be described using the following three dimensionless parameters; S/D, L/S, and α, where L, S, and D are the thickness of the soil specimen, spacing between the electrodes, and radial spacing between the outer electrode and the outer boundary of the tested specimen, respectively, as shown in Fig. 3.2. The term α is expressed as:

$$\alpha = \frac{Th_{ps}\rho_{ps}}{Th_T\rho_{Exp}} \tag{3.2}$$

where Th_{ps}, Th_T, ρ_{Exp} and ρ_{ps} are the thickness of the porous stone, total thickness of the porous stone and the testing specimen, experimental electrical resistivity of soil specimen and electrical resistivity of the porous stone, respectively. Therefore, the first two parameters (S/D and L/S) describe the geometric conditions and the last parameter, α, expresses the effect of the electrical resistivity and thickness of the bottom boundary (porous stone). The deviation of the measured electrical resistivity, ρ_{Exp}, using the proposed cell and Eq. 3.1 from the actual electrical resistivity, ρ_{act}, can be expressed as:

$$\beta = \frac{\rho_{act}}{\rho_{Exp}} \tag{3.3}$$

where β is the boundary condition calibration factor that is controlled by the proposed three dimensionless parameters (S/D, L/S, α). Therefore, Eq. 3.1 can be modified to determine the actual resistivity (electrical resistivity) using the proposed cell as:

$$\rho_{act} = 2\pi\beta\frac{V}{I} \tag{3.4}$$

It should be mentioned that when $L/S = \infty$, it follows that $D/S = \infty$, $\alpha = 0$ (Wenner method condition) and $\beta = 1.0$. A calibration process was conducted to determine the evolution of β as the three dimensionless boundary condition parameters (S/D, L/S, α) deviate from the Wenner method condition.

3.5 Calibration methodology

In general, the calibration process involves testing samples of known properties using the proposed measuring technique to establish a relationship (calibration equation) between the

measured property and the known property value of the tested sample. In other words, the calibration process involves generating an extensive, well-trusted, experimental database for the problem under consideration. Then, while exploiting this database, a strong mathematical expression can be developed between the output of the proposed measuring technique and the known property of the tested samples using a robust statistical data-processing tool. The success of the developed calibration equation is usually assessed by its accuracy in determining the known value of the tested material from the output of the proposed measurement technique and its ability to consider precisely the effect of the changes in boundary conditions.

In this study, generating the calibration database by experimental means is not an easy task (costly and time consuming) since the proposed calibration factor, β, is affected by several parameters (S/D, L/S and α); thus, a different approach should be considered. Instead, the calibration database is generated by conducting an extensive numerical experimental programme as it saves both time and cost. Furthermore, it also eludes the following uncertainties that might affect the outcomes of the investigation if a laboratory experimental approach is used: homogeneity of the tested soil specimens and repeatability of the measurements; and level of saturation of the tested soil specimen.

3.5.1 Numerical Calibration Programme

To develop the required calibration database in this study, 72 numerical experiments were conducted using different combinations of the three dimensionless boundary condition parameters (S/D, L/S and α) to investigate their effect on the calibration parameter, β. Based on the electrodes' configuration in the top cap (as shown in Fig. 3.2), the geometric boundary-condition parameter D/S was set constant at a value of 0.4 corresponding to the experimental set-up. Furthermore, to cover most of the practical cases, the numerical study for the calibration purposes has been limited to the conditions where $0.25 \leq L/S \leq 2$ and $50 \ \Omega \cdot m \leq \rho_{ps} \leq 500000$ $\Omega \cdot m$.

The finite-element solver FlexPDE^{TM} (PDE Solution Inc 2016) was used to solve the following governing equation for the three-dimensional steady state electricity flow in soils:

$$\Gamma_E = L_E \nabla(-\Phi_E) \tag{3.5}$$

where Γ_E, L_E and Φ_E are the electrical current, conductivity of electrical flow, and electrical gradient, respectively. The boundary conditions for the conducted numerical simulation can be described as follows:

- Constant electrical potential is applied at the outer electrodes; and
- No current flow boundary is located at the top of the specimen, at the sides of the testing specimen, and at the bottom porous stone.

The following assumptions were also adopted in this study:

- No voltage losses between the electrodes and the soil (perfect contact condition);
- Ohm's law is applicable; and
- The electrical properties of the considered porous medium (i.e. soil) are isotropic and homogenous.

Fig. 3.3 shows a representative numerical test model representing the case of $L/S = 2$ and $D/S = 0.4$. It has 13695 nodes and 9003 elements. On average, one numerical test would require half an hour to complete.
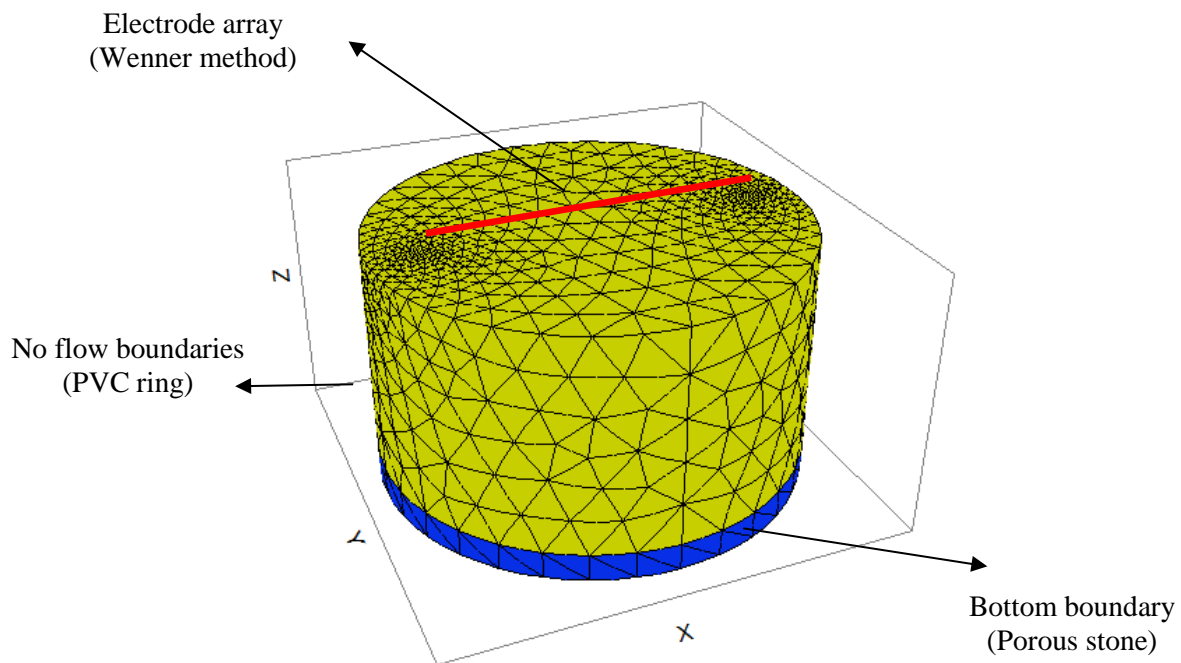
Fig. 3.3 A representative model used in numerical analysis (specimen diameter and height of model are 76 mm 40 mm, respectively)

3.5.2 Numerical calibration results

Fig. 3.4 shows the effect of α and L/S on the calibration factor, β, for $D/S = 0.4$. The results indicated that for different L/S, the calibration factor, β, remains constant for $\alpha > 1$. However, for $\alpha < 1$, the calibration factor, β, increases as α decreases for different L/S values.

As $Th_T > Th_{ps}$ and ρ_{Exp} is a function of ρ_{act} and ρ_{ps}, the condition of $\alpha > 1$ represents the case where $\rho_{act} < \rho_{ps}$. Thus, $\alpha = 1$ would be a threshold value and beyond that, electrical resistance of the bottom porous stone will have an insignificant effect on the current flow configuration; consequently, β remains constant for $\alpha > 1$. On the other hand, in the case of $\alpha \leq 1$, decreasing the electrical resistance of the bottom porous stone will affect the current flow configuration; consequently, β changes for $\alpha \leq 1$. Furthermore, the results shown in Fig. 3.4 illustrate that at constant α, as L/S increases, β increases. Figure 3.5 shows the evolution of β as L/S increases for $D/S = 0.4$ and $\alpha > 1$.
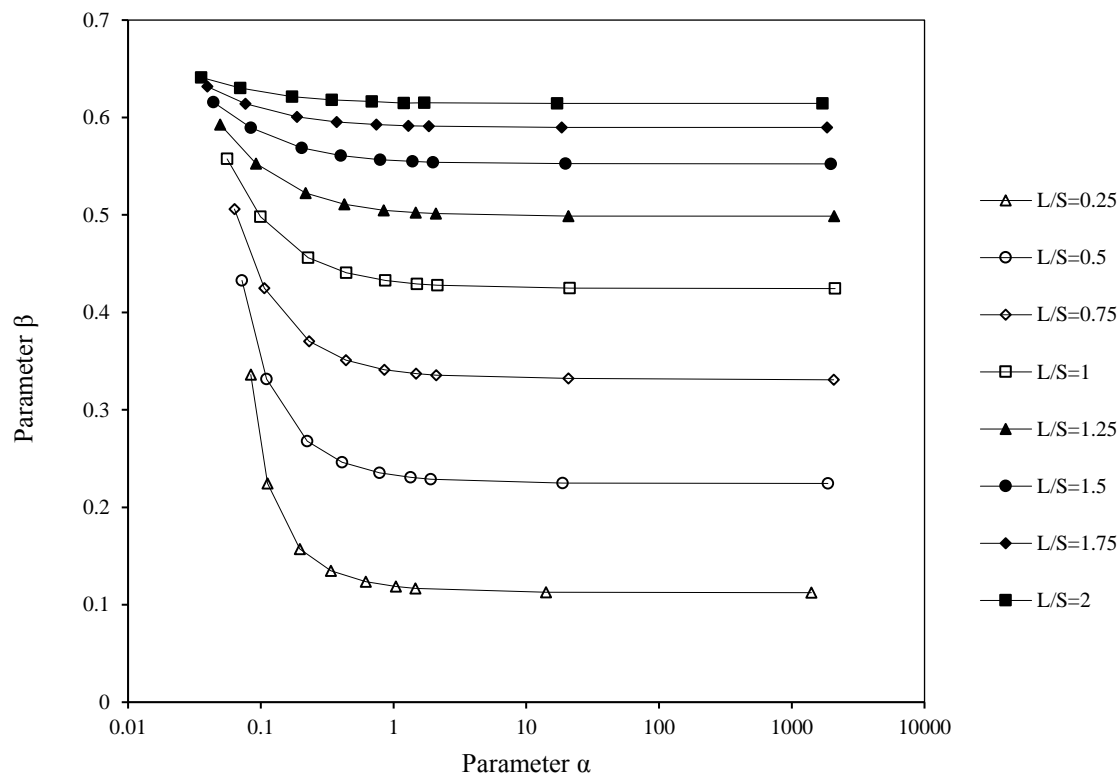
Fig. 3.4 Relationship between α and calibration factor, β ($D/S = 0.4$)
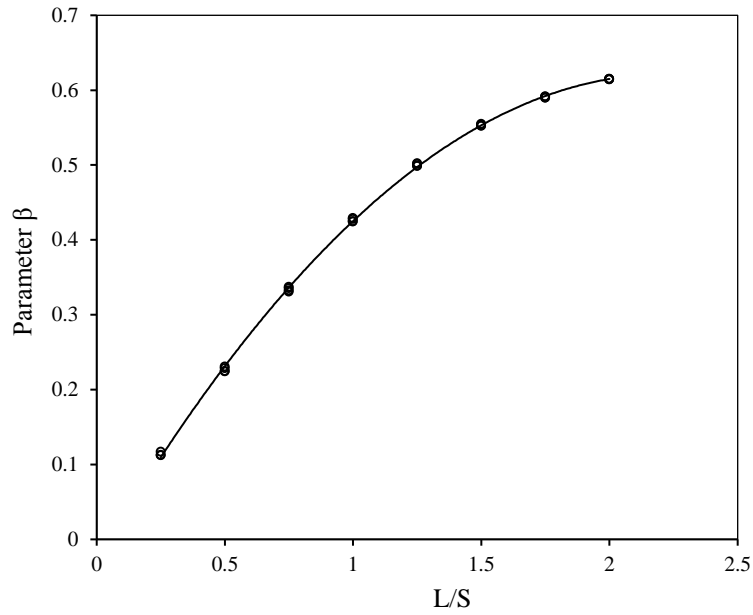
Fig. 3.5 Calibration curve for $\alpha > 1$ ($D/S = 0.4$)

This trend can be explained in terms of the ratio between the thickness of the tested specimen, L, and the effective depth of Wenner method, d_e, which can be defined as the depth below which insignificant current passes through the soil. For the Wenner condition, the ratio $L/d_e = \infty$; therefore, as L increases, L/d_e increases, and the value of β should move closer to Wenner condition ($\beta = 1$). Thus, β will increase as L/S increases.

Using the results shown in Fig. 3.4, a correlation equation using MATLAB$^{\text{TM}}$ (The MathWorks Inc 2015) is developed to predict β as follows.

$$\beta = 0.3885 - 0.128\left(\frac{L}{S}\right)^2 + 0.157\alpha\left(\frac{L}{S}\right) - 0.629\alpha + 0.48\left(\frac{L}{S}\right) + 0.202 \qquad (3.6)$$

The correlation factor for the above equation, R^2, is 0.93. On the other hand, for $\alpha > 1$, the following equation could be obtained:

$$\beta = -0.132\left(\frac{L}{S}\right)^2 + 0.586\left(\frac{L}{S}\right) - 0.029 \qquad (3.7)$$

where $R^2 = 0.999$. Note that as mentioned above, the above equations are valid for the experimental set-up used in the tests, i.e. $D/S = 0.4$ and for the range $0.25 \leq D/S \leq 2$. For cell dimensions different from the one employed here, the proposed calibration approach could be

extended and used to develop suitable calibration equations. However, it is worthy to mention that subsequent numerical analyses showed that within the normal range of D/S (i.e. $0.2 < D/S \leq 1.0$), the values of electrical resistivity are not significantly affected by changes in D/S.

3.5.3 Experimental validation of the numerical results

3.5.3.1 Tested Soil properties

The experimental programme was conducted on New Zealand kaolin clay. This kaolin clay has liquid and plastic limits of 71% and 27% respectively, and can be categorised as inorganic, highly plastic clay. The activity of this clay is 0.44. The geotechnical and chemical properties of this kaolin clay is shown in Table 3.1. In the table, S_a is the specific area while G_s is the specific gravity.

Table 3.1 Characteristics of New Zealand kaolin clay

Geotechnical properties	
Property	**Value**
LL (%)	71
PL (%)	27
PI	44
Sensitivity	0.44
Classification	Inorganic highly plastic clay
Sa (m^2/g)	20
G_s	2.57
Chemical properties	
SiO_2 (%)	57.5
Al_2O_3 (%)	41.8
Fe_2O_3 (%)	0.32
Others (TiO_2, CaO, MgO, K_2O, Na_2O) (%)	0.38
pH of Slurry at 20% Solid (by weight)	4.8-5
Cation Exchange Capacity (meq./100g of clay)	10

In addition, at some stage during the experimental investigations, Mercer river sand was also used to reduce the amount of fine-grained material in the soil and investigate the effect of soil sensitivity on the evolution of electrical resistivity of the soil. Fig. 3.6 shows the particle size distribution of Mercer river sand.
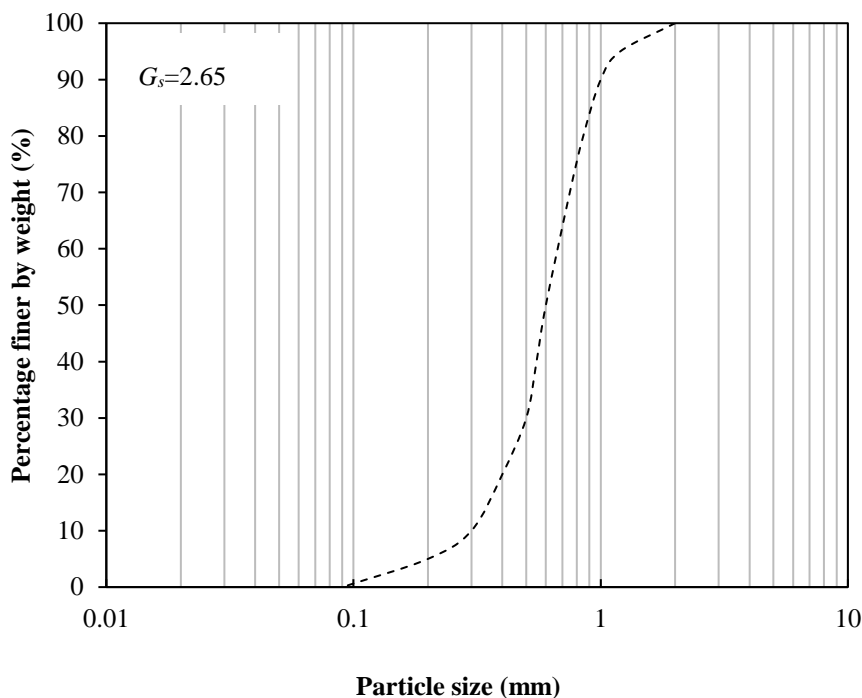
Fig. 3.6 Mercer sand particle size distribution

3.5.3.2 Case of $\alpha > 1$

To check the validity of the proposed numerically generated calibration factor for the case where $\alpha > 1$, a special test setup was designed and fabricated. The test setup involved the use of PVC inner oedometer ring and the modified PVC top cap that included the Wenner four-electrode arrangement. The top cap was attached to the bottom of the oedometer ring as shown in Fig. 3.7 and the top boundary of the oedometer ring was open to air (perfect electrical insulator).

The oedometer ring was filled with deaerated water with varying salinity levels, including distilled water, with 0.1 N NaCl, and with 0.2 N NaCl. The height of liquid in the ring varied between 5 to 19 mm to allow assessing the effect of L/S on β. Tests were conducted at a room

temperature of 20 °C. A total of 21 electrical resistivity experiments were conducted as part of the verification stage. A summary of the conducted tests is given in Table 3.2.
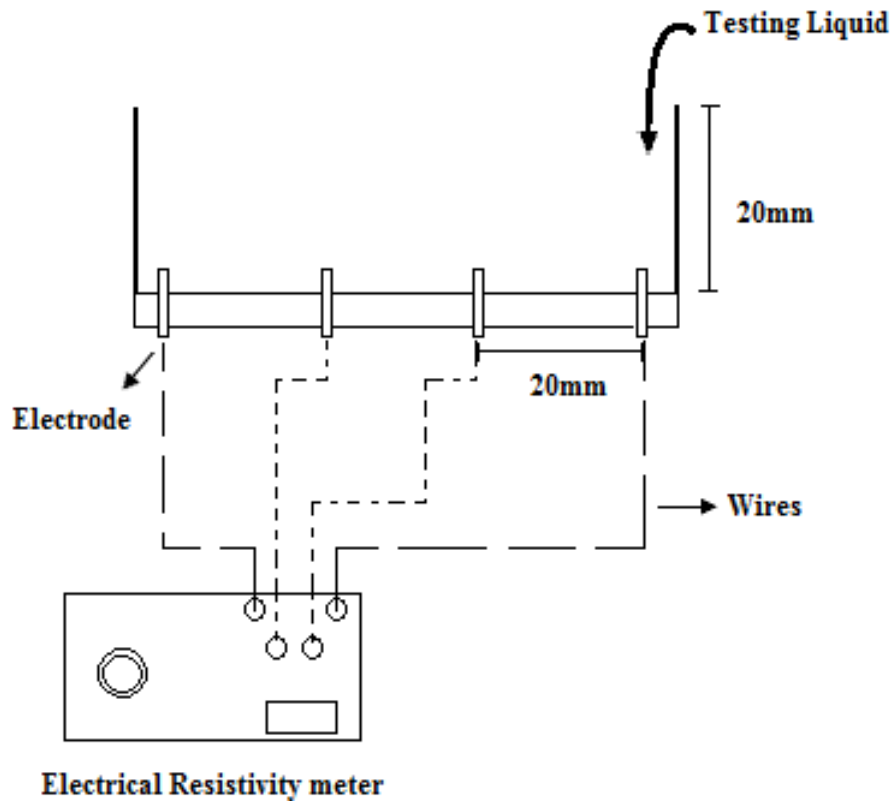
Fig. 3.7 Experimental apparatus for calibrating non-conductive boundaries (D/S=0.4)

In addition, the data from Rinaldi and Cuestas (2002) and ASTM standard D6431-99 (1999) were used for comparison.

As mentioned earlier, the top boundary in the test setup was open to air, which is a perfect electrical insulator; therefore, $\alpha > 1.0$. In addition, the height of the water in the ring was varied between 5 to 19 mm to be able to test various liquid depths. Figure 3.8 shows a comparison between the ρ_{act} - L/S relationships produced in this study (measured experimentally and calibrated numerically) and previous literature (Rinaldi and Cuestas, 2002; ASTM, 1999) for different solutions. As a good agreement can be observed, the validity of the numerical calibration method is confirmed for the case of $\alpha > 1.0$.

Table 3.2 Summary of tests conducted on nonconductive boundary calibration

Test ID	Water Thickness (mm)	Salinity level
1	19	Distilled water
2	17	Distilled water
3	15	Distilled water
4	13	Distilled water
5	11	Distilled water
6	9	Distilled water
7	7	Distilled water
8	19	0.1 M of NaCl
9	17	0.1 M of NaCl
10	15	0.1 M of NaCl
11	13	0.1 M of NaCl
12	11	0.1 M of NaCl
13	9	0.1 M of NaCl
14	7	0.1 M of NaCl
15	19	0.2 M of NaCl
16	17	0.2 M of NaCl
17	15	0.2 M of NaCl
18	13	0.2 M of NaCl
19	11	0.2 M of NaCl
20	9	0.2 M of NaCl
21	7	0.2 M of NaCl
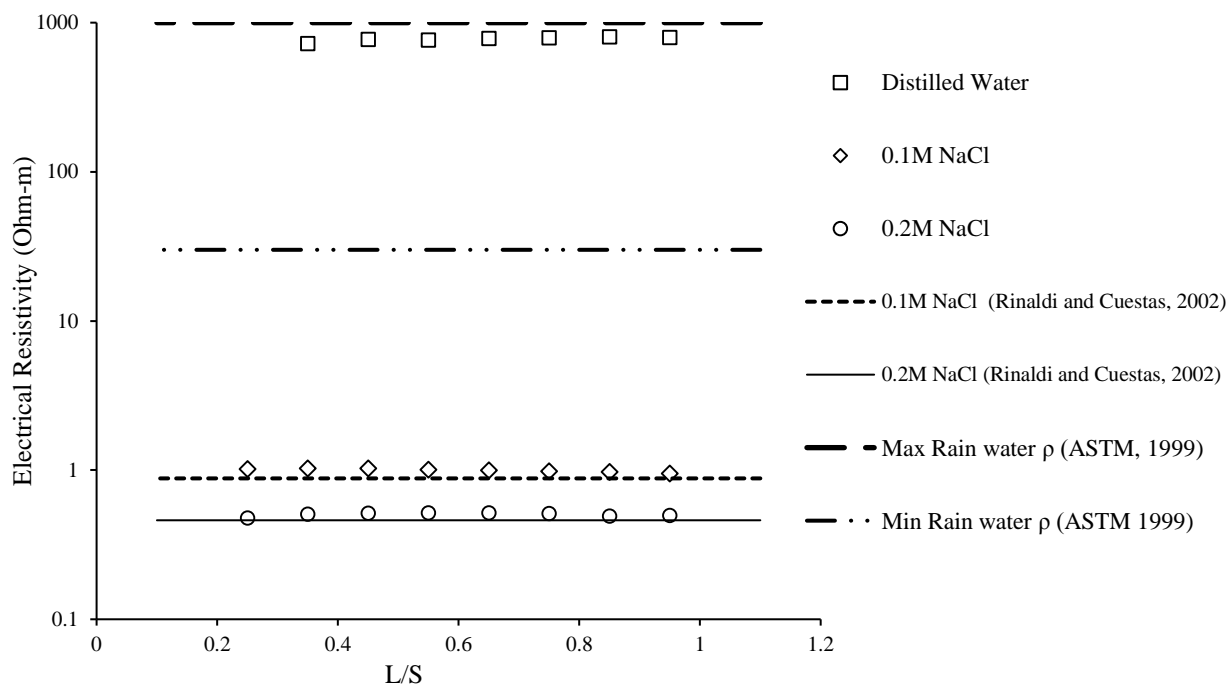
Fig. 3.8 Evaluation of numerical calibration factors for different testing liquids ($\alpha > 1.0$)

Note: Maximum and minimum water electrical resistivity is based on ASTM (1999)

3.5.3.3 Case of $\alpha \leq 1$

To evaluate the calibration factors for $\alpha \leq 1$, the proposed set up shown in Fig. 3.9 was used.
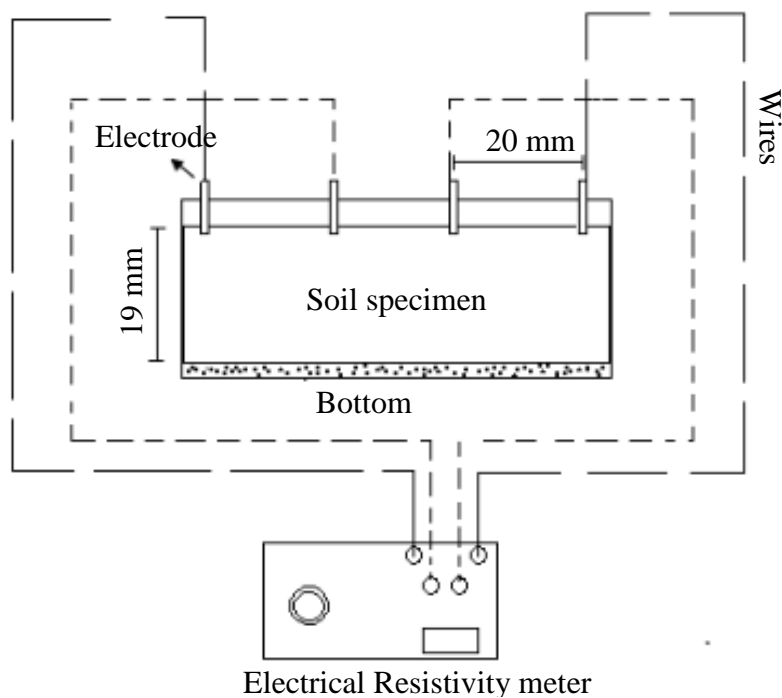
Fig. 3.9 Experimental apparatus for calibrating conductive boundaries (D/S=0.4)

Reconstituted specimens compacted at different moisture contents with different bottom boundary conditions were used as listed in Table 3.3 (i.e. PVC, saturated porous stone).

Table 3.3 Summary of tests conducted on conductive boundary calibration

Test ID	Moisture content	Bottom boundary
1	0.30	PVC
2	0.34	PVC
3	0.37	PVC
4	0.40	PVC
5	0.42	PVC
6	0.51	PVC
7	0.58	PVC
8	0.65	PVC
9	0.30	Porous stone
10	0.34	Porous stone
11	0.37	Porous stone
12	0.40	Porous stone
13	0.42	Porous stone
14	0.51	Porous stone
15	0.58	Porous stone
16	0.65	Porous stone

The electrical resistivity of the saturated porous stone is also determined using the setup shown in Fig. 3.9. The validation process involved using the PVC bottom boundary condition (electrical insulator) to determine the actual electrical resistivity value of the tested soil specimen. In this case, $\alpha > 1.0$ and the calibration equation was already validated in the previous section. Then, the PVC bottom boundary condition was replaced by the saturated

porous stone after which the experimental electrical resistivity of each specimen was measured (using porous stone). Then, the parameter α was calculated for each specimen using Eq. 3.2 considering the experimental electrical resistivity. Figure 3.10 shows the relationship between measured ρ_{Exp} and the corresponding α using porous stone ($\alpha \leq 1$). Then, the calibration factors were calculated using Eq. 3.6. Finally, the calibrated electrical resistivity under this condition using Eq. 3.4 was compared with the actual electrical resistivity value of the tested soil specimen. Figure 3.11 shows the results of the validation process where the calibrated electrical resistivity values using PVC (is denoted by PV) and porous stone (is denoted by PS) are compared at different moisture contents and good agreement can be observed. Therefore, the calibration equation successfully calibrates the experimental results for boundary effects in various conditions.

$$\alpha = 79.18\ (\rho_{EXP})^{-1}$$
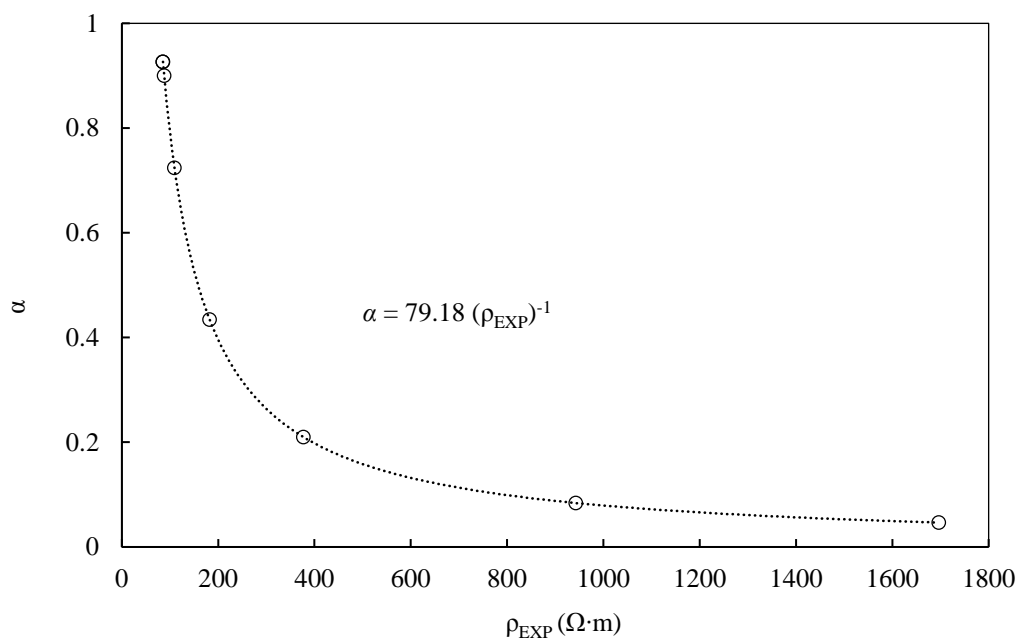
Fig. 3.10 Relationship between geophysical number (α) and measured electrical resistivity for pure New Zealand kaolin clay and porous stone
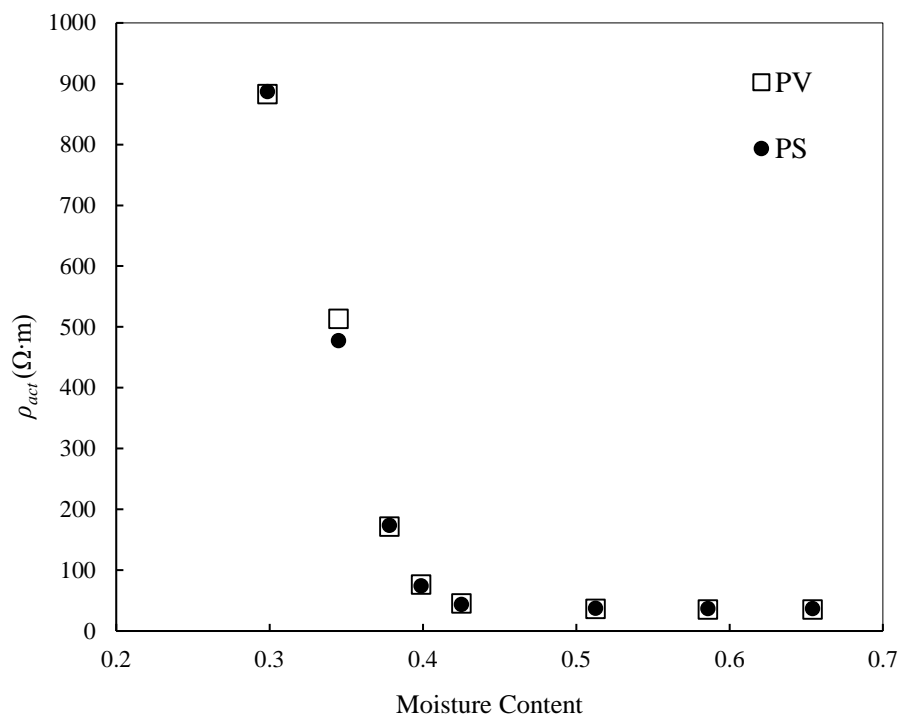
Fig. 3.11 Evaluation of calibration factors for $\alpha \leq 1$

3.6 Calibrated experimental measurements of electrical resistivity

With the proposed robust calibration factors, the modified oedometer can be trusted to measure the electrical resistivity of soils during the consolidation processes. Several series of consolidation experiments were conducted to examine the changes in the electrical resistivity due to changes in effective stress levels.

The changes in electrical resistivity during consolidation were evaluated in specimens M-0-0, M-1-0 and M-2-0 as listed in the Table 3.4. The values obtained are plotted versus the soil's volumetric water content (θ) in Fig. 3.12. The results show an exponential trend consistent with the modified Archie's law that has been developed for clays (Archie, 1942; Atkins and Smith, 1961; Salem and Chilingarian, 1999; Shah and Singh, 2005). Soil electrical resistivity depends on the water content, electrical resistivity of water, and surface conductivity of bulk soil (Rhoades et al., 1989; Olsen et al., 1999; Bolt, 1979; Mojid et al., 2007; Kibria and Hossain, 2012; Long et al., 2012). In this experimental programme, the electrical resistivity of water was

maintained constant during the consolidation tests and, as a result, the electrical resistivity deviation can be attributed only to the water content and surface conductivity.

Table 3.4 Summary of conducted electrical resistivity tests on New Zealand kaolin clay

Test ID	Kaolin Content (%)	Sand Content (%)
M-0-0	100	0
M-1-0	90	10
M-2-0	80	20
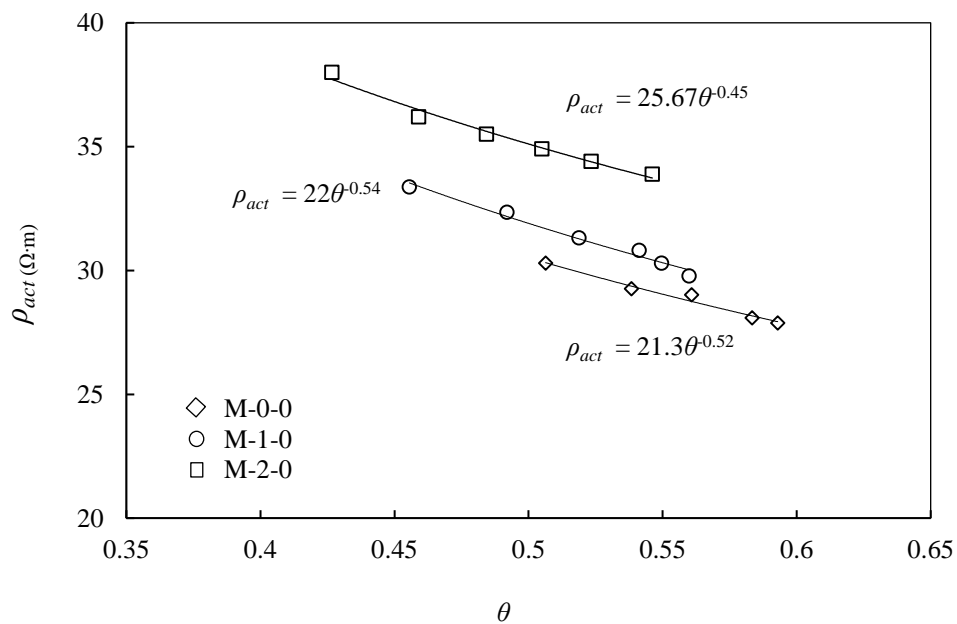
Fig. 3.12 Electrical resistivity of various kaolin samples

As the volumetric water content decreases during the consolidation process, the water content drops, and consequently the electrical resistivity increases. For instance, a reduction of ~10% in the volumetric water content of pure kaolin clay causes ~20% increase in electrical resistivity. In addition, negative charges on the clay surfaces attract the cations from the soil water and form a high concentration of electrically unbalanced layer of counter ions called diffuse double layer (DDL) close to the clay surfaces (Sheriff, 1973; Bolt, 1979; Mojid and

Cho, 2006; Mojid et al., 2007; Bergaya and Lagaly, 2013). The existence of the diffuse double layer around clay structures causes surface conduction. Further discussion about DDL is presented in Section 4.5. By adding sand to pure kaolin clay, the amount of surface charges per unit volume of soil as well as the number of ions and the volume of water in the diffuse double layer within that specified volume will decrease. Consequently, the surface conductivity decreases and the bulk soil electrical resistivity increases, as shown in Fig. 3.12 for the two mixtures. A thorough investigation on the collective effects of these parameters is presented in the next chapter. As these experiments were conducted in a saturated state in the oedometer cell and fully calibrated by well-verified calibration factors, the measured values of the electrical resistivity can be used directly to predict the EO consolidation efficiency. Therefore, the amount of power consumption can be accurately predicted during the electro-osmosis consolidation process to efficiently design the electro-osmosis improvement programme. In addition, the electrical resistivity results, which varies with volumetric water content (and consequently with time), is directly implemented in a numerical model to estimate the electric potential difference in the soil body during EO consolidation in Chapter 6.

3.7 Summary

A modified electro-oedometer was developed using the configuration of the Wenner four-electrode field testing method to measure the change in electrical resistivity of soil as the effective stress changes. A coupled numerical-experimental calibration approach was proposed in this study to account for the effect of the deviation of the proposed cell boundary conditions from the Wenner methods. Three dimensionless calibration parameters were used to describe the cell boundary conditions. Two of these parameters described the relation between the size of the specimen and the configuration of the electrodes (S/D and L/S), whereas the third parameter expressed the relative thickness and electrical resistance of the bottom porous stone compared to the test specimen (α). For $\alpha > 1.0$, the boundary calibration factor (β) solely depends on the L/S; however, for $\alpha \leq 1$ the parameter β was influenced by the values of L/S and α. Therefore, two zones were identified to take the boundary effects into the account. A calibration equation was introduced and validated for each zone. Moreover, the calibration equations were applied to the modified oedometer cell which was utilised in this study. Note that for cell dimensions different from the ones used here, the proposed calibration approach in this study could be extended and used to develop suitable calibration equations.

4 ELECTRICAL RESISTIVITY OF FINE-GRAINED SOILS DURING CONSOLIDATION: NUMERICAL APPROACH

4.1 Introduction

The electrical resistivity of soil has been measured based on standardised, calibrated apparatus as discussed in Chapter 2. Apart from the experimental measurements, the electrical resistivity of soil can be estimated using electrical resistivity models. In that case, the model can be used to estimate the electrical resistivity of soil and then it can be implemented into the EO model to predict its EHM behaviour. The previously developed electrical resistivity models did not consider all available paths for current transmission and the majority of them neglected the surface conductivity of solid particles. Herein, a conceptual-numerical electrical resistivity model was developed considering the surface conductivity of particles. Then, the numerical model was validated using the experimental results. The experimental electrical resistivity results utilised for validation were obtained using the apparatus developed and calibrated in Chapter 3. The results from this numerical model can be directly incorporated into the EO model developed in Chapter 6 to estimate the EHM behaviour of the soil. In addition, the results will be used to estimate the efficiency of EO consolidation in Chapter 8.

4.2 Existing electrical resistivity models

Several studies have shown that the electrical resistivity of soils is a function of a number of soil properties, including soil mineralogy, particle size distribution, volumetric water content,

pore size distribution, connectivity, degree of water saturation, pore water salinity, electrical resistivity of the fluid and temperature (Kalinski and Kelly, 1993, 1994; Abu-Hassanein et al., 1996; McCarter and Desmazes, 1997; Revil et al., 1998; Samouelian et al., 2005; Ekwue and Bartholomew, 2011; Kim et al, 2011; Long et al., 2012; Oh et al., 2014). In real cases, these factors change from site to site and experimental measurement of electrical resistivity requires consideration of these factors. However, extensive experimental measurement of electrical resistivity is not always economically practical and is time consuming. Therefore, electrical resistivity models were developed to address this issue. Several electrical resistivity models available in the literature link the soil's volumetric water content and moisture content with its electrical resistivity, as listed in Table 4.1.

Electrical resistivity models are developed mainly based on the current passages available in soil body. Archie (1942) proposed a widely accepted model for predicting the electrical resistivity of sandy soils by assuming that the electrical current passes only through the pore water. Thus, the Archie's model was expressed based on the porosity and electrical resistivity of the soil solution as:

$$\rho = \rho_w \theta^{-m} \tag{4.1}$$

where ρ and ρ_w are the soil and pore water electrical resistivity, respectively, θ is the volumetric water content and m denotes the cementation factor. This model was able to estimate the average electrical resistivity values of sands in the range of 1.67 to 3.33 $\Omega \cdot m$ (Mitchell and Soga, 2005). However, since the effect of surface charge on soil electrical resistivity was neglected, Archie's model failed to efficiently predict the electrical resistivity of fine-grained soils.

Several researchers attempted to fit this model to fine-grained soils and proposed a modified Archie's model (Atkins and Smith, 1961; Salem and Chilingarian, 1999) as:

$$\rho = a\rho_w \theta^{-m} \tag{4.2}$$

where a is a fitting parameter. The modified Archie's model can be used as a generic model to predict the electrical resistivity of wide range of soil types. However, as it was not established based on a robust theoretical background, the modified Archie's model is case-dependent and requires a large volume of experimental tests for parameter identification. To overcome this limitation, Waxman and Smith (1968) added another pathway to the Archie's model. Pore

water and solid surfaces were assumed as two parallel conduction paths for electric current through the soil medium, as shown in Table 4.1, and the following relationship was introduced:

$$\rho_T = C(\rho_w + \rho_s) \tag{4.3}$$

where ρ_T, ρ_w and ρ_S are the electrical resistivity of the total soil, water and solid particles, respectively, and C denotes a fitting parameter which should be determined experimentally for every type of soil. In line with the model of Waxman and Smith (1968), Rhoades et al. (1976) incorporated the volumetric water content, θ, in their model and proposed the following relationship:

$$\sigma_T = \sigma_w (d\theta^2 + e\theta) + \sigma_s \tag{4.4a}$$

$$\rho = \frac{1}{\sigma_T} \tag{4.4b}$$

where σ_T, σ_w and σ_s denote the electrical conductivity of the bulk soil, water and solid particles, respectively, while d and e are fitting parameters. The model was able to predict the lower range of electrical resistivity, but it predicted negative values of solid particle's conductivity for special types of clays (Shah and Singh, 2005). Therefore, Rhoades et al. (1989) added a series pathway for electric flow through the mixture of soil solids and pore water as shown in Table 4.1. Thus, the soil conductivity, σ_T, was expressed as follows:
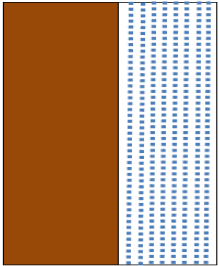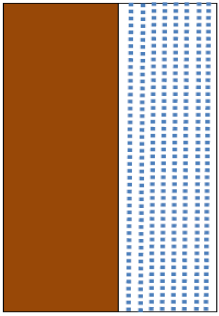
$$\sigma_T = \frac{a\sigma_w\sigma_s}{(1-e)\sigma_w + e\sigma_e} + b\sigma_s + c\sigma_w \tag{4.5a}$$
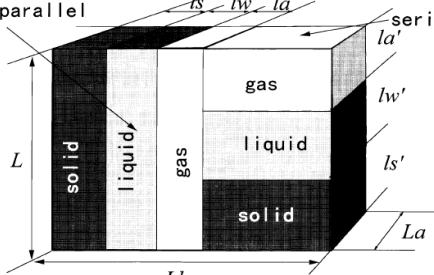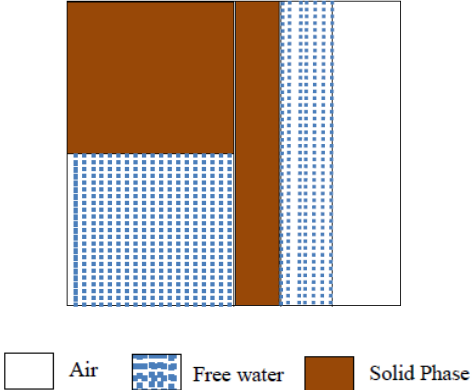
$$\rho = \frac{1}{\sigma_T} \tag{4.5b}$$
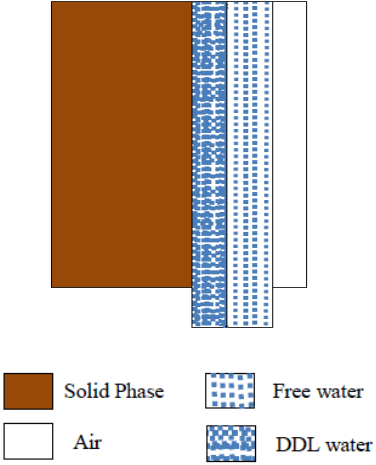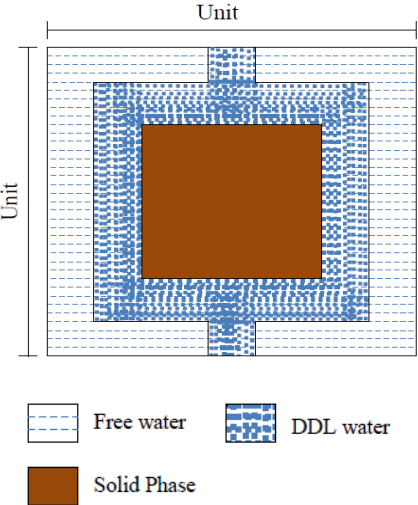
where a, b, c and e are fitting parameters. This model provides a reasonable prediction over the full range of electrical resistivity data (Mitchell and Soga, 2005). However, the determination of the fitting parameters associated with this model requires an extensive experimental database making it difficult to apply in practice.

To reduce the amount of experimental effort, Mualem and Friedman (1991) and Fukue et al. (1999) proposed different relationships based on assumptions similar to that adopted in the Rhoades et al. (1989) model. Although these models need less experimental effort to determine the fitting parameters, the effect of soil mineralogy was neglected.

Table 4.1 Electrical resistivity models

Models	Equation	Model representation	Fitting parameters	Parameter Identification
Modified Archie (1942)	$r = a r_w q^{-m}$	No physical representation	a, m	Curve fitting
Waxman and Smith (1968)	$\rho_T = C(\rho_w + \rho_s)$	Free water — Solid Phase	C	Curve fitting
Rhoades et al. (1976)	$\sigma_T = \sigma_w(d\theta^2 + e\theta) + \sigma_s$ $\rho = \dfrac{1}{\sigma_T}$	Free water — Solid Phase	d, e	Curve fitting

Mualem and Freedman (1991)	$$\sigma_T = \sigma_w F(\lambda) \frac{\theta^{n+2}}{\theta_{sat}}$$ $$F(\lambda) = \frac{1 + \frac{2}{\lambda}}{(1 + \frac{1}{\lambda})^2}$$ $$\rho = \frac{1}{\sigma_T}$$	No physical representation	n, λ, θ_{sat}	Curve fitting/experimental relationships
Fukue et al. (1999)	$$\sigma_T = \frac{\pi r}{\omega G_s (1-n)} \frac{\sigma_w}{(1-F)}$$ $$\rho = \frac{1}{\sigma_T}$$		F	Curve fitting
Rhoades et al. (1989); Mitchell and Soga (2005)	$$\sigma_T = \frac{a\sigma_w \sigma_s}{(1-e)\sigma_w + e\sigma_s} + b\sigma_s + c\sigma_w$$ $$\rho = \frac{1}{\sigma_T}$$	Air Free water Solid Phase	a, b, c	Curve fitting

Mojid et al. 2007	$\sigma_T = T\left[(\theta - \theta_{ddl})\sigma_w + \theta_{ddl}\sigma_{ddl}\right]$ $\rho = \dfrac{1}{\sigma_T}$	 ■ Solid Phase ▦ Free water ☐ Air ▩ DDL water	T, σ_{DDL}	Curve fitting
Proposed model	$I = \int \sigma(\dfrac{dV}{dy})A$ $\rho = \dfrac{VA}{IL}$	 ▦ Free water ▦ DDL water ■ Solid Phase	σ_{DDL}	Finite element model

Note that soil mineralogy controls the amount of attraction applied from the soil surface to the pore solution and the level of attraction affects the electrical behaviour of the pore solution and, consequently, the electrical resistivity of the bulk soil. To address this issue, Mojid et al. (2007) proposed a model considering different pore solution behaviours as follows:

$$\sigma_T = T[\sigma_w(\theta - \theta_{DDL}) + \theta_{DDL}\sigma_{DDL}] \tag{4.6a}$$

$$\rho = \frac{1}{\sigma_T} \tag{4.6b}$$

where T, θ_{DDL} and σ_{DDL} denote the transmission coefficient, volumetric water content of diffused double layer (DDL) and electrical conductivity of DDL, respectively. Although various water forms are incorporated in the model by Mojid et al. (2007), all the possible current pathways are not considered since only parallel conduction paths are taken into account. Therefore, there is still a need for a comprehensive model to accurately take the surface conduction of fine-grained soil into account.

4.3 Proposed Model

4.3.1 Theoretical Background

4.3.1.1 Diffuse Double Layer (DDL)

The electrical resistivity of bulk soil and the behaviour of pore solution highly depend on soil mineralogy. The effect of mineralogy on bulk electrical resistivity of soils is insignificant in sandy soils, but complexities arise in the prediction of electrical resistivity in clays due to the presence of surface charges. The clay particle surface is negatively charged and to maintain the electrical charge neutrality, the particle attracts positive ions from the pore solution. Stern (1924) assumed two different regions for the combination of anions and cations close to the clay particle surface. The inner region comprises fixed and highly packed cations attached to the particle surface and strongly attracted by clay minerals, named as the Stern layer. The thickness of this region is in the order of 0.5 nm for clay systems (Mitchell and Soga, 2005). The outer layer includes the combination of cations and anions called Diffuse Double layer (DDL). Counter ions in this region are under the influence of clay surfaces and are maintained in place by inter-particle forces. Far enough from the clay surfaces where the attraction of the

surfaces diminishes, the pore solution is electrically neutral and is named as free water. The different regions adjacent to the soil surfaces are illustrated in Fig. 4.1.
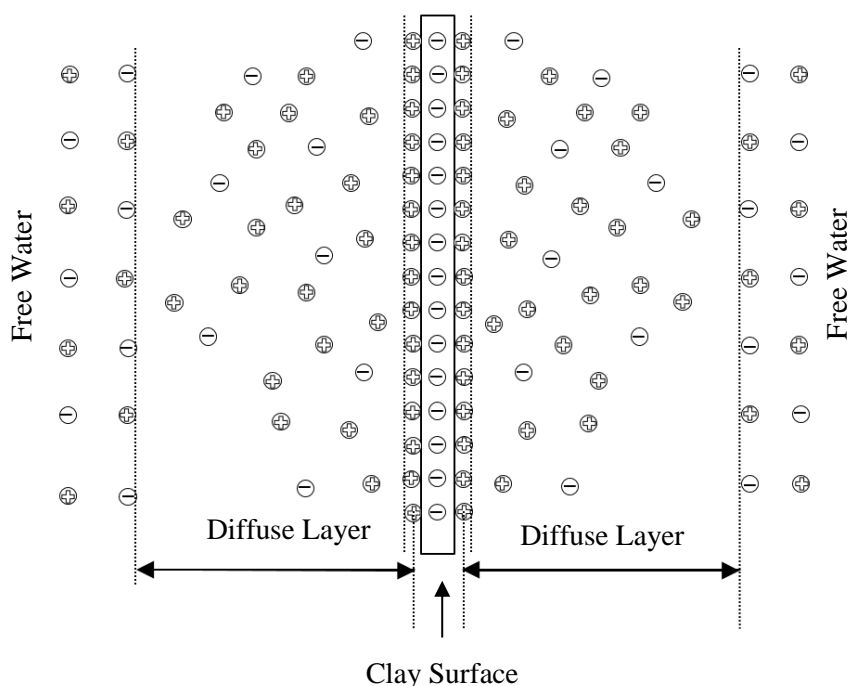
Fig. 4.1 Different electrical layers close to the clay surface (after Stern, 1924)

Based on experimental investigations, the electrical resistivity of the DDL is less than that of the free water in fine-grained soils (Mojid et al., 2007). More importantly, that difference in electrical resistivity of water considerably changes the magnitude of electrical resistivity of the bulk soil. Therefore, to achieve better prediction of electrical resistivity of fine-grained soils, the properties of the DDL layer (volume and electrical resistivity) should be incorporated in the model formulation.

4.3.1.2 Thickness of DDL

The volume of water in the DDL can be calculated from the product of the DDL thickness, η, and the surface area of the clay. The term η depends on the strength of attraction between counter ions in the clay system whereas the surface area is governed by the amount of clay content in the bulk soil.

Schofield (1947) developed and successfully tested a general relationship to estimate η.

$$\eta = \frac{q}{\sqrt{v\beta n}} - \frac{4}{v\beta\omega} \tag{4.7}$$

where q is a factor that depends on the valence, v, of the cation, β is the DDL constant, n is the normality of pore solution and ω is the adsorption of repelled ions per unit area. The second term on the right-hand side of this relationship is much smaller than the first term and it can be ignored in DDL thickness calculations (Mojid et al., 2007).

Following Schofield's theory, Theng (2012) proposed an equation for predicting η based on Boltzman's equation which describes the ion concentration near the clay/solution interface as an exponential function. Based on ion concentration, the charge density and, consequently, the extension of hydrated ions into the clay system can be calculated. That extension of hydrated ions is a measure of DDL thickness and is called Deby length ($1/k$) and is expressed as follows:

$$\frac{1}{k} = \frac{0.3}{\sqrt{I}} \tag{4.8}$$

$$I = \sum nZ^2 \tag{4.9}$$

where n is the pore solution concentration, Z is the ion valency, and I is the ionic strength.

4.3.1.3 Electrical behaviour of DDL

The electrical behaviour of the DDL is mainly controlled by the influence of ion mobility which depends on the pore solution salinity level and the clay surface density of electrical charges. The amount of surface density of negative electrical charges is proportional to the amount of isomorphous substitutions and the type of clay. In this case, kaolin and montmorillonite clays have the highest and lowest order, respectively, of surface density of charges among various types of clays. Also, the pore water solution provides the system with the positive charges. More positive charges in pore solution indicate stronger attraction between the soil surfaces and the pore water and, as a result, lower ion mobility. The ions in the free water are completely mobile. Closer to the surface, within the DDL, ions are attracted to the surface negative charges; thus, the mobility of the ions is reduced in this region. The closest cations to the surface are held firmly by the negative charges and are immobile (Bolt,

1979; Mitchell and Soga, 2005). Bolt (1979) postulated that by increasing the concentration of ions in the pore solution, the electrical resistivity of DDL becomes proportional to the free water electrical resistivity, ρ_{FW}, with the coefficient of proportionality defined as K:

$$\rho_{FW} = K \rho_{DDL} \tag{4.7}$$

Therefore, the parameter K should be a complex parameter covering all contributing factors, such as geometry, ion mobility and ion concentration.

4.3.2 Physical representation of the proposed model

In a typical clay system, current could pass through three routes as follows (Fig. 4.2 a): (1) continuously conductive paths that could be formed by the diffused double layer (DDL) water and the clay particles that are in close contact; (2) free water between soil particles; and (3) DDL and free water in series with each other. To model these three routes considering the existence of the solid particles (non-conductive medium), a unit soil element is assumed where the solid particles are represented as a square concentrated at the centre of the unit block of soil as shown in Fig. 4.2 (b).

The DDL water is represented as a uniform layer that covers the central block of solid particles, but it also extends to the sides of the soil element, as shown in Fig. 4.2 (b), to consider the possible electrical current flow route through the DDL (Route No. 1). As the soil is fully saturated, free water fills the remaining space of the element. The representative unit soil is assumed to have electrical behaviour that can be modelled in 2D.
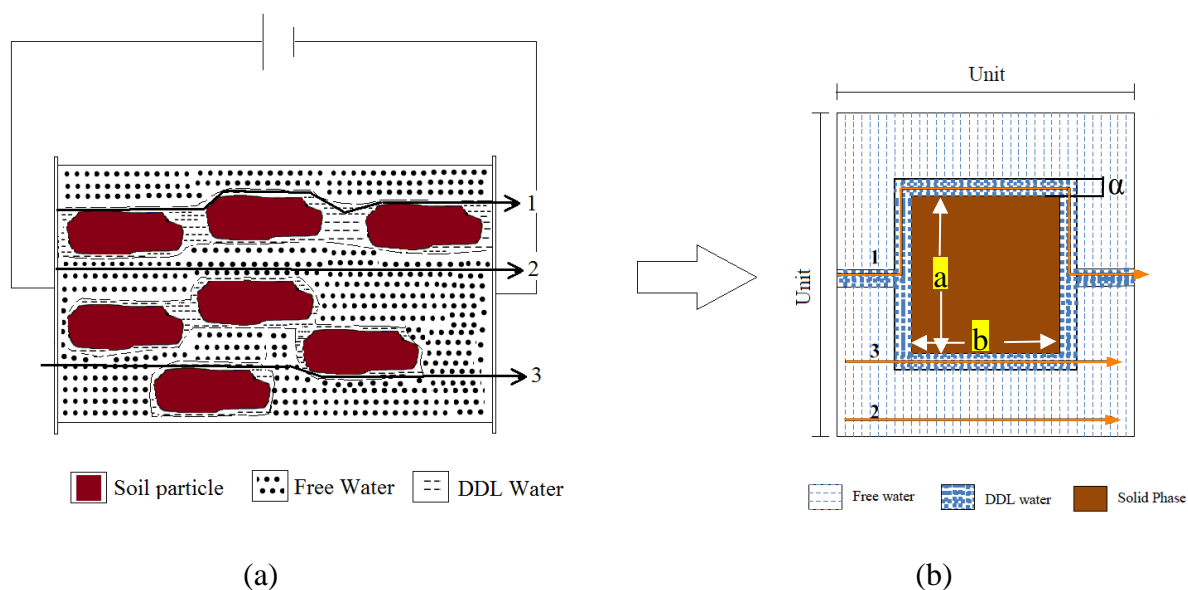
Fig. 4.2 (a) Physical representation of the electrical current passage through the soil medium; (b) Physical interpretation of the proposed electrical resistivity model

The thickness of the DDL water around the solid particles is expressed as α. The terms a and b in Fig. 4.2 (b) are the dimensions of the solid particle block at the middle of the unit soil. In this study, the soil is considered as fully saturated and isotropic material. Therefore, it is assumed that $a=b$. However, it should also be mentioned that $a \neq b$ case could be used to model anisotropic soil condition in terms of electrical resistivity behaviour.

The following quadratic equation which is proposed based on model geometry, can be used to determine α where θ_{DDL} is the DDL volumetric water content:

$$2\alpha^2 + [2b + a + 1]\alpha - \theta_{DDL} = 0 \qquad (4.8)$$

$$\theta_{DDL} = S\eta = \frac{qS}{\sqrt{v\beta n}} \qquad (4.9)$$

$$S = S_a \gamma \qquad (4.10)$$

where q is a parameter that depends on valency, η is the thickness of the DDL, β is the DDL constant, v is the valence of cation, n is the concentration of the bulk solution, S is the surface area of soil per unit volume, S_a is the specific surface area of clay (m²/kg) and γ denotes the dry density of the soil (kg/m³).

4.4 Numerical simulation

The parameters that could affect the electrical resistivity of saturated soils, in addition to its volumetric water content, were expressed in terms of two dimensionless numbers: F and K, as follows:

$$F = \frac{\theta_{DDL}}{\theta_{FW}} \qquad (\theta_{FW} \neq 0) \qquad (4.14a)$$

$$K = \frac{\rho_{FW}}{\rho_{DDL}} \qquad (4.14b)$$

where θ_{FW} is the volumetric water content of the free water and can be determined as follows:

$$\theta_{FW} = \theta - \theta_{DDL} \qquad (4.15)$$

In addition, to generalise the electrical resistivity measurements, a parameter R was defined as follows, where ρ_s and ρ_{FW} are the electrical resistivity of bulk soil, and free water, respectively:

$$R = \frac{\rho_s}{\rho_{FW}} \qquad (4.16)$$

The parameter F shows the level of attraction of the solid phase on the pore water and how the water phases are formed in terms of the quantity (volume) of DDL water and free water. On the other hand, the parameter K represents the effect of surface charges on the electrical behaviour of the DDL in relation to the free water. Finally, the parameter R shows the computed electrical resistivity of the soil in relation to the electrical resistivity of the free water. As the parameters F, K and R are dimensionless, they can be generalised for any type of fine-grained soil. These parameters are discussed further in following sections.

FlexPDE software was used to solve the governing equations of the electrical flow through the proposed representative soil unit (Fig. 4.2 b) at different values of θ, K, and F. The numerical results were used to calculate the bulk soil electrical resistivity. Fig. 4.3 shows an example of mesh used and the results obtained when current passed through the unit specimen.

Based on the coupled flow theory, the electric current flow in the soil under the influence of electrical gradient and in the absence of any other types of gradient, is called Ohm's rule:

$$J_E = -\sigma(\nabla V) \qquad (4.17)$$

where J_E is the electrical current density caused by the electric potential, σ is the electrical conductivity and V is the electrical gradient. By applying the continuity of the current to the Ohm's rule, the main governing equation can be obtained:

$$\nabla J_E = \nabla(-\sigma.\nabla V) = 0 \tag{4.18}$$

By solving Eq. 4.18 over the representative unit soil, the distribution of electric gradient can be measured over the specimen and, consequently, the current can be computed as:

$$I = -\sigma(\frac{\partial V}{\partial x})A \tag{4.19}$$

and the soil electrical resistivity, ρ, can be determined as follows:

$$\rho = \frac{VA}{IL} \tag{4.20}$$

where A is the cross-section area of soil sample, I is the current passing through the soil specimen and L is the height of the specimen.

As mentioned, FlexPDE software was used to solve the above equations. An example of a unit soil in the numerical model is shown in Fig. 4.3 for the case of $\theta=0.5$, $\theta_{DDL}=0.12$ and $K=1.2$.

.
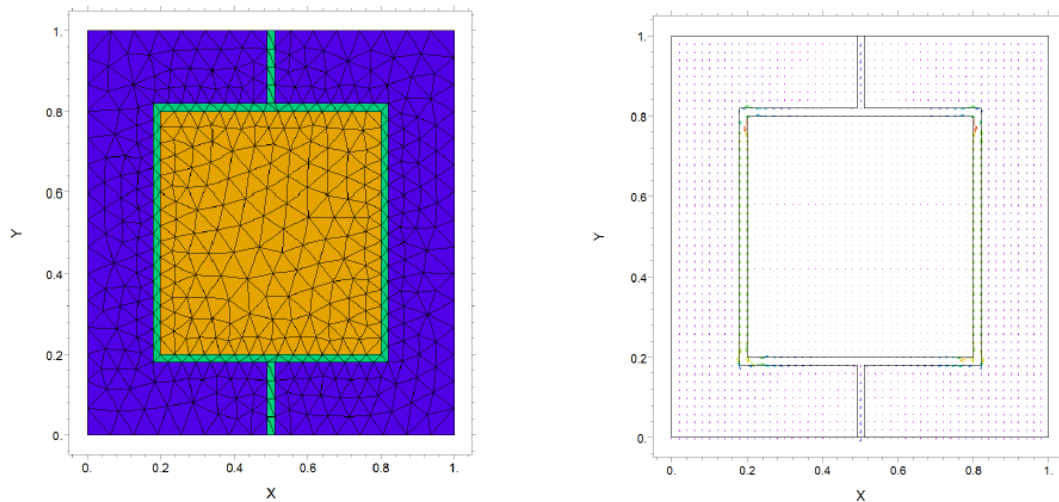
(a) Example of mesh in numerical model   (b) Example of flow through the soil

Fig. 4.3 Model representation of electrical current passage through the unit soil medium
$\theta=0.5$, $\theta_{DDL}=0.12$, $K=1.2$

Using the above-mentioned model, a numerical database was developed to propose a generic model for the prediction of electrical resistivity of fine-grained soils. To achieve that, numerical tests were carried out using various values of θ, F and K. In addition, to develop the database, some limitations were imposed on these parameters. According to Das (2013), the volumetric water content of soil in saturated, natural state varies from 0.23 to 0.76, corresponding to Glacial till and soft organic clay, respectively. The typical values of volumetric water content (fully saturated) in natural state, for fine-grained soils are listed in Table 4.2. Therefore, the range of θ chosen for numerical modelling was between 0.2 to 0.8 to cover all possible cases (i.e. $\theta = 0.2, 0.3, 0.4, 0.5, 0.6, 0.7$ and 0.8). Thus, the proposed database is valid for $0.2 \leq \theta \leq 0.8$.

In the case of the parameter K, which represents the effect of surface charges on pore water electrical resistivity, values of 1.11 to 1.39 were reported by Mojid et al. (2007) for sandy clay and clay loam, respectively. K values for numerical modelling were chosen to cover all types of fine-grained soils plus higher values to define some trends (i.e. $K = 1, 1.1, 1.2, 1.4, 1.6, 2, 4, 6, 10$) and therefore, the generated database covers $1 \leq K \leq 10$. The measurement of parameter K requires a single test for each soil type which will be discussed in the validation section.

Table 4.2 Typical values of volumetric water content in various soil types (Das, 2013)

Type of soil	Volumetric water content in natural state [*]
Stiff clay	0.375
Soft clay	0.47-0.58
Loess	0.47
Soft organic clay	0.71-0.76
Glacial till	0.23

*Fully saturated

On the other hand, the parameter F varies in a wider range. Theoretically, F varies between 0 to ∞, with $F = 0$ occurring when $\theta_{DDL} = 0$; in other words, no attraction is applied by solid particles to the pore water. In addition, $F = \infty$ happens when $\theta_{FW} = 0$. Extensive initial numerical modelling was carried out to identify a viable range of F for the numerical database. As shown

in Fig. 4.2, the DDL water covers the concentrated solid. For a constant θ, as the attraction of solid particles on pore water (DDL and free water) decreases, the K value decreases whereas the thickness of the DDL water (α) increases. The increase in α continues until all pore water becomes DDL water. Fig. 4.4 shows a comparison of soil units with various θ_{DDL} and θ_{FW} and constant $\theta = 0.5$. Fig. 4.4 (a) shows $\theta_{DDL} = 0.1$ (typical in natural clays) and $\theta_{FW} = 0.4$. In Fig. 4.4 (b) θ_{DDL} was increased to 0.25 and in Fig. 4.4 (c) θ_{DDL} was increased further to the maximum threshold of 0.455. Above this maximum threshold of θ_{DDL} which will be denoted by $\theta_{DDL,T}$, the soil boundaries remain constant (whole water will be DDL water) and therefore, the electrical resistivity remains constant for a specific K. The numerical results (R) for various θ and K are presented in Fig. 4.5 (a) to Fig. 4.5 (f). For a specific θ, the electrical resistivity of soil depends on the value of F and K. However, the electrical resistivity shows constant behaviour for $F > F_T$, where F_T is the value of F corresponding to $\theta_{DDL,T}$. For example, when $\theta = 0.5$, $\theta_{DDL,T} = 0.455$ as shown in Fig. 4.4 (c). It implies that from $F_T = 0.455 / (0.5-0.455) = 10.1$, the electrical resistivity of soil remains constant for a specific K (Fig. 4.5 f). This fact can be observed for different values of θ, as shown in Fig. 4.5 (a) to Fig. 4.5 (f) with various values of $\theta_{DDL,T}$.
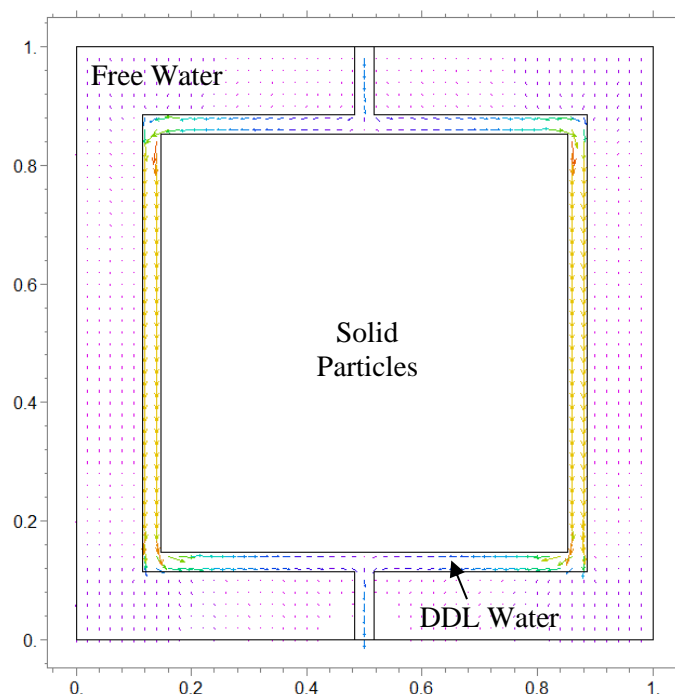
(a) $\theta = 0.5$, $\theta_{DDL} = 0.1$, $\theta_{FW} = 0.4$

Fig 4.4 Electric flow developed in the unit soil for various states
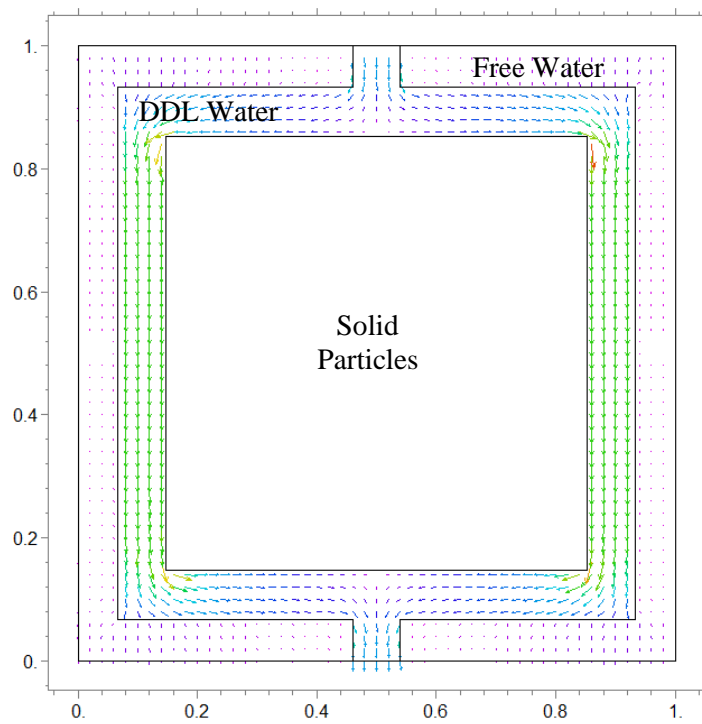
(b) $\theta = 0.5$, $\theta_{DDL} = 0.25$, $\theta_{FW} = 0.25$
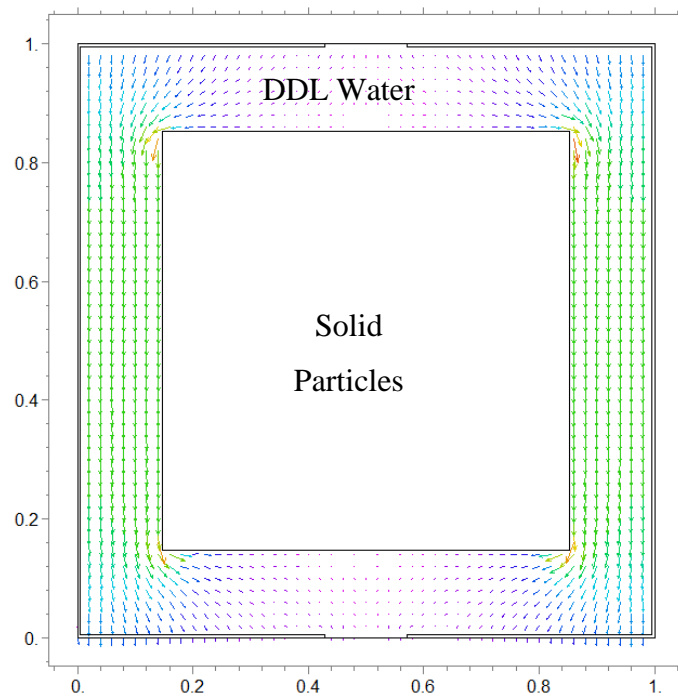
(c) $\theta = 0.5$, $\theta_{DDL} = 0.455$, $\theta_{FW} = 0.045$

Fig. 4.4 Electric flow developed in the unit soil for various states (Cont'd)
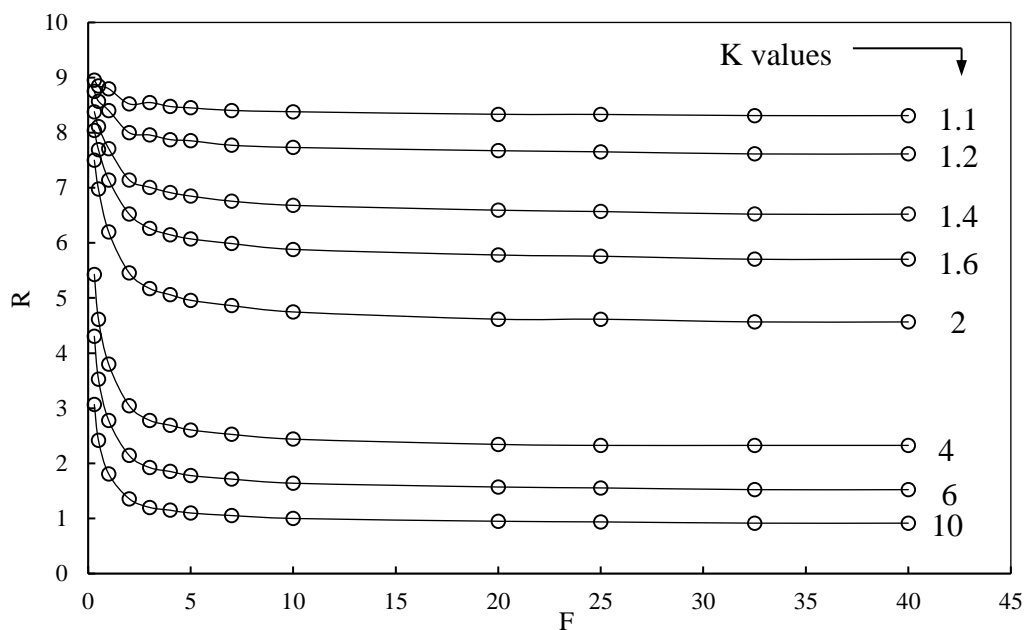
(a) $\theta = 0.2$
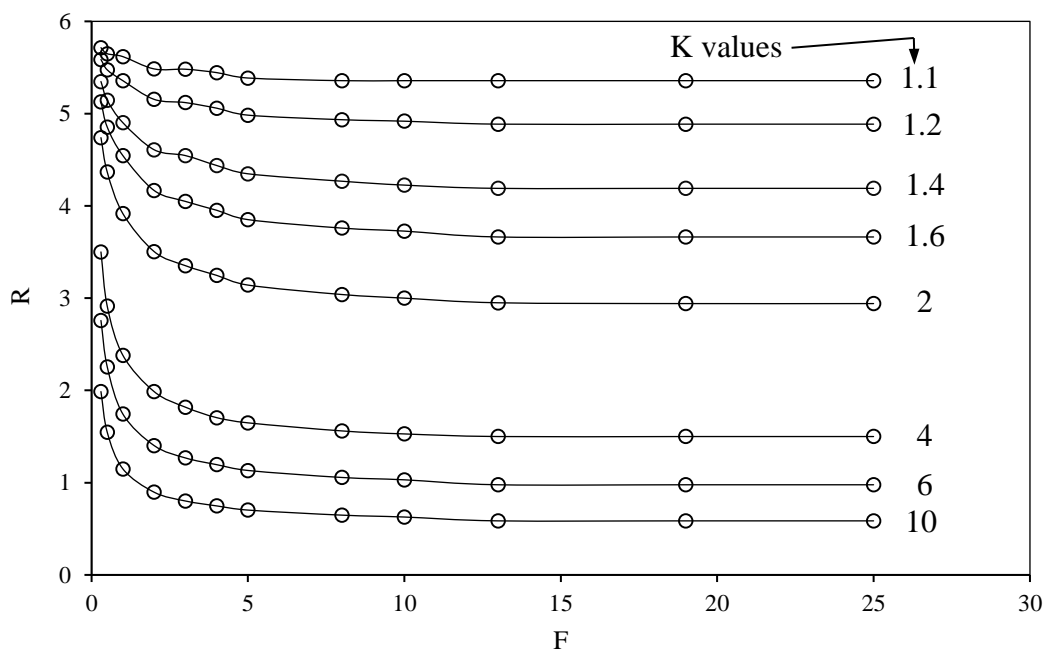
(b) $\theta = 0.3$

Fig. 4.5 Variation of parameter R (electrical resistivity) with K and F for various values of θ
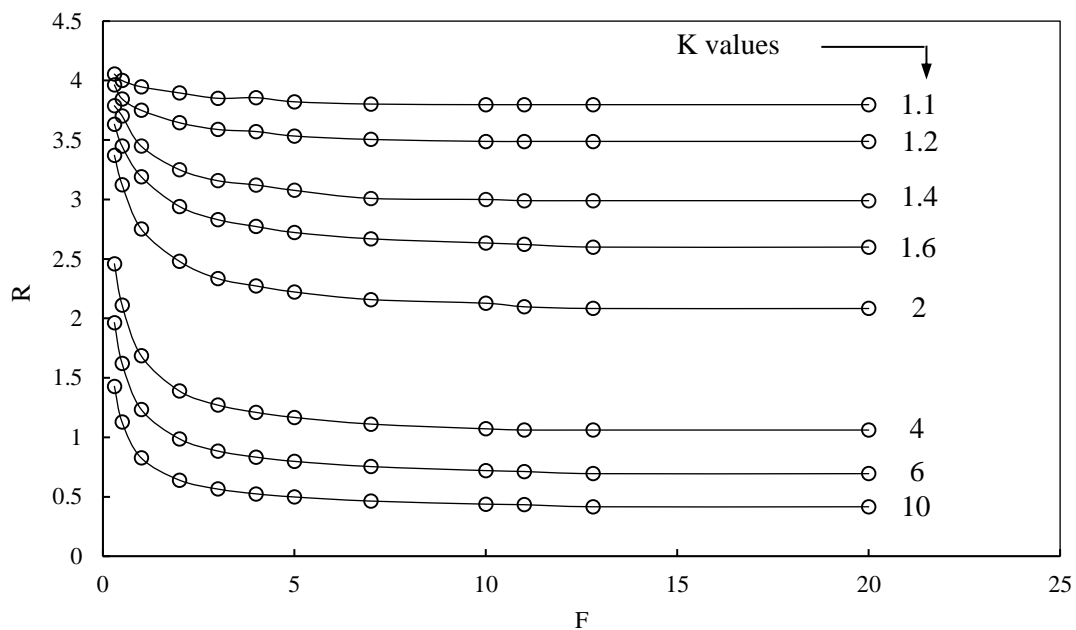
(c) $\theta = 0.4$
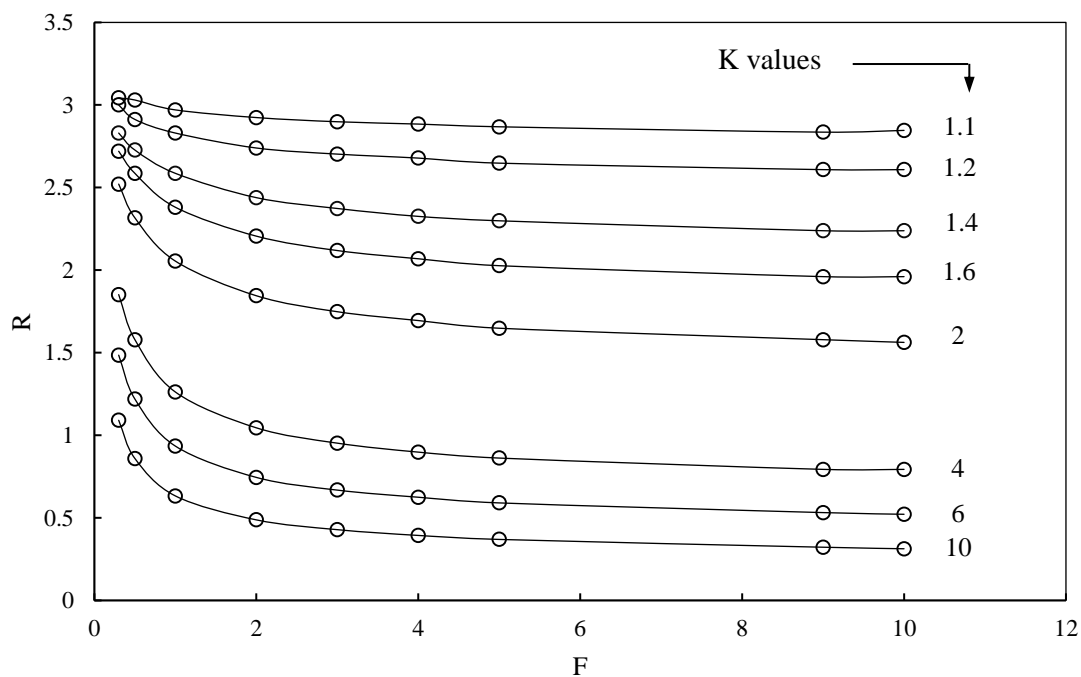
(d) $\theta = 0.5$

Fig. 4.5 Variation of parameter R (electrical resistivity) with K and F for various values of θ
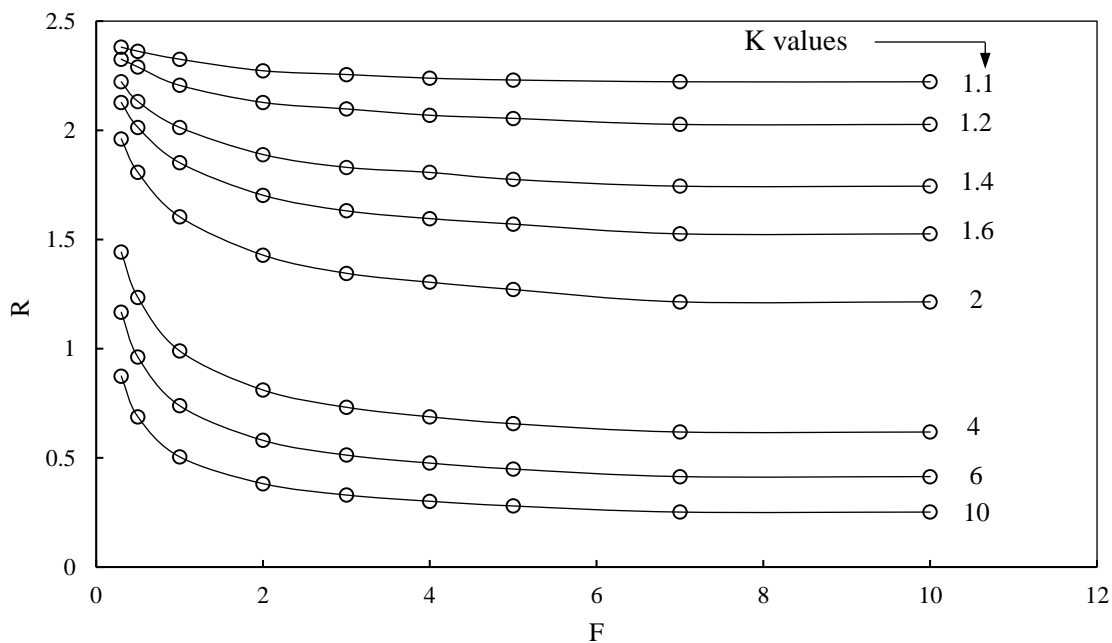
(cont'd)

(e) $\theta = 0.6$
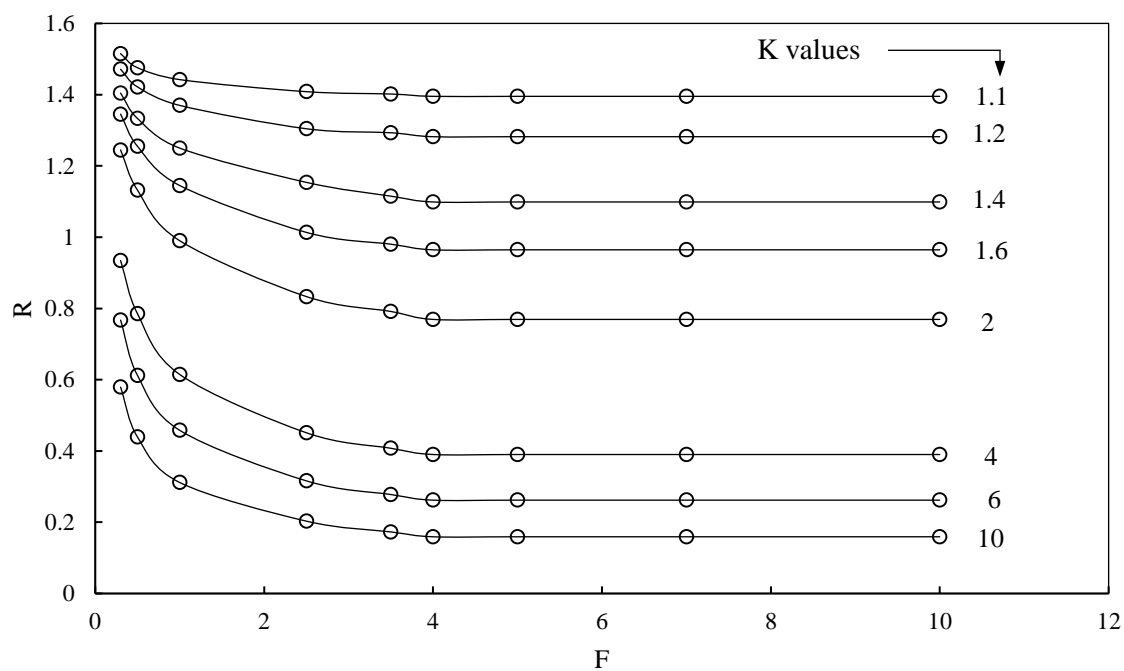
(f) $\theta = 0.8$

Fig. 4.5 Variation of parameter R (electrical resistivity) with K and F for various values of θ

(cont'd)

In addition, from the results presented in Fig. 4.5, it is concluded that the values of $\theta_{DDL,T}$ and F_T are constant for various K and solely depend on θ. Therefore, as shown in Fig. 4.6, a unique relationship was proposed for estimation of F_T as a function only of θ as:

$$F_T = 3.447 \times \theta^{-1.421} \qquad (4.21)$$

with correlation factor of $R^2 = 0.987$.
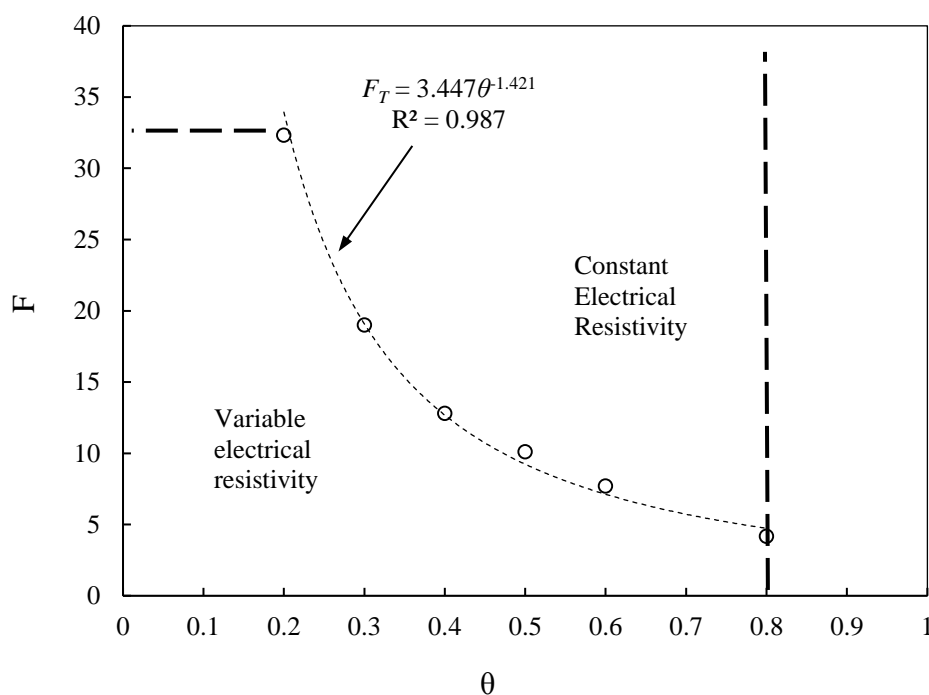
Fig. 4.6 Maximum threshold of parameter F

Therefore, in the case of $F \geq F_T$, F_T will be used in the numerical model, while in the case of $F < F_T$, the parameter F will be used which is independent of the parameter K. Therefore, to develop the database, the parameter F has been chosen to be between 0 and F_T to cover all possible cases.

A summary of the parameters utilised to develop the numerical database is presented in Table 4.3.

Table 4.3 Parameters used to develop the numerical database

Parameter	Range used	Values used for numerical model
θ	0.2 to 0.8	0.2, 0.3, 0.4,0.5,0.6, 0.7, 0.8
K	1.1 to 10	1.1, 1.2, 1.4, 1.6, 2, 4, 6, 10
F	0 to F_T	$F_T = 3.447\theta^{-1.421}$

In addition, since the values of F depend on θ, the values used for F in the development of the database are listed in Table 4.4 for various values of θ.

Table 4.4 Details of parameter F used to develop the numerical database

θ	Values of F used	Total number of tests
0.2	0, 0.1, 0.2, 0.3, 0.5, 7, 10, 20, 25, 32.3(F_T)	10
0.3	0, 0.1, 0.2, 0.3, 0.5, 1, 2, 3, 4, 5, 8, 10, 19 (F_T)	13
0.4	0, 0.1, 0.2, 0.3, 0.5, 1, 2, 3, 4, 5, 8, 10, 11, 12.8 (F_T)	14
0.5	0, 0.1, 0.2, 0.3, 0.5, 1, 2, 3, 4, 5, 8, 9 ,10.11 (F_T)	14
0.6	0, 0.1, 0.2, 0.3, 0.5, 1, 2, 3, 4, 5, 7, 7.7 (F_T)	12
0.8	0, 0.1, 0.2, 0.3, 0.5, 1,2.5, 3.5, 4, 4.2 (F_T)	10
		Total = 73 tests

In addition, the cases listed in Table 4.4 were repeated for each K as listed in Table 4.3 except for $F=0$, and since R is independent of K, a total of 6 numerical tests will suffice. For each of the other values of F (listed in Table 4.4), 8 values of K were used. Therefore, a total of 542 numerical tests were conducted to develop the numerical database and to develop a generic model for electrical resistivity. In addition, referring to Fig. 4.5 (a) to Fig. 4.5 (f), in the case of

$F \geq F_T$, the parameter R is constant; therefore, when $F \geq F_T$, the value of F_T is used to compute the electrical resistivity of the soil.

4.5 Development of electrical resistivity model

As discussed above, a database of 542 numerical tests was conducted to develop a generic model to estimate the electrical resistivity of fine-grained soils. It was found that the electrical resistivity of soil for various K and F is proportional to the electrical resistivity of soil when there is no surface charge ($\theta_{DDL} = 0$ which implies $F = 0$). In addition, it implies $K=1$. The electrical resistivity in that situation is the reference electrical resistivity, which is denoted as R'. Therefore, Eq. 4.22 is established for the database.

$$R \propto R' \tag{4.22}$$

R' can be determined using Fig. 4.7.
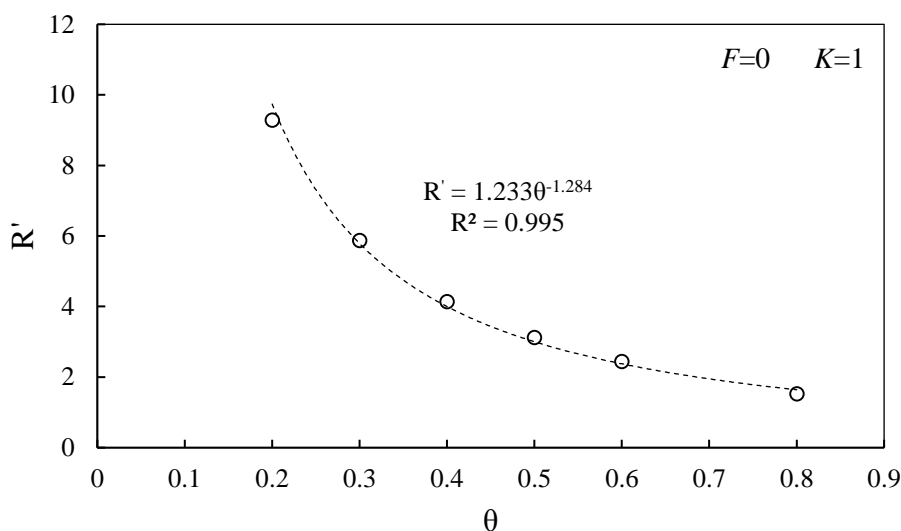
Fig. 4.7 Reference electrical resistivity (R')

To be able to estimate the electrical resistivity of the soil, Eq. 4.22 was converted to an equation by defining a coefficient of the proportionality λ as:

$$R = \lambda R' \tag{4.23}$$

Then, λ was determined for the database and plotted against K and F as shown in Fig. 4.8.
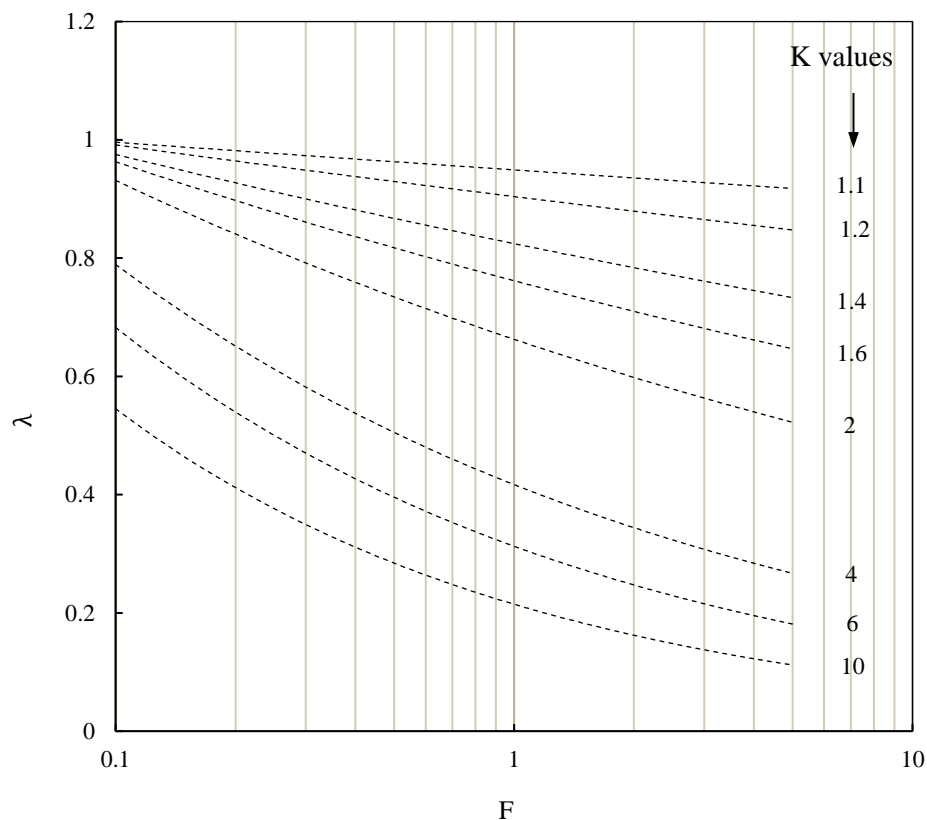
Fig. 4.8 Parameter λ for estimation of electrical resistivity of soil

Therefore, the electrical resistivity of soil can be estimated through two graphical steps: (1) determination of R' knowing θ; and (2) determination of λ knowing K and F (as discussed in Sections 4.3 and 4.5).

This graphical presentation of the numerical test results demonstrates the proposed electrical resistivity model in non-dimensional space. For constant K and θ, the graph shown indicates that the electrical resistivity of the bulk soil increases as F decreases. A decrease in F under constant θ condition leads to a lower level of DDL water volume. As DDL water has lower electrical resistivity compared to the free water, a higher electrical resistivity of bulk soil is observed. The numerical results in Fig. 4.7 and Fig. 4.8 also show that for constant θ and F, the parameter K increases as the soil electrical resistivity decreases. This is attributed to the increase in the electrical conductivity of DDL water as K increases.

4.6 Validation of the model (comparison with laboratory results)

The experimental programme discussed in Chapter 3 was used to assess the validity of the proposed electrical resistivity model. The reconstituted samples were prepared by mixing Kaolin clay and sand at different weight ratios, with water at different salinities as outlined in Table 4.5. The results of the experimental programme are shown in Fig. 4.9 (a) to Fig. 4.9(d). The results show that as the salinity of the pore water increases the electrical resistivity decreases. Furthermore, the results also indicated that as the sand content increases the resistivity increases. This behaviour reflects the effect of θ_{DDL} on the electrical resistivity of soil, i.e. θ_{DDL} decreases as the sand content increases.

To predict the electrical resistivity evolution as θ changes for the tested reconstituted soils, the values of F and K should be determined. Eq. 4.7, 4.11, 4.12, 4.13, 4.14 a, 4.14 b and 4.15 were used to determine F. The parameter K can be determined by back-calculation method, where only one electrical resistivity test is used for a sample with known θ, F, and R. To achieve that, the parameters θ and F are set in the model and numerical tests are conducted using different values of K to achieve the most accurate value of R (value similar to the experimental one). Then the back-calculated K is assumed to be constant and used to estimate R for other conditions.

Alternatively, K can be back-calculated using Figs. 4.7 and 4.8 and a single experimental result (experimentally measured ρ for a specific θ). Then, R' can be determined using Fig. 4.7 corresponding to the value of θ. Then, the parameter λ can be calculated using Eqs. 4.16 and 4.23. Knowing λ and F (which can be calculated using Eq. 4.14a) the value of K can be back-calculated using Fig. 4.8. For example, for soil M-1-1, when θ=0.49, ρ = 3.08 $\Omega\cdot$m. As discussed in Chapter 3, ρ_{FW} = 1.05 $\Omega\cdot$m and therefore, R = 2.9. In addition, θ=0.48 implies R'=3.08 and thus, λ =0.95. In this case, F was calculated as 0.14 using Eq. 4.16. Details of the calculation of F are discussed in Section 4.3. Based on known parameters λ and F, the value of K lies between 1.1 and 1.2 which can be estimated as 1.15 using the graphical method (Fig. 4.8). This value is consistent with the value obtained using FlexPDE software for back-calculation (K=1.17).

Table 4.5 lists the values of K and F of the laboratory-tested samples in this study. It should be mentioned that during the consolidation process, only F will change as the volume of free water changes whereas K remains unchanged. Fig. 4.9 also shows the comparison between the

laboratory test results for all tested soils and the prediction using the proposed model (Fig. 4.7 and Fig. 4.8) and good agreement can be observed. Therefore, the model is able to consider successfully the effect of DDL on the electrical resistivity of soils.

Table 4.5 Chemical properties and numerical parameters of tested materials

Soil Type	CEC* (meq/100g)	Pore water salinity (eq/lit) **	Parameter K (back calculated)	Range of parameter F
M-1-1	9	0.1	1.17	0.1 to 0.2
M-1-2	9	0.2	1.25	0.1 to 0.15
M-2-1	8	0.1	1.17	0.1 to 0.2
M-2-2	8	0.2	1.25	0.1 to 0.12

* Cation exchange capacity which is a measure for soil chemistry

** Equivalent/litre
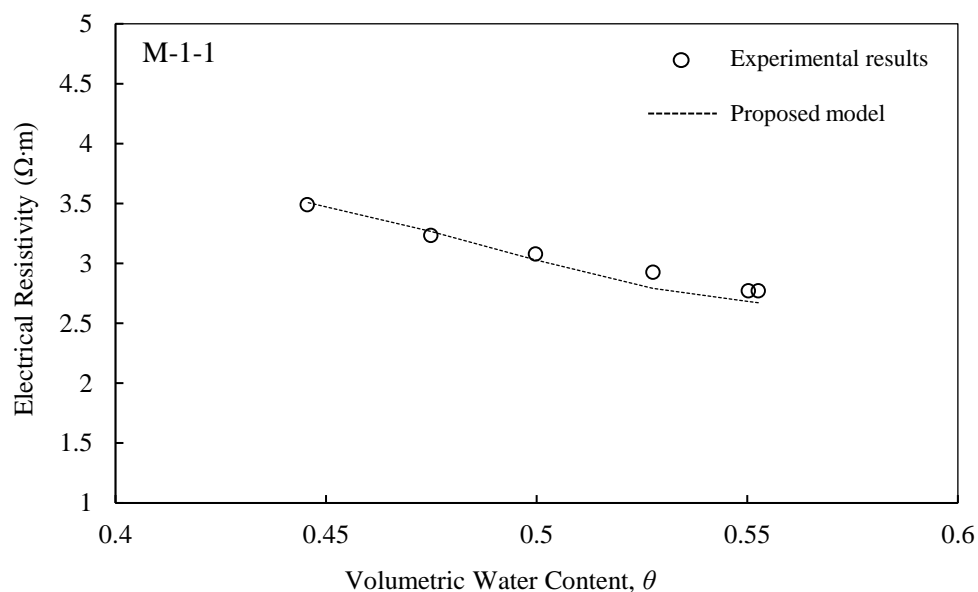
(a)

Fig. 4.9 Evaluation of proposed electrical resistivity model
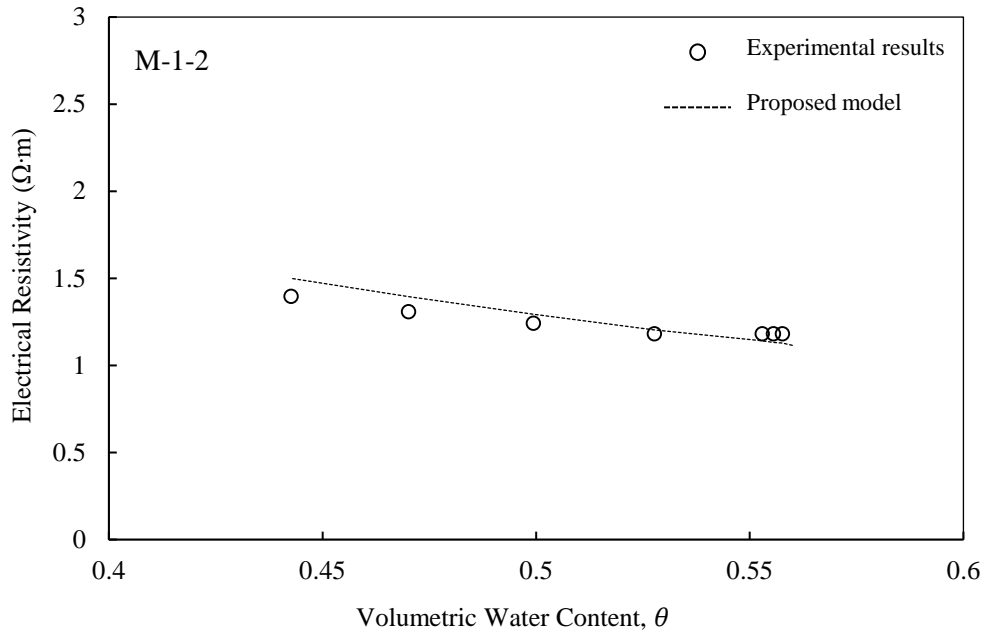
(b)
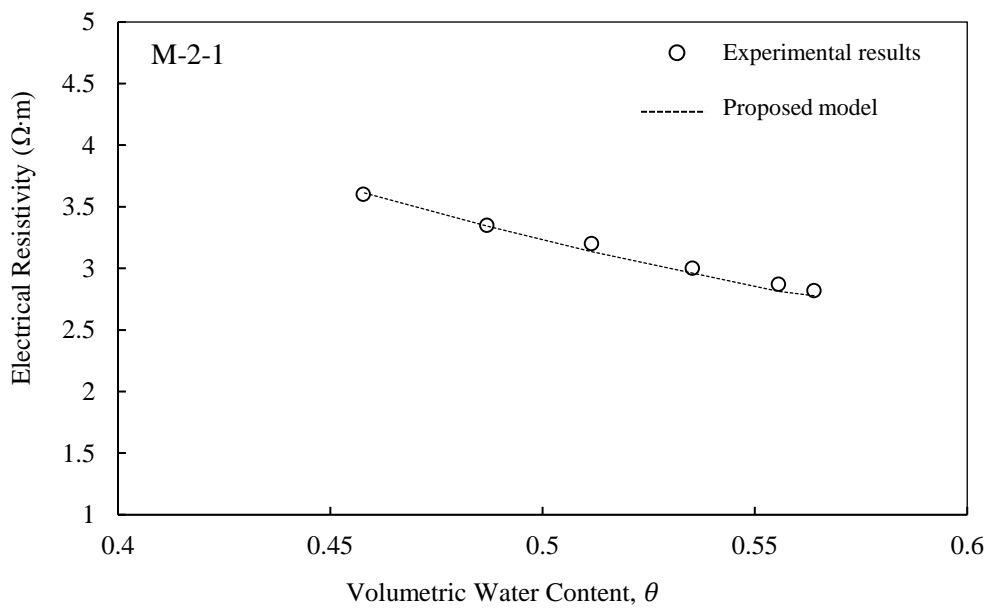
(c)

Fig. 4.9 Evaluation of proposed electrical resistivity model (Cont'd)
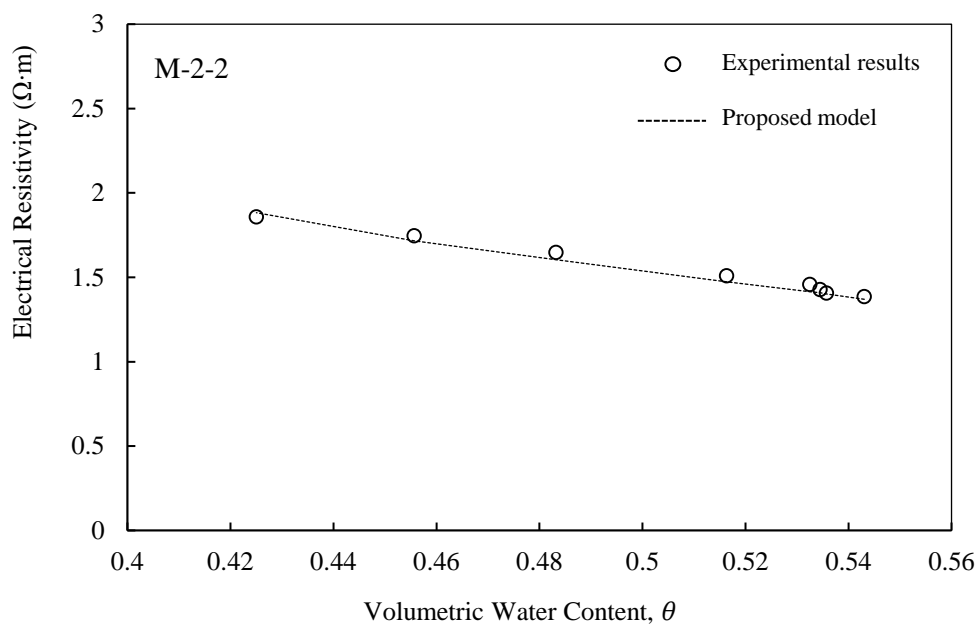
(d)

Fig. 4.9 Evaluation of proposed electrical resistivity model (Cont'd)

To quantify the difference between experiment and prediction over the range of volumetric water content employed, the Absolute Error (*AE*) was used, i.e.

$$AE_i\% = \frac{\left|\rho_{\exp i} - \rho_{num i}\right|}{\rho_{\exp i}} \times 100\%$$ (4.11)

Boxplots were used to represent the error between experiment and prediction for each tested sample, as shown in Figure 4.10. Note that a boxplot is a convenient way of visualising the distribution of a group of data based on its quartiles, as well as its smallest and largest values. The boxplots in the figure correspond to lower and upper quartiles, while the horizontal line inside the boxplot represents the median of the data. The boxplots also have lines extending vertically from the boxes (called whiskers), indicating variability from its smallest to largest values. Based on the results shown in Fig. 4.10, a median *AE* between experiment and prediction of less than 2% have been observed for M-2-2 sample, while values between 2-4% are noted for the other samples. Therefore, the model is able to consider successfully the effect of DDL on the electrical resistivity of soils.
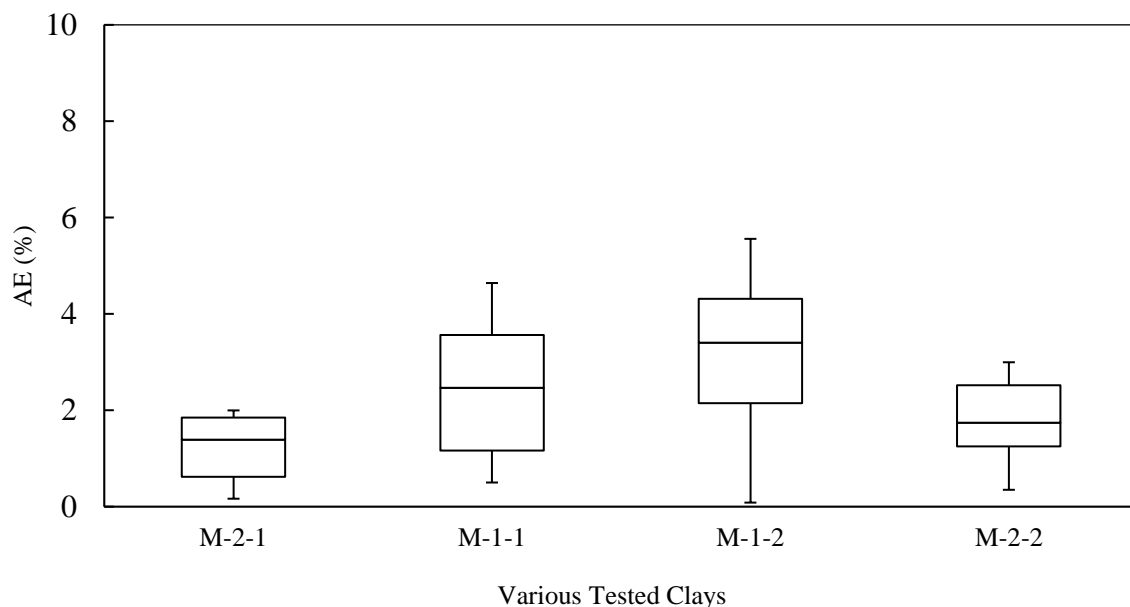
Fig. 4.10 Absolute error between experimental and numerical results

4.7 Summary

A new numerical model has been proposed to estimate the electrical resistivity of saturated fine-grained soils. In this model, solid particles are concentrated at the centre of the soil medium and surrounded by diffuse double layer (DDL) and free water. Therefore, all possible paths for current passage are addressed in the model, which received limited attention in currently available models. A combination of coupled flow and continuity equation for electrical current flow governing equations was solved over the proposed representative soil unit by finite element method utilising FlexPDE software. The validity of the proposed model has been tested against experimental results. Good agreement was observed between the experimental and the numerical data. In addition, this model is able to predict the electrical resistivity of soil in various conditions with minimal experimental tests (i.e. only one test). Therefore, it can be used as a replacement for experiment-intensive models, such as the Archie and the three element models.

5 ELECTRO-OSMOSIS CONSOLIDATION: LABORATORY TESTS

5.1 Introduction

EO consolidation test is not a conventional experiment in the laboratory. Therefore, various researchers tried to modify the conventional oedometer and triaxial apparatus to apply the electric potential to the soil specimen. As discussed in Chapter 2, the main drawbacks of the modified apparatus are:

- In some cases, there is no (or limited) ability for load application; therefore, the effect of different levels of preconsolidation and overconsolidation ratio (OCR) on EO consolidation cannot be investigated; and
- In many cases, the electric cell is designed to just apply the electric potential difference; the specimen is then disassembled and removed from the electric cell and tested in a conventional apparatus, such as triaxial cell or oedometer. Therefore, the specimen will be able to rebound, which changes the state of interconnected void network and can impact the laboratory results

In this chapter, a conventional oedometer cell is modified to address the issues mentioned above. Then, the proposed apparatus is used in the laboratory, the parameters affecting EO consolidation are identified and measured and the results are discussed. In addition, as the type

of soil tested is the same as previously discussed, the electrical resistivity results from Chapters 3 and 4 of can be used to investigate the effect of electrical resistivity on EO consolidation.

5.2 Experimental apparatus

In addition to measuring all contributing parameters to EO consolidation, the experimental apparatus was designed to apply the electric potential difference and hydraulic loading in a single cell. The specimen can be loaded and unloaded as desired before and after the EO consolidation process in the same cell. Fig. 5.1 shows a schematic diagram of the apparatus utilised for EO consolidation which was developed by modifying a conventional oedometer cell. As shown, the soil specimen was placed in a PVC ring which has height and diameter of 19 mm and 76 mm, respectively. Fig. 5.2 shows the loading cap, PVC ring and cathode dense mesh along with the power connections. The ring was placed on the cathode which was made of dense stainless-steel mesh. Using the mesh as a cathode enabled the system to drain at the cathode side. In addition, as the volume of the mesh was very small in relation to the soil volume (approximately 1%), its effect on any volume calculation was neglected.
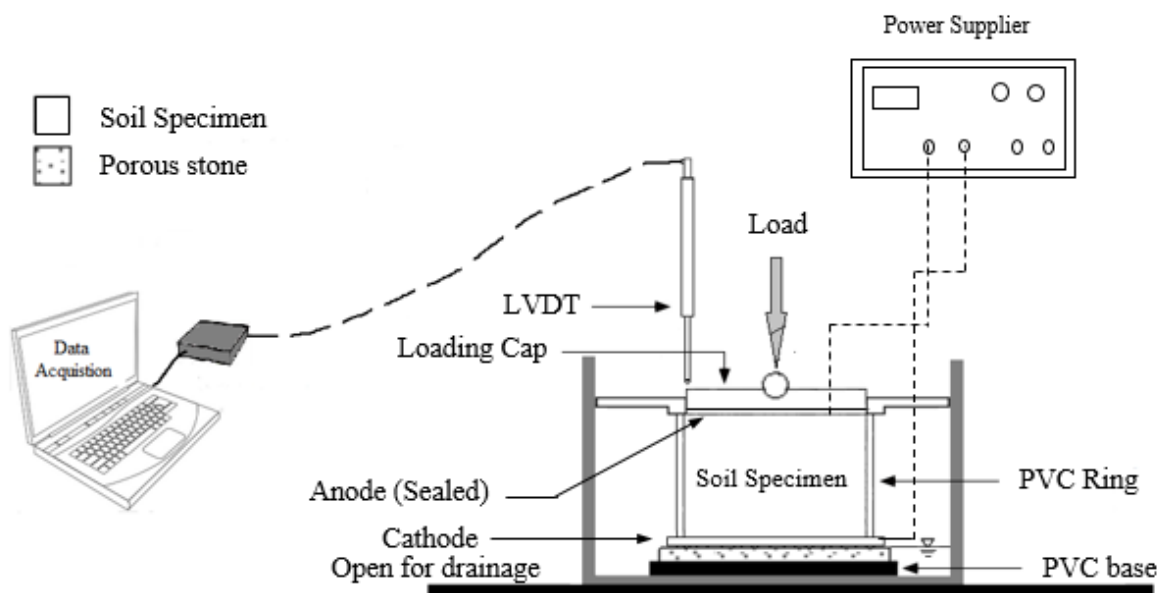
Fig. 5.1 Schematic diagram of the developed EO cell

Power
connection

Anode

Loading cap with attached anode

PVC ring

Cathode

Power
connection

Porous stone

PVC plate

Consolidation ring with cathode
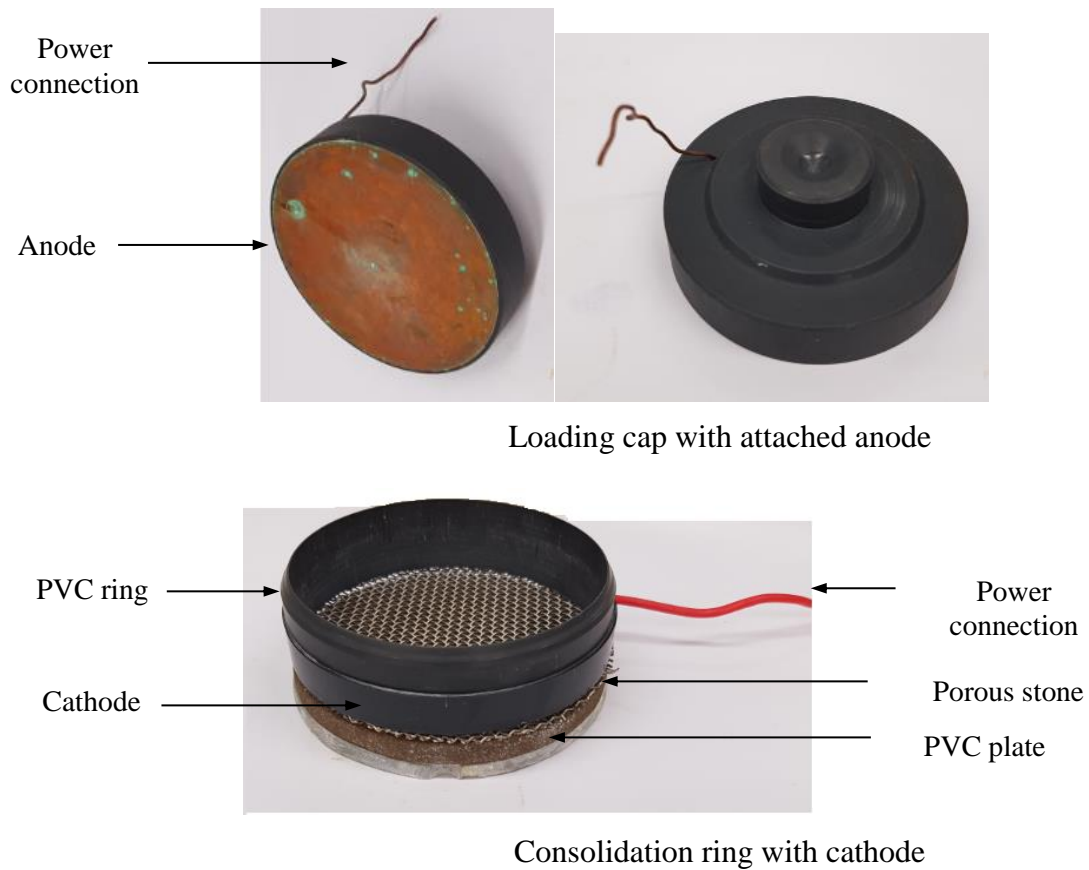
Fig. 5.2 EO system used in EO cell

The ring and the cathode were then placed on top of the porous stone which sat on a PVC plate. The PVC plate was used to minimise the current leak from the bottom of the cell and provided similar boundary as that in the electrical resistivity test. The loading cap was also modified to allow the application of load and electric potential gradient at the same time. The loading cap was made of PVC and a solid bronze disc was attached to the bottom of the cap. The solid disc was in contact with the soil specimen and provided the sealed anode in the system. Finally, the cathode and the anode were connected to the power supply by means of wires. Fig. 5.3 shows a view of the oedometer apparatus developed in the laboratory.

LVDT

Power supply
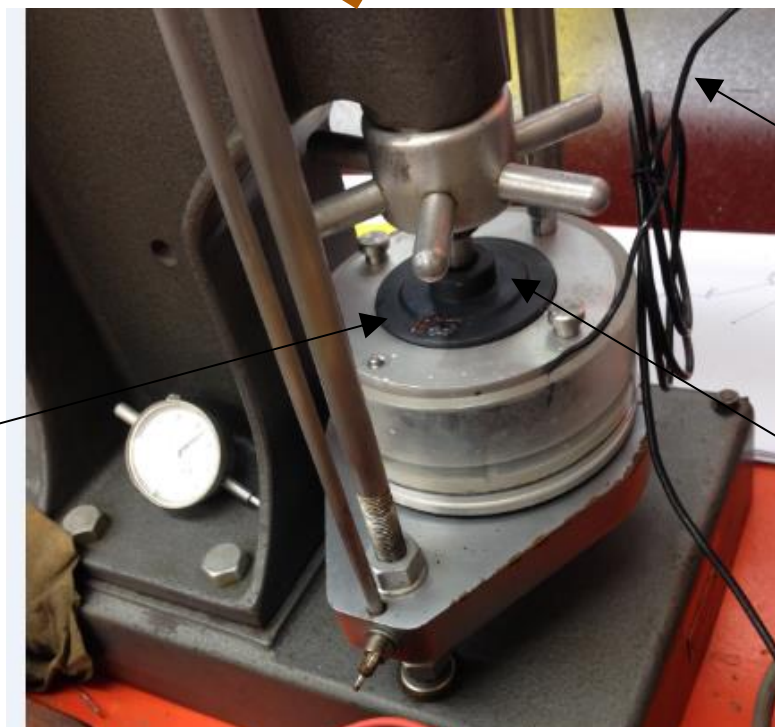
Cathode
connection -Wire

Anode
connection -Wire

PVC top cap

Fig. 5.3 A view of the developed EO cell

In addition, a new PVC ring was specifically designed and fabricated to measure the potential loss at electrodes during EO consolidation. It had three potential probes located on the side and the probes were connected to a voltmeter, allowing the measurement of the potential at each point with time. The detail of the new ring is shown in Fig. 5.4.
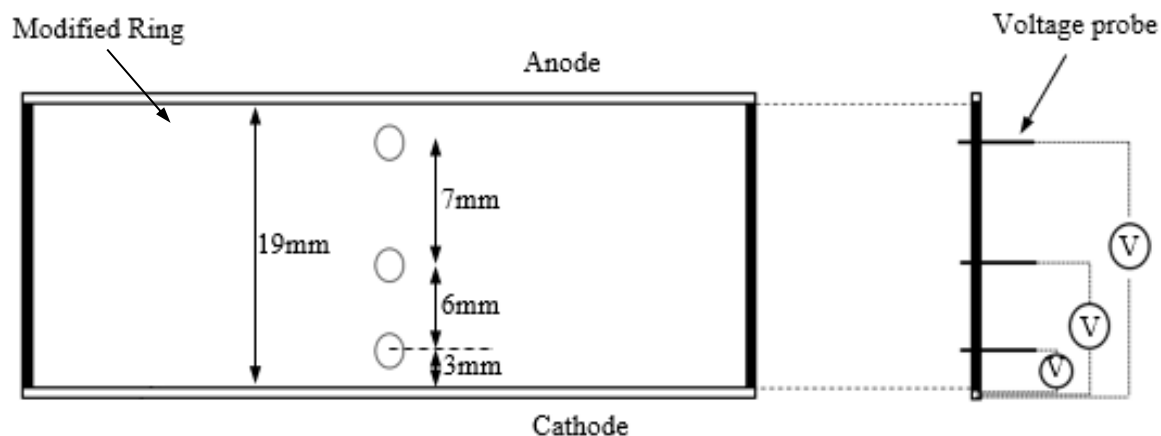
Fig. 5.4 Modified ring to measure the voltage drop at electrodes

5.3 Specimen preparation

To prepare the specimen, the soil was thoroughly mixed with water to obtain a moisture content which was 1.5 times the soil's liquid limit. Then, the soil was poured into a split mould and installed to a loading cell, as shown in Fig. 5.5. A pressure of 10 kPa was applied to the specimen using another oedometer apparatus and the specimen was left to saturate for about 3 days. A constant displacement was recorded between 1 and 3 days using an LVDT; this was used as a way of ensuring that full saturation was achieved. Then, the system was disassembled, and the specimen was trimmed and installed in the EO cell as shown in Fig. 5.1. By this method, a saturation ratio of about 1.0 was measured based on the initial and final soil heights, before starting the consolidation process.
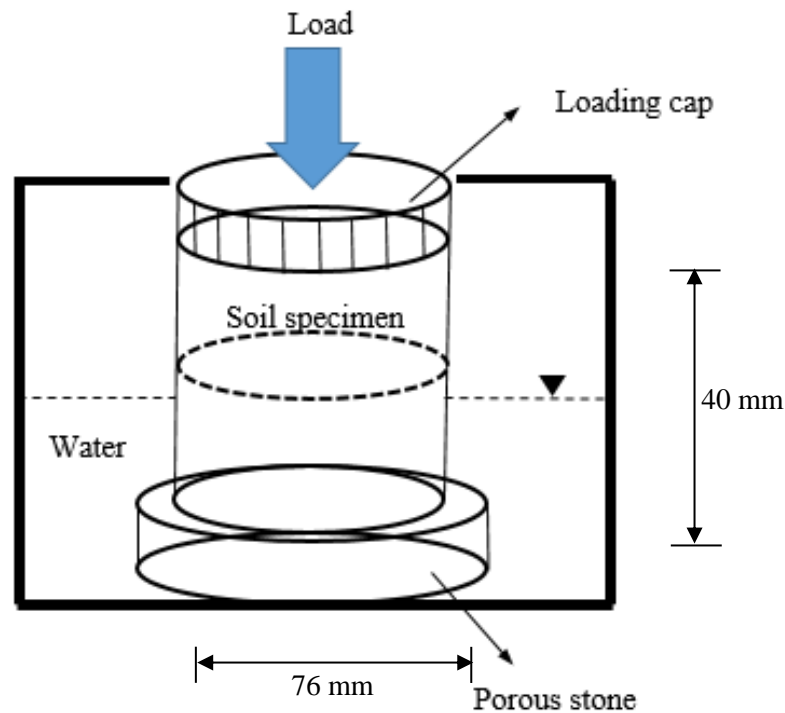
Fig. 5.5 Schematic apparatus for specimen preparation

5.4 Testing programme

The experimental programme adopted in this research involved seven sets of hydraulic and electrical consolidation tests at a constant level of electric potential difference of 4 V. The first three sets of tests were conducted on normally consolidated (NC) samples at various stress levels. In test L-1 (Low preconsolidation pressure, Overconsolidation Ratio (OCR) =1), the specimen was consolidated up to 86 kPa, unloaded to 21.6 kPa and again loaded to 86 kPa to achieve OCR=1 and preconsolidation pressure of 86 kPa. Then an electric potential was applied to the specimen and finally the sample underwent another loading-unloading cycle. Similarly, in tests M-1 (Medium preconsolidation pressure, OCR=1) and H-1 (High preconsolidation pressure, OCR=1) the specimens were loaded, unloaded and again re-loaded to achieve the desired stress level. Three more tests were done on overconsolidated (OC) samples at different OCR. In M-2 (Medium preconsolidation pressure, OCR=2) test, the specimen was initially loaded up to 172 kPa, was unloaded to 86 kPa to obtain an OCR=2, then an electric potential gradient was applied, and the sample underwent a loading-unloading cycle afterwards. For M-4 (Medium preconsolidation pressure, OCR=4) and M-8 (Medium preconsolidation pressure,

OCR=8), the level of initial loading was maintained constant at 172 kPa and then unloaded to 43 and 21 kPa, respectively, before the electric potential gradient application. Fig. 5.6 shows schematically the different mechanical and electrical paths used in the tests in void ratio-effective stress (e - σ') and applied voltage - effective stress (V - σ') plots, while Table 5.1 summarises the conducted EO consolidation tests considering various soil stress histories.

In addition, to measure the level of potential loss due to electrochemical effects at the soil-electrode interface, a separate EO consolidation test was carried out. For this test, a specimen of kaolin clay was placed in the consolidation ring and loaded up to 10 kPa. Details of the consolidation ring utilised for this test are shown in Fig. 5.4. Then, an electric potential gradient of 4 V was applied across the soil specimen and the electric potentials were measured using the installed probes.

Table 5.1 Summary of conducted EO consolidation tests considering stress history

Test ID	Preconsolidation pressure (kPa)	OCR	Applied Voltage (V)
L-1	86	1	4
M-1	172	1	4
H-1	345	1	4
M-2	172	2	4
M-4	172	4	4
M-8	172	8	4

(a) NC samples   (b) OC samples
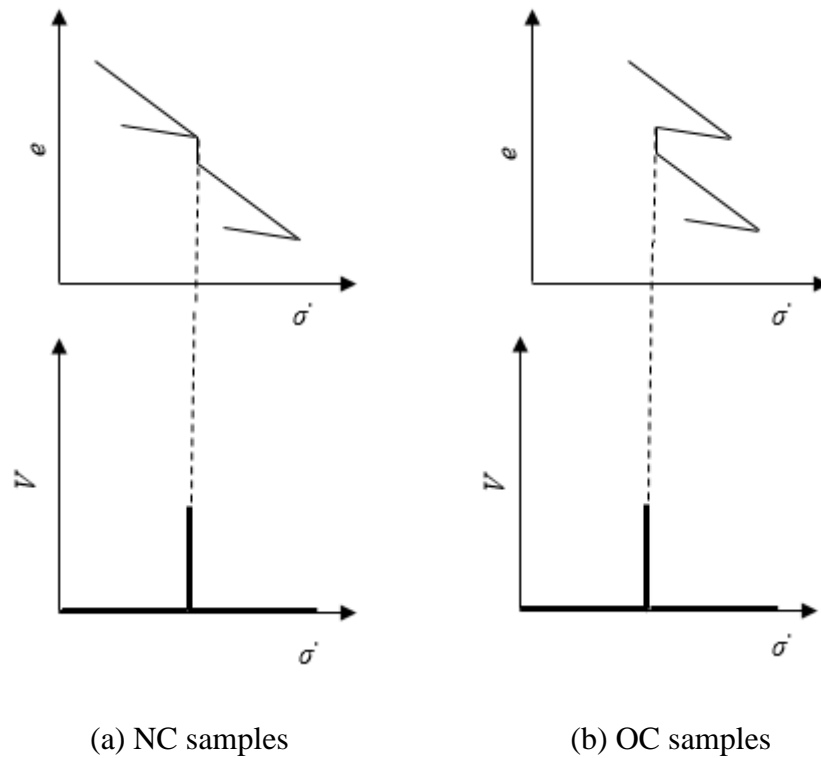
Fig. 5.6 Schematic diagram of mechanical and electrical paths applied in this study

5.5 Experimental results

5.5.1 Electrically-induced soil settlement

The soil settlements during the hydraulic and EO consolidation phases were recorded for the soil specimens outlined in Table 5.1. The experimental results are shown in Fig. 5.7 to Fig. 5.12. For each soil specimen, the results are plotted in the e - log σ' plane. In addition, the soil settlement during the voltage application phase (EO consolidation) is presented in each case.
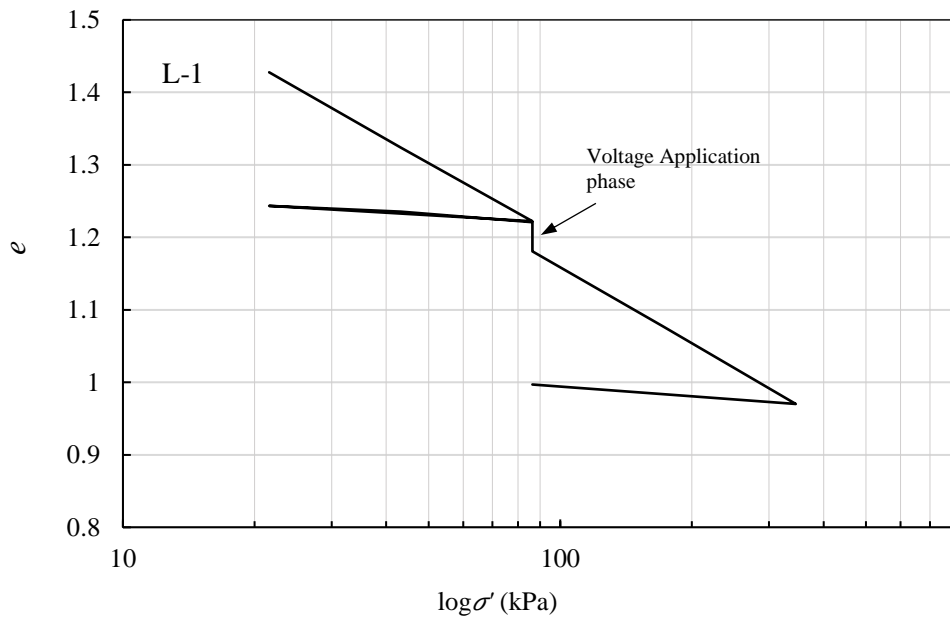
(a) e versus $\log \sigma'$
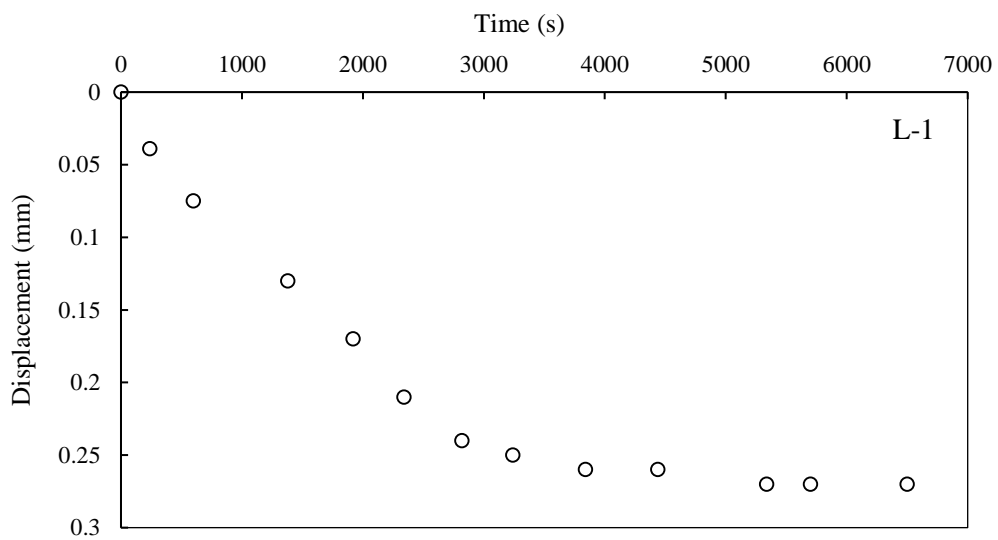
(b) Soil settlement during voltage application phase (V=4 V)

Fig. 5.7 Consolidation characteristics for L-1 sample
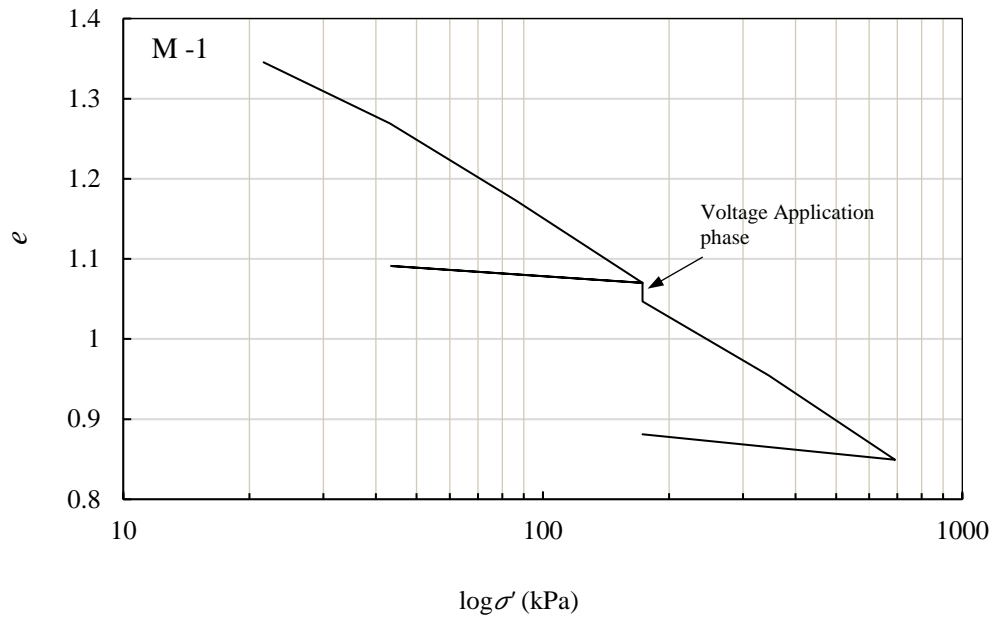
(a) e versus $\log\sigma'$
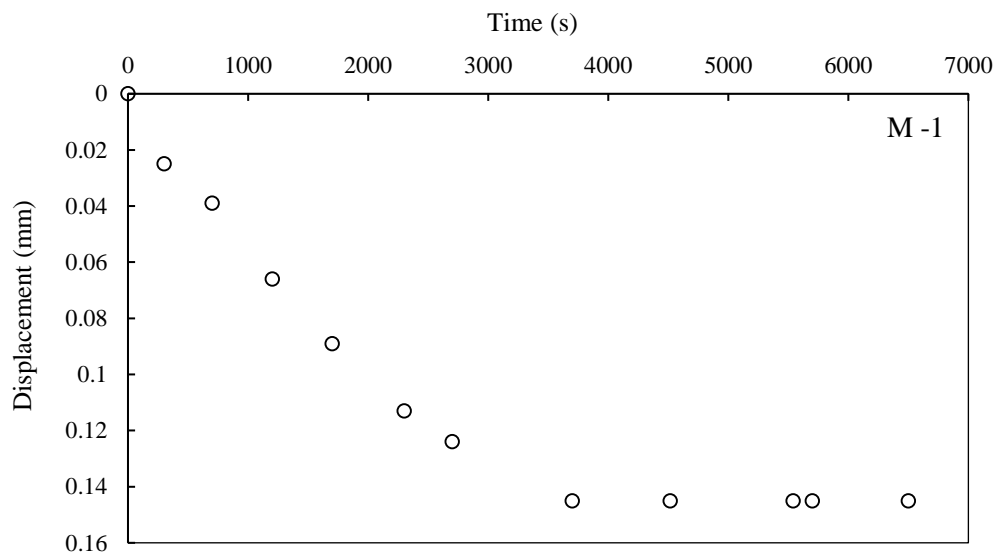
(b) Soil settlement during voltage application phase (V=4 V)

Fig. 5.8 Consolidation characteristics for M-1 sample

(a) *e* versus logσ'
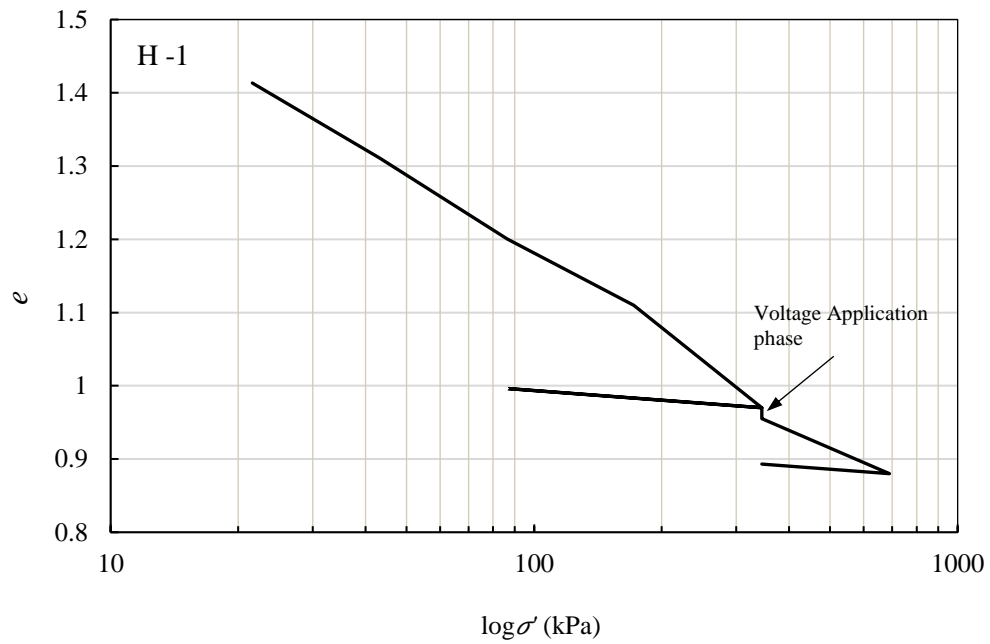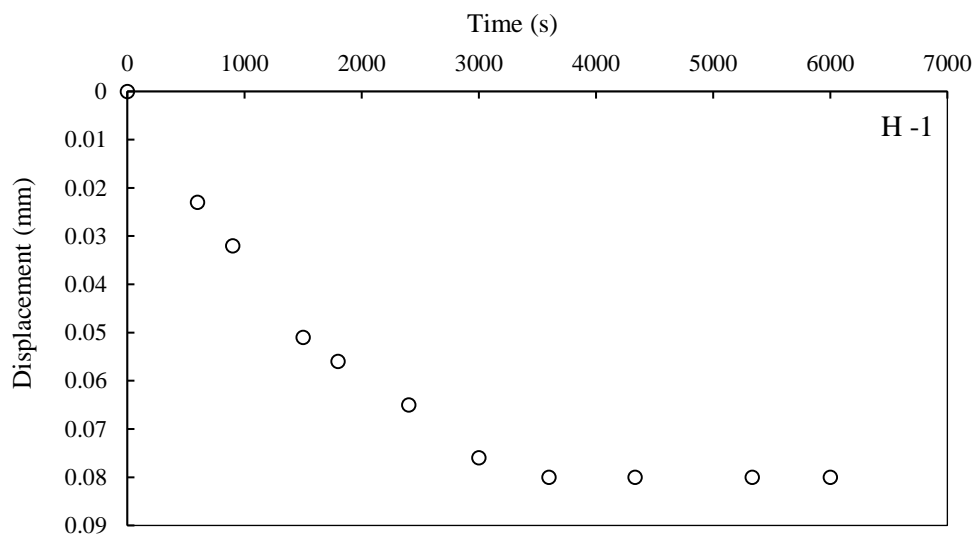
(b) Soil settlement during voltage application phase (*V*=4 V)

Fig. 5.9 Consolidation characteristics for H-1 sample
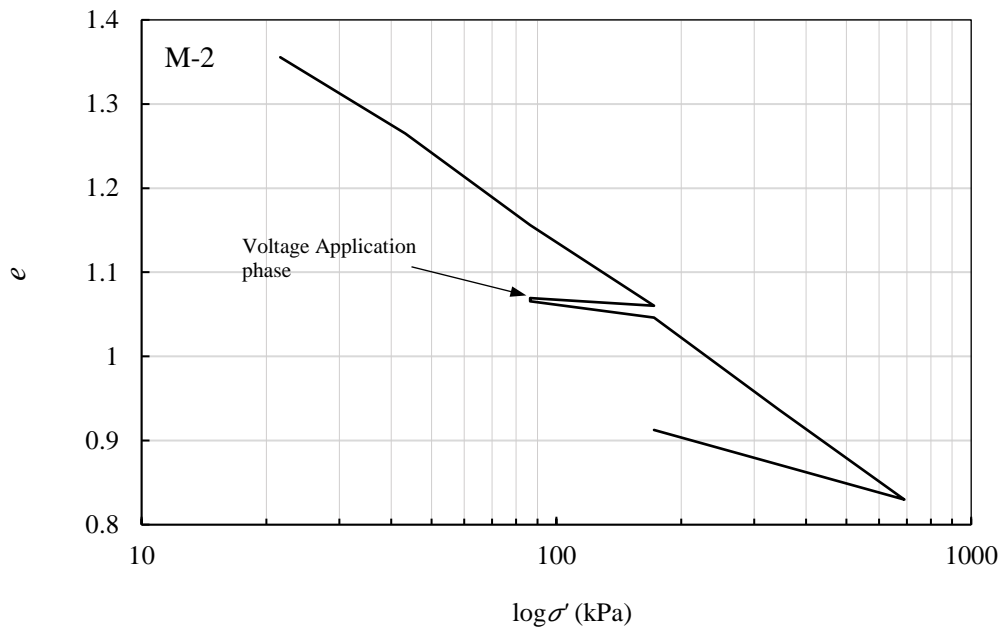
(a) e versus $\log\sigma'$
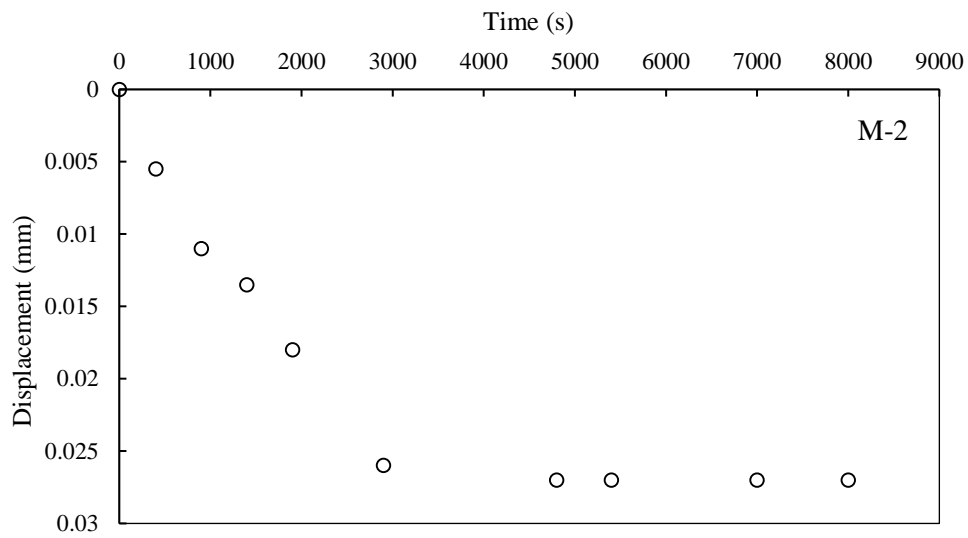
(b) Soil settlement during voltage application phase (V=4 V)

Fig. 5.10 Consolidation characteristics for M-2 sample
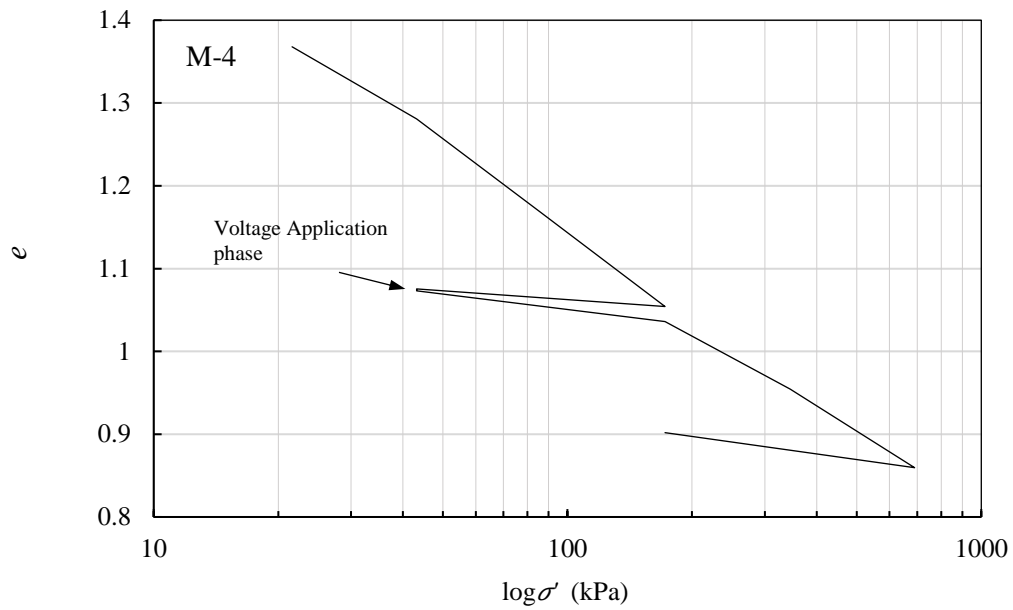
(a) e versus $\log\sigma'$
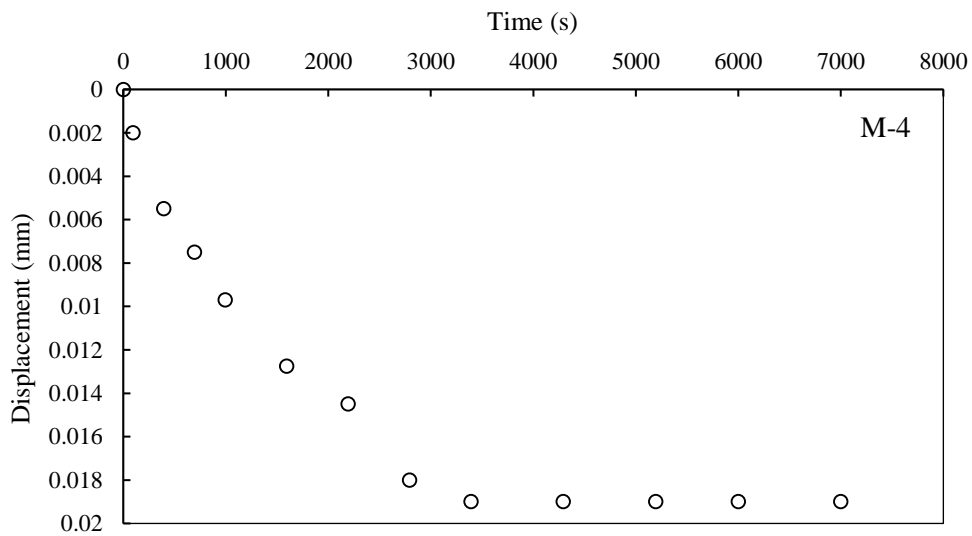
(b) Soil settlement during voltage application phase (V=4 V)

Fig. 5.11 Consolidation characteristics for M-4 sample

(a) *e* versus logσ'
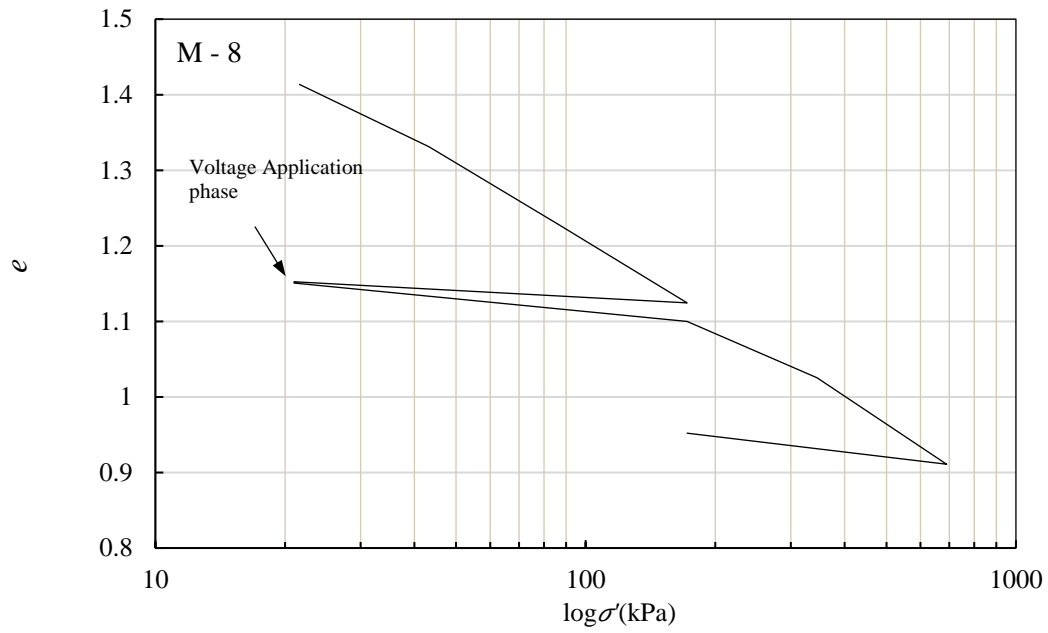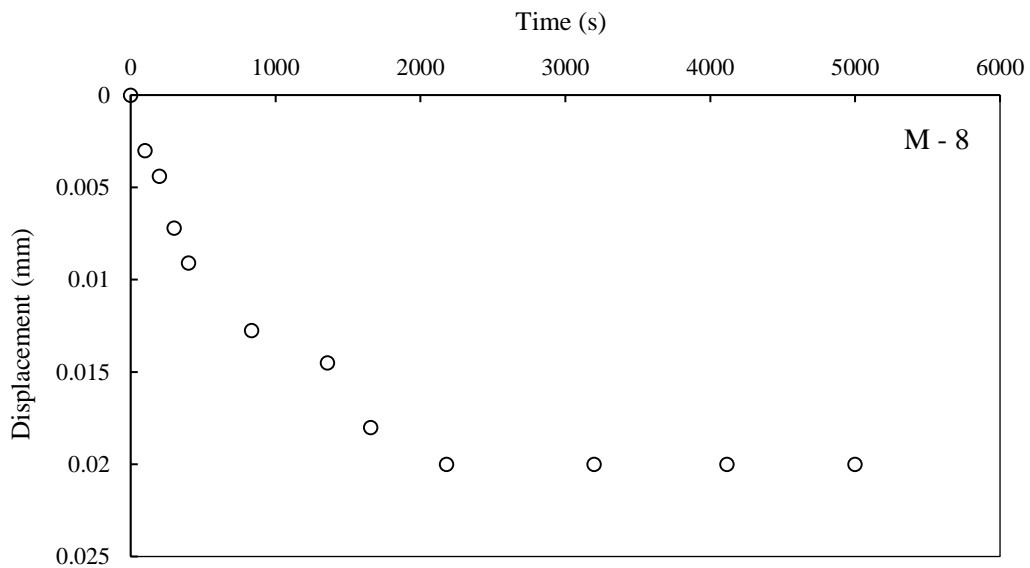
(b) Soil settlement during voltage application phase (*V*=4 V)

Fig. 5.12 Consolidation characteristics for M-8 sample

To date, there is no well-documented observation in existing literature on the behaviour of compression index (C_c) and the swelling index (C_s) during EO consolidation. Based on the results obtained from current study, the C_c and C_s were computed before and after EO consolidation. C_c showed very limited deviation before and after EO consolidation as shown in Table 5.2. Therefore, the value of C_c can be assumed to be constant before and after EO consolidation. However, the effect of EO consolidation on C_s was more apparent. In NC soils, the rate of increase in C_s before and after EO increases with overconsolidation pressure; however, in OC samples C_s was consistently doubled after voltage application. This deviation in C_s can be attributed to the reversibility of EO consolidation. Concurrent electrochemical processes occur during EO consolidation. These chemical processes are partially reversible which could lead to soil rebound. This rebound is more noticeable in unloading phases which leads to increase in the swelling index. In addition, the results imply that the rate of reversibility of EO consolidation effects depends on the overconsolidation pressure and stress history. This can be due to additional swelling which occurs because of reduction of suction as water moves back into the soil matrix. In addition, it can be attributed to the effect of electrically-induced suction which changes the soil structure and leads to more water moving back into the soil matrix.

Table 5.2 Experimental results of compression and swelling indexes before and after EO test

Test	Before EO		After EO	
	C_c	C_s	C_c	C_s
L-1	0.34	0.038	0.35	0.044
M-1	0.33	0.032	0.33	0.052
H-1	0.35	0.040	0.30	-[a]
M-2	0.33	0.031	0.35	0.064
M-4	0.31	0.035	0.29	0.070
M-8	0.32	0.031	0.32	0.070

[a] No measurement due to system malfunction

5.5.2 Coefficient of Consolidation

The coefficient of consolidation (C_v) holds great importance in EO consolidation investigation as it controls the rate of consolidation in the soil body and it is also a key parameter in numerical modelling of EO consolidation. Generally, there are two methods available for calculation of C_v: (1) logarithm-of-time and (2) square-root-of-time. In this research, logarithm-of-time method was chosen to calculate C_v. According to this method:

$$C_v = \frac{0.197 H_{dr}^2}{t_{50}}$$

(5.1)

where H_{dr} is the longest drainage path and t_{50} is the time for 50% consolidation to occur. Therefore, for each loading cycle during the consolidation test, a C_v value should be calculated before and after the EO consolidation phase for each tested specimen. The value 0.197 corresponds to the time factor T_v at 50% average degree of consolidation, where T_v is defined as:

$$T_v = \frac{C_v t_{50}}{H_{dr}^2}$$

(5.2)

The details of the logarithm-of-time method can be found in the literature (e.g. Das, 2013).

The measured coefficients of consolidation for the various specimens outlined in Table 5.1 are presented in Fig. 5.13.
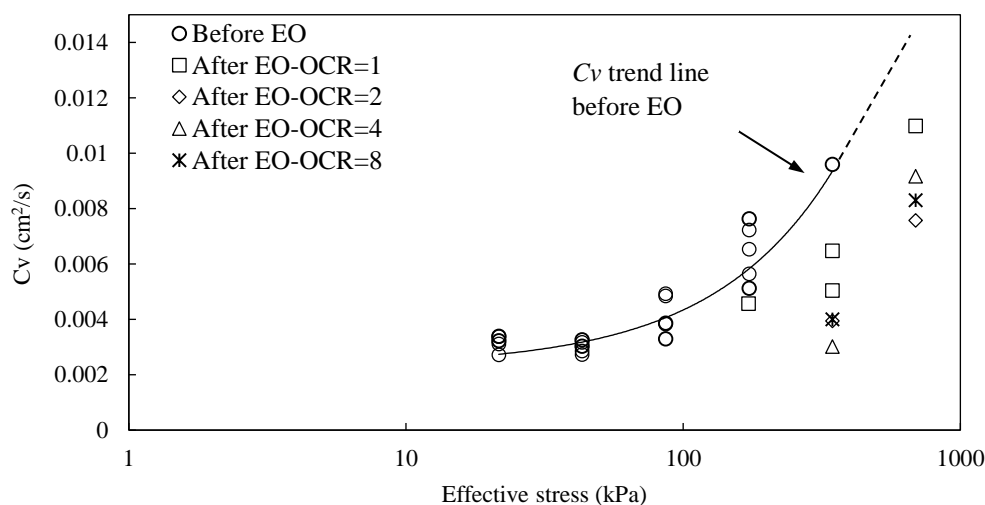
Fig. 5.13 Coefficient of EO consolidation before and after EO consolidation

Generally, C_v in kaolin clay increases with the increase in the level of applied effective stress. However, at a specific effective stress, C_v decreases after EO consolidation compared to that before EO consolidation. In addition, it can be concluded that in OC soil, the level of OCR has a limited effect on C_v. For OCR=2, OCR=4 and OCR=8, the C_v varies from 0.0031 and 0.0039 cm^2/s at effective stress of 345 kPa, and from 0.008 to 0.009 cm^2/s at effective stress of 690 kPa.

The parameter C_v was calculated during the hydraulic loading and it does not indicate the rate of consolidation during the EO consolidation phase. To investigate the coefficient of EO consolidation and to compare its magnitude to the C_v during hydraulic loading, C_v was also calculated during the EO consolidation phase and this is denoted as C_{ve}. Similar to the calculation of C_v, the logarithm-of-time method was used to compute C_{ve} during EO consolidation. However, referring to Section 2.6.3 and based on Esrig's theory, the time factor at 50% average degree of EO consolidation equals to 0.3; therefore, C_{ve} is calculated as:

$$C_{ve} = \frac{0.3H_{dr}^2}{t_{50}}$$

(5.3)

Because there is only a single cycle of EO consolidation during each consolidation test, a value of C_{ve} is calculated for each specimen listed in Table 5.1. Fig. 5.14 shows the C_{ve} measured in the tested specimens. Based on the results on NC and OC specimens, C_{ve} is approximately 1/10 of C_v. In addition, in NC soil, the value of C_{ve} was constant and was independent of the preconsolidation pressure and void ratios. However, with the increase in OCR, the C_{ve} increases. The highest value of $C_{ve} = 0.0008$ cm^2/s is observed in the specimen with OCR=8.

Usually, the value of C_v is used to investigate EO consolidation. However, the actual coefficient of consolidation during EO consolidation is C_{ve} and C_v is accurate only during the hydraulic loading phase. In addition, the differences between the values of these parameters are noticeable. Therefore, these results imply the importance of C_{ve} and it should be measured in any EO consolidation investigation.
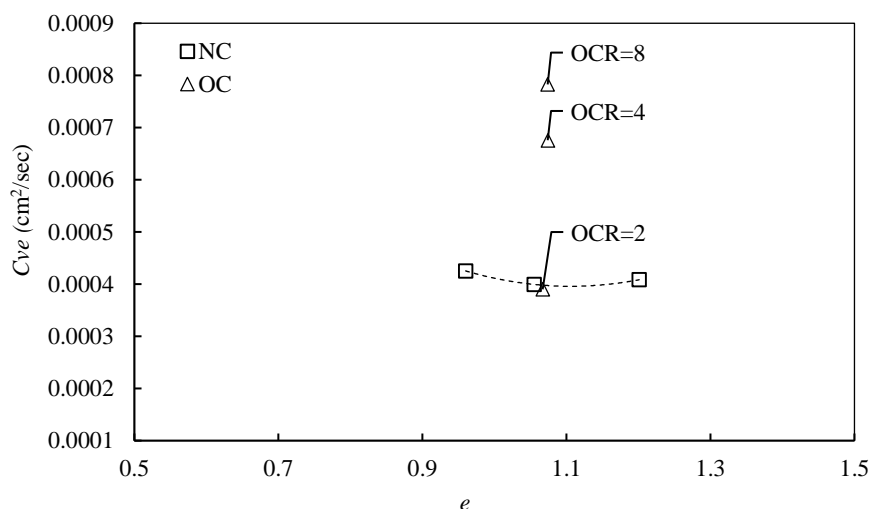
Fig. 5.14 Coefficient of EO consolidation during voltage gradient application

5.5.3 Hydraulic permeability (k_h)

Referring to the governing equation of the EO consolidation (Chapter 2, Eq. 2.27), the hydraulic permeability is a controlling factor in the negative pore water pressure development during EO consolidation. Therefore, k_h should be closely monitored during the EO process. In addition, to investigate the effect of EO consolidation on k_h, it was measured before and after the EO consolidation phase. To measure k_h before and after EO, Eq. 5.4 was used.

$$C_v = \frac{k_h}{m_v \gamma_w}$$
(5.4)

where m_v is the coefficient of volume compressibility.

Generally, k_h depends on numerous mechanical and physico-chemical parameters, such as geometrical arrangement, tortuosity and individual flow channel sizes. Therefore, for kaolin clay, k_h was calculated at various void ratios. Each void ratio corresponds to a loading cycle. For each loading cycle, the parameter m_v was measured and then using C_v, k_h was calculated. Fig. 5.15 shows the results of k_h before the EO consolidation phase. Based on the results, k_h decreases as the void ratio decreases and k_h varies in the range of 2.76×10^{-9} to 8.24×10^{-9} m/s, depending on the void ratio of the soil before the EO consolidation phase.
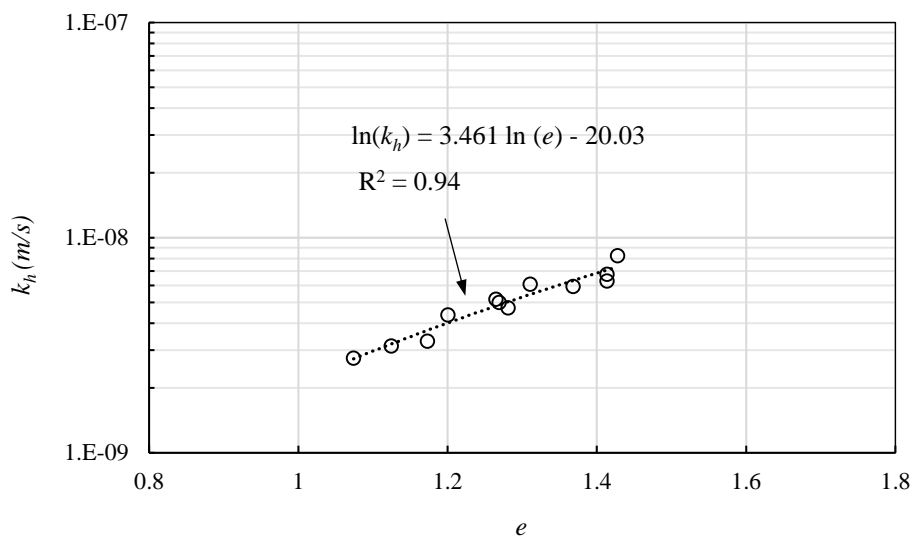
Fig. 5.15 Hydraulic permeability before EO consolidation

In addition, a unique equation can be fitted to the experimental results with correlation factor of $R^2=0.94$ as:

$$\ln(k_h) = 3.46\ln(e) - 20.03 \tag{5.5}$$

This equation can be used to predict the k_h of kaolin clay at various void ratios before the EO consolidation. The effect of EO consolidation on k_h was also investigated by measuring the k_h after EO consolidation phase. To achieve this, Eq. 5.4 was used. k_h measured after EO consolidation phase is shown against the predicted k_h before EO in Fig. 5.16.
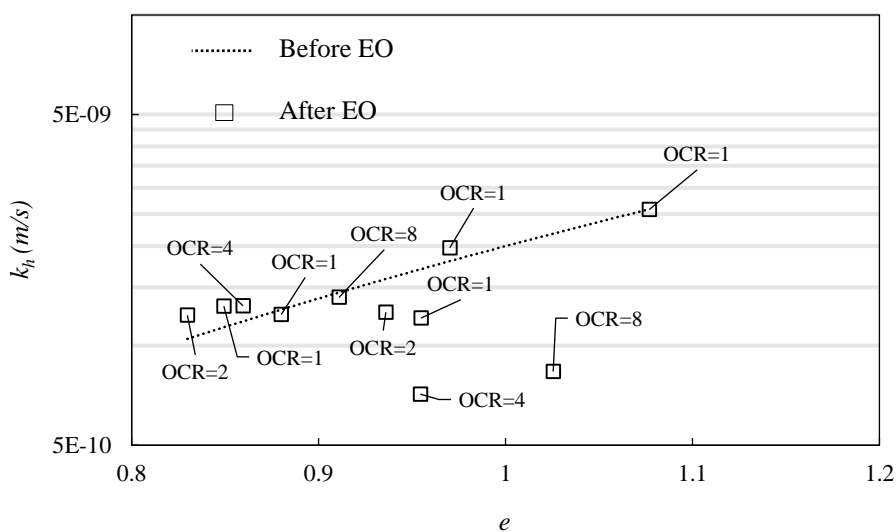
Fig. 5.16 Hydraulic permeability before and after EO consolidation

The values of k_h before and after EO consolidation are summarised in Table 5.3. To quantify the difference between k_h before and after EO consolidation, $\Delta k_h\%$ is used, which is defined as:

$$\Delta k_h\% = \frac{|k_{h1} - k_{h2}|}{k_{h1}} \times 100\%$$

(5.6)

where k_{h1} is the predicted hydraulic permeability before EO consolidation and k_{h2} denotes the measured hydraulic permeability after EO consolidation process.

Table 5.3 Comparison of hydraulic permeabilities before and after EO consolidation

Test No	Initial Void ratio	OCR	k_{h1} (m/s)	k_{h2} (m/s)	$\Delta k_h\%$
1	1.07	1	2.52×10^{-09}	2.6×10^{-09}	3
2	0.97	1	1.71×10^{-09}	2×10^{-09}	16
3	0.95	1	1.61×10^{-09}	1.2×10^{-09}	25
4	0.85	1	1.05×10^{-09}	1.3×10^{-09}	24
5	0.88	1	1.19×10^{-09}	1.2×10^{-09}	0.8
6	0.94	2	1.49×10^{-09}	1.3×10^{-09}	12
7	0.83	2	1×10^{-09}	1.2×10^{-09}	20
8	0.95	4	1.61×10^{-09}	7.1×10^{-10}	56
9	0.86	4	1.1×10^{-09}	1.3×10^{-09}	15
10	1.03	8	2.1×10^{-09}	8.4×10^{-10}	60
11	0.91	8	1.35×10^{-09}	1.4×10^{-09}	5

In the case of NC soil, k_h after EO shows a difference of 0.8% to 25% while the difference for OCR=2 is between 12% to 20%. These values imply that in NC soil and in soil with OCR=2, the value of k_h before EO consolidation can be used to represent the hydraulic permeability of the sample. However, a maximum of 25% deviation should be expected in some points after EO consolidation. In the case of soil with OCR > 2, a higher level of deviation in k_h of post-treated soil should be expected. For example, in the case of OCR= 4 a deviation of 15% to 56% while in OCR=8, 5% to 60% difference were observed. The difference in the value of k_h between pre- and post-treated soil can be attributed to the effect of the collective electrochemical processes on the soil. The electrochemical effects are mainly the variation in the pH of the soil and gas generation at the cathode vicinity, which were discussed in Chapter 2.

5.5.4 EO permeability (k_e)

As discussed earlier, as a result of the movement of the hydrated ions under the influence of the applied electric potential difference, a drag force is induced in the free water adjacent to the hydrated ions. The developed drag force in the soil body leads to suction and consequently a negative pore water pressure. The level of induced drag force depends on k_e. In addition, the higher level of k_e in a soil, assuming constant k_h, implies more hydrated ions have moved from the anode to the cathode and, consequently, more water molecules are transported. These, in turn, generate more drag force leading to higher level of negative pore water pressure being developed. The value of k_e is usually calculated using Casagrande's formula:

$$k_e = \frac{Q_e}{i_e A} \tag{5.7}$$

where Q_e is the electrically-induced water discharge in soil body. However, due to electrolysis that occurs at the electrodes, especially at the cathode, a noticeable part of the applied voltage is lost at the electrode, which impacts the effective parameter i_e and the calculation of Q_e.

In this study, the value of k_e was calculated considering C_{ve}. Similar to k_h, k_e can be calculated as:

$$k_e = C_{ve} \times \gamma_w \times m_v \tag{5.8}$$

Also:

$$m_v = \frac{a_v}{1 + e_0} \tag{5.9}$$

where e_0 is the initial void ratio. In addition, a_v denotes the coefficient of compressibility. Assuming linear relationship between effective stress (decrease in pore water pressure) and void ratio, a_v is defined as:

$$a_v = -\frac{\partial e}{\partial(\Delta \sigma')} \tag{5.10}$$

Also, assuming the effective stress applied to soil during the electro-osmosis consolidation is equal to the developed negative pore pressure, Eq. 5.10 can be written as:

$$a_v = \frac{\partial e}{\partial u} \tag{5.11}$$

Based on Esrig's theory (Chapter 2, Eq. 2.33):

$$\partial u = \frac{k_e}{k_h} \gamma_w V \tag{5.12}$$

where V is the effective voltage which, considering potential loss at electrodes, can be written as:

$$\partial u = \frac{k_e}{k_h} \gamma_w n(t) V \tag{5.13}$$

where n is the efficiency factor of applied voltage and is a function of time.

On the other hand, k_e can also be calculated from Casagrande's formula as:

$$k_e = \frac{Q_e}{\dfrac{n(t)V}{L} A} \tag{5.14}$$

By introducing Eq. 5.14 to Eq. 5.13:

$$\partial u = \frac{Q_e L \gamma_w}{A k_h} \tag{5.15}$$

Then by substituting Eq. 5.15 into Eq. 5.8, k_e can be calculated to be independent of the applied voltage:

$$k_e = C_{ve}\gamma_w m_v = \frac{C_{ve}k_h A\Delta e}{Q_e L(1+e_0)}$$

(5.16)

Fig. 5.17 shows the calculated k_e for the tested specimens. k_e varies within a limited range of 1.7×10^{-9} to 4.2×10^{-9} m^2/V·s, with average value of 3×10^{-9} m^2/V·s. These values are consistent with the ranges proposed by other researchers, that is between 1×10^{-9} to 1×10^{-8} m^2/V·s (Win et al. 2001; Mitchell and Soga 2005).
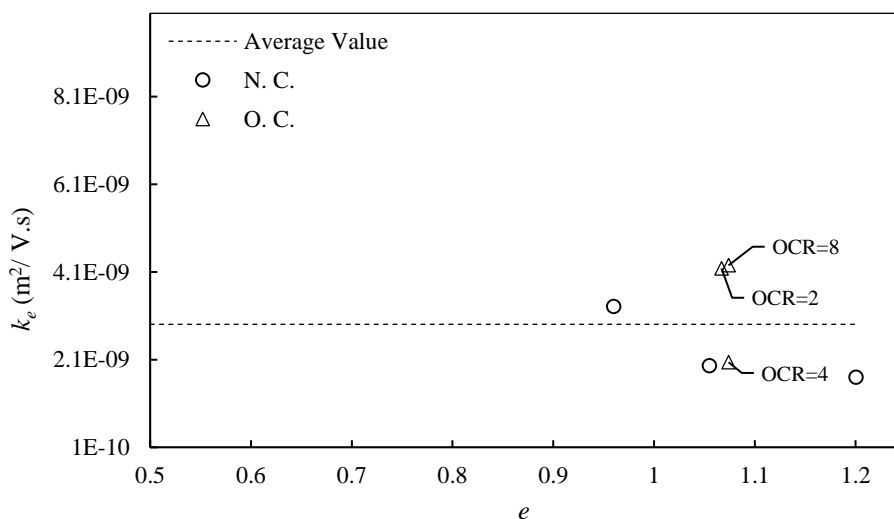
Fig. 5.17 Electro-osmosis permeability

5.5.5 Potential loss at electrodes (electrolysis effects)

As discussed in Section 2.5.6, during the EO consolidation various electrochemical processes lead to electrolysis and consequently gas generation in the soil-electrode vicinity. Due to the presence of generated gases, high-resistivity layers are formed in the soil-electrode interfaces. To consider this effect, the soil body was divided into two zones: (1) high-resistivity zones which appear in the soil-electrode vicinity due to gas generation; and (2) actual resistivity section (soil body). The defined zones are shown in Fig. 5.18.
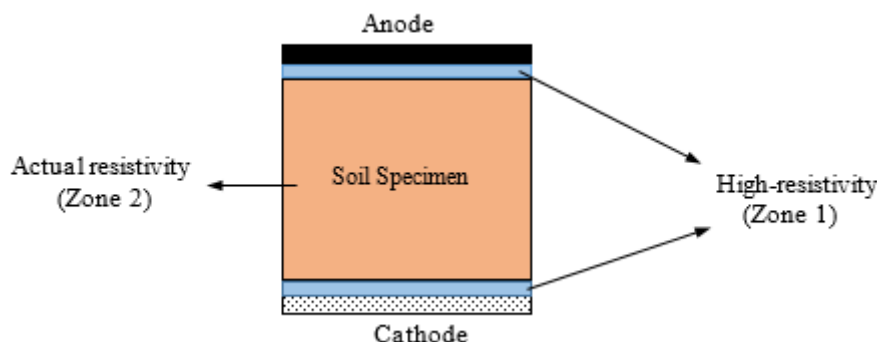
Fig. 5.18 Schematic of various resistivity zones in the soil body

The extent of Zone 1 is mainly a function of soil type, electrode materials and level of applied voltage (Zhuang and Wang, 2007; Wu et al. 2015) however further research is required to accurately determine the thickness of Zone 1. Because of high resistivity, a considerable portion of the applied voltage is lost in Zone 1. Therefore, the effective voltage received by the soil body is less than the applied voltage and the following relationship is valid:

$$V_{app} = V_{loss} + V_{eff}$$
(5.17)

where V_{app}, V_{loss} and V_{eff} are the applied, lost and effective voltages, respectively.

Jeyakanthan et al. (2011) experimentally verified that the effective voltage is independent of the stress level and level of applied voltage. However, the level of observed effective voltage depends on the soil-electrode materials (Jeyakanthan et al. 2011, Mohamedelhassan, 2009). In addition, Bjerrum et al. (1967) found that the measured effective voltage in EO consolidation varied from 75% to 45% depending on the duration of treatment in the field. However, there is no evidence that the same trend can be observed for the potential loss in the laboratory. Similarly, in the case of the current EO tests, the potential losses at the soil-electrode vicinity can be assumed to be independent from the preconsolidation pressure and the level of applied voltage. However, it is a function of time and soil-electrode material. Therefore, by knowing the potential loss for the current case during EO consolidation, the value of V_{eff} can be calculated as a function of time, considering constant applied electric potential.

The potential loss at soil-electrode interfaces (Zone 1) is measured experimentally during EO consolidation phase, using the apparatus shown in Fig. 5.1, along with the modified ring, as depicted in Fig. 5.4. Fig. 5.19 shows the time-dependent measured voltages at various locations

for 15 hours of voltage application. The locations and effective voltages are shown in normalised form where:

$$\text{Normalised distance from anode} = \frac{\text{distance from anode}}{L} \qquad (5.18a)$$

and

$$\text{Normalised effective voltage} = \frac{\text{effective voltage}}{V_{applied}} \qquad (5.18b)$$
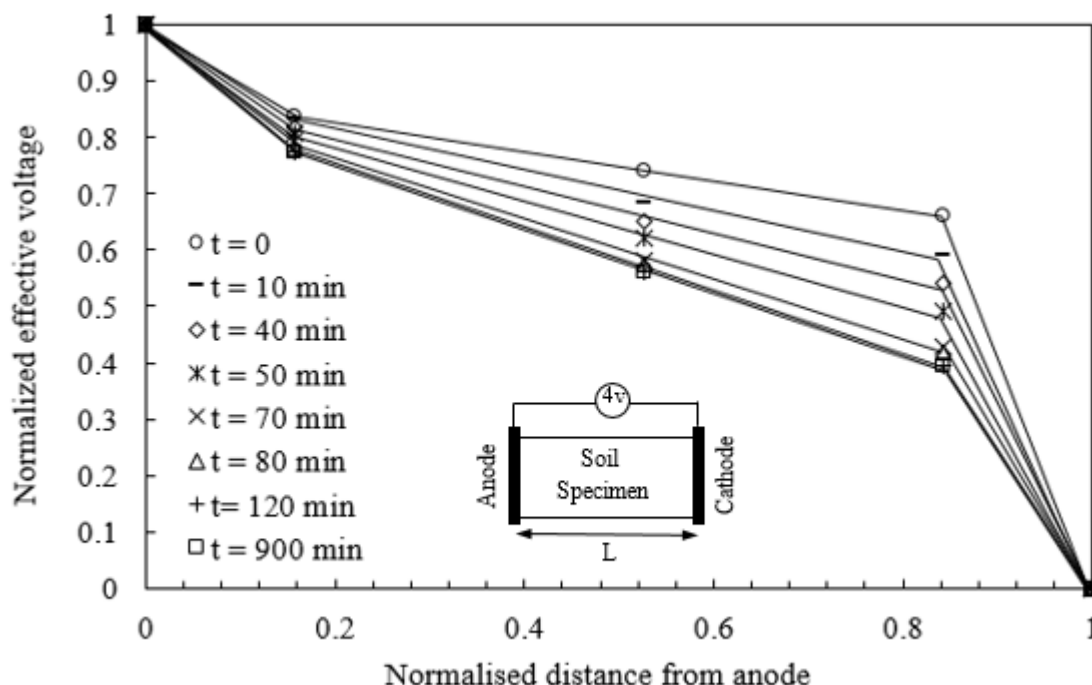
Fig. 5.19 Voltage profiles across soil specimen at various elapsed time

By choosing bronze as anode material, negligible potential loss was observed at the anode side. However, a time-dependent potential loss was measured at the stainless-steel cathode. Before the start of voltage application ($t = 0$), approximately 0.37 potential loss was measured at the cathode. In fact, in the absence of voltage application, no chemical process takes place and therefore, the observed potential loss can be attributed to the loose contact between the cathode and soil body. The rate of potential loss at the cathode is higher in first hour of voltage

application. The level of potential loss increased from 0.3 to approximately 0.6 in two hours. Then, from $t = 120$ min to $t = 900$ min, the level of potential loss is maintained at approximately constant value.

Based on the measured voltages shown in Fig. 5.18 the efficiency factor (n) is calculated and presented in Fig. 5.20, where

$$n = \frac{V_{effecive}}{V_{applied}} \qquad (5.19)$$
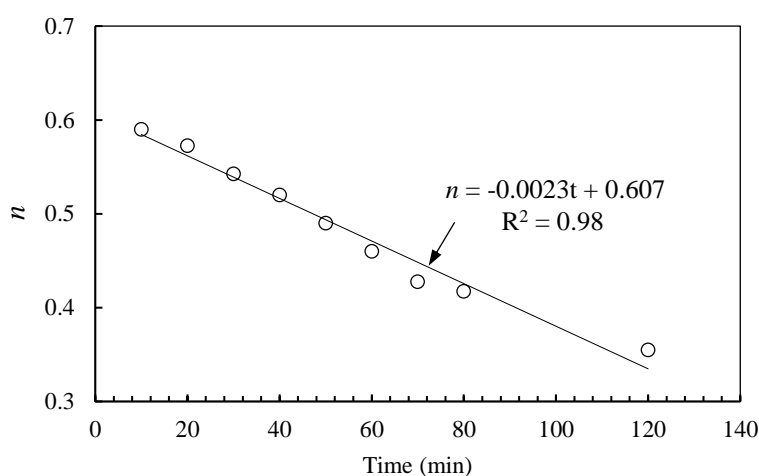
Fig. 5.20 Time-dependent efficiency factor

The efficiency factor over time shows a linear trend with correlation factor of R^2=0.98. The efficiency factor lies in the range of 0.35 to 0.6 during the EO consolidation. Jeyakanthan et al. (2011) found that, on average, 60% of the applied voltage is effective (n=0.6). In addition, Bjerrum et al (1967) observed 45% to 75% of potential drop in the field, which can be translated to globally $n = 0.5$ (Lefebvre and Burnotte, 2002). These results are more or less in the same range (considering approximately $n = 0.5$ in the current case). However, as the potential loss varies with time, it should be investigated during the EO consolidation and the average value may not be capable of showing an accurate picture of the potential loss at the electrodes during EO consolidation.

5.6 Summary

A new electric oedometer cell was designed, fabricated and tested in the laboratory. Using this cell, high levels of load and voltage were applied. The effect of electric potential gradient on the soil was investigated at various stress levels and OCR. The compression index of the soil before and after the EO consolidation remained approximately constant. However, the swelling index increased after EO consolidation compared to that before voltage application.

In addition, the coefficient of consolidation during EO consolidation (C_{ve}) was approximately ten times lower than that during hydraulic consolidation (C_v). Moreover, the EO process had a limited effect on C_v. However, the hydraulic permeability of the soil depended on the void ratio and the application of voltage has limited effect on hydraulic permeability of the soil. It was noted that the average value of 3×10^{-9} m^2/V·s was measured as the EO permeability of the New Zealand kaolin clay. Finally, the potential loss at the bronze anode was found to be negligible. However, the potential loss at the cathode was time-dependent. A maximum of 60% potential loss has been recorded after two hours at the cathode vicinity.

6 ELECTRO-OSMOSIS CONSOLIDATION: NUMERICAL MODELLING

6.1 Introduction

In parallel with the experimental investigation of EO consolidation, numerical modelling can be used to extend the EO consolidation to various situations. In addition, an accurate numerical model can be used as a powerful tool to design an efficient EO consolidation scheme in the field. However, the available EO consolidation models are not popular in geotechnical engineering. This can be attributed to the following drawbacks of available EO models:

- The effect of C_{ve} is neglected in all models;
- The effect of electrical resistivity of soil is neglected in majority of the proposed models; and
- The electrochemical effects which lead to potential loss at electrodes are neglected in the EO models

As discussed previously, the coupled hydraulic and electrical governing equation for EO consolidation is given by

$$\frac{\partial^2 u_e}{\partial y^2} + \frac{k_e \gamma_w}{k_h} \frac{\partial^2 V}{\partial y^2} = \frac{1}{C_v} \frac{\partial u_e}{\partial t}$$

(6.1)

The maximum negative pore water pressure developed in the soil body highly depends on the ratio of k_e/k_h and the level of the applied effective electric potential gradient. The latter parameter is governed by the soil and soil-electrode interface resistivity. In addition, the rate of consolidation process is controlled by the coefficient of consolidation during the EO process. Finally, the electrical resistivity of soil, which is varying with the void ratio, controls the voltage distribution in the soil body. Therefore, the electrical resistivity of soil needs to be incorporated in the EO model. However, these parameters are neglected in the current available models. Table 6.1 shows a summary of the parameters used to model the EO consolidation of soils in the previously developed EO models. Apart from the neglected parameters, the majority of these parameters are assumed or adopted from the literature or measured in the laboratory using multiple cells which impose errors to the EO model analysis. Therefore, to accurately model the EO consolidation, the important parameters affecting EO consolidation should be accurately measured and incorporated in the EO model.

In this chapter, a numerical EO consolidation model is developed using coupled flow theory and conservation of electric charge law. Then, the contributing parameters to EO consolidation are fully investigated and discussed. The governing equations implemented in the model are solved over the desired boundary using FlexPDE software. Finally, the model is verified in various soil situations, including different preconsolidation pressures and stress histories, and the results are discussed.

Table 6.1 Parameters utilised by various researchers to model EO consolidation

Researcher/s	Parameters					
	k_e	k_h	σ	Voltage loss	C_v	C_{ve}
Esrig (1968)	Constant	Constant	×	×	Constant	×
Wan and Mitchell (1976)	Constant	Constant	×	×	Constant	×
Shang (1998)	Constant	Constant	×	×	Constant	×
Su and Wang (2003)	Constant	Constant	Constant	×	Constant	×
Rittirong and Shang (2008)	Constant	Constant	×	Constant	Constant	×
Jayakanthan et al. (2011)	Constant	Void ratio-dependent	Constant	Constant	Constant	×
Hu et al. (2012)	Time-Dependent	Time-Dependent	Time-Dependent	×	Constant	×
Yuan and Hicks (2015)	Constant	Constant	Constant	×	Constant	×

6.2 Proposed EO model

The proposed EO model comprised of two parallel partial differential equations. The first part was a modification of Eq. 6.1. As discussed in Section 5.5.2, C_{ve} controls the rate of EO consolidation and C_v governs the rate of consolidation during hydraulic loading. Therefore, to model EO consolidation, C_{ve} should be used. In the second part, as discussed in Section 5.5.4, the potential loss at soil-electrode interface is a function of time, thus time-dependent voltage was incorporated in the EO model. Therefore, the first equation was defined as:

$$\frac{\partial^2 u_e}{\partial y^2} + \frac{k_e \gamma_w}{k_h} \frac{\partial^2 (Vf(t))}{\partial y^2} = \frac{1}{C_{ve}} \frac{\partial u_e}{\partial t} \tag{6.2}$$

The effect of electrical resistivity of soil was incorporated into the EO model through the conservation of electric charge as:

$$-\nabla \cdot j = C_p \frac{\partial V}{\partial t} \tag{6.3}$$

where j is current flux and C_p is soil capacitance. j is also given by

$$j = \sigma \cdot \nabla V \tag{6.4}$$

These equations were incorporated into a single EO model and u_e was solved simultaneously, over the desired boundaries, using FlexPDE software.

6.3 Parameter identification and numerical simulation

The proposed EO governing equations were solved over the boundaries similar to the tested specimens described in Chapter 5. The details of the experimental EO tests were outlined in Section 5.4. To solve the proposed partial differential equations over the boundaries similar to the experimental tests, the contributing parameters, namely k_e, k_h, C_{ve}, $f(t)$ and ρ, need to be identified for each specimen.

As discussed in Section 5.5.3, k_e varied within a limited range and the average value of 3×10^{-9} m^2/V·s can be assumed. In addition, k_h depends on the void ratio of the soil as shown in Fig. 5.14. Therefore, for each test a k_h value, corresponding to the void ratio of the soil before EO consolidation phase, was used. The parameter C_{ve} was measured for each specimen in Chapter 5 (Section 5.5.2 and shown in Fig. 5.13) and used in the numerical tests. In addition, the

measurements of potential loss at the soil-electrode from Section 5.5.4 were used to identify *f(t)*. To achieve this, the voltages measured at 4 points were considered: V_{anode} = 4 V, $V_{cathode}$ = 0 and the voltage midway between the electrodes and close to the cathode, as shown in Fig. 6.1. The voltages midway between the electrodes and close to the cathode vary with time. To identify the time-dependent equations for these two voltages, two new parameters, namely; n_1 and n_2, are defined as:

$$n_1 = \frac{V_1}{4}$$

$$n_2 = \frac{V_2}{4}$$

(6.5)
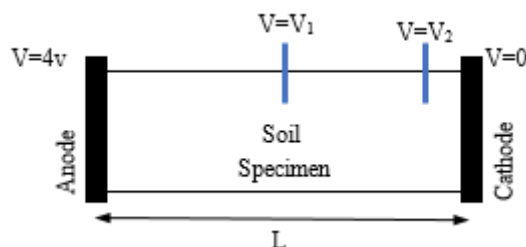
Fig. 6.1 Schematic diagram of utilised voltages in the numerical investigation of EO consolidation

These parameters show the efficiency factor of the applied voltages at various locations. By knowing these parameters, the exact voltage profile can be defined across the soil specimen. The parameters n_1 and n_2 were identified experimentally based on the voltage measurements during EO consolidation phase. The details of the conducted tests and the measurement technique for V_1 and V_2 were discussed in Section 5.5.4. Fig. 6.2 shows the equations for n_1 and n_2 as functions of time. These equations were then implemented into the numerical model for each soil specimen to achieve the actual voltage profile developed within the soil.

Finally, for the parameter ρ which depends on many factors, the results from Chapter 3 were used considering the soil volumetric water content. A summary of the parameters used for the numerical model is provided in Table 6.2.

Table 6.2 Summary of utilised parameters in numerical modelling of EO consolidation

Parameter	Assumptions	Reference section
k_e	Constant	5.5.4
k_h	Void ratio-dependent	5.5.3
C_{ve}	Void ratio-dependent	5.5.2
$f(t)$	Time-dependent	6.3
ρ	Void ratio-dependent	3.6

The identified parameters were adopted in the proposed EO model for each soil type. Then, the equations were solved simultaneously for u_e and the results were verified using the experimental results.
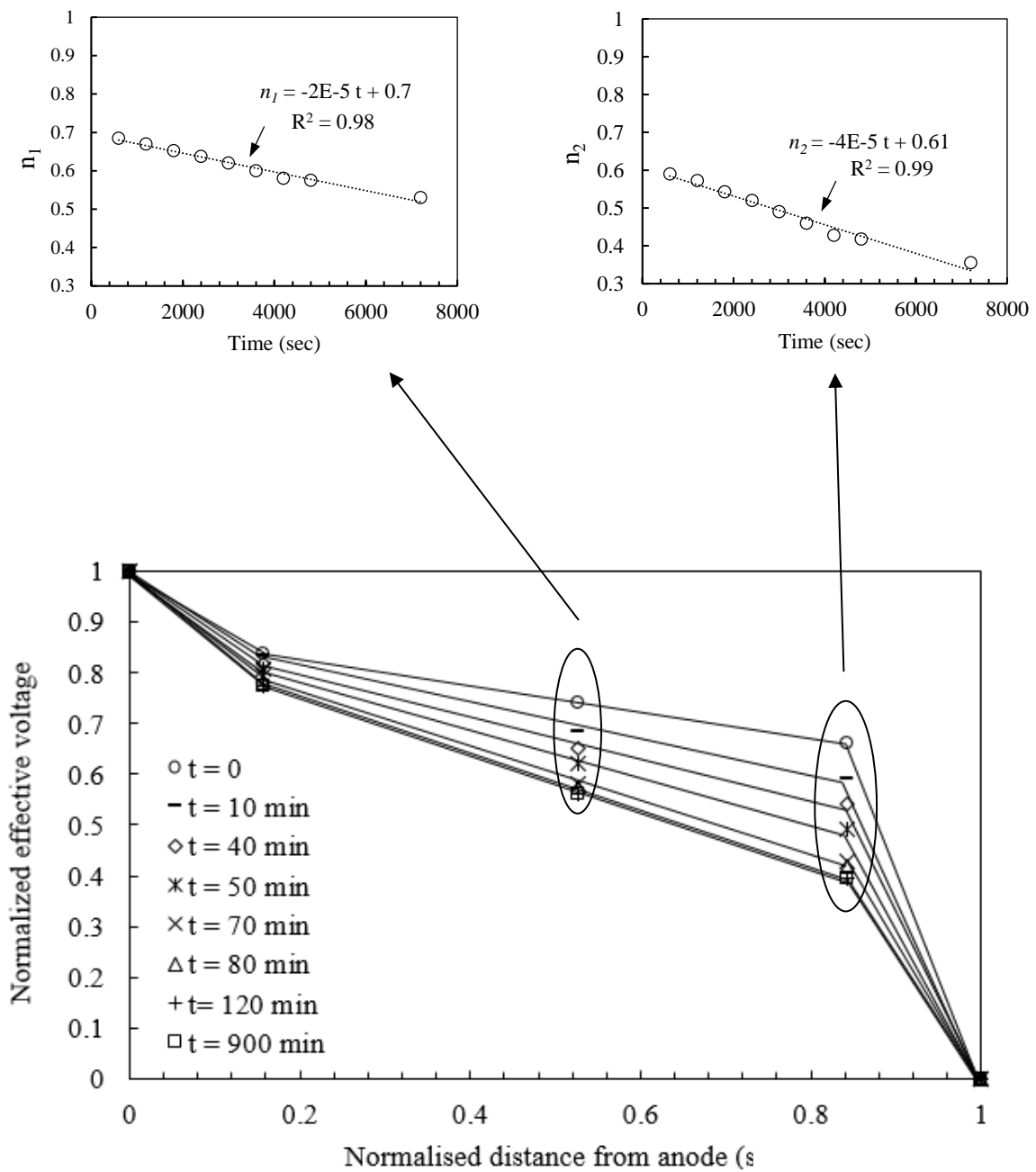
Fig. 6.2 Electric potential profiles utilised in numerical investigation

6.4 Validation of the model

6.4.1 Validation against experimental tests

The numerical tests were validated using all experimental data presented in Chapter 5. To achieve this, the pore water pressure was computed during EO consolidation for each soil sample at various locations. Then, from the developed pore water pressure the temporal soil settlement was calculated and compared against experimental data. To calculate the soil settlement during EO consolidation, Terzaghi's theory was used, where the soil settlement can be determined by the following relationship:

$$\text{For NC soil:}\quad S_p = \frac{C_c H}{1+e_0}\log(\frac{\sigma_0'+\Delta\sigma'}{\sigma_0'})$$

$$\text{For OC soil:}\quad S_p = \frac{C_s H}{1+e_0}\log(\frac{\sigma_p'}{\sigma_0'}) + \frac{C_c H}{1+e_0}\log(\frac{\sigma_0'+\Delta\sigma'}{\sigma_0'})$$

(6.6)

H, e_0 and σ_0' are constant for a specific test and can be measured before the electric potential application. $\Delta\sigma'$ is the induced porewater pressure over the soil layer while σ_p' is the preconsolidation pressure. As the pore water pressure developed varies over the thickness of the specimen, the soil specimen was divided into smaller sublayers with constant thickness as thin as 0.19 mm (the thickness of the sublayers adopted was equal to the FlexPDE adaptive mesh) and Eq. 5.17 was modified into:

$$\text{For NC soil:}\quad dS_p = \frac{C_c H}{1+e_0}\log(\frac{\sigma_0'+\Delta\sigma'}{\sigma_0'})dy$$

$$\text{For OC soil:}\quad dS_p = [\frac{C_s H}{1+e_0}\log(\frac{\sigma_p'}{\sigma_0'}) + \frac{C_c H}{1+e_0}\log(\frac{\sigma_0'+\Delta\sigma'}{\sigma_0'})]dy$$

(6.7)

Then, the temporal developed pore water pressure was computed at each sublayer over the desired boundaries and the total soil settlement at a specific time was computed by integration of dS_p. For example, for specimen H-1, at $t = 600$ s, the developed pore water pressure was computed over the soil boundary in each soil element. Then the dS_p was calculated for each sublayer and finally integrated over the soil depth to find the settlement of the specimen at that particular time. This process was repeated for every time step for all tested specimens. Fig. 6.3 compares the experimental and numerical results. As the recorded settlements for M-8 soil is more or less similar to M-2 and M-4, they were not plotted in Fig. 6.3.
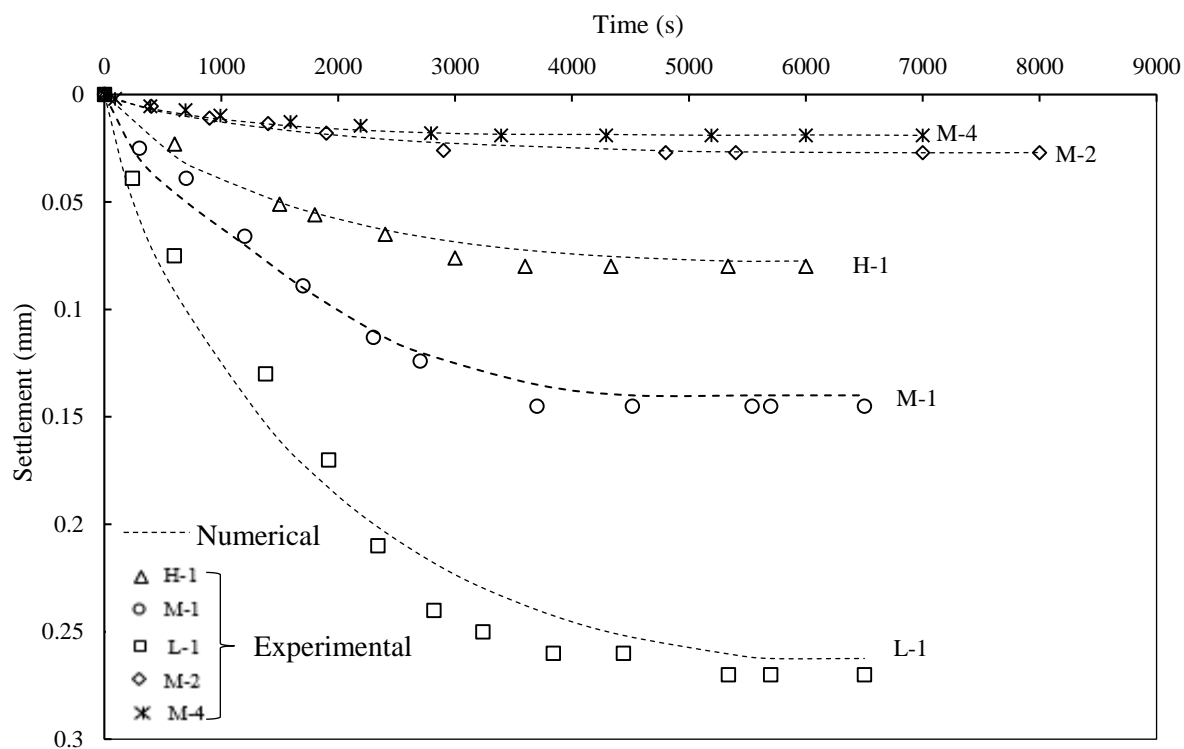
Fig. 6.3 Comparison of numerical soil settlements with experimental results

The level of accuracy of the proposed model was checked against the numerical results using Absolute Error (*AE*). Fig. 6.4 shows the box plots of *AE* during EO consolidation for each tested specimen. Comparing the numerical results with the experimental data, generally a median *AE* of less than 7% was observed for all specimens. Therefore, it can be said that good agreement was observed between the numerical model and experimental results.

In addition, a maximum of 25% *AE* was observed in few points (L-1 and M-1), all during the first $t = 600$ s of EO consolidation.
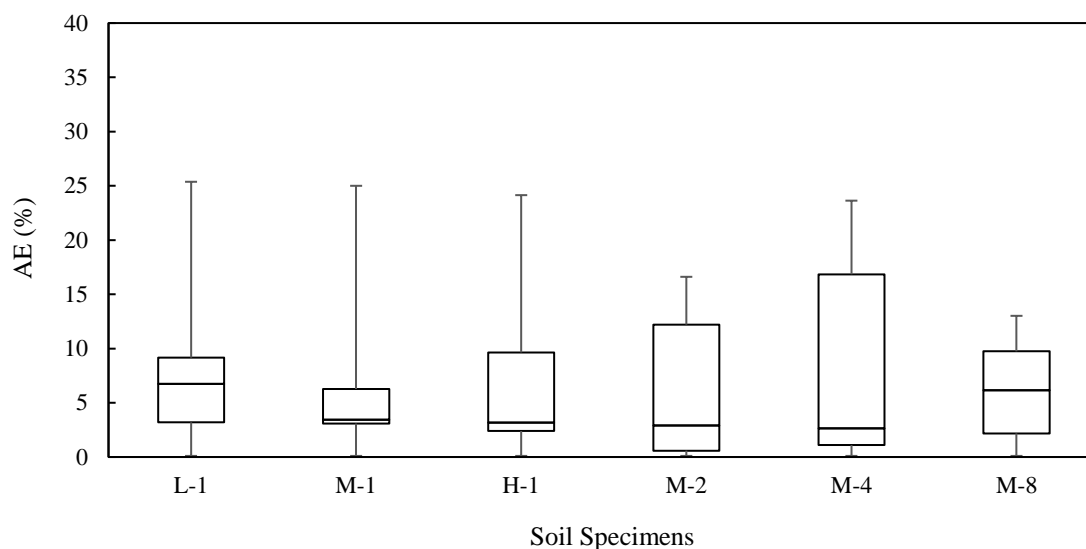
Fig. 6.4 Error between estimated and measured settlements during EO consolidation

The error during the first $t = 600$ s of consolidation can be due to the precision of the LVDT sensors, as the difference between experimental and numerical results are in the order of 0.001 mm. In addition, during the EO consolidation, parameters such as k_h, k_e, ρ and C_{ve} show some variations (as shown in Chapter 5), however they are assumed to be constant during EO consolidation; this may be another source of error.

Therefore, the implementation of the time-dependent (unsteady) potential loss at electrodes and the accurate distribution of the voltage across the electrodes will lead to an acceptable estimation of the developed pore water pressure and soil settlement.

6.4.2 Comparison with previous models

Generally, the EO governing equation, along with various assumptions and simplifications, was used to compute the negative pore water pressure during EO consolidation in the majority of previously developed popular models (Esrig 1968; Wan and Mitchell 1976; Shang 1998; Jayakanthan et al. 2011; Yuan and Hicks 2015). Then, using the computed negative pore water pressure, soil settlement and shear strength were estimated using various methods, such as Terzaghi's equation, Cam clay model, etc. (Jayakanthan et al. 2011; Yuan and Hicks 2015). These methods should be used with caution as the voltage application will affect the constants used in the models, such as the Cam clay model's friction constant (M) and Poisson's ratio (v),

and consequently the estimation of soil settlement and shear strength. This fact was neglected in the previous models and constant parameters were used before and after voltage application. However, the effect of voltage on the Terzaghi's parameters were investigated in Chapter 5 and this theory was used to estimate the soil settlement.

On the other hand, as noticeable amount of applied voltage was lost at the soil-electrode interface, assuming no potential loss during the EO consolidation process is not realistic. Therefore, a factor of efficiency of approximately 60% (i.e. 40% potential loss at soil-electrode interface) was proposed by various researchers for EO consolidation albeit independent from the level of applied electric potential gradient (Mohamedelhassan 2009; Jayakanthan et al. 2011). In addition, the applied potential gradient was assumed to be in steady state and with linear, spatial trend. However, it was concluded in Chapter 5 that the potential loss at soil-electrode vicinity and, consequently the applied electric potential gradient, is an unsteady parameter and its distribution is controlled by the electrical resistivity through the conservation of electric charge.

In addition, the hydraulic and EO coefficients of consolidation (C_v and C_{ve}) are quite different. Utilising C_v instead of C_{ve} is popular in many EO models (Wan and Mitchell 1976; Shang 1998; Jayakanthan et al. 2011; Yuan and Hicks 2015). Using C_v instead of C_{ve} leads to relatively accurate prediction of the maximum negative pore water pressure if no potential loss is considered; however, the rate of consolidation cannot be predicted accurately. As C_{ve} is smaller than C_v, using C_v leads to faster consolidation rate. Therefore, the negative pore water pressure cannot be estimated/extended accurately during consolidation in the field (Bjerrum et al. 1967; Lamont-Black et al. 2016).

The estimated soil settlements using the above-mentioned four assumptions are summarised in Fig. 6.5 for two sets of experimental data from the current research (M-1 and M-4). To achieve this, the initial negative pore water was computed using the EO governing equation (given by Eq. 6.1, but the proposed model used Eq. 6.4 instead) with assumptions similar to those adopted by various researchers. Then, the computed negative pore water pressure was substituted into the Terzaghi's theory (Eq. 6.6) to calculate the soil settlement in each case.
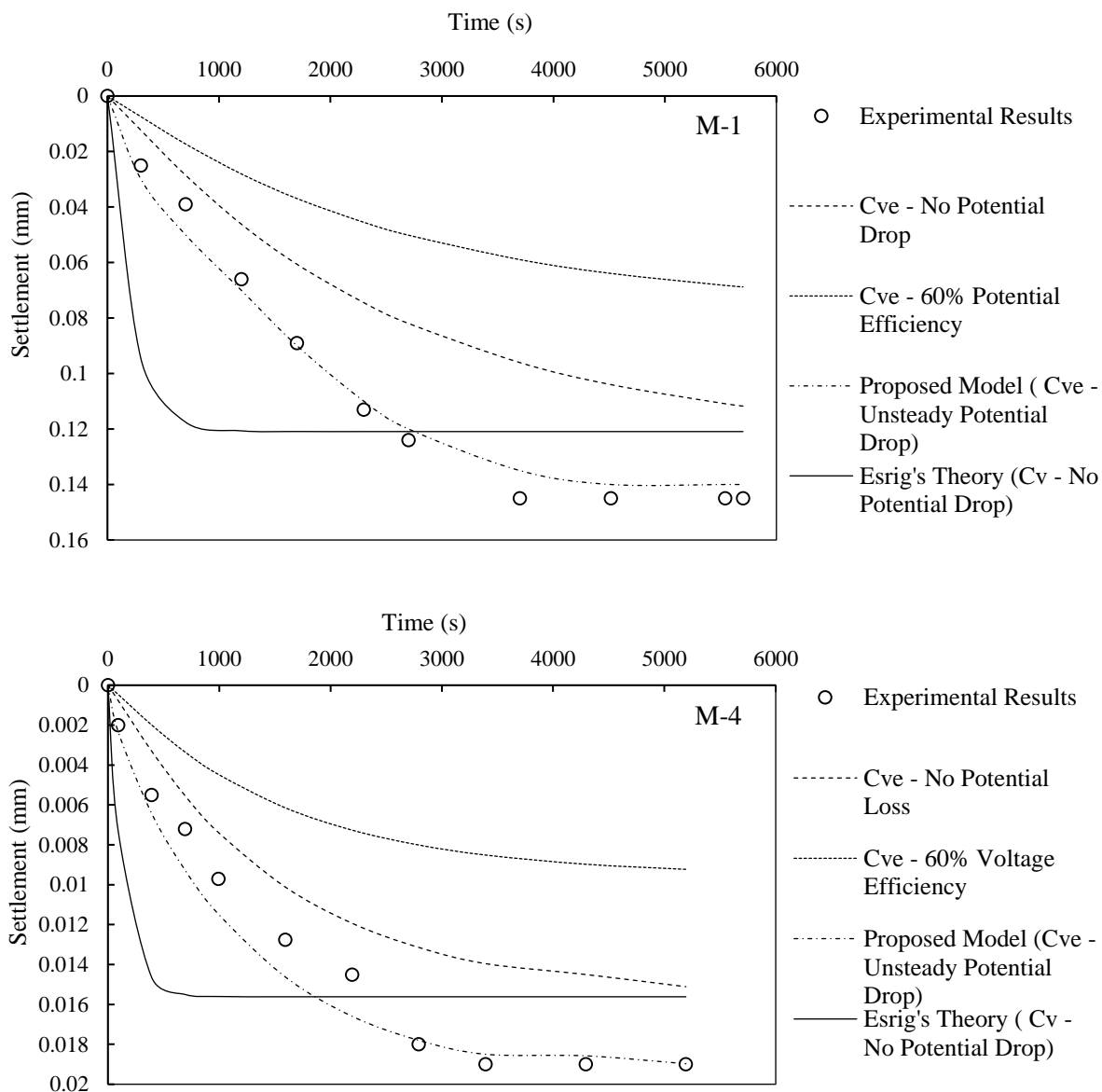
Fig. 6.5 Comparison between various assumptions in EO consolidation

By considering C_v and no potential loss (Esrig 1968; Wan and Mitchell 1976; Shang 1998; Yuan and Hicks 2015), the soil settlement was initially overestimated. However, this model slightly underestimated the final soil settlement. Considering C_{ve} and no potential drop, the estimated trend for the soil settlement is closer to the experimental data. Therefore, using C_{ve} instead of C_v improved the estimation of the negative pore water pressure and consequently the soil settlement. As can be observed from Fig. 6.5, the approach of using constant potential loss (Mohamedelhassan 2009; Jeyakanthan et al. 2011) and considering C_{ve} for coefficient of

consolidation shows similar trend as the case of no potential loss but it also obviously underestimates the soil settlement. Finally, the best results were achieved using realistic combination of C_{ve} and unsteady voltage profile considering the electrical resistivity of the soil.

6.5 Discussion of numerical results

6.5.1 Numerical pore water pressure development

Figs. 6.6 to 6.11 show the normalised developed pore water pressure (u/u_{max}) along with maximum negative pore water pressure developed at various time factors, for each experimental case considered in the current research. In part (a) of the figures, the unsteady trend of the potential drop at the cathode vicinity can be observed. At small time factors which indicate the start of EO consolidation, the potential loss at the cathode is minimal. Therefore, most of the applied voltage is effective at that location and the negative pore water pressure are greater than those at higher time factors. The generated negative pore water pressure draws the water from the anode to the cathode side. As drainage is provided at the cathode, the water is drained out and the pore water pressure is zero. On the other hand, the total overburden pressure is maintained constant. Therefore, the effective pressure increases in the soil (mostly at the vicinity of anode) and consolidation takes place. In addition, in response to the water movement from the anode to the cathode, a hydraulic head is developed at the cathode side. Because of the developed hydraulic gradient, the water moves from the cathode to the anode side. As the EO consolidation continues, the potential loss at the cathode increases and the effective voltage decreases. Therefore, the developed negative pore water pressure decreases with time at the cathode vicinity. This effect decreases the rate of water transport from the anode to the cathode, however the counter-flow from the cathode to the anode continuously occurs. The reduction in EO water flow and the increase in hydraulic flow continues until these flows become equal and the consolidation is completed. In this case, the pore water pressure becomes approximately linear as shown in Fig. 6.6 to Fig. 6.11 and the maximum generated negative pore water pressure remains constant (part b in Figs. 6.6 to 6.11).
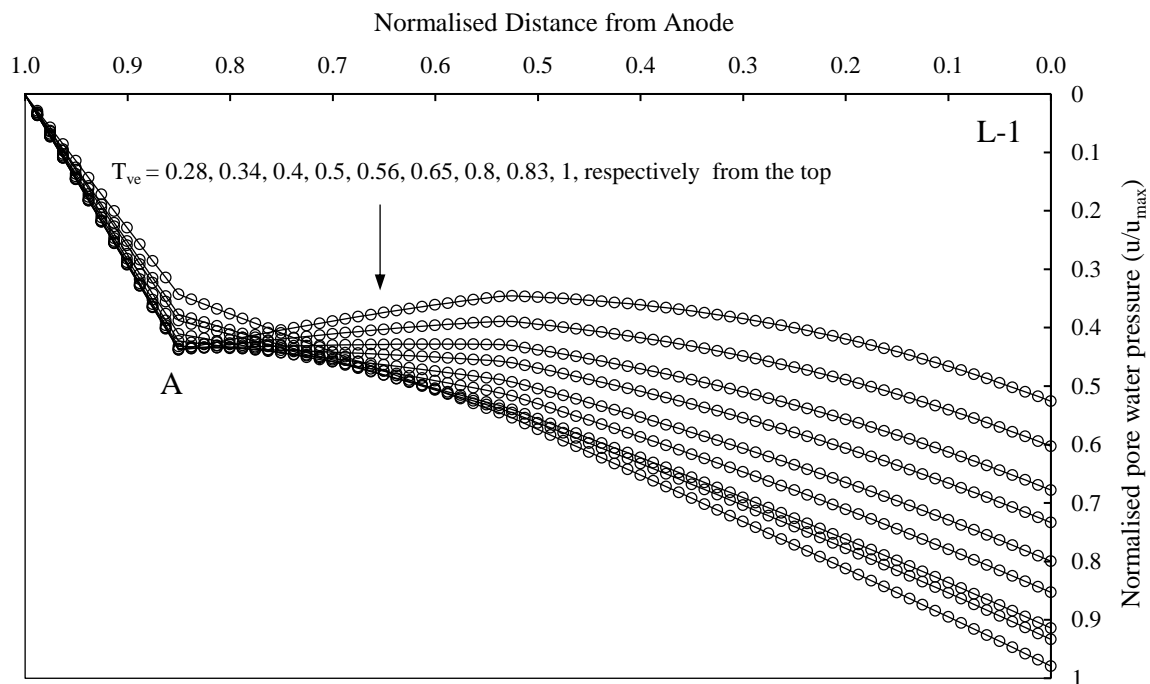
Normalised Distance from Anode

(a) Temporal and spatial variation of developed negative pore water pressure
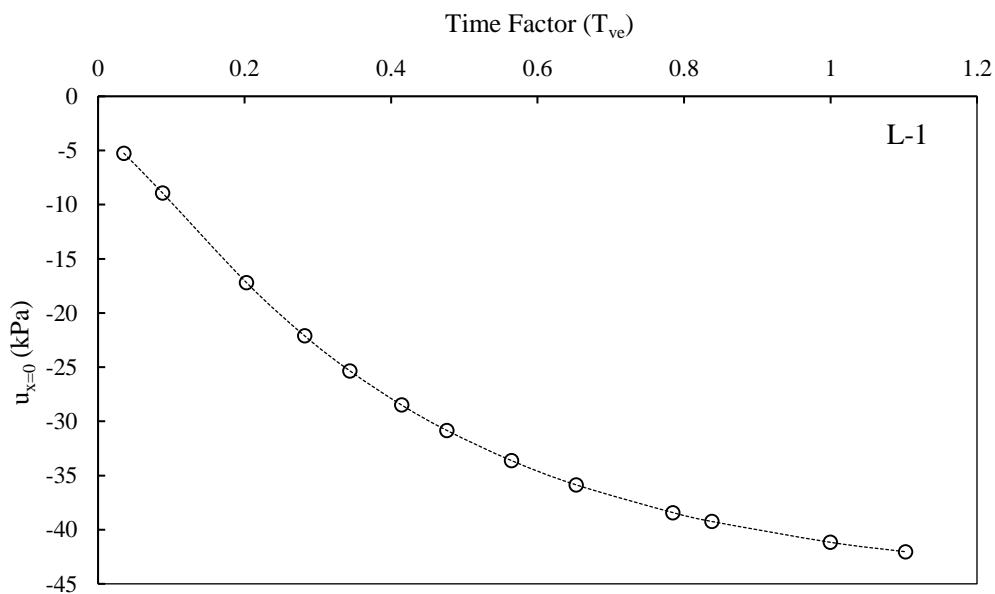
Time Factor (T_{ve})

(b) Negative pore water pressure development at the anode at various time factors

Fig. 6.6 Numerically simulated negative pore water pressure at various locations and time factors in soil L-1
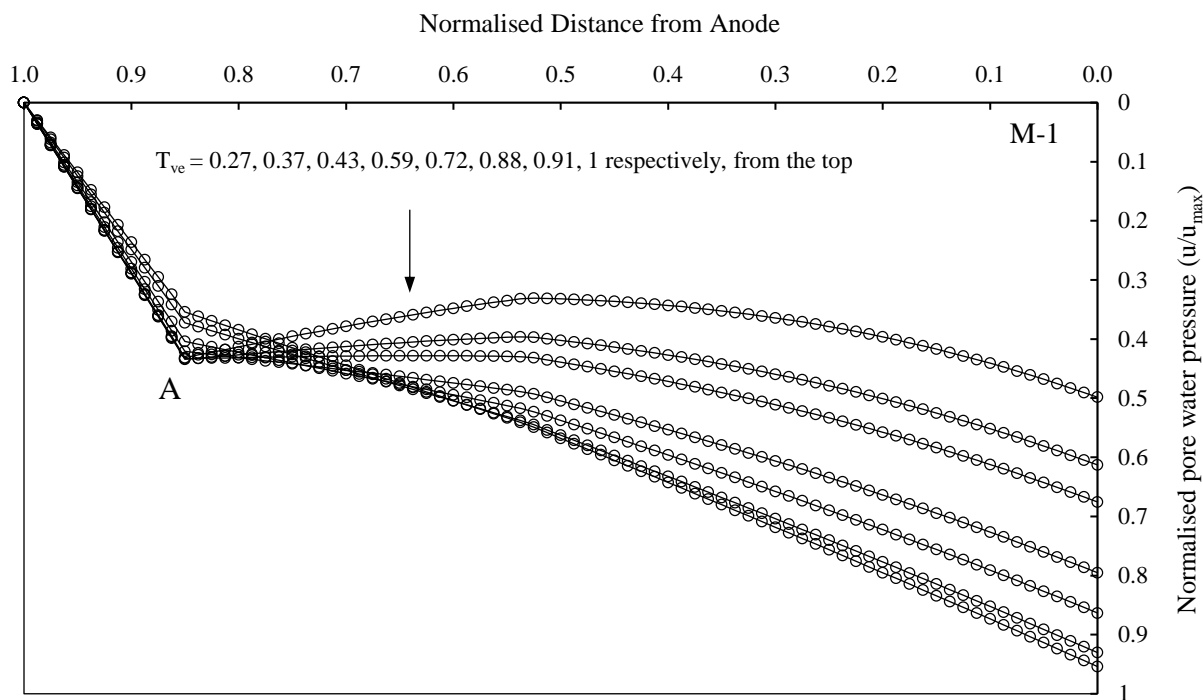
(a) Temporal and spatial variation of developed negative pore water pressure
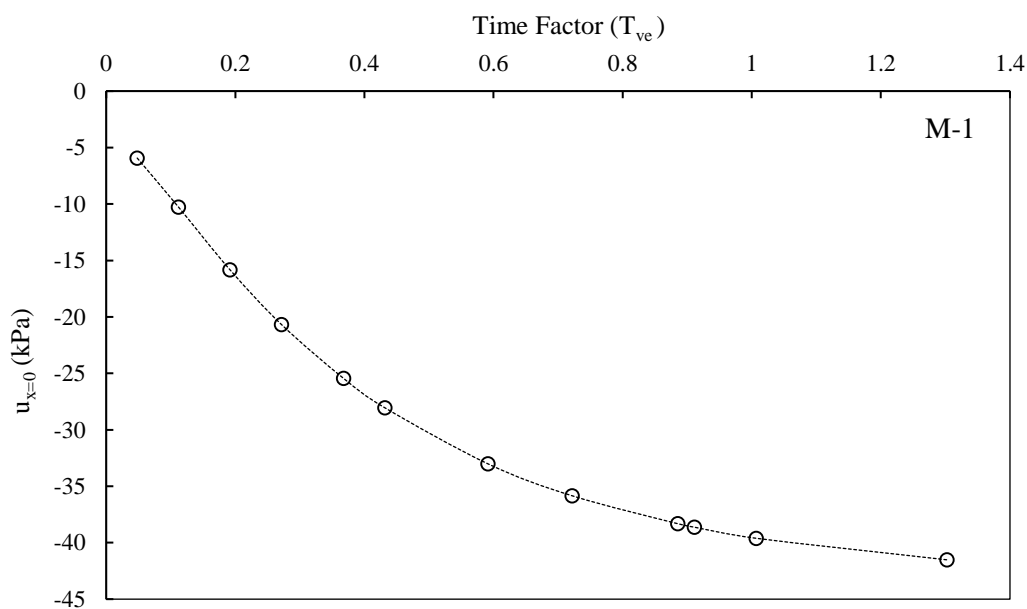
(b) Negative pore water pressure development at the anode at various time factors

Fig. 6.7 Numerically simulated negative pore water pressure at various locations and time factors in soil M-1
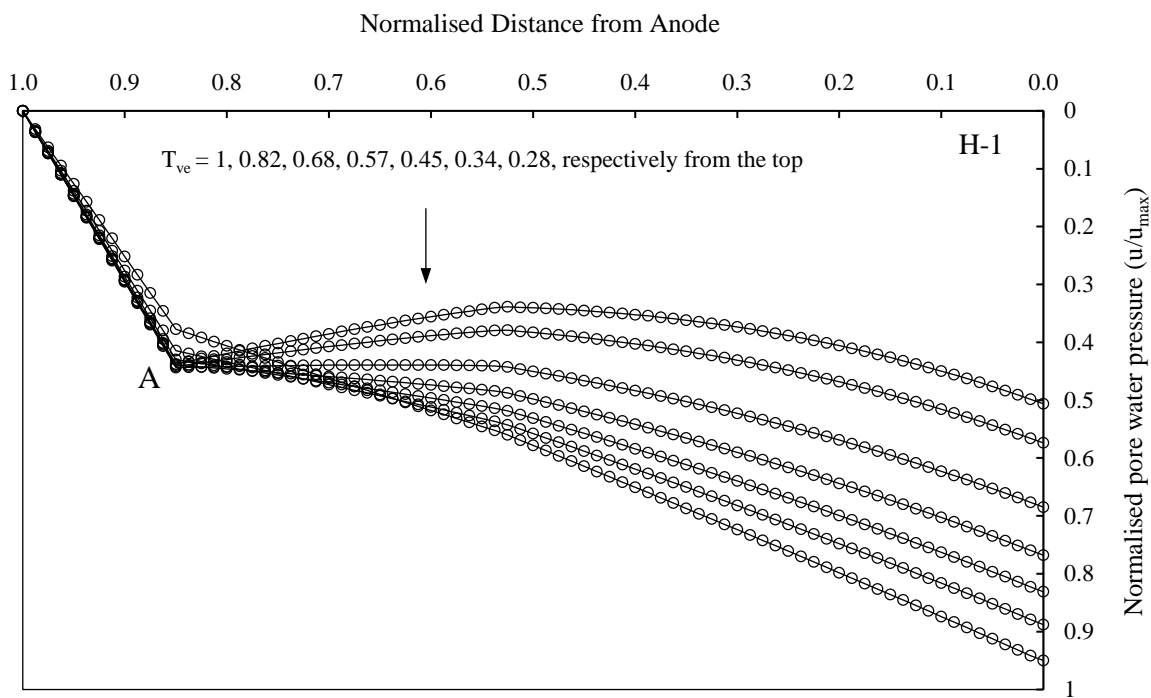
(a) Temporal and spatial variation of developed negative pore water pressure
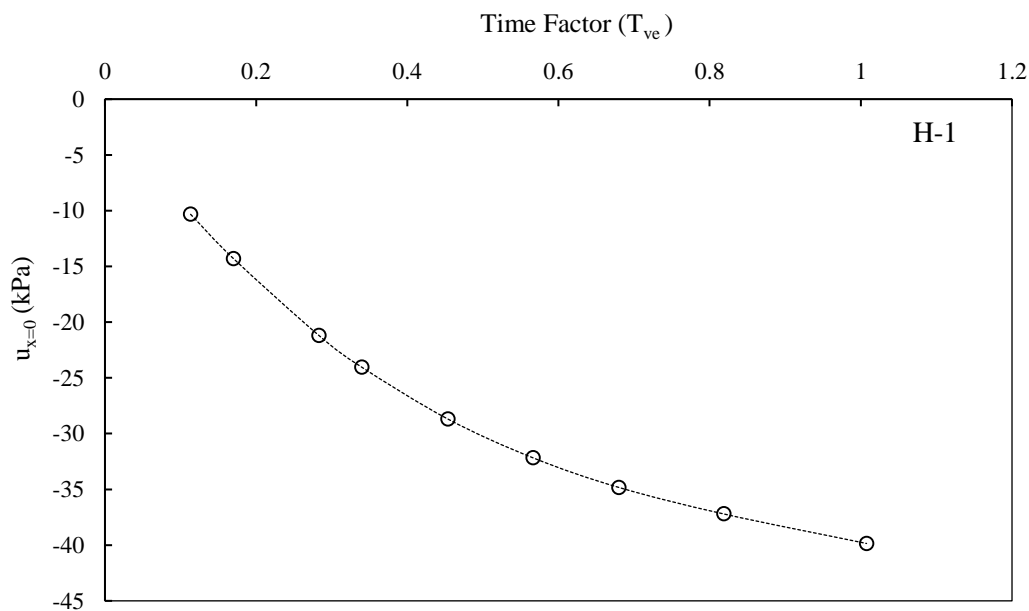
(b) Negative pore water pressure development at the anode at various time factors

Fig. 6.8 Numerically simulated negative pore water pressure at various locations and time factors in soil H-1
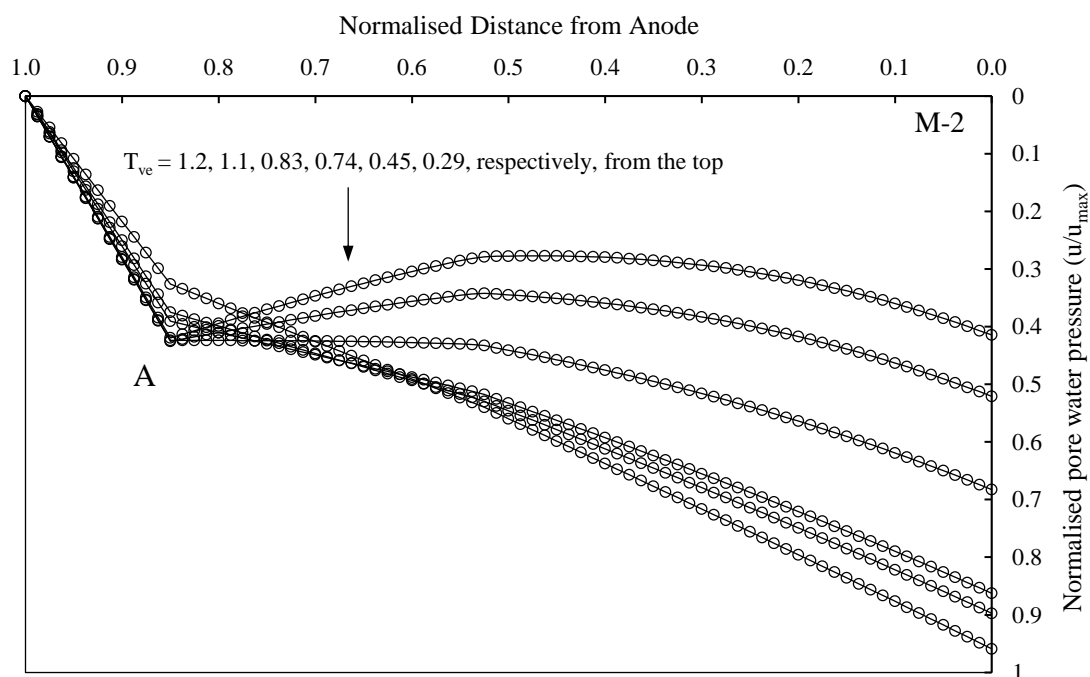
(a) Temporal and spatial variation of developed negative pore water pressure
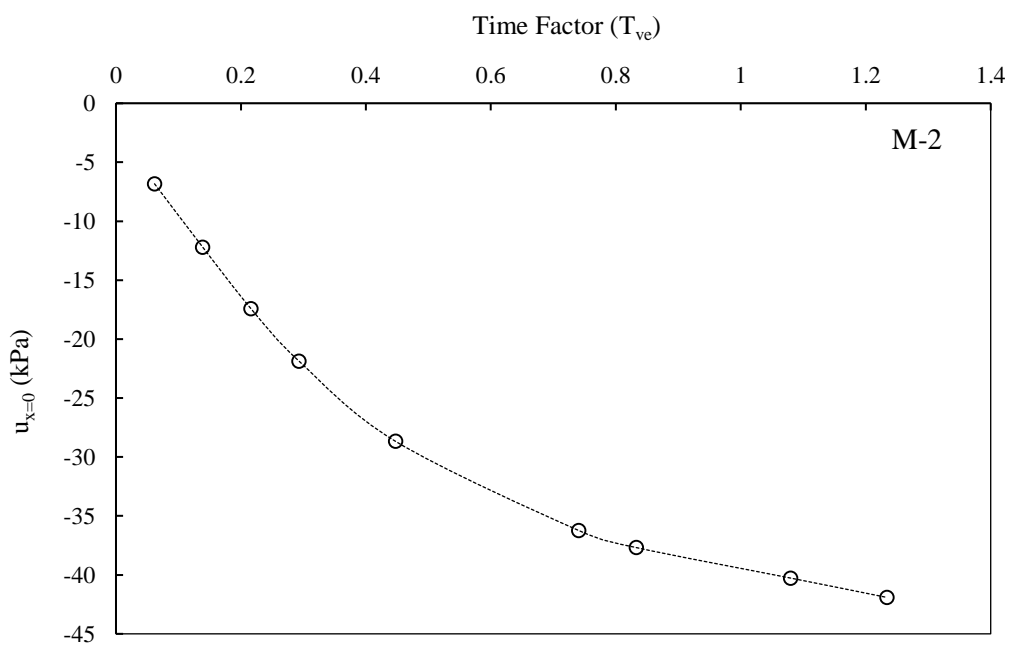
(b) Negative pore water pressure development at the anode at various time factors

Fig. 6.9 Numerically simulated negative pore water pressure at various locations and time factors in soil M-2
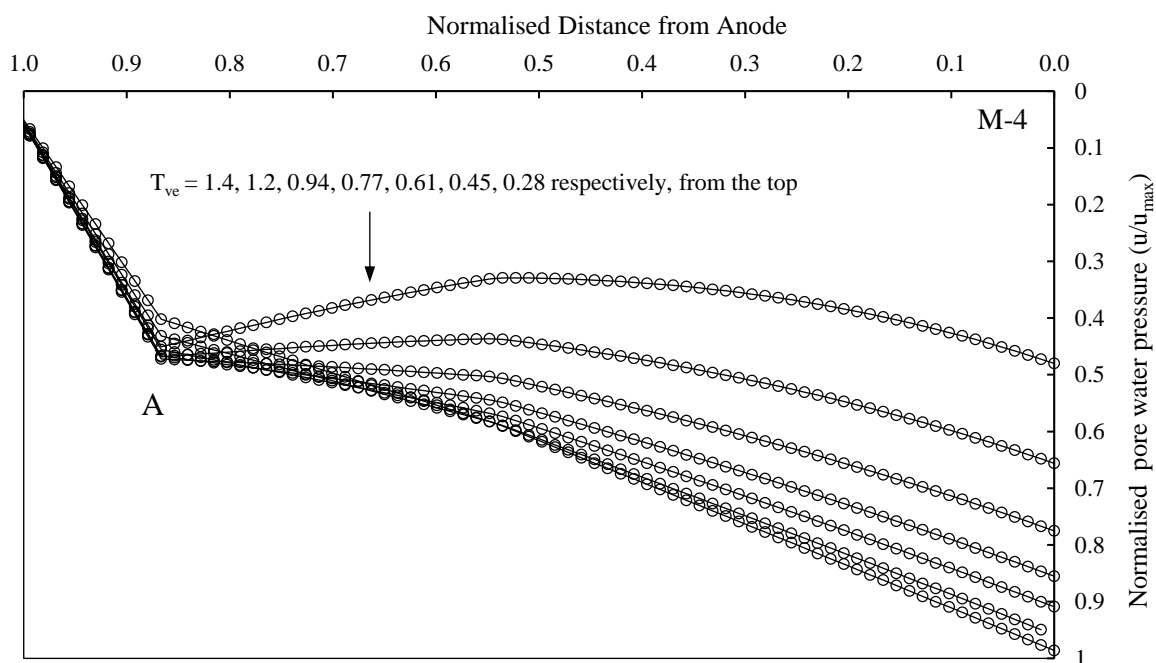
(a) Temporal and spatial variation of developed negative pore water pressure
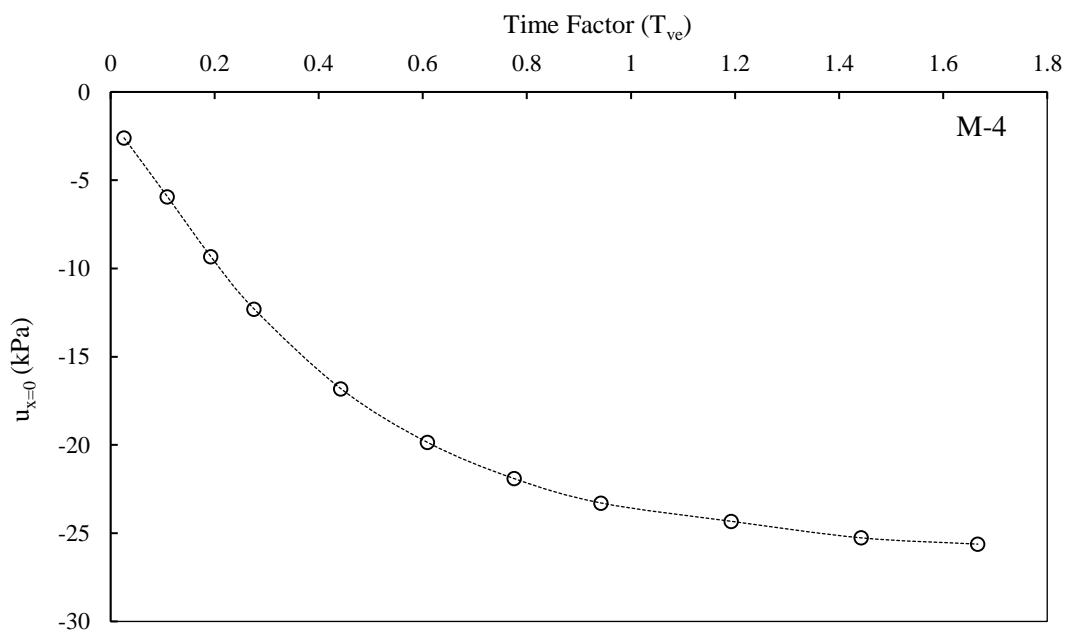
(b) Negative pore water pressure development at the anode at various time factors

Fig. 6.10 Numerically simulated negative pore water pressure at various locations and time factors in soil M-4
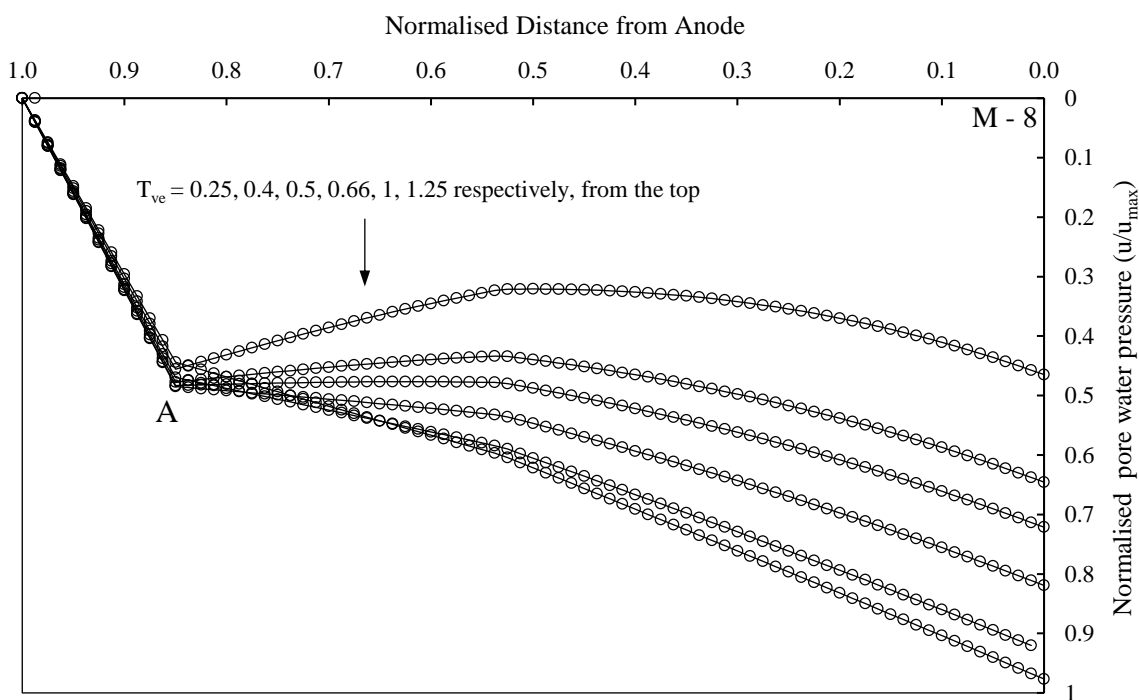
(a) Temporal and spatial variation of developed negative pore water pressure
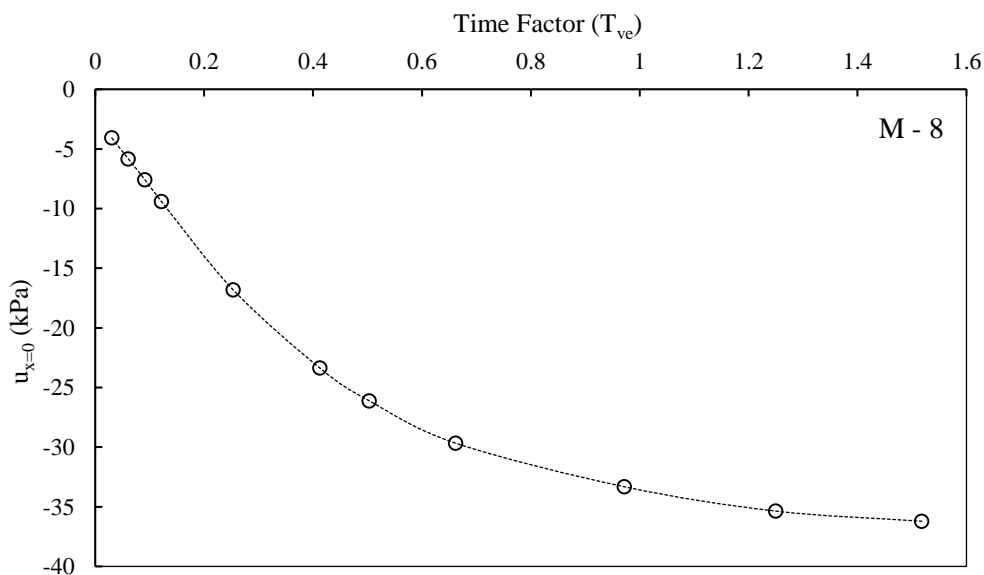
(b) Negative pore water pressure development at the anode at various time factors

Fig. 6.11 Numerically simulated negative pore water pressure at various locations and time factors in soil M-8

In addition, the level of potential drop at the cathode increases temporally. Therefore, for lower T_v, lower potential drop and consequently higher negative pore water pressure was observed. As consolidation proceeds, the potential loss at the cathode increases and therefore the level of developed pore water pressure decreases at the cathode side. This trend can be observed at point A in Figs. 6.6 to 6.11. In case of NC soil, the maximum negative pore water pressure was about -40 kPa whereas for OC soil it varied between -25 kPa to -40 kPa. As the k_e is a constant parameter, the difference in the maximum pore water pressure developed can be attributed to the difference in k_h values for the different soil samples.

6.5.2 Effect of various voltages

The effect of various voltages on EO consolidation was also checked using the proposed model. Apart from the V=4V condition, the induced EO settlements using three other voltages (V = 1, 2 and 6 V) were tested numerically on two NC specimens with various preconsolidation pressures (M-1 and H - 1) and one OC sample (M-4). To achieve this, the same validated proposed model which was discussed in Section 6.2 was used. Initially the negative pore water pressure developed was computed over the specimen height for various voltages. Then, the soil settlement was computed using Terzaghi's theory. The results are presented in Fig. 6.12 to Fig. 6.14.
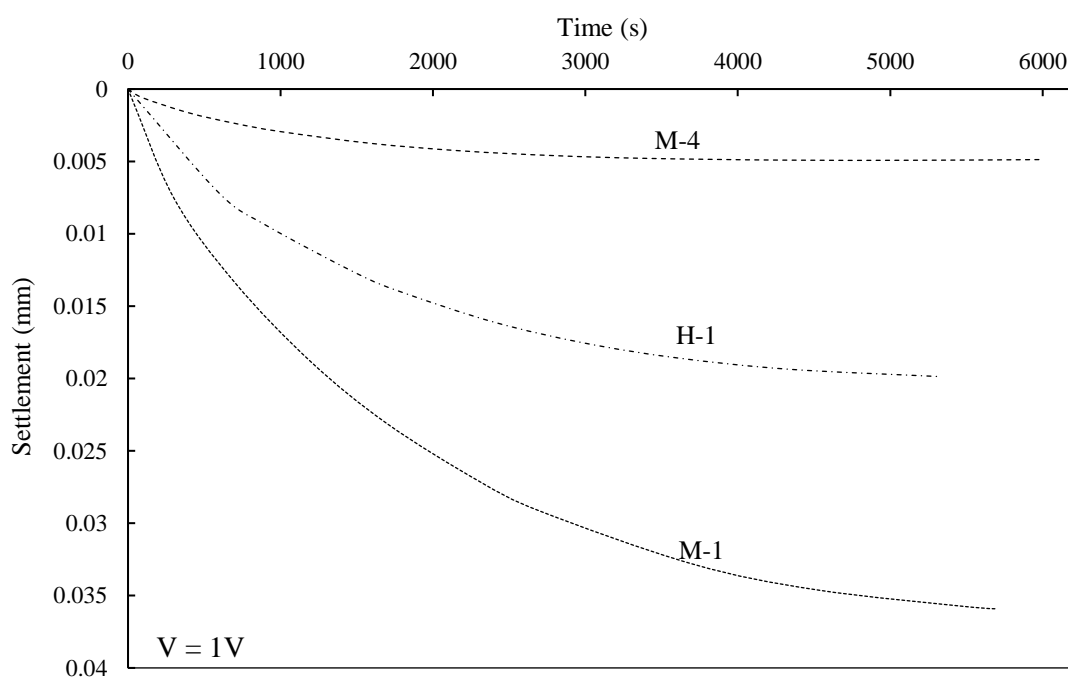
Fig. 6.12 Estimated soil settlement for V =1 V

Time (s)
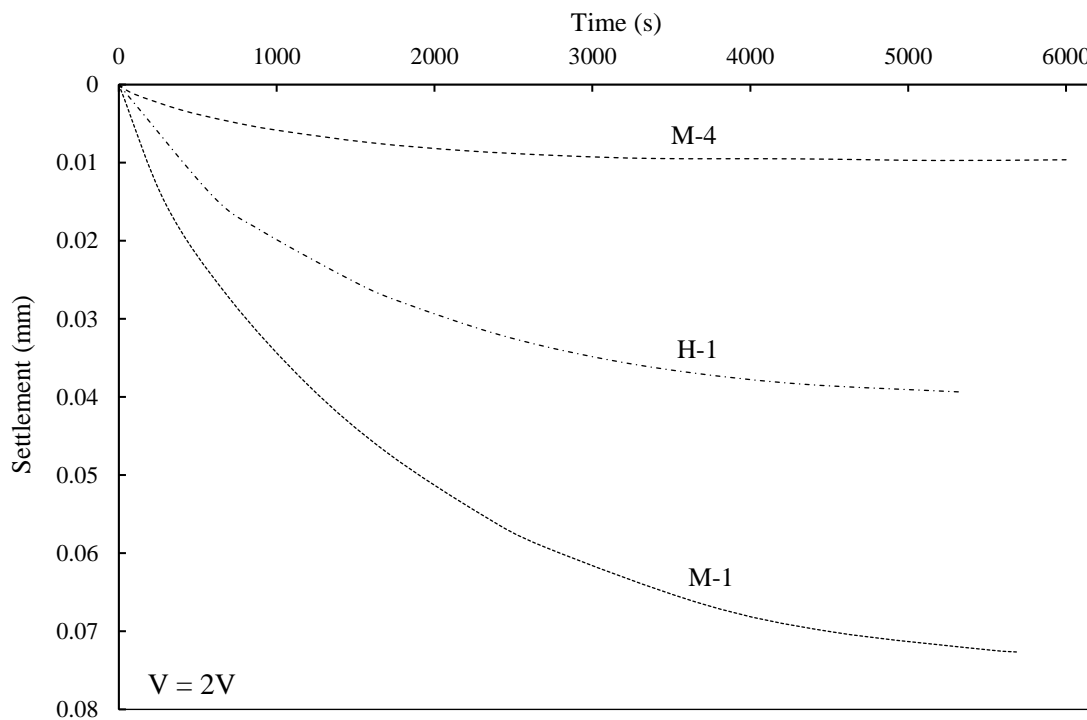
Fig. 6.13 Estimated soil settlement for *V* = 2 V

Time (s)
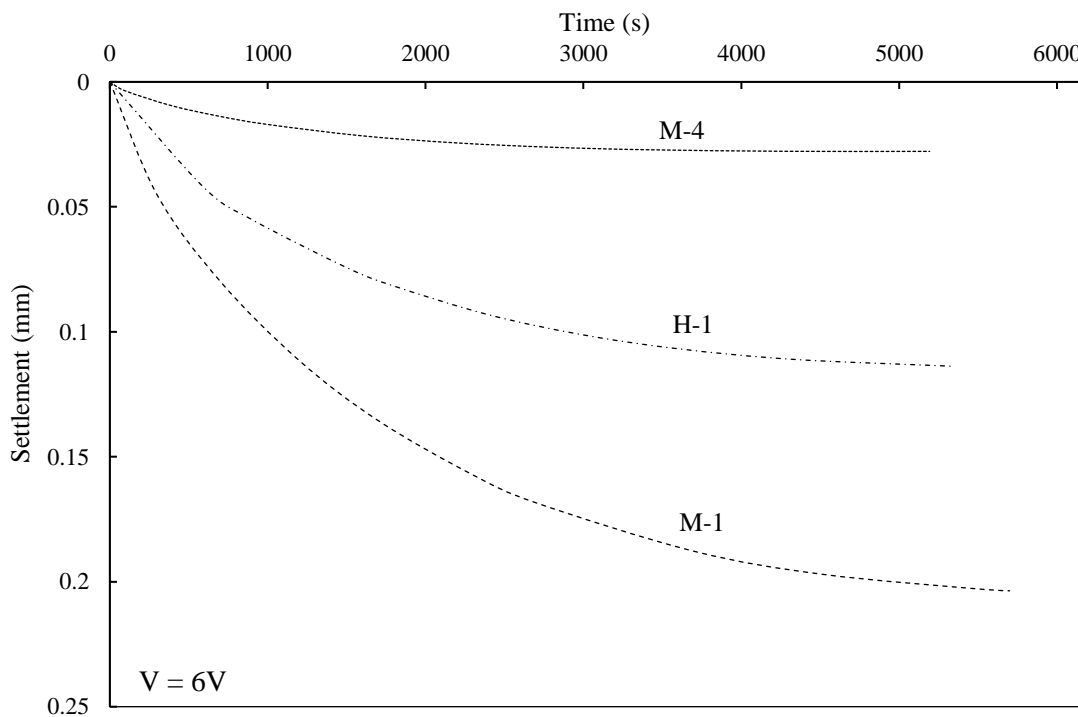
Fig. 6.14 Estimated soil settlement for *V* = 6 V

As expected, the negative pore water pressure developed and consequently the soil settlement was proportional to the level of the voltage applied at a specific time. For higher level of voltage, more hydrated ions move from the anode to the cathode and consequently higher drag force is exerted to the free water. Therefore, larger volume of water is transported from the anode to the cathode and more settlement occurred. In addition, the EO consolidation was more efficient in terms of inducing settlement in NC soils rather than in OC soils. For example, the maximum induced settlement in M-1 for 1 V ($S_t = 0.034$ mm), is larger than that in M-4 with 6 V applied ($S_t = 0.027$ mm).

6.5.3 Electrically induced shear strength

Generally, vane shear test is used to measure the shear strength of the pre/post treated soil in the field and in the laboratory. For a normally consolidated soil, the initial shear strength of the soil directly depends on the soil preconsolidation pressure, as indicated in Eq. 6.8 (Bjerrum et al. 1967; Burnotte et al. 2004; Jeyakanthan et al. 2011)

$$C_u = \alpha_u \, \sigma_p'$$ (6.8)

where C_u is the undrained shear strength of the soil, σ_p' is the preconsolidation pressure of the soil and α_u is a constant parameter that denotes the shear strength ratio. In addition, as the maximum negative pore water pressure occurs in the anode side and no pore water pressure develops in the cathode, the maximum and minimum shear strengths are observed in the anode and the cathode, respectively.

Considering α_u to be constant for the tested soil before and after the EO consolidation (Burnotte et al. 2004; Jeyakanthan et al. 2011), the level of achieved shear strength during EO (C_{uf} / C_{ui}) can be estimated through the shear strength ratio:

$$\frac{C_{uf}}{C_{ui}} = \frac{\sigma_{pf}'}{\sigma_p'}$$ (6.9)

where i and f subscripts denote the initial (before EO treatment) and final (after EO treatment) condition. In addition, the achieved preconsolidation pressure during EO at a specific time is equal to the developed negative pore water pressure (u_t). Therefore, the total preconsolidation σ'_{pt} can be estimated as:

$$\sigma_{pf}' = \sigma_p' - u_t$$ (6.10)

Figs. 6.15 and 6.16 show the average and maximum shear strength ratios, respectively, before and after EO consolidation for the soils L-1, M-1 and H-1. To calculate these, the average negative pore water pressure developed was calculated by integration of the negative pore water pressure over the soil height (as in Eq. 6.11) and then the result was substituted into Eq. 6.9.
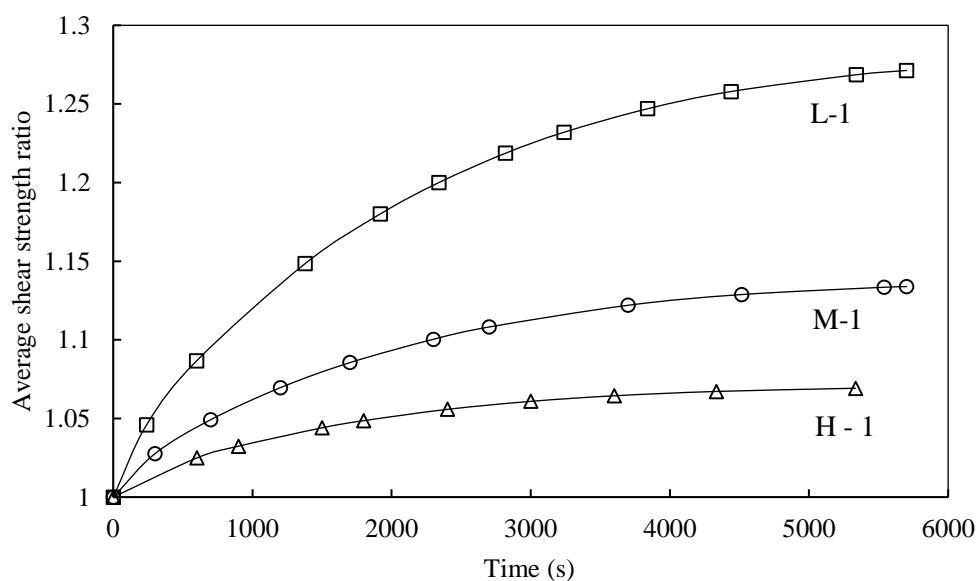
Fig. 6.15 Increase in average soil shear strength during EO consolidation at $V = 4$ V
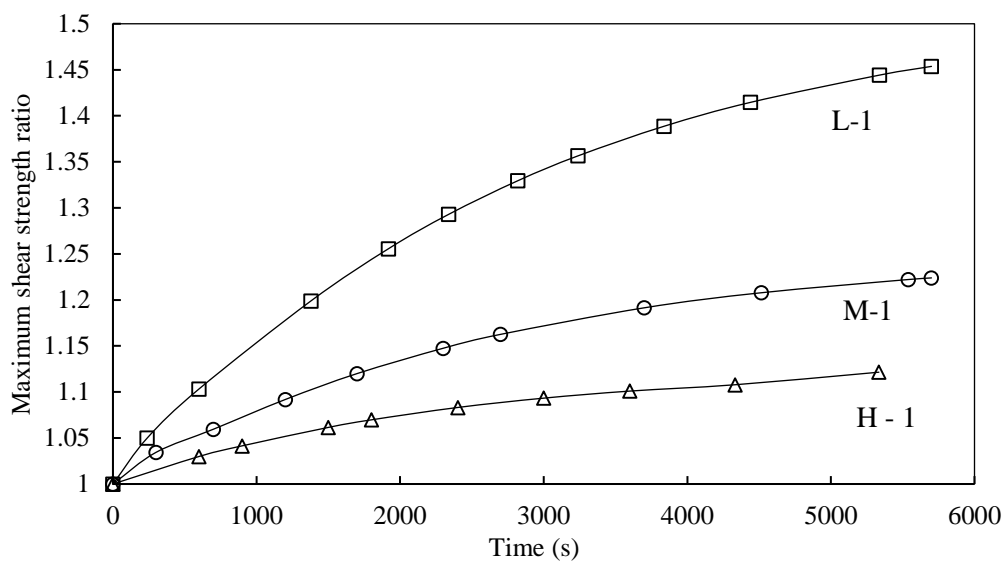
Fig. 6.16 Increase in maximum soil shear strength during EO consolidation at $V = 4$ V

Average shear strength ratios of approximately 1.27, 1.14 and 1.06 were observed in L-1, M-1 and H-1, respectively, at the end of the EO consolidation. This implies that in NC soil specimens, the EO consolidation is more effective on specimens with lower preconsolidation pressure. This can be attributed to the lower negative pore water pressure developed in the soil with higher preconsolidation pressure. In this case, based on Eq. 6.10, lower negative pore water pressure developed leads to lower induced excess preconsolidation pressure and therefore, referring to Eqs. 6.6 and 6.9, lower soil settlement and lower shear strength ratio were observed. Therefore, the maximum shear strength ratio of 1.45 was calculated in the vicinity of the anode of L-1 specimen.

Moreover, Fig. 6.17 shows a comparison of the average shear strength ratio and the shear strength ratio midway between the electrodes. The results indicate that the two values are approximately similar during the EO process. This implies that the results from midway between the electrodes can be assumed as the average value. However, a small deviation between the two values was observed at the beginning of the EO consolidation. This deviation can be attributed to the higher rate of negative pore water development at the vicinity of the anode. As the consolidation process progresses, the deviation between midway and the maximum developed negative pore pressure decreases and, at the end of the consolidation process, the average shear strength ratio (over whole specimen length) and shear strength ratio midway between the electrodes become equal.
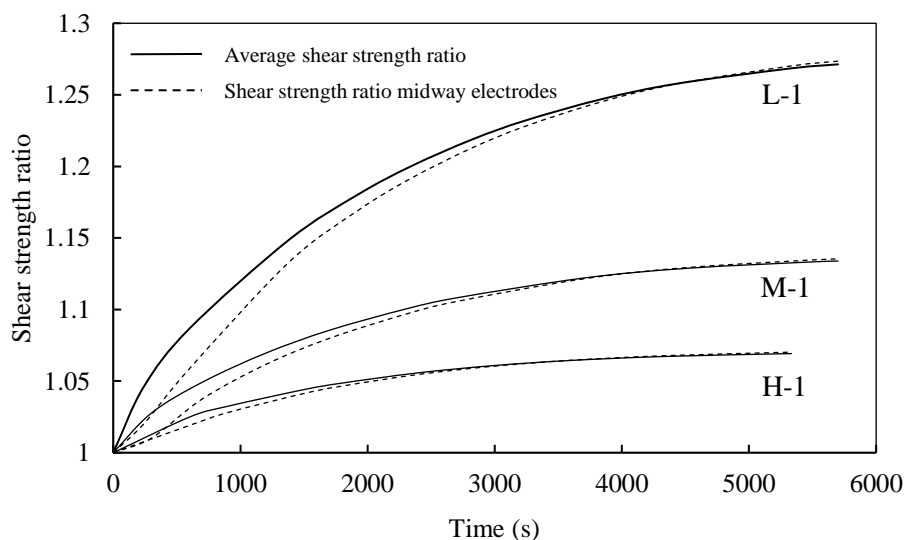
Fig. 6.17 Level of increase in soil shear strength during EO consolidation

148

The shear strength ratio plots can also be used to apply the EO process more efficiently. By having an estimate of the required shear strength at the site and knowing the initial shear strength of the soil, the target shear strength ratio can be defined. Knowing the shear strength ratio and desired and the practical applied voltage, the required duration of voltage application can be estimated. Therefore, to reduce the level of power consumption and cost of the project, the power supply can be disconnected once the target is achieved.

6.6 Summary

A new numerical model was proposed for EO consolidation. The model was developed by modifying the general governing equation of EO consolidation and incorporating the law of conservation of electric charge. To modify the general governing equation of EO consolidation, the coefficient of consolidation (C_v) was replaced by the coefficient of consolidation during EO process (C_{ve}). In addition, the electrochemical effects were considered by incorporating the unsteady potential loss in the model. Moreover, the law of conservation of electric charge was used in parallel with the modified governing equation of EO consolidation to accurately model the voltage distribution in the soil body. Then the model was verified using the experimental data from this research. In addition, the proposed model was compared with other available assumptions and models. It was found that using C_{ve} instead of C_v improved the EO model in terms of estimation of consolidation rate during EO consolidation. In addition, utilising unsteady potential drop close to the cathode and in the soil body improved the prediction of the negative pore water pressure developed in the soil. A maximum of 7% median absolute error between the predicted and the measured soil settlements was observed in the tested soils. In addition, it was found that the EO consolidation was more effective on NC soils with low preconsolidation pressure. Finally, the maximum shear strength ratio, representing the shear strength increase after EO consolidation, was estimated to be 1.45 for L-1 kaolin clay.

7 ELECTRO-OSMOSIS CONSOLIDATION IN THE FIELD

7.1 Introduction

Generally, the design of large-scale EO consolidation schemes is based on laboratory test results. A number of laboratory tests have been conducted by various researchers to identify the effect of various parameters on EO consolidation efficiency and behaviour of post-treated soil. The results from those laboratory tests show noticeable differences compared with those observed in field trials. These differences signify that the laboratory scale experiments should be carried out with less simplifications. In addition, the extension of laboratory results should be conducted more accurately using numerical techniques. A systematic review and comparison of laboratory and field results highlight two simplifications which are currently used widely in laboratory tests: (1) the voltage distribution, which depends mainly on electrical resistivity of soil, is considered to be linear across the electrodes; and (2) the potential drop at soil-electrode medium is neglected in many cases. Therefore, these two parameters should be closely monitored during the EO consolidation tests, in addition to other commonly measured parameters, such as electro-osmosis permeability and coefficient of consolidation. In addition to monitoring all important parameters contributing to EO consolidation, the laboratory results should be more accurately extended to the field using numerical models.

In this chapter, in addition to a comparison of the post-treated soil behaviour in the laboratory and field, the calibrated model which was developed in Chapter 6 was extended to the field case. The model comprised the main governing equation of EO consolidation which has been

modified by incorporating time-dependent potential loss at soil-electrode. In addition, the distribution of voltage was estimated using the law of conservation of electrical charge using variable electrical resistivity. The equations were integrated into a single model and solved over the desired boundary using FEM technique through FlexPDE software. Finally, the developed model was verified against the experimental data and previous numerical models.

7.2 Field and laboratory scale EO consolidation trials

The reviewed laboratory and field tests are listed in Table 7.1, where the test IDs of L and F represent laboratory and field tests, respectively. In total, four groups of laboratory and field tests on similar soils, in terms of liquid and plastic limits, clay contents and minerology and soil types were reviewed (columns 1-4). In addition, the application of potential difference to the soil was carried out by means of conductive electrodes with various materials and shapes. The electrodes can be oriented in different alignments (vertically and horizontally) depending on applications, as schematically shown in Fig. 7.1. In ground improvement application, the electrodes are mainly oriented vertically whereas in slope stabilisation applications, the electrodes are generally oriented horizontally. However, as the soil is assumed to be isotropic, the effect of electrode orientation was neglected in all EO consolidation investigations (Bjerrum et al. 1967; Lo et al., 1991). Lo et al. (1991) carried out field tests with electrical intensity of up to 0.4 V/cm. This intensity was, more or less equal to that used in their laboratory tests (Lo et al. 1991) on the same soil (up to 0.39 V/cm was used in the laboratory). Although the soil type, electrode materials and electric field intensity were similar in the laboratory and field trials, the alignment of the electrodes was different. Horizontal and vertical electrode arrangements were used in the laboratory and field tests, respectively.

Lefebvre and Burnotte (2002) tested a clay from Mount St-Hilaire of Canada in the laboratory with electric field intensity of 0.3-0.37 V/cm. Two types of electrodes were tested: (1) conventional perforated steel tubes with constant electric field intensity of 0.35 V/cm; and (2) conventional perforated steel tubes with soil-electrode resistance improvement using saline solution injections. In the latter case, the electric field intensity was varied from 0.3 V/cm at the beginning of the test to 0.37 V/cm (average of 0.34 V/cm). However, a field test was carried out at the same site from which laboratory samples were extracted, with electric field intensity of 0.33 V/cm by Burnotte et al. (2004). Burnotte et al. (2004) used solid steel tube as electrodes without soil-electrode resistance improvement.

Table 7.1 Properties of EO systems used in field and laboratory EO tests

Test ID	Soil type	LL (%)	PL (%)	Clay Content (%)	Electrode materials	Electrode Diameter (mm)	Reference
L-1	Sensitive Leda clay	48	24	48	Copper disc	101.6	Lo et al. (1991)
F-1	Sensitive Leda clay	48	24	48	Perforated copper pipes	60	Lo et al. (1991)
L-2a	Mount St-Hilaire	42-78	22-24	˜80	Perforated steel tube	10	Lefebvre and Burnotte (2002)
L-2b	Mount St-Hilaire	42-78	22-24	˜ 80	Perforated steel tube Treated soil-electrode interface	10	Lefebvre and Burnotte (2002)
L-2c	Mount St-Hilaire	42-78	22-24	˜ 80	Perforated steel tube Treated soil-electrode interface	10	Lefebvre and Burnotte (2002)
F-2	Mount St-Hilaire	42-79	22-25	˜80	Steel tube	170	Burnotte et al. (2004)
L-3	Singapore marine clay	71	28	-	Copper disc	70	Win et al. (2001)
F-3	Singapore marine clay	80	35	44	EVD with copper wires	-	Chew et al. (2004)

Win et al. (2001) conducted laboratory experiments on Singapore marine clay using horizontal perforated copper electrodes. The electric field intensity of 0.14 to 1 V/cm was applied. Chew et al. (2004) carried out field tests on Singapore marine clay using vertical copper drains with electric field intensity of 0.12 V/cm.
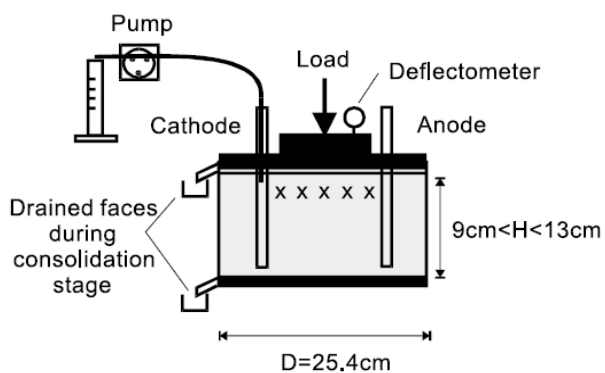
(a) Vertical electrodes - laboratory test
(Lefebvre and Burnotte, 2002)

(b) Vertical electrodes - field test
(Burnotte et al., 2004)
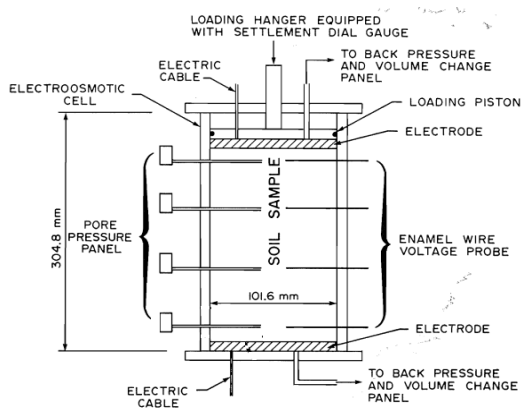
(c) Horizontal electrodes - laboratory test
(Lo et al., 1991)
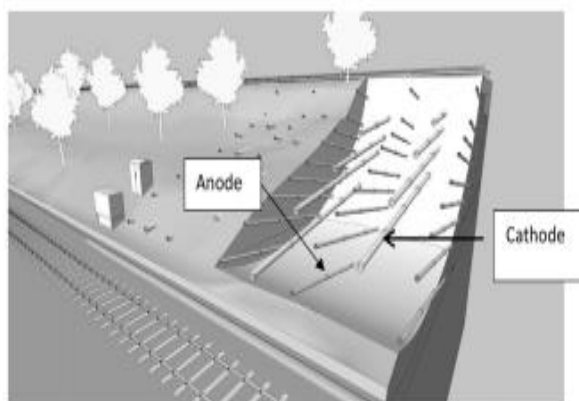
(d) Horizontal electrodes - field test
(Lamont-Black et al., 2016)

Fig. 7.1 Electrode alignments used in EO consolidation

7.3 EO improvement verification and comparison criteria

Basically, the applicability of EO ground improvement technique is verified through comparison of the behaviour of post-treated soil with pre-treated soil. These behaviours include induced shear strength, developed negative pore water pressure and electrically-induced soil settlement. Various researchers tried to estimate the feasibility of EO consolidation in the laboratory; however, different results have been reported from the field compared to those observed in the laboratory. The negatively developed pore water pressure, soil settlement and post-treated shear strength are usually reported higher in the laboratory than those observed in the field trials. This issue leads to overestimation of the post-treated soil behaviour in the field and imposes uncertainties in the EO consolidation technique. The results from laboratory and field trials corresponding to Table 7.1 are summarised in Table 7.2.

7.3.1 Electrically-induced shear strength

The vane shear test is usually used to measure the shear strength of the pre/post-treated soil in the laboratory and in the field. Usually, the average shear strength indicates the shear strength of the soil midway between the electrodes. This is also verified numerically in Chapter 6. Fig. 7.2 shows the measurements of initial and average post-treated shear strengths of the soil corresponding to Tables 7.1 and 7.2. In a few cases shown in Table 7.2, the developed negative pore water pressures have been calculated based on Eq. 7.1. Chew et al. (2004) tested Singapore marine clay with a preconsolidation pressure of 100 kPa in the laboratory and an average value of 30 kPa was reported for the shear strength of the soil. Therefore, the parameter α_u for Singapore marine clay can be estimated as 0.3 in the laboratory (reported as 0.26-0.28 by Chew et al. (2004) in the field). Win et al. (2001) also tested the same soil type (Singapore marine clay) with a preconsolidation pressure of 120 kPa and reported an estimated increase of 93 kPa in the preconsolidation pressure in the laboratory. Therefore, the initial shear strength can be estimated as 36 kPa and the final shear strength can be translated to 63.9 kPa, which implies approximately 78% increase in shear strength of the soil as shown in Fig. 7.2. In addition, the developed pore water pressures can be estimated based on Eq. 2.33, which is a numerically derived formula for the developed negative pore water pressure ($u_e = - (k_e \gamma_w/k_h) \times V$).

Electro-osmosis consolidation in the field

Table 7.2 Soil behaviour in field and laboratory before and after EO tests

Test ID	Preconsolidation pressure (kPa)	Average developed pore pressure (kPa)	Induced vertical strain (%)	Initial shear strength (kPa)	Final shear strength (kPa)	Reference
L-1	100	-75	9.8	11	30	Lo et al. (1991)
F-1	86*	-44.5*	2	18.2	27.4	Lo et al. (1991)
L-2a	175	-101*	4.3	47	76	Lefebvre and Burnotte (2002)
L-2b	105	-98*	12.4	29	57	Lefebvre and Burnotte (2002)
L-2c	175	-263*	10.4	47	123	Lefebvre and Burnotte (2002)
F-2	105	-135*	12	30	60	Burnotte et al. (2004)
L-3	120	-93	3.5	36*	63.9*	Win et al. (2001)
F-3	100	-10	0	30	46	Chew et al. (2004)

* Estimated by the author

Lo et al. (1991) consolidated Leda clay samples up to 100 kPa similar to the field, then an electric field intensity of 0.29 to 0.39 V/cm was applied. An increase from 113.6% to 172.7% in average shear strength was observed in the laboratory. However, a maximum of 50.8% increase in the average shear strength was reported in the field with an electric intensity from 0.1 to 0.4 V/cm.

Lefebvre and Burnotte (2002) tested one specimen with σ'_p=175 kPa using the conventional method (test L-2a) and two other specimens with σ'_p =105 and 175 kPa using a treated EO system (tests L-2b & c). The average initial shear strengths of the soil with σ'_p =105 and 175 kPa were 29 kPa (test L-2b) and 47-48 kPa (tests L-2a & c), respectively. The post-treatment shear strengths of the specimen in test L-2b, L-2c and L-2a were reported to be 57, 123 and 76 kPa, respectively. Burnotte et al. (2004) reported 30 kPa for the initial shear strength of the soil in the field, which has been improved to an average of 60 kPa. A major improvement in shear strength has been observed in the anode vicinity.

In the case of the Singapore marine clay, a maximum of approximately 50% shear strength increase was reported by Chew et al. (2004) in the field. However, Win et al. (2001) extracted a sample of similar clay from a depth of 17-17.8 m (more or less similar to depth investigated by Chew et al. 2004) and tested it in the laboratory. Approximately σ'_p= 93 kPa achievement has been observed at the end of the EO process.
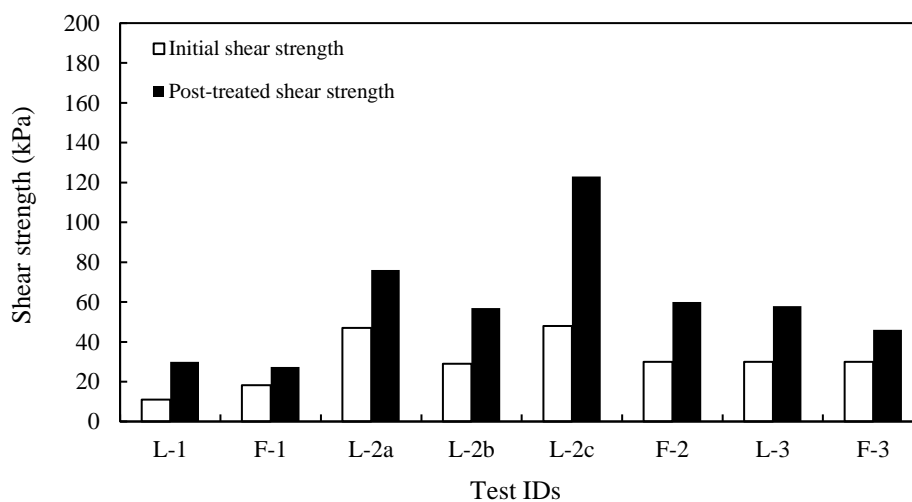
Fig. 7.2 Comparison between measured initial and post-treated shear strengths from laboratory and field trials

Based on the presented results, the deviation between the laboratory and field estimation of shear strength of the post-treated soils is apparent even in same types of the soil. Therefore, a more accurate approach needs to be adopted to estimate the developed pore water pressure and consequently the shear strength of the post-treated soil in the laboratory and in the field.

7.3.2 Electrically-induced settlement

As the maximum and minimum negative pore pressures are developed in the anode and cathode vicinities, respectively, the maximum settlement occurs near the anode whereas no settlement takes place near the cathode. Usually, the settlement in the soil body is reported in terms of vertical strain (δ/L) or volume strain (V_s/V) where δ, L, V_s, V denote the soil settlement, initial soil thickness, volumetric change and initial volume of the soil, respectively. Fig. 7.3 shows the results from laboratory and field tests corresponding to Table 7.1. Lo et al. (1991) reported 9.8% vertical strain in the laboratory scale whereas only about 2% vertical strain was observed in the field test. Lefebvre and Burnotte (2002) reported 4.3%, 12.4% and 10.4% volumetric strains for L-2a, b & c respectively. However, Burnotte et al. (2004) reported 12% volumetric/vertical strains based on measurement of surface settlement on top of the treated soil. Finally, Win et al. (2001) reported about 3.5% vertical strain in Singapore marine clay whereas no settlement could be measured (i.e. not measurable) by Chew et al. (2004) in the field.
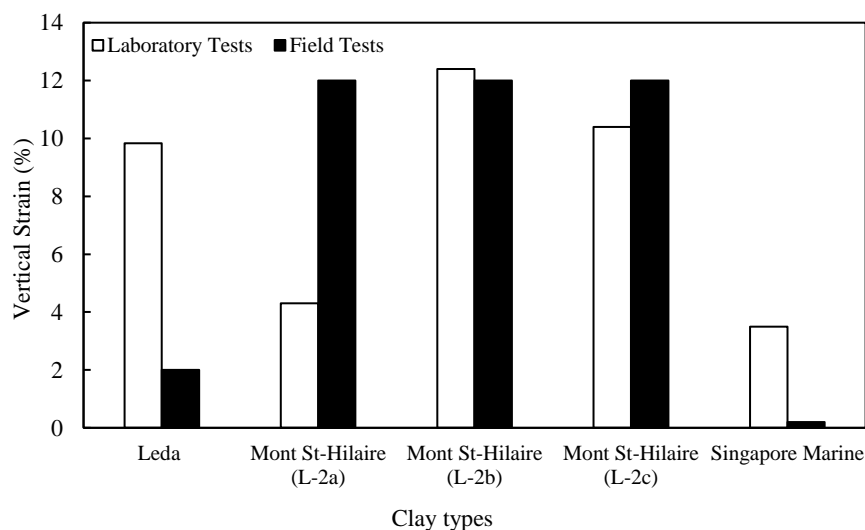
Fig. 7.3 Comparison between vertical strains from laboratory and field trials

7.3.3 Negative pore water pressure

Negative pore water pressure that develops during EO consolidation pressure as a result of water transport from the anode to the cathode accounts for enhancement of soil behaviour. However, discrepancies have been observed between laboratory and field results in terms of negative pore water pressure developed during the EO consolidation. The developed negative pore water pressures are shown in Fig. 7.4 for laboratory and field trials.
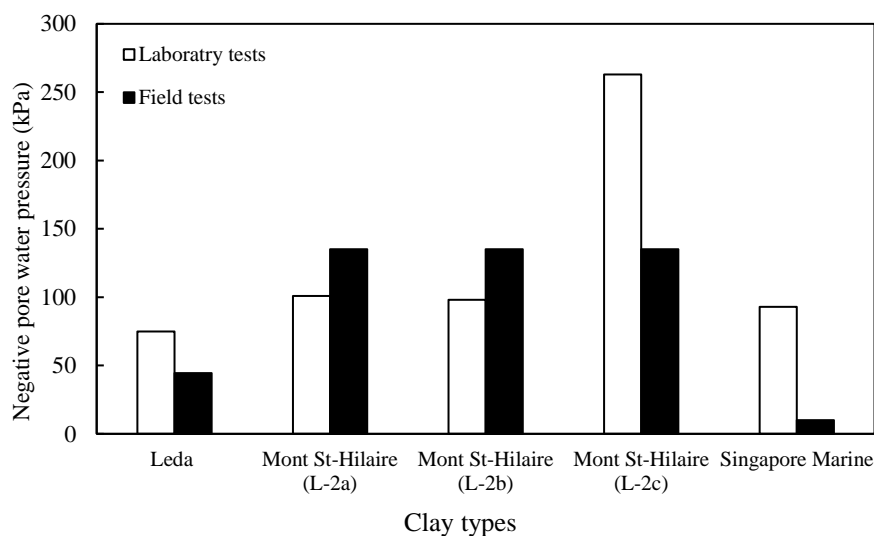
Fig. 7.4 Comparison between negative pore water pressure from laboratory and field trials

Lo et al. (1991) reported development of -75 kPa of pore water pressure during EO test in the laboratory. In the field case, the pore water pressure development was estimated based on Eq. 7.1. The average initial shear strength in the field was 18.2 kPa corresponding to a treatment depth of approximately 4 m (i.e. depth of 2-6 m below the surface). The preconsolidation pressure at the same site was reported by Leroueil et al. (1983) as 62-110 kPa which implies an average value of 86 kPa for the same depth. Therefore, the parameter α_u can be estimated as 0.21. Consequently, the negative pore pressure can be estimated as -44.5 kPa. In the case of Mont St-Hilaire clay, α_u was reported as 0.25 to 0.33, with an average of 0.285 in the laboratory (for specimens L-2a & c) and 0.25 in the field; therefore, the developed pore water pressure can be estimated as -101, -98 and -263 kPa for L-2a, b & c, respectively. However, the developed negative pore water pressure estimated in the field shows a value of -135 kPa. In the

case of Singapore marine clay, the value of -93 kPa of pore water pressure was reported by Win et al. (2001). A maximum of -10 kPa was reported by Chew et al. (2004) for the pore water pressure in the field.

7.3.4 Discussion of the results

The results from the laboratory and field tests carried out on Leda and Singapore marine clays were in agreement in terms of the observation that laboratory experiments overestimated the developed negative pore pressure, the induced settlement and the post-treated soil shear strength in the field. However, results for Mont St-Hilaire clay showed that the laboratory results were either in agreement or slightly underestimated the soil behaviour in the field. The deviation observed between laboratory and field tests can be attributed to several factors, which were neglected in the experimental testing framework adopted in majority of the previous research: (1) chemical reactions; (2) soil electrode contacts; and (3) electrical resistivity of the soil. The effect of the first two factors may appear in terms of potential loss at soil-electrode interfaces.

Once the electric potential gradient is applied to the soil, chemical and EO processes take place concurrently. The most important chemical effect during EO consolidation is electrolysis at the soil-electrode interfaces. Electrolysis at electrodes causes gas generation (O_2 and H_2) at the electrode vicinities which increases the electrical resistance of soil-electrode interface. This resistance leads to noticeable potential loss at the electrode medium. Therefore, only a fraction of the applied voltage will be effective. The level of gas generation at the electrode vicinity depends on the chemistry of the soil and the electrodes. Therefore, care should be taken in selecting the electrode while the soil material should be similar to the field trials or properly calibrated before extending the laboratory results to the field. In addition, the value of the potential drop is a time-dependent factor and should be experimentally measured in the laboratory within a time frame equal to that in the field test. As discussed earlier, it is known that the oxygen gas generated at the anode side is able to react with certain types of electrodes, such as bronze, copper and stainless steel, and forms metal oxide, which in itself is conductive. Therefore, no loss is recorded in those anodes (Mohamedelhassan 2009; Jeyakanthan et al. 2011). Thus, by effective selection of electrode materials, the level of potential loss can be reduced to zero in the anode. These effects can be clearly observed in the reported field and laboratory results as listed in Tables 7.1 and 7.2. In addition, loose contact between the soil and

the electrodes leads to the existence of trapped air in the soil-electrode medium which increases the soil-electrode interface resistance and dissipates a portion of the electric potential gradient. The soil-electrode contact can be related to the electrode alignment. In the case of Leda and Singapore marine clay, the electrode materials, soil type and level of applied electric field intensity were maintained more or less the same in the field and in the laboratory tests. However, the electrode alignments were different. In the laboratory tests, the electrodes were laid horizontally; therefore, the soil-electrode contact was improved by the vertical overburden load. In the field, the electrodes were installed vertically, and no stress existed to keep the soil-electrode contact in place. Therefore, better contact and less potential loss in the laboratory scale were provided which lead to higher shear strength achievement in the laboratory compared to that in the field. However, in the case of Mont St-Hilaire clay, vertical electrodes were used in the laboratory and field cases. The results showed slightly better contact in the field as the level of the achieved shear strength in the field was slightly higher compared to that in the laboratory (L-2a). Once the soil-electrode interface in the field was treated by saline solution (L-2b), the level of soil-electrode interface resistance dropped to the same level as in the field and similar shear strength increases can be observed; similar trend was seen in soil settlement and vertical/volumetric strains.

Moreover, the laboratory apparatus should be designed to capture the electrical resistivity of the soil during the EO consolidation. Electrical resistivity governs the distribution of the voltage across the soil body accurately, as discussed fully in Chapters 4 and 5.

In the reviewed cases of laboratory and field experiments, the EO system properties and soil characteristics, namely the electrode materials, the level of applied electric potential gradient, the soil minerology and the chemical reactions at the soil-electrode interfaces can be assumed to be constant in each case between laboratory and field. Consequently, the deviation between laboratory and field results can be attributed to the effective potential gradient. In turn, the effective potential gradient depends on soil-electrode contact which, in itself, is dependent on electrode alignment.

To take the electrode alignment into account, monitoring the time-dependent potential drop at soil-electrode interface and the electrical resistivity during EO consolidation is crucial. Therefore, the testing apparatus should be designed considering the field application to select the appropriate alignment of electrodes and having the identical pattern of potential loss at the

soil-electrode interface between laboratory and field. In addition, there is a need for a robust numerical model to consider these parameters and to be able to implement all contributing parameters and accurately extend the laboratory results to the field. As discussed in Chapter 6, the proposed numerical model considers all contributing parameters in the laboratory and in this Chapter, the proposed EO model is extended to the field. The results are verified using a well-documented EO consolidation field test reported by Burnotte et al. (2004). In addition, the proposed model is compared with the numerical model proposed by Yuan and Hicks (2015).

7.4 Extension of proposed EO numerical model to the field

7.4.1 Numerical model

The proposed model was fully discussed in Chapter 6. It was established based on two relationships: (1) modified EO governing equation; and (2) conservation of electric charges. For field application, the 2D model can be used and the soil behaviour can be estimated in each desired plan (Shang 1997; Rittitong and Shang, 2008; Hu et al. 2012; Yuan and Hicks, 2015). Therefore, the proposed model was extended to establish a 2D numerical model:

$$\frac{\partial^2 u_e}{\partial y^2} + \frac{k_e \gamma_w}{k_h} \frac{\partial^2 (f(t).V)}{\partial y^2} + \frac{\partial^2 u_e}{\partial z^2} + \frac{k_e \gamma_w}{k_h} \frac{\partial^2 (f(t).V)}{\partial z^2} = \frac{1}{C_{ve}} \frac{\partial u_e}{\partial t} \qquad (7.1)$$

$$-\nabla \cdot j = C_p \frac{\partial V}{\partial t} \qquad (7.2)$$

and

$$j = \sigma \cdot (\frac{\partial V}{\partial y} + \frac{\partial V}{\partial z}) \qquad (7.3)$$

The field test, which was essentially a 3D case, was simplified as plane strain problem and numerically modelled in 2D; hence, the third dimension was assumed to be of unit width and the electrodes were modelled as plates. As a result, the water movement was assumed to occur only in the lateral direction and no water movement was allowed across the rows of the electrodes. Such simplification was acceptable, since modelling the 3D response is beyond the scope of current available EO consolidation modelling techniques.

By solving the above equations over the desired boundaries, the excess negative pore water pressure across the soil body could be defined. Then the soil settlement and the shear strength ratio at various locations could be estimated as discussed in Chapter 5. In addition, the soil was assumed to be homogeneous and isotropic and therefore a constant value of k_h can be adopted for the soil.

7.4.2 Numerical analysis of a field test

The proposed numerical model was used to simulate a EO consolidation field test reported by Burnotte et al. (2004). The site was located near Mont St-Hilaire, in the St Lawrence Valley, east of Montreal in Canada (Mont St-Hilaire clay). The soil profile at the site is shown in Fig. 7.5.
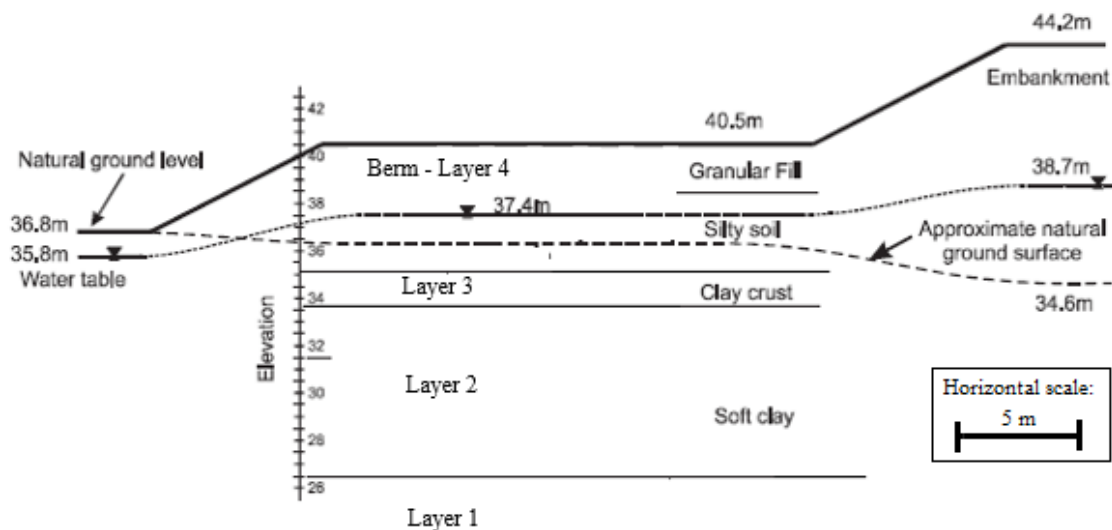
Fig. 7.5 Soil profile at Mont St-Hilaire site (Burnotte et al., 2004)

The actual EO consolidation test was conducted in an area measuring 9 m × 10 m using 17 cm diameter steel electrodes. The electrodes were placed in 2 m × 3 m grids. An overview of the electrodes and electrode arrangement used are shown in Fig. 7.6. The voltage was altered during the field test. 0.33 V/m was applied during the first 22 days, then reduced to 0.23 V/m from day 23 to 29. The voltage was again restored to 0.33 V/m after day 29. However, for the numerical model the value of 0.33 V/m was considered as the average applied voltage throughout the duration of the field test.
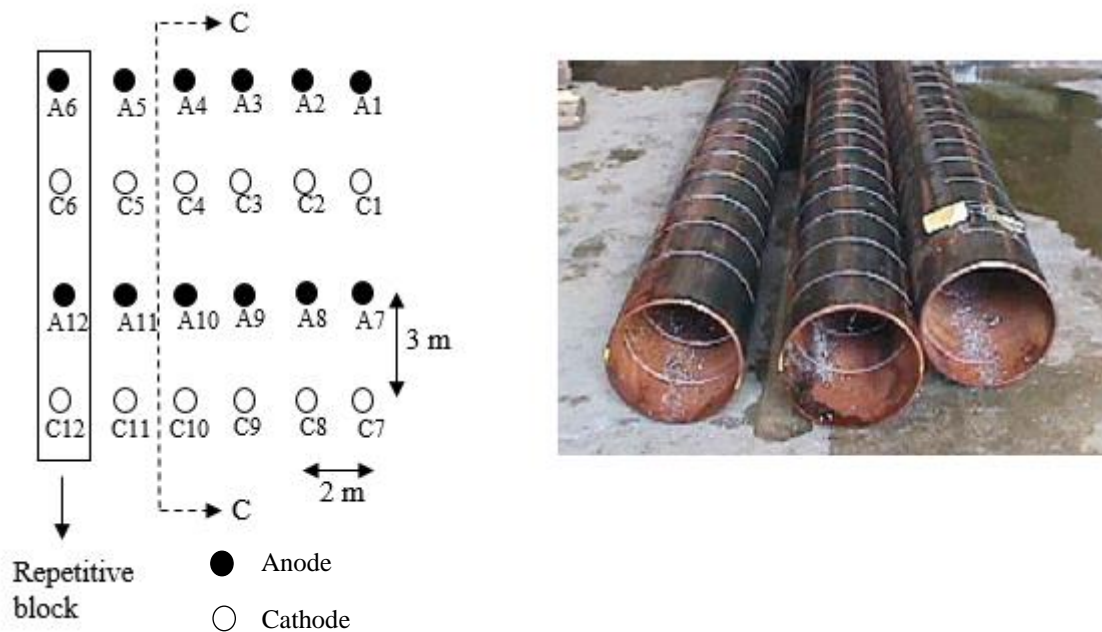
Fig. 7.6 Overview of electrode arrangement and actual electrodes used in EO consolidation at Mont St-Hilaire site (Burnotte et al., 2004)

As shown in Fig. 7.6, the tested area comprised repetitive sub-areas, therefore the cross-section C-C was considered for numerical analysis. The analysed area and the elements used in the numerical analysis are shown in Fig. 7.7. To minimise the possible effect of boundaries on the numerical analysis, the clay layer was extended for 20 m laterally and 0.5 m from the bottom of electrodes. Analysis of this case would allow the comparison of the proposed model with that of Yuan and Hicks (2015). As in the field test, a PVC cover was put above the electrodes up to the top of the first layer in order to protect the electrodes from potential loss in layers other than in clay. In addition, the soil boundaries are defined as natural boundaries which implies no electric flow and no pore water pressure changes. These boundaries are shown with solid lines in Fig. 7.7. Also, as the developed pore water value is zero at cathodes, zero-value boundaries are defined for pore water pressure at the cathode electrodes.
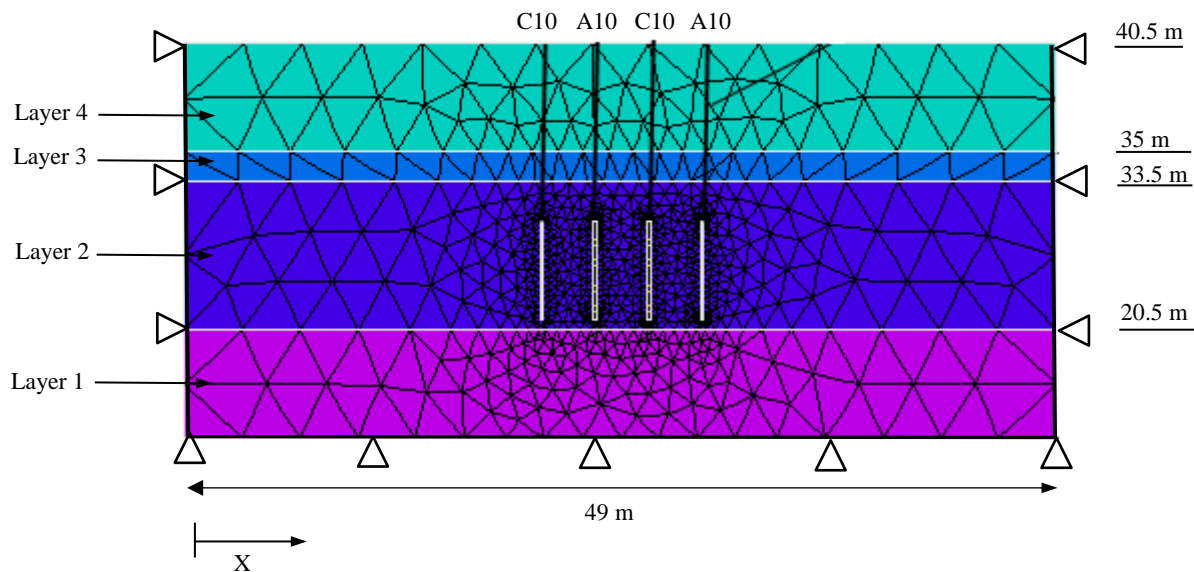
Fig. 7.7 Mesh used in numerical modelling of EO consolidation of Mont St-Hilaire site

In addition to the soil boundaries, the required parameters need to be identified, as discussed in Chapter 5. k_e and k_h were experimentally measured and reported by Burnotte et al. (2004) as 3.5×10^{-9} m²/V·s and 1.5×10^{-9} m/s, respectively. In addition, ρ of the clay was reported as approximately 1 Ω·m. However, to identify the required parameters for the proposed model, C_{ve} and voltage profile were also required. For estimating the voltage profile, the data from Lefebvre and Burnotte (2002), which was carried out on similar clay type, was used. Based on their research, the time-dependent voltage profiles between the two circular steel electrodes in a laboratory-scale modified EO oedometer cell as shown in Fig. 7.8 were experimentally described at various locations.
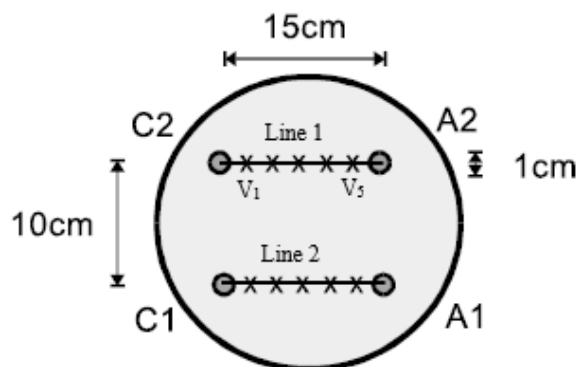
Fig. 7.8 A view of the laboratory apparatus used for EO consolidation test on Mont St-Hilaire clay (Lefebvre and Burnotte, 2002)

Fig. 7.9 shows the measured voltages across Line 1 and Line 2 for NC Mont St-Hilaire clay with preconsolidation pressure of 175 kPa.
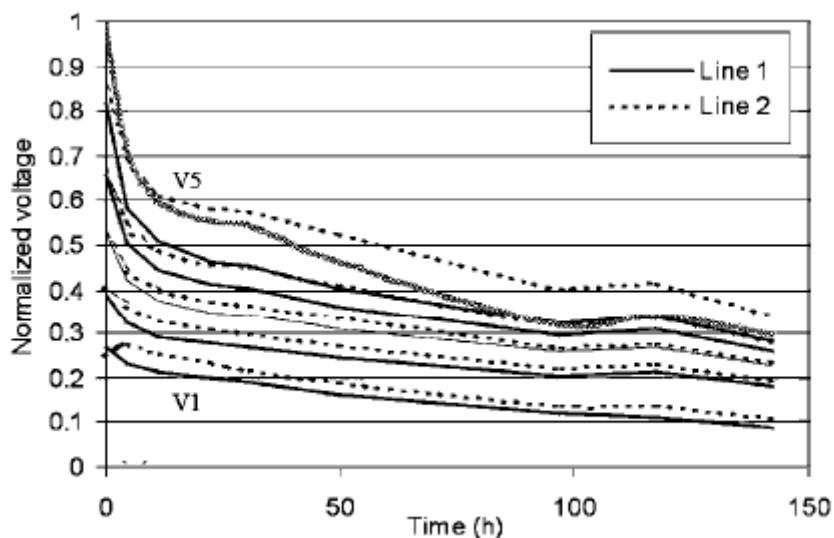
Fig. 7.9 Laboratory measured voltage efficiency between electrodes during EO consolidation of Mont St-Hilaire clay (Lefebvre and Burnotte, 2002)

To implement the voltage profile, the solid line (Line 1) was used. For each set of measurements (V1 to V5) a curve was fitted to the data points and then implemented into Eq. 7.1. The equations of the fitted curves are listed in Table 7.3, where n is the normalised voltage at specific location and specific time, t.

Table 7.3 Voltage efficiency versus time during EO consolidation of Mont St-Hilaire clay

Location	Equation	R^2
V_5	$n = 2.8t^{-0.163}$	$R^2 = 0.97$
V_4	$n = 1.8t^{-0.135}$	$R^2 = 0.94$
V_3	$n = 1.32t^{-0.123}$	$R^2 = 0.94$
V_2	$n = 0.87t^{-0.102}$	$R^2 = 0.94$
V_1	$n = 0.87t^{-0.152}$	$R^2 = 0.93$

Finally, to complete the parameter identification for the proposed model, C_{ve} needs to be determined. As no experimental data was available for C_{ve}, this parameter was initially

estimated using C_v. Note that as discussed in Chapter 5 and based on Figs. (3.13) and (5.14), the C_{ve} / C_v for kaolin clay when $\sigma'_0 = 120$ kPa was approximately 0.15. Hence, the same trend was assumed for Mont St-Hilaire clay and consequently when C_v is known, the C_{ve} can be estimated for Mont St-Hilaire clay. C_v was also calculated based on the hydraulic consolidation curve shown in Fig. 7.10, for preconsolidation pressure of 120 kPa (under the berm and before EO consolidation) to 300 kPa (assuming approximately -200 kPa as the maximum negative pore water pressure developed).
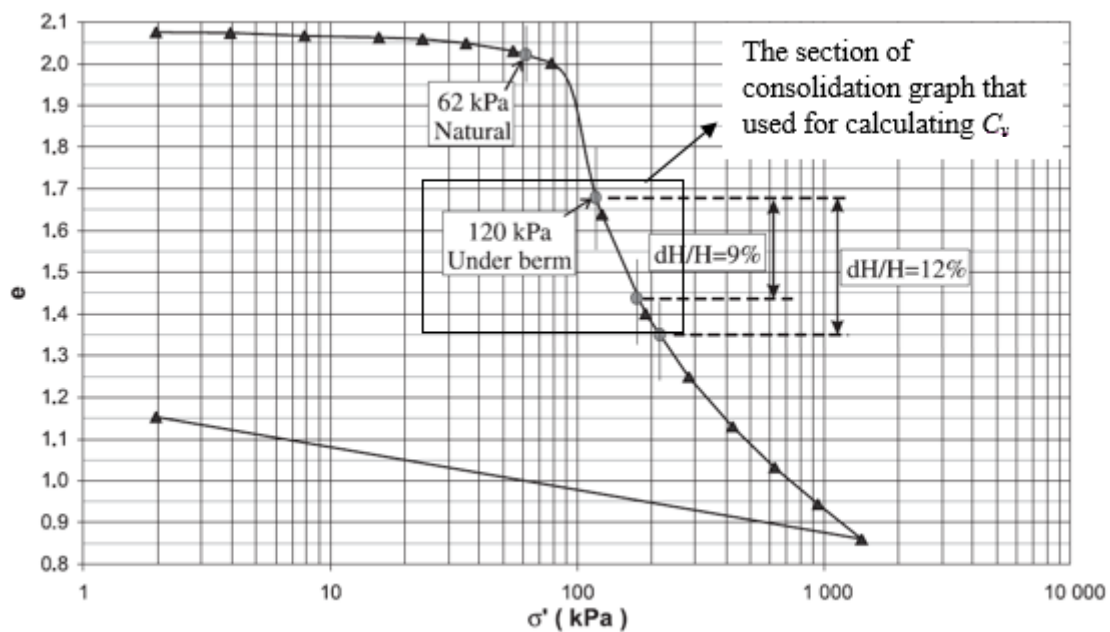
Fig. 7.10 Hydraulic consolidation curve for Mont St-Hilaire clay where e denotes void ratio (Burnotte et al., 2004)

Based on the graph, for $\sigma' = 120$ kPa the void ratio (e) is 1.68 and for $\sigma' = 300$ kPa, $e = 1.25$. Thus, $m_v = 0.00096$ m^2/kN and $C_v = 1.8 \times 10^{-7}$ m^2/sec. Therefore, $C_{ve} = 3 \times 10^{-8}$ m^2/sec was used as initial estimate. Then, C_{ve} was counterchecked and adjusted using a single experimental result of soil settlement at $X = 20.5$ m (refer to Fig. 7.7) and $t = 15$ days. After a few steps of adjustment, $C_{ve} = 3.8 \times 10^{-8}$ m^2/sec was obtained which was used as a constant parameter in the numerical model at various situations. A summary of the parameters used in numerical model is presented in Table 7.4.

Table 7.4 Summary of parameters used in EO consolidation numerical model

Parameter	Value
k_e	$3.5 \times 10^{-9}\ m^2/V \cdot s$
k_h	$1.5 \times 10^{-9}\ m/s$
P	$1\ \Omega.m$
C_{ve}	$3.8 \times 10^{-8}\ m^2/sec$
V	$V_0 \times f(t)$
$f(t)$	Refer to Table 7.3
V_0/L	$0.33\ V/m$
C_c	0.316
C_s	0.045
σ'_p	$120\ kPa$

7.5 Results and discussion

The electrically-induced soil settlement calculated from the numerical model was compared to the field data for Mont St-Hilaire clay. The results are presented after $t = 15$ days (short-term) and $t = 48$ days of voltage application in various locations. In addition, the numerical results from Yuan and Hicks (2015) were compared with the proposed model. Yuan and Hicks (2015) proposed a 2D EO consolidation model for St. Hilaire clay based on EO consolidation governing equation and conservation of electric charge law. The finite element method (FEM) was used to solve the mentioned equations over the desired boundaries similar to those shown in Fig. 7.7. For this purpose, Cam clay model was used to estimate the soil behaviour and soil settlement. Note however that the important parameters in Yuan and Hicks (2015) model were identified before any voltage application. Thus, the effect of voltage application and potential loss on those important parameters was ignored. After comparing the proposed model with that developed by Yuan and Hicks (2015), the shear strength improvement of the soil in the field was estimated and verified.

7.5.1 Electrically-induced soil settlement

Fig. 7.11 shows the numerical results using the proposed model and Yuan and Hicks (2015) model along with the experimental data. In addition, the absolute errors from the two numerical models are compared as box plots for different times in Fig. 7.12.
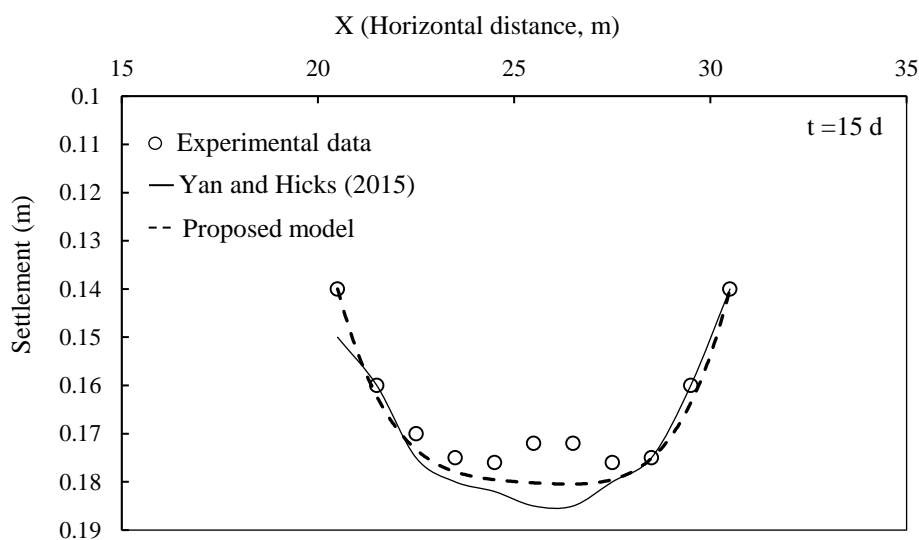
(a) Soil settlement after $t = 15$ d of voltage application (short-term consolidation)
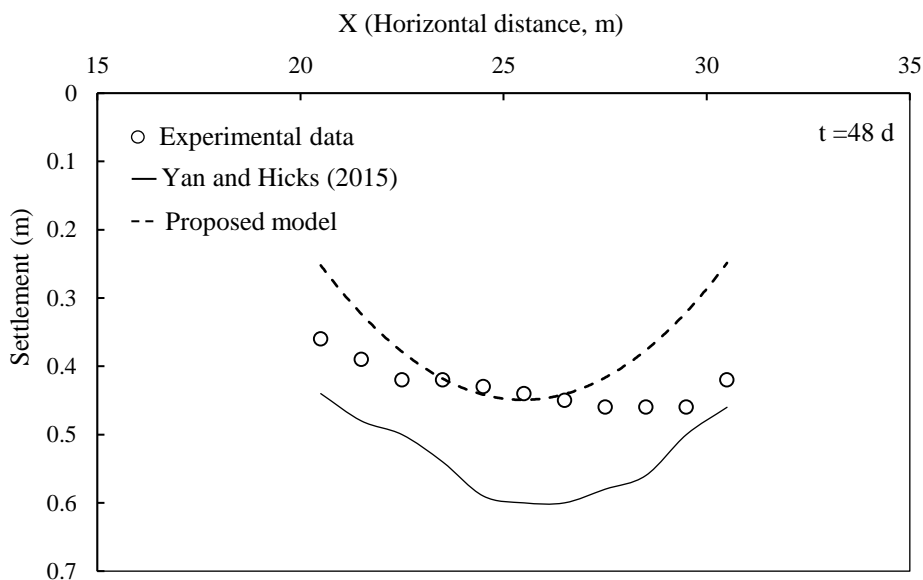
(b) Soil settlement after $t = 48$ d of voltage application

Fig. 7.11 Estimation of EO-induced settlement of Mont St-Hilaire clay in the field
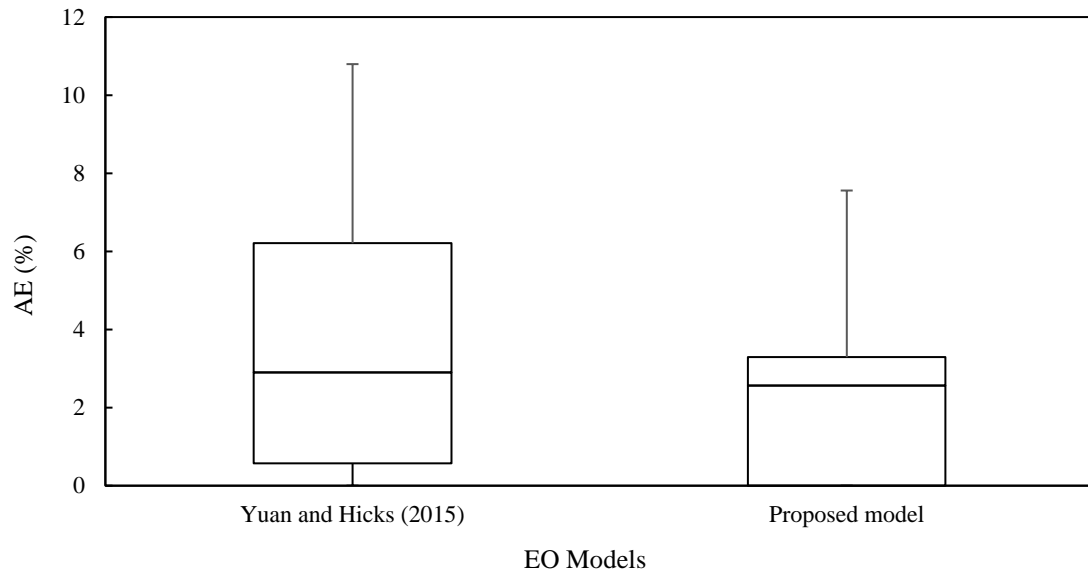
(a) Box plot of errors generated by EO model after $t = 15$ d of voltage application
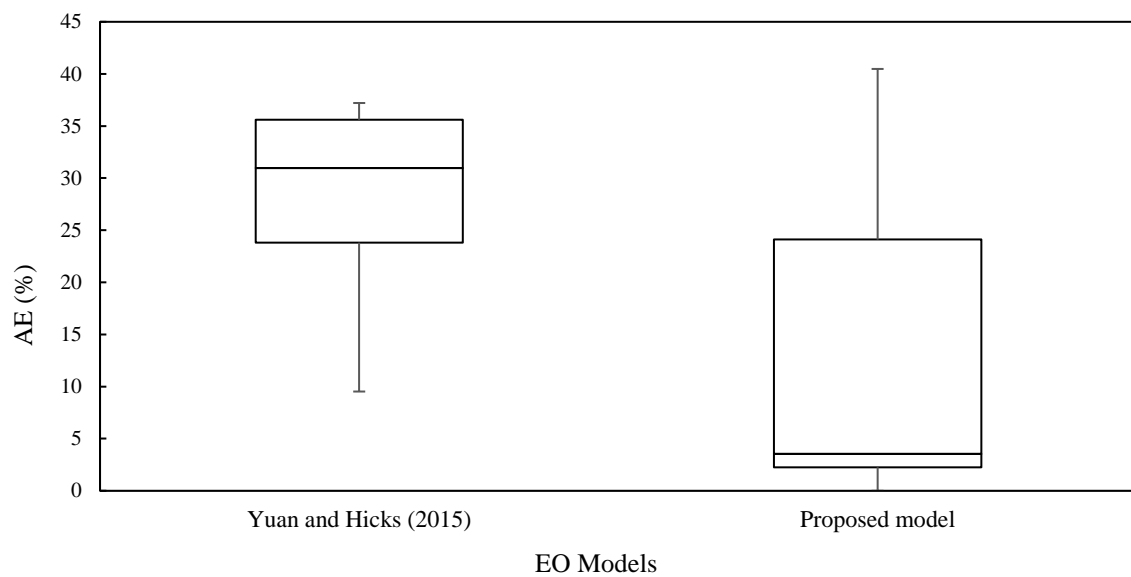
(b) Box plot of errors generated by EO model after $t = 48$ d of voltage application

Fig. 7.12 Errors generated by EO models in estimation of EO-induced soil settlement in the field

The results from Yuan and Hicks (2015) model are in good agreement with the experimental data for 15 days, with median error of 3%. However, after 48 days the model considerably overestimates the soil settlement. The median error of 30% was observed with the maximum

error of approximately 37%. The massive error generated after 48 days can be attributed to some simplifications and assumptions adopted by Yuan and Hicks (2015). The potential loss at soil-electrode interface was neglected and the C_v was used as coefficient of EO consolidation. As discussed in Chapter 6, assuming C_v as the coefficient of EO consolidation and no potential loss leads to reasonable estimate of soil settlement in the short term. Therefore, the model showed reasonable estimate of soil settlement at the beginning of the EO consolidation for 15 days and then overestimated for 48 days duration. In addition, the Cam clay model was used as a part of their model to estimate the soil settlement; however, the Cam clay model parameters were all assumed to be constant which may actually change during voltage application and need to be verified before using the model.

On the other hand, in the proposed model, C_{ve} was used as the coefficient of EO consolidation and the potential loss at soil-electrode interfaces were incorporated in the model. Based on the results, the proposed model was reasonably in good agreement with the experimental data in all situations, showing median errors of 3% and 4% after 15 and 48 days of voltage application, respectively, compared to the experimental data. In addition, the maximum error of 40% was calculated based on the boxplot in a single point close to anode. The observed errors can be related to the different potential loss at soil-electrode interface in the laboratory and the 2D assumption. In addition, in 2D plan, the electric field between electrode rows were neglected. In this case, the model estimates stronger current than in the actual 3D case. This was also confirmed by Yuan and Hicks, 2015.

7.5.2 Electrically-induced shear strength

The shear strength of post-treated soil was investigated as discussed in Chapters 5 and 6. Based on the vane shear test at the middle of clay layer, $\alpha_u = 0.23$ and the initial shear strength of the soil was reported as 30 kPa (Burnotte et al. 2004). Fig. 7.13 shows the predicted shear strength using the proposed model against the laboratory-measured, field-measured and the initial shear strength of the Mont St-Hilaire clay. The experimental data were reported based on vane shear test at three locations and the linear shear strength behaviour was assumed between the tested locations (Burnotte et al. 2004). To estimate the post-treated shear strength numerically, the developed average pore water pressure was computed at each point over the length of the electrodes and substituted into Eq. 6.8. Based on the results, a good agreement was observed between the numerical and experimental post- treated shear strength up to the mid distance of

the electrodes and it was underestimated close to the anode. However, Burnotte et al. (2004) stated that "the phenomenon responsible for drastic C_u increase in the field was not modelled in the laboratory." This fact can also be related to the different patterns of potential loss at the soil-electrode interfaces between laboratory and field conditions. However, the numerically derived post-treated shear strengths of the soil are within the range of experimental results.
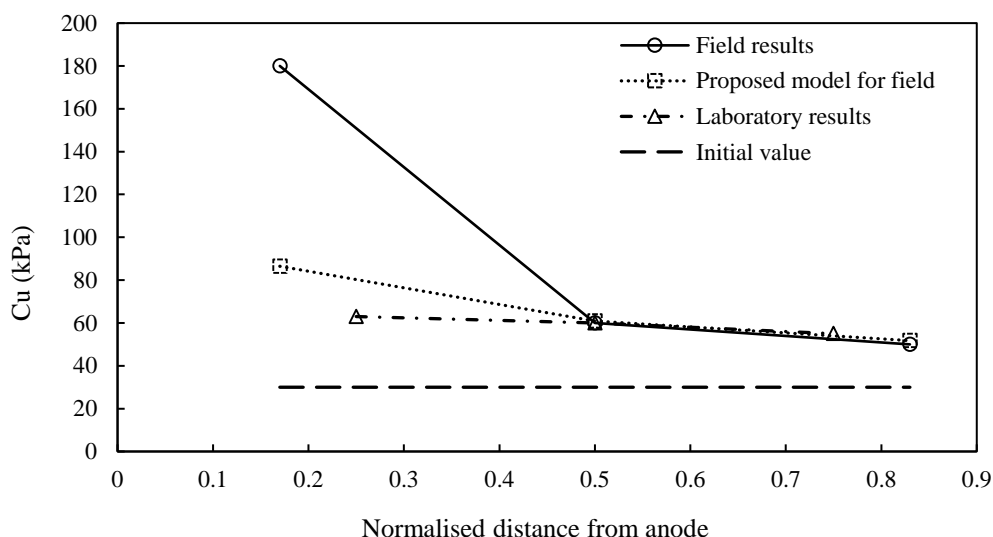
Fig. 7.13 Initial and post-treated shear strengths of Mont St-Hilaire clay

7.6 Summary

A numerical model for EO consolidation was proposed to simulate EO consolidation in the field. Basically, the proposed EO consolidation model was a successful extension of the EO model which was developed in Chapter 6. The coefficient of EO consolidation and the potential drop at soil-electrode interfaces were implemented into proposed model. The model was validated using the results of a set of well-documented field test conducted on Mont St-Hilaire clay. In addition, the proposed model was compared with a previous EO numerical model available in the literature. Although the proposed model considered only 2D scenario, the results in terms of soil settlement and post-treated shear strength were in good agreement with the experimental data. A median error of up to 4% was observed compared with the experimental data. In addition, the proposed model and the existing model were able to provide reasonable prediction of EO-induced soil settlement for 15 days after voltage application. However, over long term (48 days), the proposed model was able to provide better prediction of soil settlement than the existing model.

8 ENHANCEMENT OF ELECTRO-OSMOSIS

8.1 Introduction

The cost of the EO consolidation scheme is a controlling factor in determining its feasibility. Generally, the cost of the project is controlled by two parameters: (1) efficiency of EO consolidation; and (2) level of power consumption. Therefore, accurate estimation of these parameters leads to a more efficient design of an EO consolidation scheme in the field. Estimation of consolidation efficiency depends on the electrical resistivity of the soil which should be measured using standard methods in the field and in the laboratory. As discussed in earlier chapters, due to electrochemical processes and consequently gas generation in the vicinity of the soil-electrode interface, a large portion of the applied voltage will be lost at the soil-electrode interfaces which increases the level of power consumption and consequently the cost of the project. Therefore, an accurate estimation of the EO consolidation efficiency and the level of power consumption is crucial in the design of an efficient EO scheme and in justifying its feasibility. In addition, there is a need for a new technique to reduce the level of potential loss at the soil-electrode interface and therefore reduce the power consumption and consequently the cost of the project.

 In this chapter, the feasibility of EO consolidation was investigated in the light of EO efficiency and power consumption using the electrical resistivity of the soil, which was measured experimentally in Section 3.6. Apart from the electrical resistivity, the other parameters required were also measured experimentally in Section 5.6. Then, a unique type of

electrode was proposed, developed and tested in the laboratory in order to reduce the level of power loss at the soil-electrode interface.

8.2 EO feasibility

Generally, the feasibility of the EO ground improvement technique is controlled by the level of extracted water versus the consumed power (cost). The level of extracted water is studied under the framework of EO efficiency whereas the cost of project is studied in the light of power consumption. It should be mentioned that the power consumption is a variable part of the project cost and other expenses, such as transport of equipment, electrode drilling, wiring, fencing etc., are relatively constant for each project.

Accurate determination of the EO efficiency and the level of power consumption can lead to accurate estimation of the EO project cost and feasibility. The common important parameter affecting the extracted water and power consumption is identified as the electrical resistivity. Under a specific applied voltage gradient, electrical resistivity controls the level of extracted water and also governs the level of current developed in the soil body and, consequently, determines the level of power consumption of the EO ground improvement technique.

Estimation of EO efficiency and power consumption

As discussed in Section 2.7.1, the efficiency of the EO system is defined as the amount of transported water per unit charge that passed through the soil. The efficiency, denoted by η, is given by:

$$\eta = \rho k_e \tag{8.1}$$

The electrical resistivity, ρ, of natural clays varies between 1 to 100 $\Omega \cdot$m and the k_e ranges from 1×10^{-8} to 1×10^{-9} m^2/V$\cdot$s Therefore, the maximum theoretical efficiency is 1×10^{-6} m^3/C where C is unit charge (Coulomb). To represent the EO efficiency of each type of soil as a percentage and for more convenient comparison, the EO efficiency is normalised by the maximum theoretical efficiency (1×10^{-6} m^3/C), which is assumed as 100% efficiency. Therefore, the percentage efficiency ($\eta\%$) has been defined as:

$$\eta\% = \frac{\eta}{\eta_{max}} \times 100\% \tag{8.2}$$

Based on the above definition, the isochrones for EO efficiency were generated and shown in Fig. 8.1 as dotted lines. To investigate the level of EO efficiency of various types of soils, and to compare with the tested soil, the results from the current study on kaolin and the experimental results from case histories and large-scale experiments on different clays are utilised. The available case histories and experiments are listed in Table 8.1. However, ignoring the electrical resistivity of soil and the diversity of experimental procedures in determining the required parameters, including ρ and k_e, impose orders of errors on the measured EO efficiency. In the current study, ρ and k_e can be determined by similar standardised and calibrated methods as developed in Chapters 4, 5 and 6. In the case of previous case histories and available data, the reported values of ρ and k_e were used regardless of the experimental procedures adopted and/or assumptions used. In addition, in the majority of field and laboratory trials, the effect of electrical resistivity of the soil is ignored. In such cases, the results of electrical resistivity measurements from other research on similar types of soil are used to calculate the EO efficiency.
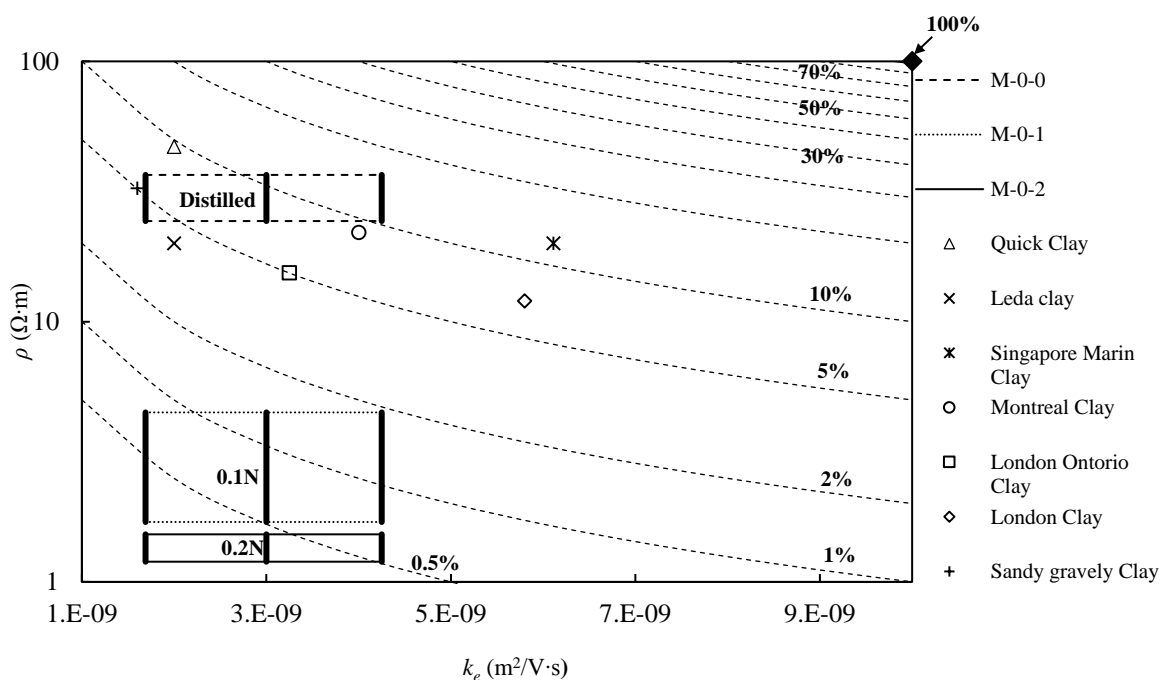
Fig. 8.1 EO efficiency for various types of clays

As the effects of soil salinity, void ratio deviation and soil boundaries on the electrical resistivity were neglected during EO consolidation in previous studies, a constant number was

reported for electrical resistivity for each type of soil in the saturated phase (Yuan and Hicks 2015) and, considering k_e as a constant parameter, a single number was calculated as the EO efficiency for each type of clay in various situations. However, the electrical resistivity of kaolin clay was measured according to Chapters 3 and 4, considering the effect of void ratio reduction and boundary conditions (Naghibi et al., 2017). In addition, the experimental results as presented in Chapter 5 were used to determine the parameter k_e. Therefore, the EO efficiency ($\eta\%$) varies depending on the salinity level, variable void ratio and EO permeability. The EO efficiency of soil can be directly affected by these factors and shows drastic drop in soil with higher level of salinity. The EO efficiencies for clays with salinities of 0.1 N and 0.2 N were investigated using the results from Chapters 3 and 5 and by assuming a similar level of k_e at different salinity levels.

The EO efficiency of various tested materials along with efficiency curves are shown in Fig. 8.1. For all tested materials, at low salinity levels, $\eta\%$ varies within a narrow range of 4% to 12%. In addition, the softer the soil the higher the EO efficiency. For soils which are categorised as soft soils, the efficiency is approximately 10% to 12%. However, all tested stiff clays show efficiency between 4 to 10%. Therefore, by determining one of the two parameters, ρ or k_e, the other one can be estimated using Fig. 8.1. The results for kaolin clay from the current study also show very good agreement of $\eta\%$ with those available in the literature, which lie between 4% and 14% for different situations.

However, by increasing the pore water salinity to 0.1 N and 0.2 N, maximum efficiencies of 2% and 0.6% were observed, respectively. This fact implies that pore water salinity should be closely monitored before choosing EO as an option for ground improvement.

Knowledge of the required level of improvement and accurate determination of EO efficiency lead to an estimation of the required voltage, which holds an immense importance in the estimation of the consumed power. In addition to the level of the applied voltages, the level of power consumption depends on the electrical response of the soil to the applied voltage (current). Based on Ohm's law, the level of power consumption in the EO system can be estimated as:

$$P = \frac{V^2}{R} \qquad (8.3)$$

where R is the soil resistance. To extend the estimated power consumption to the field, P is normalised by the volume of treated soil.

Therefore:

$$\frac{P}{vol} = \frac{V_L^{\,2}}{\rho} \qquad\qquad (8.4)$$

where V_L is electric field intensity which is defined as V/L (V/m) and vol denotes the volume of the treated soil. In addition, based on the experimental results in laboratory scale, approximately 40% of the applied potential will be lost, which should be considered in Eq. 8.3. Therefore, considering 40% potential loss at the soil-electrode interface, and knowing the electrical resistivity of the soil and the applied electrical potential gradient, the level of power consumption can be estimated by Eq. 8.4.

Table 8.1 Laboratory experiments and case histories of EO consolidation

Test No	Location	Test Type	Clay type	Duration (days)	Potential difference (v)	V/cm	Electrode materials	Embedded electrode length (m)	Spacing (m)	USSR (%)	k_h (m/s) $\times10^{-10}$	Potential loss factor	k_e (m²/V·s) $\times10^{-9}$	Electrical Resistivity (Ω.m)	Energy consumption (kWh/m³)	Reference
1	Norway	Field	Quick Clay	120	40*	0.25	Steel	9.6	2	380	2	25%-50%	2	47	17	Bjerrum, L. (1967)
2	Canada	Field	Sensitive Leda clay	32	25-120	0.2	Copper	5.5	3	182	2	55%-85%	0.2	20	10	Lo et al. (1991)
3	Malaysia	Lab test	Kaolin clay	-	5-30	0.27-1.7	Copper	Horizontal	0.18	-	10	25%-50%	3	47	-	Hamir et al. (2001)
4	Singapore	Lab test	Soft marine clay and stiff clay	-	2	1	Stainless-steel	Horizontal	0.02	-	11.71	-	6.11	20	14-28	Chew et al. (2004)
5	Singapore	Lab test	Soft marine clay and stiff clay	-	3	1.5	Stainless-steel	Horizontal	0.02		11.71	-	6.11	20	14-28	Chew et al. (2004)
6	Singapore	Large Scale Lab test	Soft marine clay and stiff clay	3.125	20	0.7	Conductive plastic	0.15	0.3	160-350	11.71	-	6.11	20	14-28	Chew et al. (2004)
7	Singapore	Field	Soft marine clay and stiff clay	13.12	14	0.12	Conductive plastic	35	1.2	132	11.71	-	6.11	20	1.8(3.6)	Chew et al. (2004)
8	Canada	Field	Soft clay (Montreal)	48	93	0.31	Steel	5	3	214	-	-	4	22	148	Burnotte et al. (2004)

9	Malaysia	Field	Very soft to soft clayey silt	14	7-29	0.05-0.21	Copper foil and C.P.	6	1.4	439			-	1.5		0.7	Rittirong et al. (2008)
10	Malaysia	Large scale Lab test	London Ontario clay	11	25	1.38	Copper foil and C.P.	0.2	0.18	-		11%-0.72%		3.25	15.4	200	Rittirong et al. (2008)
11	Malaysia	Large scale Lab test	London Ontario clay	11	45	2.5	Copper foil and C.P.	0.2	0.18	-		11%-0.72%		3.1	13.3	430	Rittirong et al. (2008))
12	UK	Field	Mainly London clay	42	60-80	0.3-0.4	EKG		2	-	1		-	5.8	12	11.5	Jones et al. (2011)
13	UK	Field	Sewage sludge**	63	10-30	0.33	EKG	-	-	-	-	-		1.5	-	128	Glendinning et al. (2007)
14	UK	Lab test	Silty sandy Clay	1.7	2.5	0.5	EKG		0.05	-	1.38		-	1.4	40	4	Lamont-Black et al. (2016)
15	UK	Lab test	Sandy gravely Clay	1.7	2.5	0.5	EKG		0.05	-	0.59		-	1.4	25-40	8.1	Lamont-Black et al. (2016)
16	UK	Lab test	Mainly Sandy Clay	1.7	2.5	0.5	EKG		0.05	-	2.10		-	1.6	25-40	4.5	Lamont-Black et al. (2016)
17	UK	Field	Mixture of silt, sand, gravel and clay	42	80-10	0.5	EKG		1.5-2	-	-		-	1.6	25-40	6.14	Lamont-Black et al. (2016)

*Average value

** Very low initial shear strength which was assumed to be 1 kPa

Fig. 8.2 shows the calculated power consumption based on Ohm's rule considering the potential loss at soil-electrode interface. Each dotted graph shows a specific level of power consumption in kW/m^3. For comparison, the consumed power for available field trials are also shown.

In majority of the field trials, the field-measured power consumption indicates a higher level compared to the calculated power consumption. These results signify more than 40% of potential loss in the field compared to that observed in the laboratory tests. In other words, the level of potential losses observed in the field are much higher than those measured in the laboratory. The reasons for this difference can be attributed to the lack of voltage calibration in the laboratory, short-term measurement of voltage drops and perfect contact of soil-electrode in horizontal electrode configuration in the laboratory.
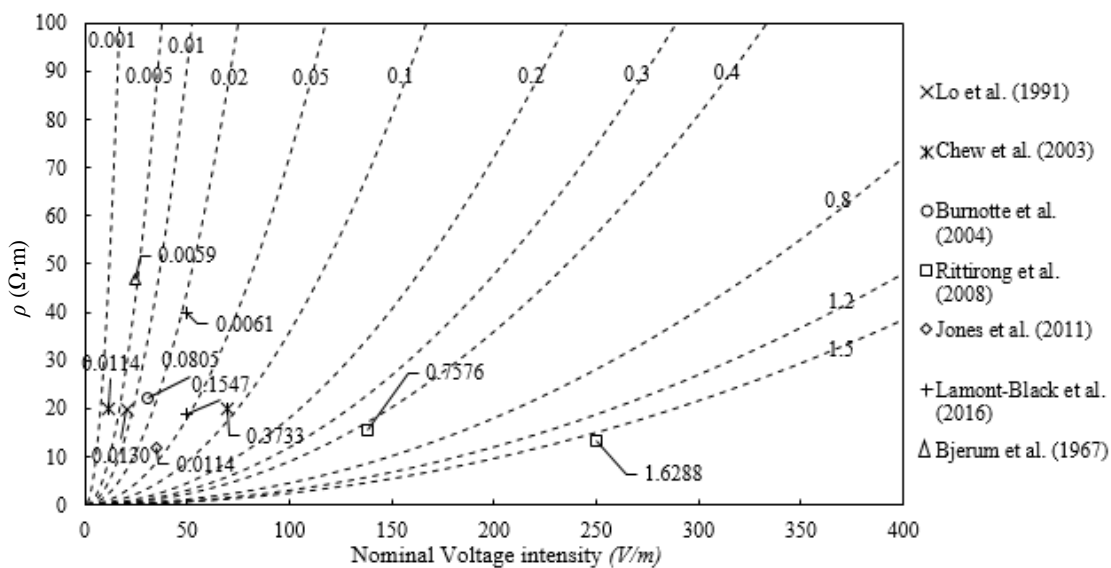
Fig. 8.2 Power consumption (in kW/m^3) for various types of clays

To tackle this issue and to minimise the level of power consumption in the field, two options are available: (1) increasing the electrical resistivity of the soil; and (2) decreasing the potential loss at the soil-electrode interface. Generally, improving the soil properties, such as electrical resistivity, is not practical in real case. Therefore, reducing the potential loss is considered.

Usually, injection of chemicals, such as saline solution, calcium chloride and sodium silicate, is used to reduce the electrical resistivity at the soil-electrode interface and decrease the level

of power consumption. As discussed, although increasing the level of chemicals in the pore solution leads to a lower electrical resistivity and lower potential loss at soil-electrode interface, it decreases the efficiency of the EO process simultaneously and less volume of water drained from the soil body should be expected. Therefore, a detailed EO efficiency study is required for individual chemical injection in a specific type of soil. In this research, a physical approach has been considered to decrease the resistivity of soil-electrode interface resistance and consequently, the consumed power. To achieve this goal, a physical modification is made on the cathode to reduce the level of gas production and enhance the capability of the system to remove the generated gas.

8.3 Proposed electrode system

To decrease the level of potential loss at the soil-electrode interface, a physical modification was made on the electrode of the laboratory set up and, as no chemical has been injected, the EO efficiency of the soil was maintained constant. The proposed electrode is shown in Fig. 8.3. The body of the electrode was made of steel grinds. A thin geosynthetic material was also placed at the middle of the grind electrode to facilitate the water drainage at the cathode. To apply the electrical potential gradient, a conductive cap with a conductive tag was fabricated and positioned on the top of the steel grinds. The grind electrode body allowed the generated gas in soil-electrode vicinity to move to the surface and be flushed out from the conductive cap. The removal of generated gases leads to a lower electrical resistivity at soil-electrode vicinity and lower level of potential loss. In addition, this system enhanced the contact between the soil and electrode through increasing the contact surface and provided more uniform electric field inside the soil throughout the electrode length. Furthermore, as the full length of the electrode was performing as a drainage surface, the drainage was increased in the system compared to that in conventional perforated cathodes. To check the capability of the proposed electrode, an extensive experimental programme utilising a large oedometer cell was conducted.
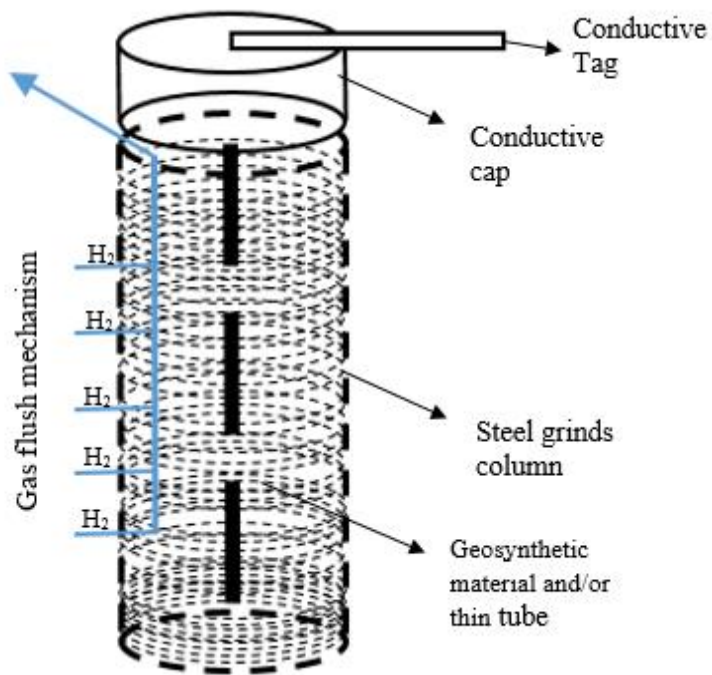
(a) Schematic diagram of the proposed electrode and gas flush mechanism

(b) Steel grinds used in the experiments   (c) Conductive cap and electrode sleeve
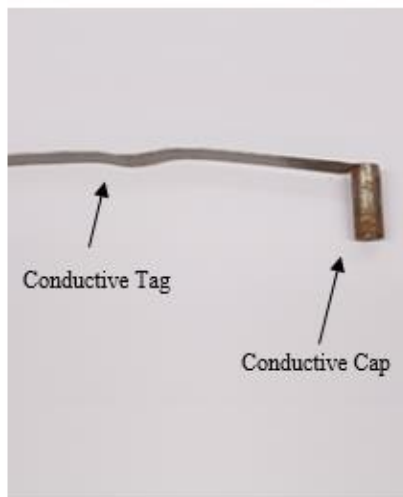
Fig. 8.3 Overview of the proposed system for the cathode

8.3.1 Apparatus for testing the proposed electrode

To investigate the applicability of the proposed electrode, a bench-scale oedometer cell was developed and fabricated as shown in Fig. 8.4. A 150 mm diameter PVC cell was designed to accommodate the EO consolidation system.

The EO consolidation system which confined a 380 mm high soil specimen included four circumferential steel electrodes (A1-A4) located in a rectangular configuration, as shown in section C-C in Fig. 8.5. The electrodes were inserted through the top cap which was made of PVC with the same diameter as the cell. The anodes were identical, with diameter of 10 mm made of solid steel. An electrode as a cathode (C) was also located at the centre of the cell at 60 mm distance from the anodes. Two types of electrodes were used in the test programme: perforated solid steel, as shown in Fig. 8.6, and steel grinds (proposed electrodes). A smaller diameter PVC loading cap was fabricated to apply the load before starting the EO consolidation process. A large groove was made at the bottom surface of the loading cap to give the conductive cap enough room to be lifted and to flush the gas out of the cathode medium during the test. In addition, to measure the potential loss at electrode vicinities, 4 stainless-steel probes were located on the top cap at various distances from the cathode. As the potential loss at the cathode was more problematic, the probes were placed closer to the cathode and one of the probes was designed to specifically check the potential loss at the anode. The material utilised for voltage probes held a great importance in the voltage measurements, especially in the laboratory scale. To address this issue, extensive calibration experiments were conducted as outlined in the following section.

8.3.2 Experimental programme

The experimental procedure involved EO consolidation experiments, as outlined in Table 8.2. Initially, a control experiment was conducted using a conventional EO consolidation system. Then, an EO consolidation test was carried out in the same EO cell, as illustrated in Fig. 8.4, using the proposed electrode shown in Fig. 8.3 as cathode. The applied electric potential gradient was maintained constant at a level of 0.67 V/cm.
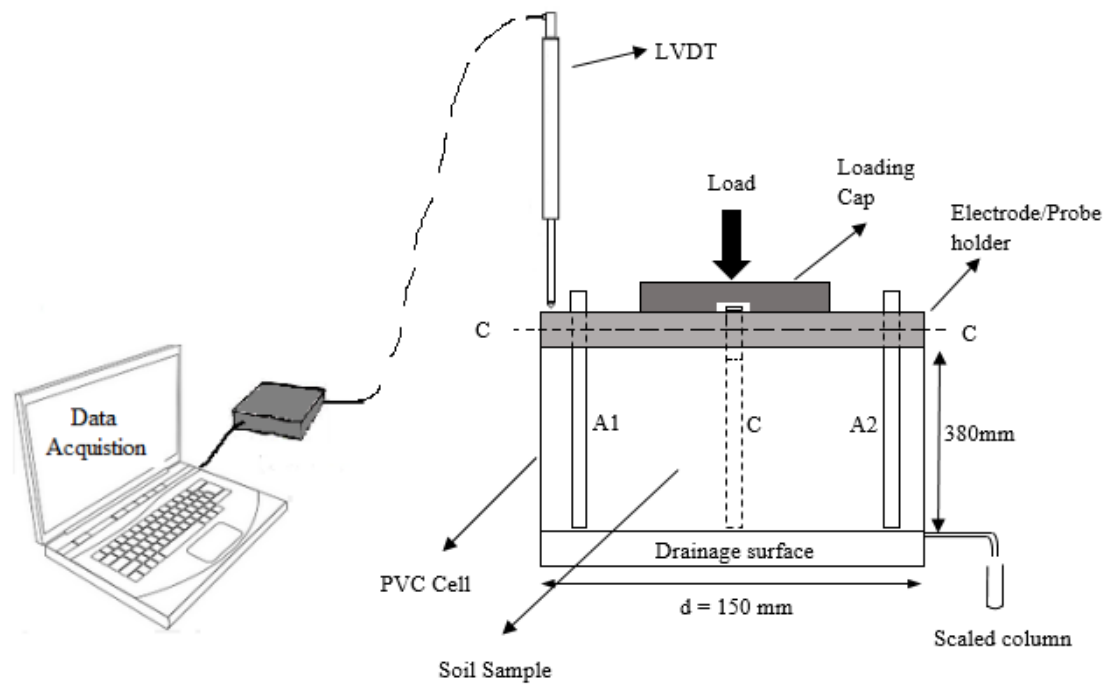
Fig. 8.4 View of large oedometer cell
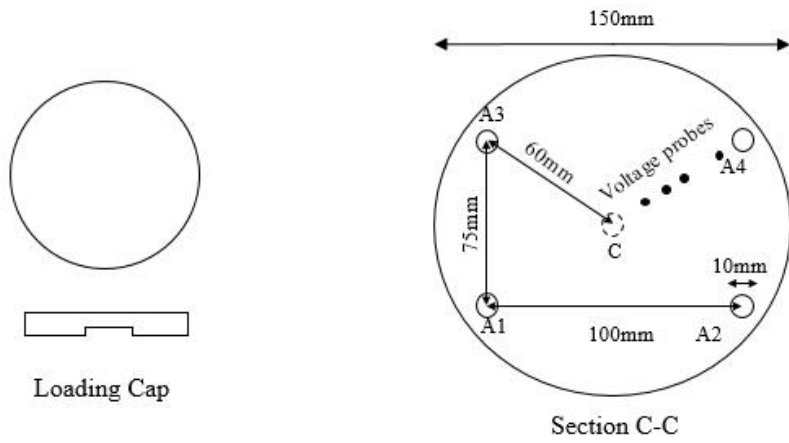
(a) Loading cap   (b) Electrode/probe holder (PVC)

Fig. 8.5 Electrode configuration and loading cap

(a) Cathode   (b) Anode

Fig. 8.6 Conventional electrodes

Table 8.2 Summary of EO consolidation tests

Test No	Applied potential gradient (V/cm)	Cathode	Anode	Preconsolidation pressure (kPa)
EO-4-CC	0.67	Perforated Solid steel	Solid steel	10
EO-4-GC	0.67	Steel grinds	Solid steel	10

8.3.3 Calibration of voltage measurements

In the absence of an electric gradient, when a metallic electrode is immersed in an electrolyte such as saturated soil, oxidation and reduction take place in the vicinity of the soil-electrodes interfaces.

$$oO + ne^- \leftrightarrow rR \qquad (8.5)$$

Here, ne is charge transfer, o and r are coefficients related to oxidation and reduction, respectively. Oxidation and reduction causes flow of electrons from the soil solution to the electrode (anodic current) and from the electrode to the soil solution (cathodic current), respectively. Those currents are dynamic and an equilibrium situation is established at a relatively constant potential, which is known as equilibrium potential at the soil-electrode interfaces. The amount and sign of the potential generated at the electrodes depend on the electrode materials. The total potential gradient generated at the two electrodes can be calculated as:

$$E_{cell} = E_+ - E_- \qquad (8.6)$$

where E_+ and E_- are the potentials at the electrodes and E_{cell} is the potential gradient between the two electrodes. The values of E_+ and E_- are usually measured in a standard situation and are available in electro-chemistry literature (e.g. Bagotsky, 2005).

Utilising stainless steel wire as a probe in the testing apparatus, as shown in Fig. 8.4, leads to the generation of a new electro-chemical cell between the probe and electrodes in the soil body in the proposed cell and generates secondary electric potential gradient (E_{cell}). Therefore, the measured electrical potential from the probes includes E_{cell} and, as a result, less potential loss at electrodes will be observed.

To measure E_{cell} and calibrate the results, an apparatus was designed as outlined in Fig. 8.7. A steel electrode with 10 mm diameter was immersed into the kaolin clay, then probes of various materials, including stainless steel, were placed in a PVC spacer located beside the electrode. The voltage generated by each electro-chemical cell was recorded at four locations to consider the possible effect of distance between the electrodes. The tests conducted are listed in Table 8.3.
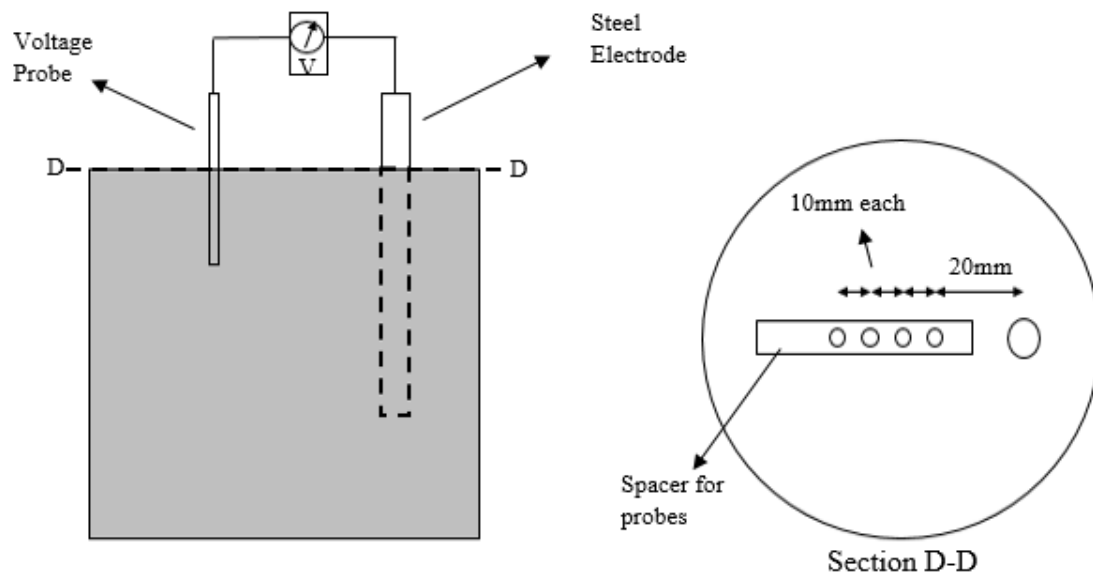
(a) Profile and plan view of voltage calibration apparatus

(b) Probe spacer

(c) Utilised probes

Fig. 8.7 Voltage calibration apparatus

Table 8.3 Summary of calibration tests

Test No	Probe	Electrode
CA1	Steel	Steel
CA2	Copper	Steel
CA3	Stainless steel	Steel
CA4	Brass	Steel

8.4 Experimental results and discussion

The feasibility of the proposed electrodes was checked against the conventional solid steel electrodes. The effective electric potential gradient, developed current, induced volumetric strain, void ratio reduction and drained water, were compared and discussed for both cases.

8.4.1 Voltage profiles

To verify the feasibility of the proposed electrodes, the potential loss at soil-electrode system should be measured. To measure the voltage between the electrodes, the apparatus shown in Fig. 8.4 was used. However, as the probes used in this test were different from the electrode materials, the calibration test results were also utilised. Fig. 8.8 shows the results of the calibration tests. The steel probe, which was made of steel similar to the electrodes, showed no generated voltage in the absence of applied electric potential gradient. However, by using different materials as voltage probes, approximately a constant level of 0.6 V of generated voltage was recorded. In addition, the generated voltage was recorded at various locations between the electrode and voltage probes. Limited variations, in the order of few mV, were observed at different locations.
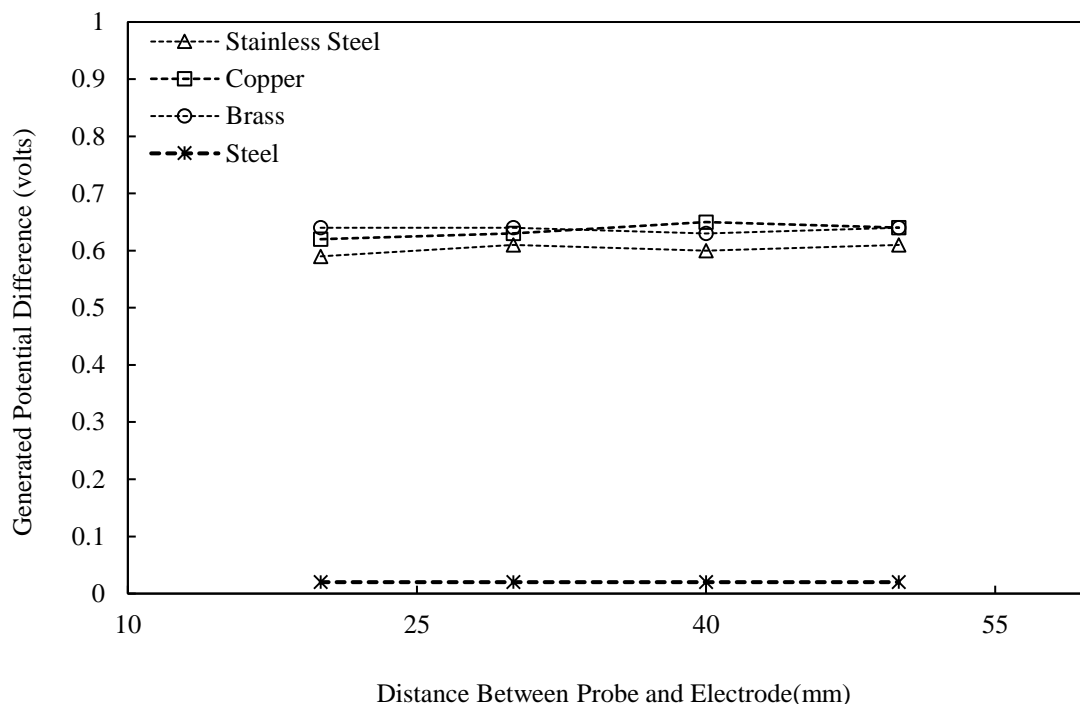
Fig. 8.8 Generated voltage at various locations in the absence of electric field in the soil body

As the generated voltage was independent of the location of probe, the voltage can be negligible in the field where voltages of 30-100 V are generally applied to the soil by means of electrodes. However, in the laboratory scale, the applied voltage is usually in the order of 1-5 V and therefore 0.6 V can noticeably impact the results. Hence, the potential loss at electrodes should be recorded considering the material of voltage probes and it should be fully calibrated.

The potential loss at the electrodes was measured during the consolidation test in a large oedometer cell, which is shown in Figs. 8.4 and 8.5. In addition, copper voltage probes were used in the test. Fig. 8.9 shows the calibrated voltage gradient profiles across a pair of electrodes in the soil body. The experimental results are presented for two different time steps: 10 minutes after voltage application and approximately 15 hours after voltage application, at various locations for the conventional cathode (solid, perforated) and the proposed cathode. 10 minutes after voltage application is assumed to be prior to gas generation because some initial soil displacement was observed during that time. In addition, 15 hours can be assumed to be the end of EO consolidation process (constant displacement recorded for more than an hour) and accounted for the "after gas generation" at the cathode. These steps are designated as

"before gas generation" and after gas generation" in Fig. 8.9. In addition, linear voltage distribution (Esrig's theory) which implies zero potential loss is also shown in the figure.

At a normalised distance (l/L) of 0.87 from the anode, normalised potential drops (V_{loss}/V_{app}) of approximately 0.6 and 0.85 were measured for the conventional electrode, before and after gas generation, respectively. Note that, l and L are illustrated in Fig. 8.9. These values are in the range of the observed values in the field (Table 8.1).
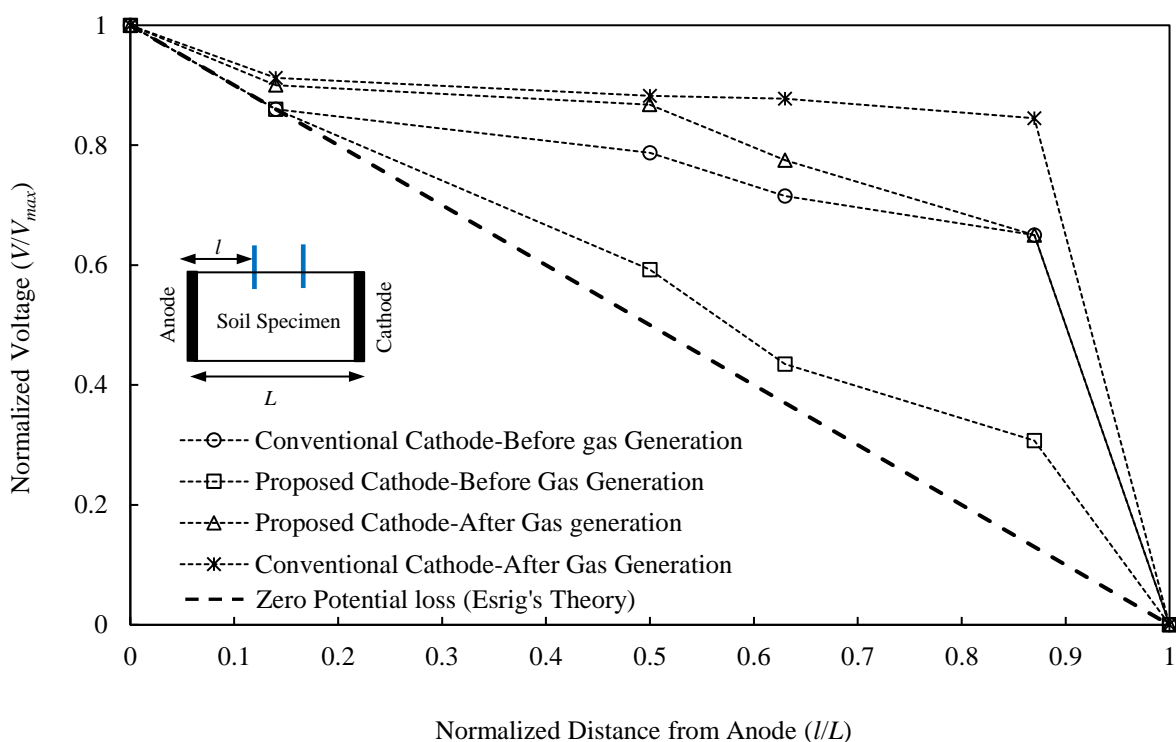
Fig. 8.9 Calibrated potential drop at electrodes

However, for the proposed electrodes, normalised potential drops of 0.31 and 0.6 were observed before and after gas generation, respectively. These values are higher than those proposed by Esrig, which shows a constant value of 0.13 at the tested location (l/L=0.87). The higher effective potential in Esrig theory is one of the factors which can lead to overestimation of soil settlement during EO consolidation. The level of potential drop before gas generation can be attributed mainly to the loose contact between the soil and electrodes. However, after gas generation, the potential loss is mainly related to two factors: (1) gas generation; and (2) movement of generated gas from the anode to the cathode. In addition, comparing the electrode alignment, the vertical electrodes show lower level of voltage efficiency as the overburden

pressure is applied directly to the electrodes and improves the soil-electrode contact. In addition, in the case of the proposed electrode, the decrease in potential drop at the soil-electrode interface can be attributed to a better contact between the soil and electrode and gas flush mechanism in the proposed electrode.

8.4.2 Electric current developed

As discussed earlier (Eq. 2.34) the current developed in the soil body during EO consolidation is a contributing factor to quantifying the volume of transported water from the anode to the cathode. Higher effective voltage received by the soil implies higher level of current passage through the sample. This is confirmed by the current evolution with time, as shown in Fig. 8.10. After 10 seconds of applying the voltage, the current measurement was commenced. At similar applied voltage, the level of developed current (corresponding to achievement of 90% consolidation) was about 55% more than that developed by conventional solid electrodes. As expected, the same level of current was recorded for the proposed and conventional electrodes at the end of the consolidation process.
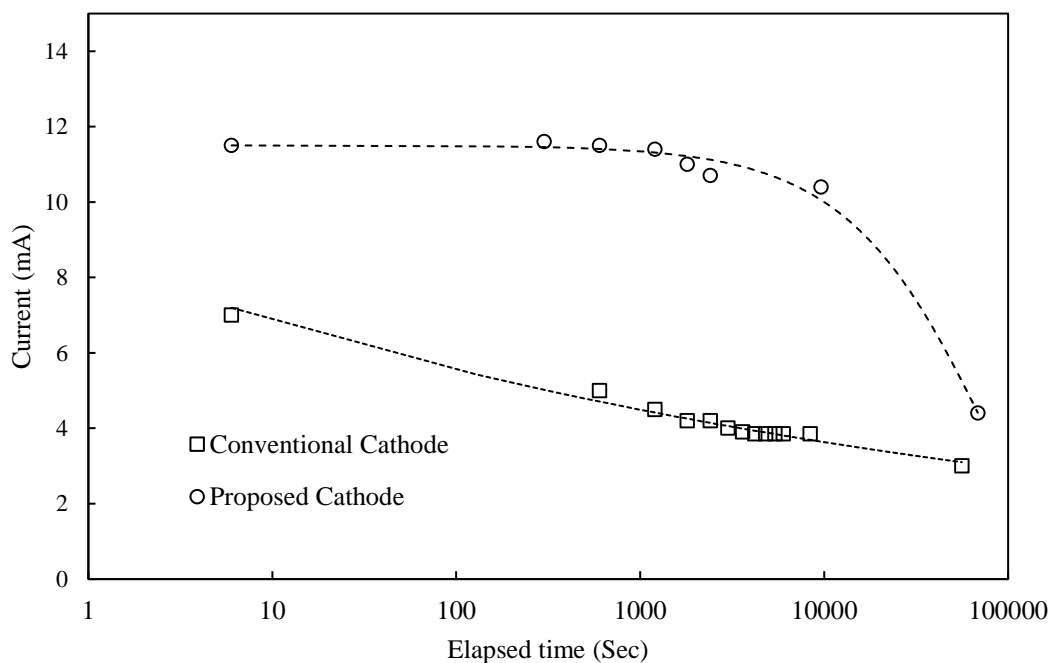
Fig. 8.10 Recorded current in conventional and proposed electrode systems

In addition, the electric flow decreases at approximately constant rate. However, the rate of decrease in electric flow during EO consolidation is higher for the proposed electrodes. The decrease in electric current can be attributed mainly to gas generation and potential drop at the cathode (referred to as Zone 1 in Chapters 4 and 5) and reduction in total electrical resistivity of the soil. The total electrical resistivity of the soil decreases due to the transport of gas from anode to cathode and the reduction of void ratio, as discussed in Chapters 4 and 5 (Zone 2).

8.4.3 Induced water flow

Generally, the application of the electric potential gradient leads to the development of EO flow and consequently the water flow increases. By increasing the EO flow from the anode to the cathode, a hydraulic gradient will develop over the soil body which triggers the counterflow from the anode to the cathode. The development of counterflow leads to a reduction in EO flow rate. The development of hydraulic gradient continues until the counterflow overcomes the EO flow and the water flow rate decreases. These behaviours were observed in the laboratory for both the conventional and proposed electrode systems. However, the proposed electrode system shows a higher level of developed EO flow. Fig. 8.11 shows the electrically-induced water flow for the proposed and conventional electrodes. As more current was developed in the proposed electrode, more water flow was induced as expected. In the case of conventional cathode, water flow of 0.5 mm^3/s was recorded at the beginning of the consolidation. The flow rate increased gently for approximately two hours to about 0.95 mm^3/s and then decreased to 0.17 mm^3/s in 15 hours. However, for the proposed electrode, water flow of approximately 0.9 mm^3/s was measured at the beginning of the EO consolidation which increased up to 2.6 mm^3/s in first hour. Then, the flow decreased to 0.25 mm^3/s at the end of the test (15 h).
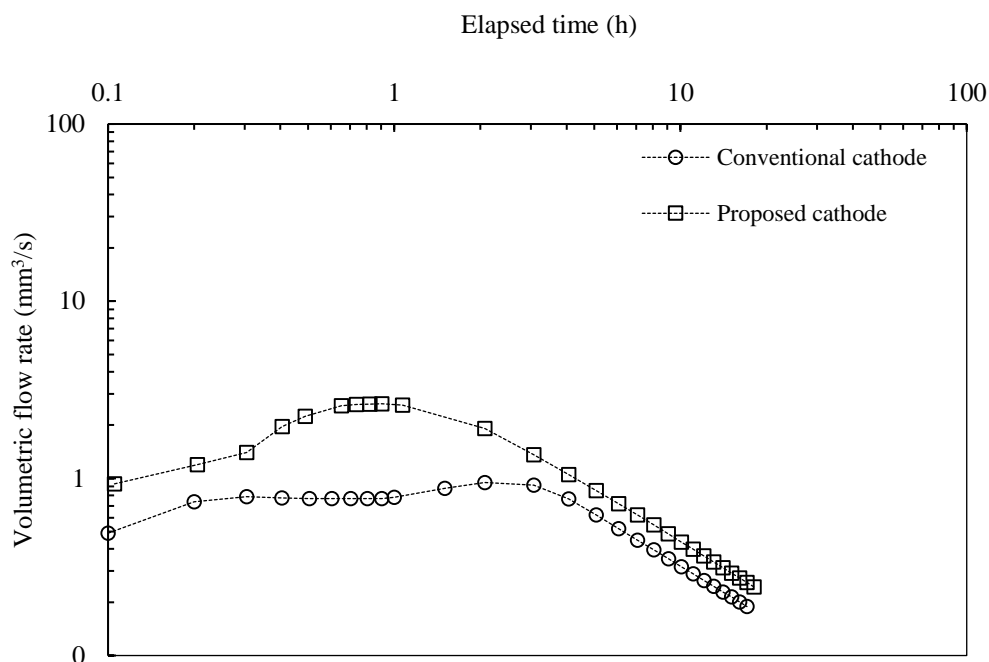
Fig. 8.11 Recorded water flow for the conventional and proposed EO systems

8.4.4 Volumetric strain and void ratio reduction

As the EO efficiency of the soil is maintained constant during the electrode modifications, a higher level of induced volumetric strain is expected by improving the effective voltage in soil-electrode vicinity. Fig. 8.12 shows the induced volumetric strain for both conventional and proposed electrode systems. In the case of the conventional electrode, the volumetric strain increased during the first three hours to 1.7% and then remained constant until the end of consolidation. However, for the proposed electrode, volumetric strain increased to approximately 3.1% in two hours and remained constant afterward. Therefore, flushing the generated gas from the cathode vicinity reduced the level of potential loss at cathode and increased the water flow in the soil body. In addition, flushing the generated gas reduced the volume of transported gas along the soil body. As shown in Fig. 8.13, these effects collectively lead to more void ratio reduction (settlement).
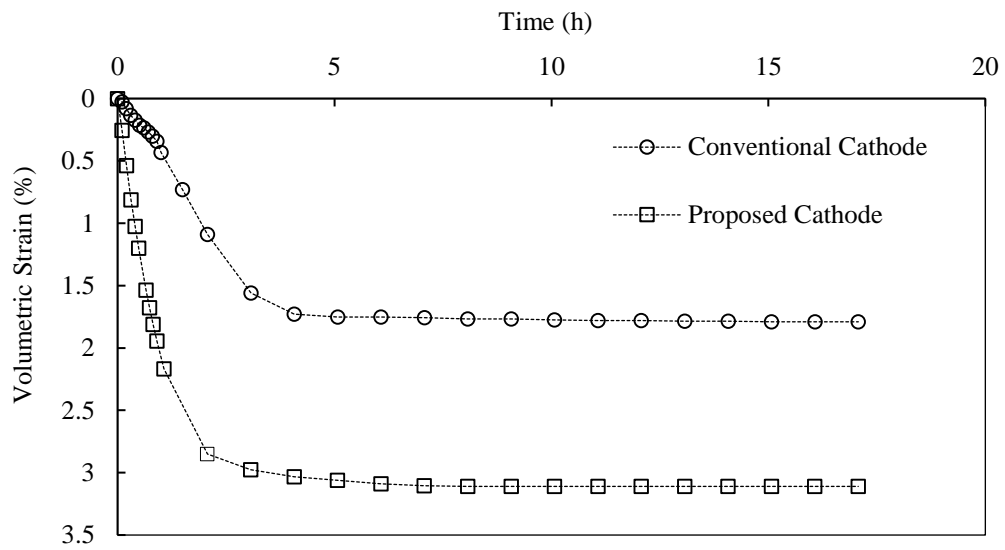
Fig. 8.12 Volumetric strain evolution in EO tests
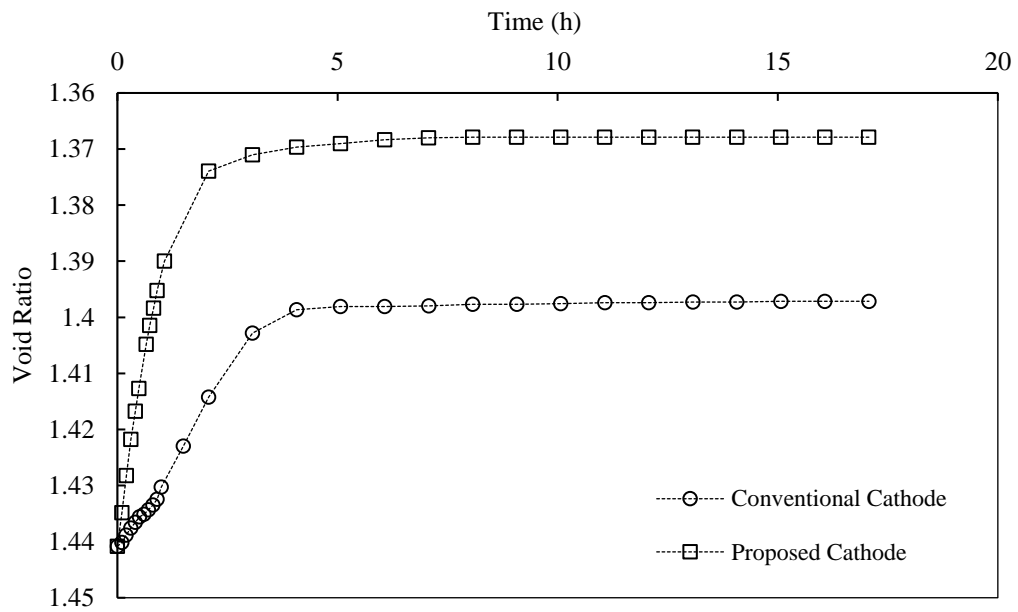
Fig. 8.13 Void ratio evolution in EO tests

8.5 Summary

The cost of EO consolidation is one of the most important concerns. Potential loss was discussed based on two parameters: (1) EO efficiency; and (2) power consumption. Therefore, these two parameters can be improved to increase the effectiveness of EO consolidation. As the EO efficiency is a constant parameter for a specific soil, a new electrode, consisting of steel grinds, was proposed to reduce the level of power consumption and consequently reduce the cost of the EO project and increase its feasibility. The proposed electrode was successfully tested on kaolin clay in a specifically-designed relatively large electric oedometer cell. Results showed that the proposed electrode increased the water flow, the developed electric current and the soil settlement compared to conventional electrodes.

9 CONCLUSIONS AND RECOMMENDATIONS

Generally, the feasibility of EO ground improvement technique depends on the EO efficiency and the post-treated behaviour of the soil, although this method is the only available technique in some cases. The efficiency of EO consolidation depends on: (1) the electrical resistivity of the soil; and (2) electro-osmosis permeability. Therefore, in order to estimate the efficiency of EO consolidation these parameters should be measured accurately for each type of soil. Apart from the mentioned parameters, hydraulic permeability, applied electric potential gradient and voltage drop at the soil-electrode interfaces are important parameters affecting the negative pore water pressure developed in the soil body. Such negative pore water pressure indicates the effective stress induced in the soil and based on this, the soil behaviour can be estimated using various theories. Therefore, to have an accurate estimation of these parameters, a robust framework is required.

A new oedometer cell was modified and fabricated to measure the electrical resistivity of the soil during the consolidation process. Then a similar-sized oedometer cell was modified and fabricated to measure the other parameters during consolidation and voltage application. These oedometers were used to conduct the laboratory tests on New Zealand kaolin clay. Then, important parameters obtained were used to estimate the efficiency of the EO consolidation technique and the behaviour of post-treated soil. In addition, the laboratory tests from the current study and the laboratory and field tests available in the literature were in agreement that a large portion of the applied electric potential was lost during consolidation. Therefore, a new

electrode was proposed to reduce the level of potential loss at the soil-electrode interface. The proposed electrode was then fabricated and successfully tested in relatively large, modified oedometer cell. In parallel with the mentioned experimental investigations, an extensive numerical study was conducted on EO consolidation. The numerical study was conducted in three phases: (1) numerical modelling of electrical resistivity and introducing a graphical method to estimate the electrical resistivity of clays considering the volumetric water content and surface conductivity; (2) numerical modelling of EO consolidation considering the electrical resistivity of soil and the time-dependent potential drop at soil-electrode interface; and (3) extension of EO consolidation numerical model to the field scale. The main conclusions extracted from the experimental and numerical investigations are presented in following sections.

9.1 Conclusions from experimental investigations

The following conclusions were made from the experimental investigations:

- The electrical resistivity of clays depends on the volumetric water content and surface conductivity. Therefore, assuming a constant value for electrical resistivity would lead to errors in the estimation of EO efficiency and post-treated soil behaviour.

- The measurement of the electrical resistivity of soil should be conducted using a standard method and the effects of the boundary on the measured electrical resistivity should be considered. To consider these factors, an oedometer was modified, fabricated and calibrated.

- Based on experimental investigation on kaolin clay and a mixture of sand and kaolin clay (up to 20%), electrical resistivity ranging from 25 to 39 $\Omega \cdot$m was measured for various volumetric water contents and zero salinity. However, by increasing the salinity of pore water to 0.1 N and 0.2 N, the measured electrical resistivity of the same soil dropped to a smaller range of 1.4 to 3.6 $\Omega \cdot$m depending on the volumetric water content.

- The experimental investigation of EO consolidation using an electrical oedometer cell showed that the effectiveness of EO consolidation was influenced by the stress history. Generally, the EO consolidation was more effective on NC soil with lower preconsolidation pressure. Using the EO apparatus described, about 1-2% of volume change was observed in soil specimens with preconsolidation pressures of 345 kPa to 86 kPa. However, in OC soil with preconsolidation pressure of 172 kPa, a maximum of

0.2% volume change was measured for OCR=2 and a constant volume change of 0.13% was observed for OCR=4 and 8.

- The effect of stress history on EO permeability (k_e) was limited. Considering constant potential loss at soil-electrode interface, a value of 3×10^{-9} m^2/V·s was found for kaolin clay with different preconsolidation pressures and OCRs, which was within the range reported in the literature. In addition, for a constant applied voltage gradient, the hydraulic permeability (k_h) of soil during EO consolidation was found to depend on the void ratio of the kaolin clay and a relationship was proposed to estimate the k_h based on the void ratio.

- Voltage application on soil had various effects on the consolidation properties. In the case of kaolin clay, the effect of voltage on compression index was limited. However, the swell index increased after voltage application. The rate of increase in swell index depended on the preconsolidation pressure. In the case of kaolin clay, a higher rate of increase in swell index was observed in OC soil and in higher preconsolidation pressure. In addition, the coefficient of consolidation during EO consolidation was approximately one tenth of the coefficient of consolidation during hydraulic loading in tested soil.

- The potential loss at the soil-electrode interface showed a temporally and spatially variable pattern based on the experimental results. A time-dependent graph of voltage efficiency during EO consolidation was proposed for kaolin clay.

- Because a substantial portion of the applied electric potential was lost at the soil-electrode interface in the laboratory and in the field, a new electrode system, consisting of steel grinds, was proposed to remove the generated gas from the electrodes, decrease the electrical resistivity of the soil-electrode interface and potential loss, and enhance the effectiveness of EO consolidation process. The proposed electrode system was tested successfully in a relatively large modified oedometer cell. It was found that the proposed electrode system reduced the level of potential by up to half in some locations close to the cathode, doubled the developed current and induced approximately twice the volumetric strain in the soil, compared to a conventional electrode system.

9.2 Conclusions from numerical investigations

As discussed earlier, the numerical study was conducted in three phases. The conclusion made from these phases are summarised below.

- Based on the results of numerical modeling of electrical resistivity of soil, a graphical procedure was proposed to estimate the electrical resistivity of soil at different volumetric water contents and surface conductivity. The proposed graph could estimate the electrical resistivity of kaolin clay at various conditions with maximum absolute error of 4%. Then, the electrical resistivity could be used to model EO consolidation of the soil.

- The numerical modeling of EO consolidation showed that less simplification than in previously available research was required to achieve better estimate of the post-treated soil behaviour. Instead of assuming zero or constant potential loss at the soil-electrode interface, the time-dependent potential loss in soil-electrode vicinity was assumed. In addition, in order to have a realistic estimate of EO consolidation, the coefficient of consolidation during the EO phase was considered in the numerical model, instead of the coefficient of consolidation during hydraulic load application.

- The electrical resistivity of soil was implemented in the EO model through the conservation law of electric charge to accurately estimate the voltage distribution across soil body. The numerical results were in very good agreement with the experimental data and had a maximum median absolute error of 7%. In addition, the level of increase in shear strength of the kaolin clay was investigated using the predicted pore water pressure developed in the soil body. A maximum of approximately 28% increase in average shear strength was observed in kaolin clay specimen with preconsolidation pressure of 86 kPa. By increasing the preconsolidation of soil, the rate of increase in shear strength was slower. Approximately 15% and 5% increase in average shear strength was found for specimens with preconsolidation pressures of 172 and 345 kPa, respectively.

- The numerical model was successfully extended to the field case. Similar to the laboratory cases, the time-dependent potential loss at soil-electrode interface, electrical resistivity of soil and coefficient of consolidation during EO consolidation were used. The results showed that this model can be used to accurately extend the laboratory-scale experimental data to the field.

- The integration of the three phases of numerical models can be used as a cost effective, reliable and accurate tool to estimate the effectiveness and efficiency of EO consolidation in the field.

9.3 Recommendations for future research

Conducting this research showed the applicability, effectiveness and efficiency of EO consolidation on kaolin clays. Based on observations from the numerical and experimental results, the following recommendations are made for future work:

- Previous research attempted to estimate the post-treated soil behaviour using critical state soil mechanics-based models, such as Cam Clay model. However, application of voltage difference to the soil may affect the behaviour of the soil and model parameters. Therefore, there is a need for an extensive research to investigate the effect of voltage application on the critical state behaviour of soil for the purpose of modelling the EHM behaviour of the soil.

- The maximum negative pore water pressure which develops at the anode surface is an important parameter in predicting the post-treated soil behaviour. To date, accurate and direct measurement of that parameter is not practical due to gas generation at electrodes. Therefore, there is a need to propose an appropriate measurement technique to tackle this issue.

- Horizontal and vertical electrodes show slightly different patterns of potential loss at the soil-electrode interface. The difference between these two possible alignments needs to be investigated further for better insights into their effects.

- During EO consolidation, different gases were generated at the electrodes. These gases were moving between electrodes within the soil body and these can change the electrical resistivity and desaturate the tested soil. These effects are neglected in the developed model; therefore, the model needs to be improved by incorporation of these effects.

- Soil type and temperature are two major limitations of this study and, obviously, the results are affected by the type of soil under the temperature considered. In this research, only New Zealand kaolin clay was tested under temperature of 20 ℃ and therefore, the proposed numerical and experimental frameworks need to be verified considering other soil types and temperature levels.

- The aspects covered by the proposed parameters could be directly measured in the field. Therefore, an extensive field test is required to measure all required parameters in the field to improve the performance of proposed model in the field cases. In addition, the modified electrode can be employed in a field test to investigate the performance of such electrodes under field conditions.

- Various cell sizes, possibly larger than the ones used in this study, can be employed to study the combined effect of electrode alignments and specimen scale on EO results and implement them into the proposed numerical model to enhance the model.

REFERENCES

Abu-hassanein, Z. S., Benson, C. H. and Blotz, L. R. (1996). "Electrical resistivity of compacted clays." *Journal of Geotechnical Engineering*, 122 (5)**,** 397-406.

Alshawabkeh, A. N., and Acar, Y. B. (1996). "Electrokinetic remediation II: theoretical model." *Journal of Geotechnical Engineering*, 122(3), 186-196.

Archie, G.E. (1942). "The electrical resistivity log as an aid in determining some reservoir characteristics." *Transactions of the AIME*, 146 (1), 54-62.

Arulanandan, K. and Smith, S. S. (1973). "Electrical dispersion in relation to soil structure." *Journal of Soil Mechanics & Foundations Div*, 99 (2), 1113-1133.

ASTM G57-06 (1995, reapproved 2012). Standard Method for Field Measurement of Soil Resistivity Using the Wenner Four-Electrode Method, Annual Book of ASTM Standards, ASTM International, West Conshohocken, PA.

ASTM D6431-99. Standard Guide for Using the Direct Current Resistivity Method for Subsurface Investigation. Annual Book of ASTM Standards, ASTM International, West Conshohocken, PA, 1999 (Reapproved 2010)

Atkins, J. E. and Smith, G. (1961). "The significance of particle shape in formation resistivity factor-porosity relationships." *Journal of Petroleum Technology*, 13(3), 285-291.

Bagotsky, V. S. (2005). "*Fundamentals of electrochemistry*, Second edition." John Wiley and Sons Press.

Bergaya, F. and Lagaly, G. (2013). *Handbook of Clay Science*, Elsevier, UK.

Bjerrum, L., Moum, J., and Eide, O. (1967). "Application of electro-osmosis to a foundation problem in a Norwegian quick clay." *Geotechnique*, 17(3), 214-235

Bolt, G. H., (1979). *Soil chemistry B: Physico-chemical models*, Elsevier Scientific Publishing Company.

Bordi, F., Cametti, C. and Gili, T. (2001). "Reduction of the contribution of electrode polarization effects in the radiowave dielectric measurements of highly conductive biological cell suspensions." *Bioelectrochemistry*, 5 (1), 53-61.

Burnotte, F., Lefebvre, G. and Grondin G. (2004). "A case record of electroosmotic consolidation of soft clay with improved soil-electrode contact." *Canadian Geotechnical Journal*, 41(6), 1038-1053.

Campanella, R. and Weemees, I. (1990). "Development and use of an electrical resistivity cone for groundwater contamination studies." *Canadian Geotechnical Journal*, 27 (5), 557-567.

Casagrande, L. (1949). "Electro-Osmosis in soils." *Geotechnique*, 1 (3), 159-177.

Cerato A.B. and Lin B. (2012). "Dielectric measurement of soil-electrolyte mixtures in a modified oedometer cell using 400 kHz to 20 MHz electromagnetic waves." *Geotechnical Testing Journal*, 35(2), 1-9.

Chew, S. H., Karunaratne, G.P., Kuma, V.M., Lim, L.H., Toh, M.L. and Hee, A.M. (2004). "A field trial for soft clay consolidation using electric vertical drains." *Geotextiles and Geomembranes*, 22(1-2), 17-35.

Choo, H., Yeboah, N. and Burns S. (2014). "Impact of unburned carbon particles on the electrical conductivity of fly ash slurry." *Journal of Geotechnical and Geoenvironmental Engineering*, 140(9), 1-9.

Das, B. M. (2013). *Fundamentals of Geotechnical Engineering*. Cengage Learning press.

Ekwue, E. and Bartholomew, J. (2011). "Electrical conductivity of some soils in Trinidad as affected by density, water and peat content." *Biosystems Engineering*, 108 (2), 95-103.

Esrig, M. I. (1968). "Pore pressures, consolidation, and electrokinetics." *Journal of the Soil Mechanics and Foundation Division*, 94 (4), 899-922.

PDE Solutions Inc. (2016). FlexPDE [Computer software]. Retrieved from http://www.pdesolutions.com

Fourie, A. B., Johns, D.G. and Jones, C. J. F. P. (2007). "Dewatering of mine tailings using electrokinetic geosynthetics." *Canadian Geotechnical Journal*, 44(2), 160-172.

Fukue, M., Minato, T., Horibe, H. and Taya, N. (1999). "The micro-structures of clay given by resistivity measurements." *Engineering Geology*, 54 (1-2), 43-53.

Gabrieli L., Jommi, C., Musso G. and Romero E. (2008). "Influence of electro-osmotic treatment on hydro-mechanical behaviour of clayey silts: Preliminary experimental results." *Journal of applied electrochemistry*, 38, 1043-1051

Glendinning, S., Lamont-Black, J. and Jones, C. J. F. P. (2007). "Treatment of sewage sludge using electrokinetic geosynthetics." *Journal of Hazardous Materials*, 139(3), 491-499.

Hamir, R. B., Jones, C. J. F. P. and Clarke, S. (2001). "Electrically conductive geosynthetics for consolidation and reinforced soil." *Geotextiles and Geomembranes*, 19(8), 455-482.

Hu, L., Wu, W. and Wu, H. (2012). "Numerical model of electro-osmosis consolidation in clay." *Geotechnique*, 62(6), 537-541.

Jeyakanthan, V., Gnanendran, C. T., and Lo, S. -C. R. (2011). "Laboratory assessment of electro-osmotic stabilisation of soft clay." *Canadian Geotechnical Journal*, 48(12), 1788-1802.

Jones, C. J. F. P., Lamont-Black, J. and Glendinning, S. (2011). "Electrokinetic geosynthetics in hydraulic applications." *Geotextiles and Geomembranes*, 29(4), 381-390.

Kalinski R, Kelly W. (1994). "Electrical-resistivity measurements for evaluating compacted-soil liners." *Journal of Geotechnical Engineering*, 120(2), 451-7.

Kalinski, R., Kelly, W. (1993) "Estimating Water Content of Soils from Electrical Resistivity." *Geotechnical Testing Journal*, 16(3), 323-329.

Karunaratne, G. (2011). "Prefabricated and electrical vertical drains for consolidation of soft clay." *Geotextiles and Geomembranes*, 29 (4), 391-401.

Kibria, G. and Hossain, M. (2012). "Investigation of Geotechnical Parameters Affecting Electrical Resistivity of Compacted Clays." *Journal of Geotechnical and Geoenviromental Engineering*, 138 (12), 1520-1529.

Kim J. H., Yoon, H., Cho S., Kim Y.S. and Lee J. (2011). "Four Electrode Resistivity Probe for Porosity Evaluation." *Geotechnical Testing Journal*, 34(6), 668-75.

Lamont-Black, J., Jones, C.J.F.P. and Alder, D. (2016). "Electrokinetic strengthening of slopes - Case history." *Geotextiles and Geomembranes*, 44(3), 319-331.

Lefebvre, G. and Burnotte, F. (2002). "Improvement of electroosmotic consolidation of soft clays by minimizing power loss at electrodes." *Canadian Geotechnical Journal*, 39(2), 399-408.

Leroueil, S., Samson L. and Bozozuk, M. (1983). "Laboratory and field determination of preconsolidation pressure at Gloucester." *Canadian Geotechnical Journal*, 20(3), 477-490.

Li, Y., Gong, X., Mengmeng, L. and Tao, Y. (2012). "Non-mechanical behaviours of soft clay in two-dimensional electro-osmosis consolidation." *Journal of rock mechanics and geotechnical engineering*, 4 (3), 282-288.

Lo, K.Y., Inculet I.I. and Ho, K.S. (1991). "Electroosmotic strengthening of soft sensitive clay." *Canadian Geotechnical Journal*, 28(1), 62-73.

Lo, K.Y., Ho, K.S. and Inculet I.I. (1991). "Field test of electroosmotic strengthening of soft sensitive clay." *Canadian Geotechnical Journal*, 28(1), 74-83.

Long, M., Donohue, S., L'Heureux, J., Solberg, I., Ronning, J. S., Limacher, R, O'Conner, P., Sauvin, G., Romoen, M., and Lecomte, I. (2012). "Relationship between Electrical Resistivity and Basic Geotechnical Parameters for Marine Clays." *Canadian Geotechnical Journal*, 49 (10), 1158-1168.

The MathWorks, Inc. (2015). MATLAB, Release 2015, Natick, Massachusetts, United States.

Mccarter, W. (1984). "The electrical resistivity characteristics of compacted clays." *Geotechnique*, 34 (02), 263-267.

Mccarter, W. and Desmazes, P. (1997). "Soil characterisation using electrical measurements." *Geotechnique*, 47(1), 179-183.

Mesri, G. and Olsen, R. E. (1971). "Mechanisms controlling the permeability of clays." *Clays and Clay Minerals*, 19(3), 151-158.

Mitchell, J. K., and Soga, K. (2005). *Fundamentals of Soil Behaviour*. John Wiley and Sons Press.

Mimic, S., Shang, J.Q., Lo, K.Y., Lee, Y.N. and Lee, S.W. (2001). "Electrokinetic strengthening of a marine sediment using intermittent current." *Canadian Geotechnical Journal*, 38(2), 287-302.

Mohamedelhassan, E. (2009). "Electrokinetic strengthening of soft clay." *Ground Improvement*, 162 (04), 157-166.

Mohamedelhassan, E. and Shang, J. (2001). "Effects of electrode materials and current intermittence in electro-osmosis." *Ground Improvement*, 5 (1), 3-11.

Mojid, M., Rose D. and Wyseure G. (2007). "A model incorporating the diffuse double layer to predict the electrical conductivity of bulk soil." *European Journal of Soil Science*, 58 (3), 560-572.

Mojid M. and Cho, H. (2006). "Estimating the fully developed diffuse double layer thickness from the bulk electrical conductivity in clay." *Applied Clay Science*, 33 (3-4), 278-286.

Morris, D. V., Hillis, S. F. and Caldwell, J. A. (1984). "Improvement of sensitive silty clay by electroosmosis" *Canadian Geotechnical Journal*, 22 (1), 17-24.

Mualem Y. and Friedman S. (1991). "Theoretical prediction of electrical conductivity in saturated and unsaturated soil." *Water Resources Research*, 27(10), 2771-2777.

Naghibi M, Abuel-Naga H, Orense R. (2017). "Modified odometer cell to measure electrical resistivity of clays undergoing consolidation process." *Journal of Testing Evaluation*, 45(4),1-9.

Oh, T., Cho G., Lee C. (2014). "Effect of soil mineralogy and pore-water chemistry on the electrical resistivity of saturated soils." *Journal of Geotechnical and Geoenvironmental Engineering*, 140 (11), 1-5.

Olesen, T., Moldrup, P. and Gamst, J. (1999). "Solute diffusion and adsorption in six soils along a soil texture gradient." *Soil Science Society of America Journal*, 63 (3), 519-524.

Ou, C., Chien, S. and Chang, H. (2009). "Soil improvement using electroosmosis with the injection of chemical solutions: field tests." *Canadian Geotechnical Journal*, 46(6), 727-733.

Ou, C., Chien, S. and Wang, Y. (2009). "On the enhancement of electroosmotic soil improvement by the injection of saline solution." *Applied Clay Science*, 44(1-2), 130-136.

Palacky, G. (1987). "Clay mapping using electromagnetic methods." *First Break*, 5,295-306

Reuss, F. F. (1809). *Memories de la societe imperiale des naturalistes de Moskou*, 2, 327.

Revil, A., Cathles, L., Losh, S. and Nunn J. (1998) "Electrical Conductivity in Shaly Sands with Geophysical Applications." *Journal of Geophysical Research*, 103 (B10), 23925-23936.

Rhoades, J., Manteghi, N., Shouse, P. and Alves, W. (1989). "Soil Electrical Conductivity and Soil Salinity: New Formulations and Calibrations." *Soil Science Society of America Journal*, 53(2),433-439.

Rhoades, J., Raats, P. and Prather, R. (1976). "Effects of Liquid-Phase Electrical Conductivity, Water Content and Surface Conductivity on Bulk Soil Electrical Conductivity." *Soil Science Society of America Journal*, 40 (5), 651-655.

Rinaldi, V. A. and Cuestas, G. A. (2002). "Ohmic conductivity of a compacted silty clay." *Journal of Geotechnical and Geoenvironmental Engineering*, 128 (10), 824-835.

Rittirong, A., Douglas, R. S., Shang J.Q. and Lee, E. C. (2008). "Electrokinetic improvement of soft clay using electrical vertical drains." *Geosynthetics International*, 15(5), 369-381.

Rust, C. (1952). "Electrical resistivity measurements on reservoir rock samples by the two-electrode and four-electrode methods." *Journal of Petroleum Technology*, 4 (09), 217-224.

Salem, H. S. and Chilingarian, G. V. (1999). "The Cementation Factor of Archie's Equation for Shaly Sandstone Reservoirs." *Journal of Petroleum Science and Engineering*, 23(2), 83-93.

Samouelian A, Cousin I, Tabbagh A, Bruand A, Richard G. (1999). "Electrical resistivity survey in soil science: a review." *Soil Tillage Research*. 83(2), 173-193.

Schofield RK. (1947). "Calculation of surface areas from measurements of negative adsorption." *Nature*. 160(40), 8-10.

Seladji, S., Cosenza, P., Tabbagh, A., Ranger, J. and Richard, G. (2010). "The effect of compaction on soil electrical resistivity: a laboratory investigation." *European Journal of Soil Science*, 61(6) 1043-1055.

Shah PH, Singh DN. (2005). "Generalized Archie's law for estimation of soil electrical conductivity." *Journal of ASTM International*, 12(5), 1-20.

Shang, J. Q. (1998). "Electroosmosis-enhanced preloading consolidation via vertical drains." *Canadian Geotechnical Journal*, 35(3), 491-499.

Sheriff, R. E. (1973). Encyclopedic dictionary of exploration geophysics. Society of Exploration Geophysicists, Tulsa, OK.

Smith-rose, R. (1934). "Electrical measurements on soil with alternating currents." *Journal of the Institution of Electrical Engineers*, 9(27) 293-309.

Stern, O. (1924). "On the theory of the electrolytic double layer." *Zeitschrift fur electrochemie* 30, 509-527

Su, J. Q. and Wang, Z. (2003). "The two-dimensional consolidation theory of Electro-osmosis." *Geotechnique*, 53(8), 759-763.

Theng BKG. (2012). *Formation and properties of clay-polymer complexes*, Oxford: Elsevier.

Wan, T. Y., and Mitchell, J. K. (1976). "Electroosmotic consolidation of soils." *Journal of Geotechnical Engineering Division*, ASCE, 102 (GT5), 473-491

Waxman MH, Smith LJM. (1968). "Electrical conductivity in oil-bearing shaly sand." *Society of Petroleum Engineers Journal*, 8(02), 107-22.

Wenner, F. (1915). "A method for measuring earth resistivity." *Journal of the Franklin Institute*, 180(3), 373-375.

Win, B.M., Choa, V. and Zeng, X.Q. (2001). "Laboratory investigation on electro-osmosis properties of Singapore clay." *Soils and Foundations*, 41(5), 15-23.

Wu, H., Hu, L. and Wen, Q. (2015). "Electro-osmotic enhancement of bentonite with reactive and inert electrodes." *Applied Clay Science*, 111, 76-82.

Xue, Z., Tang, X., Yang, Q., Wan, Y. and Yang, G. (2015). "Comparison of electro-osmosis experiments on marine sludge with different electrode materials." *Drying technology*, 33(8), 986-995.

Yuan, J. and Hicks, M. A. (2015). "Numerical analysis of electro-osmosis consolidation: a case study." *Geotechnique Letters*, 5 (03), 147-152.

Zhuang, Y and Wang, Z. (2007). "Interface electric resistance of electroosmotic consolidation." *Journal of Geotechnical and Geoenvironmental Engineering*, 133 (12), 1617-1621.

APPENDIX A

Electro-osmosis experimental database

The EO consolidation results from previous research in the laboratory and in the field, as collected from available literature, are listed in Tables A.1 to A.3. Table A.1 shows the characteristics of the tested soils and Table A.2 summarises the experimental results from laboratory tests whereas Table A.3 lists the soil characteristics and results from the field tests.

Table A.1 Properties of EO system and tested soils used for laboratory scale EO consolidation tests

Test No	Soil type	Clay content (%)	Treatment Duration (d)	Preconsolidation pressure (Vertical)	OCR during EO	V/cm	Anode materials	Cathode materials	Electrode dimension (mm)	Spacing (mm)	Electrodes Layout	Reference
1	Soft Silty Clay	35	16	390	0.077	0.4-0.6	Stainless Steel Wool;	Galvanized wire mesh	R[1] =77	250	horizontal	
2	Soft Silty Clay	35	7	260	0.115	0.4-0.6	Stainless Steel Wool;	Galvanized wire mesh	R=77	250	horizontal	Morris et. al. (1985)
3	Soft Silty Clay	35	24	130	0.23	0.4-0.6	Stainless Steel Wool;	Galvanized wire mesh	R =77	250	horizontal	
4	Soft Silty Clay	35	20	130	0.23	0.4-0.6	Stainless Steel Wool;	Galvanized wire mesh	R=77	250	horizontal	
5	Yulchon Marin Clay (Korea)	23	6	15	-	0.256	Steel Mesh	Steel Mesh	1.2(D)*110(W) *200(L)	250	Vertical (1-1)[2]	
6	Yulchon Marin Clay (Korea)	23	5	15	-	0.256	Steel Mesh	Steel Mesh	1.2(D)*110(W) *200(L)	250	Vertical (1-1)[2]	
7	Yulchon Marin Clay (Korea)	23	4	15	-	0.256	Steel Mesh	Steel Mesh	1.2(D)*110(W) *200(L)	250	Vertical (1-1)[2]	Mimic et al. (2001)
8	Yulchon Marin Clay (Korea)	23	3	15	-	0.256	Steel Mesh	Steel Mesh	1.2(D)*110(W) *200(L)	250	Vertical (1-1)[2]	
9	Yulchon Marin Clay (Korea)	23	4	15	-	0.128	Steel Mesh	Steel Mesh	1.2(D)*110(W) *200(L)	250	Vertical (1-1)[2]	

Table A.1 Properties of EO system and tested soils used for laboratory scale EO consolidation tests (cont'd)

Test No	Soil type	Clay content (%)	Treatment Duration (d)	Preconsolidation pressure (Vertical)	OCR during EO	V/cm	Anode materials	Cathode materials	Electrode dimension (mm)	Spacing (mm)	Electrodes Layout	Reference
10	Yulchon Marin Clay (Korea)	23	4	15-30	-	0.128	Steel Mesh	Steel Mesh	1.2(D)*110(W)*200(L)	250	Vertical (1-1)^2	
11	Singapore Marine Clay	-	-	150	1	0.42-0.5	Porous copper	Porous copper	R=70	120-140	Horizontal	
12	Singapore Marine Clay	-	-	150	1	0.86-1	Porous copper	Porous copper	R=70	120-140	Horizontal	Win et. al. (2001)
13	Singapore Marine Clay	-	-	120	1	0.14-0.17	Porous copper	Porous copper	R=70	120-140	Horizontal	
14	Singapore Marine Clay	-	-	150	1	0.28-0.34	Porous copper	Porous copper	R=70	120-140	Horizontal	
15	Commercial Kaolin Clay	100	0.7^3	25	1	0.22	Geosynthetic materials containing copper wires	Geosynthetic materials containing copper wires	R=150	230	Horizontal	
6	Commercial Kaolin Clay	100	0.7	25	1	0.43	Geosynthetic materials containing copper wires	Geosynthetic materials containing copper wires	R=150	230	Horizontal	Hamir et.al. (2001)
17	Commercial Kaolin Clay	100	0.7	25	1	0.65	Geosynthetic materials containing copper wires	Geosynthetic materials containing copper wires	R=150	230	Horizontal	

Table A.1 Properties of EO system and tested soils used for laboratory scale EO consolidation tests (cont'd)

Test No	Soil type	Clay content (%)	Treatment Duration (d)	Preconsolidation pressure (Vertical)	OCR during EO	V/cm	Anode materials	Cathode materials	Electrode dimension (mm)	Spacing (mm)	Electrodes Layout	Reference
18	Commercial Kaolin Clay	100	0.70	25	1	0.87	Geosynthetic materials containing copper wires	Geosynthetic materials containing copper wires	R=150	230	Horizontal	
19	Commercial Kaolin Clay	100	0.7	25	1	1.1	Geosynthetic materials containing copper wires	Geosynthetic materials containing copper wires	R=150	230	Horizontal	
20	Commercial Kaolin Clay	100	0.7	25	1	1.3	Geosynthetic materials containing copper wires	Geosynthetic materials containing copper wires	R=150	230	Horizontal	Hamir et.al. (2001)
21	Commercial Kaolin Clay	100	0.7	25	1	0.43	Geosynthetic materials with stainless steel fibre	Geosynthetic materials with stainless steel fibre	R=150	230	Horizontal	
22	Commercial Kaolin Clay	100	0.7	25	1	0.87	Geosynthetic materials with stainless steel fibre	Geosynthetic materials with stainless steel fibre	R=150	230	Horizontal	
23	Commercial Kaolin Clay	100	0.7	25	1	1.1	Geosynthetic materials with stainless steel fibre	Geosynthetic materials with stainless steel fibre	R=150	230	Horizontal	

Table A.1 Properties of EO system and tested soils used for laboratory scale EO consolidation tests (cont'd)

Test No	Soil type	Clay content (%)	Treatment Duration (d)	Preconsolidation pressure (Vertical)	OCR during EO	V/cm	Anode materials	Cathode materials	Electrode dimension (mm)	Spacing (mm)	Electrodes Layout	Reference
24	Commercial Kaolin Clay	100	0.7	25	1	1.3	Geosynthetic materials with stainless steel fibre	Geosynthetic materials with stainless steel fibre	R=150	230	Horizontal	
25	Commercial Kaolin Clay	100	0.7	25	1	1.08	Composite of polypropylene and carbon fibre	Composite of polypropylene and carbon fibre	R=150	230	Horizontal	
26	Commercial Kaolin Clay	100	0.7	25	1	0.22	Copper disk	Copper disk	R=150	230	Horizontal	
27	Commercial Kaolin Clay	100	0.7	25	1	0.43	Copper disk	Copper disk	R=150	230	Horizontal	Hamir et.al. (2001)
28	Commercial Kaolin Clay	100	0.7	25	1	0.65	Copper disk	Copper disk	R=150	230	Horizontal	
29	Commercial Kaolin Clay	100	0.7	25	1	0.87	Copper disk	Copper disk	R=150	230	Horizontal	
30	Commercial Kaolin Clay	100	0.7	25	1	1.1	Copper disk	Copper disk	R=150	230	Horizontal	
31	Commercial Kaolin Clay	100	0.7	25	1	1.3	Copper disk	Copper disk	R=150	230	Horizontal	
32	Mont St-Hilaire Clay	-	≈ 6	175	1.75	0.35	Perforated steel Tube	Perforated steel Tube	R=10	150	Vertical-	Lefebvre and Burnotte (2002)

Table A.1 Properties of EO system and tested soils used for laboratory scale EO consolidation tests (cont'd)

Test No	Soil type	Clay content (%)	Treatment Duration (d)	Preconsolidation pressure (Vertical)	OCR during EO	V/cm	Anode materials	Cathode materials	Electrode dimension (mm)	Spacing (mm)	Electrodes Layout	Reference
33	Mont St-Hilaire Clay	-	≈ 6	175	1	0.35	Perforated steel Tube	Perforated steel Tube	R=10	150	Vertical-	Lefebvre and Burnotte (2002)
34	Taipei silty clay	100	1	100	1	0.4	Perforated Tube	Perforated Tube	R=8	200	Vertical	Ou et. al. (2009)
35	Taipei silty clay	100	1	100	1	0.5	Perforated Tube	Perforated Tube	R=8	200	Vertical	
36	Taipei silty clay	100	1	100	1	0.6	Perforated Tube	Perforated Tube	R=8	200	Vertical	
37	Taipei silty clay	100	7	100	1	0.5	Perforated Tube	Perforated Tube	R=8	200	Vertical	
38	Mixed clay	44	6.7	10	1	0.31	Steel Mesh	Steel Mesh	Covers soil cross-section	320	Vertical	Mohamedelhassan (2009)
39	Mixed clay	44	6.7	10	1	0.31	Steel Mesh	Steel Mesh	Covers soil cross-section	320	Vertical	
40	High plasticity clay	54	Varying[4]	-	1	0.37	Copper	Copper	R=60	120	Horizontal	Jeyakanthan et.al. (2012)
41	High plasticity clay	54	Varying	-	1	0.4	Copper	Copper	R=60	120	Horizontal	
42	High plasticity clay	54	Varying	-	1	0.37	Copper	Copper	R=60	120	Horizontal	

Table A.1 Properties of EO system and tested soils used for laboratory scale EO consolidation tests (cont'd)

Test No	Soil type	Clay content (%)	Treatment Duration (d)	Preconsolida tion pressure (Vertical)	OCR during EO	V/cm	Anode materials	Cathode materials	Electrode dimension (mm)	Spacing (mm)	Electrodes Layout	Reference
43	Sodium bentonite	100	≈ 1	0	1	1	Copper	Copper	R=90	200	Horizontal	
44	Sodium bentonite	100	≈ 1	0	1	1	Iron	Iron	R=90	200	Horizontal	Wu et. al. (2015)
45	Sodium bentonite	100	≈ 1	0	1	1	Graphite	Graphite	R=90	200	Horizontal	
46	Sodium bentonite	100	≈ 1	0	1	1	Stainless Steel	Stainless Steel	R=90	200	Horizontal	
47	Dalian Marin sludge	-	2.3	1.5	-	0.8	Copper	Copper	3(D)*150(W) *170(L)	306	Vertical	
48	Dalian Marin sludge	-	3.7	1.5	-	0.8	Iron	Iron	3(D)*150(W) *170(L)	306	Vertical	Xue et al. (2015)
49	Dalian Marin sludge	-	4.1	1.5	-	0.8	Aluminium	Aluminium	3(D)*150(W) *170(L)	306	Vertical	

[1] R is electrode diameter

[2] one anode and one cathode are located in a line

[3] computed based on available graphs

[4] Until no displacement occurred

Table A.2 Laboratory scale experimental results from previous research- Corresponding to Table A.1

Test No	k_e (m²/V ·s)	Maximum Normalized potential drop (%)	Shear strength (kPa) Before EO	After EO	USSR%	Maximum Negative developed pore water (kPa)	Atterberg Limits Before EO LL (%)	PL (%)	After EO LL (%)	PL (%)	Moisture content Before EO (%)	After EO (%)
1		-	125	180	144	-	27	18	32.5	19	29	23
2		-	83	325	391	-	27	18	35.5	20	29	18.5
3		-	20	137.5	688[1]	-	28	18	32	20.5	27	23.5
4		-	41	170	410	-	28	18	37	20	30	18.5
5		17	1	7.1	710	-	59	32	60.9	32.9	115.1	92.5
6		17	1	5.7	570	-	59	32	61.2	32	117	95.7
7		17	1.6	5	312.5	-	59	32	59.5	32.8	108.3	98
8		17	1	2.6	260	-	59	32	60.2	32	114.2	103.6
9		28	1.8	3.5	194	-	59	32	58.9	32	99.9	98.7
10		28	4	6.3	157.5	-	59	32	59.8	32.5	100.8	91.8
11	3.35E-9	-	-	-	-	-	-	-	-	-	-	-
12	4E-9	-	-	-	-	-	-	-	-	-	-	-

Table A.2 Laboratory scale experimental results from previous research- Corresponding to Table A.1 (cont'd)

Test No	k_e (m²/V · s)	Maximum Normalized potential drop (%)	Shear strength (kPa) Before EO	Shear strength (kPa) After EO	USSR%	Maximum Negative developed pore water (kPa)	Atterberg Limits Before EO LL (%)	Atterberg Limits Before EO PL (%)	Atterberg Limits After EO LL (%)	Atterberg Limits After EO PL (%)	Moisture content Before EO (%)	Moisture content After EO (%)
13	9E-9	-	-	-	-	-	-	-	-	-	-	-
14	1E-8	-	-	-	-						-	-
15	-	-	4*	4	100	13	55	34	-	-	-	-
16	-	-	4	8	200	55	55	34	-	-	-	-
17	-	-	4	11	275	82	55	34	-	-	-	-
18	-	-	4	15	375	108	55	34	-	-	-	-
19	-	-	4	23	575	151	55	34	-	-	-	-
20	-	-	4	17	425	167	55	34	-	-	-	-
21	-	-	4	5	125	37	55	34	-	-	-	-
22	-	-	4	21	525	142	55	34	-	-	-	-

Table A.2 Laboratory scale experimental results from previous research- Corresponding to Table A.1 (cont'd)

Test No	k_e (m²/V ·s)	Maximum Normalized potential drop (%)	Shear strength (kPa) Before EO	Shear strength (kPa) After EO	USSR%	Maximum Negative developed pore water (kPa)	Atterberg Limits Before EO LL (%)	Atterberg Limits Before EO PL (%)	Atterberg Limits After EO LL (%)	Atterberg Limits After EO PL (%)	Moisture content Before EO (%)	Moisture content After EO (%)
23	-	-	4	25	625	173	55	34	-	-	-	-
24	-	-	4	26	650	210	55	34	-	-	-	-
25	-	-	4	25	625	168	55	34	-	-	-	-
26	-	-	4	7	175	21	55	34	-	-	-	-
27	-	-	4	10	250	52	55	34	-	-	-	-
28	-	-	4	13	325	89	55	34	-	-	-	-
29	-	-	4	15	375	115	55	34	-	-	-	-
30	-	-	4	18	450	147	55	34	-	-	-	-
31	-	-	4	20	500	182	55	34	-	-	-	-
32	1.3E-9	65	-	-	-	-			-	-	-	-

Table A.2 Laboratory scale experimental results from previous research- Corresponding to Table A.1 (cont'd)

Test No	k_e (m²/V ·s)	Maximum Normalized potential drop (%)	Shear strength (kPa) Before EO	Shear strength (kPa) After EO	USSR%	Maximum Negative developed pore water (kPa)	Atterberg Limits Before EO LL (%)	Atterberg Limits Before EO PL (%)	Atterberg Limits After EO LL (%)	Atterberg Limits After EO PL (%)	Moisture content Before EO (%)	Moisture content After EO (%)
33	1.5E-9	65	48	76	158	-			-	-	53	48
34	-	-	10	12.3	123	-	-	-	-	-	30	30.16
35	-	70	10	15.3	153	-	-	-	-	-	30	30.43
36	-	-	10	18	180	-	-	-	-	-	30	28.63
37	-	-	10	39.6	396	-	-	-	-	-	30	27.3
38	-	32	≈8	≈35	438	-	63	22			≈55.5	≈45
39	-	32	-	-	-	91	63	22				
40	1.197E-9	43	-	-	-	180	101	35	-	-		
41	1.197E-9	43	-	-	-	-	101	35	-	-		
42	1.197E-9	43	-	-	-	180	101	35	-	-		

Test No	k_e (m²/V ·s)	Maximum Normalized potential drop (%)	Shear strength (kPa) Before EO	After EO	USSR%	Maximum Negative developed pore water (kPa)	Atterberg Limits Before EO LL (%)	PL (%)	After EO LL (%)	PL (%)	Moisture content Before EO (%)	After EO (%)
43		58					155	31	-	-		
44		72					155	31	-	-		
45		79					155	31	-	-		
46		77					155	31	-	-		
47	-	33	-	-	-	-	52	23.1	-	-	71.8	-
48	-	65	10**	32.5	325	-	52	23.1	-	-	71.6	43.75
49	-	60	15	42	280	-	52	23.1	-	-	71.4	40.43

[1] The maximum reported value

* Value is considered equal to the shear strength of treated soil under voltage gradient of 0.22 V/cm as no value is reported for initial shear strength of soil

**Value is the undrained shear strength at the anode

Table A.3 Field scale experimental results from previous research

Test No	Location	Soil type	Duration (days)	Potential difference (v)	V/cm	Electrode materials	Embedded electrode length (m)	Electrode diameter (mm)	Spacing (m)	USSR (%)	Improvement depth (m)	Settlement (mm)	Energy consumption (kWh/m^3)	Reference
1	Norway	Quick Clay	120	50	0.25	Steel	9.6	19	2	380	7		17	Bjerrum, L. (1967)
2	Canada	Sensitive Leda clay	26-29*	120	0.39	Copper	5.5	51	3.05	179	5.5	55	6.4	Lo et al. (1991)
3	Canada	Sensitive Leda clay	32	120	0.2	Copper	5.5	51	6.1	182	5.5	47.5	6.4	Lo et al. (1991)
4	Singapore	Layer of sand fill, soft marine clay and stiff clay	0.92	14	0.12	Conductive plastic	35	-	1.2	132	-	-	1.8	Chew et al. (2003)
5	Canada	Soft clay	48	93	0.31	Steel	5	190	3	214	7	46.8		Burnotte et al. (2004)
6	South Africa	Mine tailings**	60	30	0.33	EKG	1	-	0.9	-	-	282	514	Fourie et al. (2004)
7	Malaysia	Very soft to soft clayey silt	4.16	29	0.21	Copper foil and conductive polymer	6	-	1.4	439	-	-	0.7	Rittirong et al. (2008)
8	Taiwan	Soft silty clay	13		-		5	50	2	182	5	0.9		Ou et al. (2009)
9	Taiwan	Soft silty clay	25		-		5	50	2	192	5	5.1		Ou et al. (2009)
10	UK	Mainly London clay	42	60	-	EKG	2		-	-	-	-	11.5	Jones et al. (2011)
11	UK	Sewage sludge**	63	30	0.33	EKG	-		-	-	-	-	128	Glendinning et al. (2007)

APPENDIX B

Electrical resistivity database

The numerical database of electrical resistivity for various F, K and θ are summarised in Tables B.1 to B.6

Table B.1 Electrical resistivity for various K and F and θ=0.8

K F	1.1	1.2	1.4	1.6	2	4	6	10
0.30	1.52	1.47	1.40	1.35	1.24	0.93	0.77	0.58
0.50	1.48	1.42	1.33	1.26	1.13	0.79	0.61	0.44
1.00	1.44	1.37	1.25	1.15	0.99	0.61	0.46	0.31
2.50	1.41	1.30	1.15	1.01	0.83	0.45	0.32	0.20
3.50	1.40	1.29	1.12	0.98	0.79	0.41	0.28	0.17
4.00	1.40	1.28	1.10	0.96	0.77	0.39	0.26	0.16
5.00	1.40	1.28	1.10	0.96	0.77	0.39	0.26	0.16
7.00	1.40	1.28	1.10	0.96	0.77	0.39	0.26	0.16
10.00	1.40	1.28	1.10	0.96	0.77	0.39	0.26	0.16
30.00	1.40	1.28	1.10	0.96	0.77	0.39	0.26	0.16
50.00	1.40	1.28	1.10	0.96	0.77	0.39	0.26	0.16

Table B.2 Electrical resistivity for various *K* and *F* and θ=0.6

F \ K	1.1	1.2	1.4	1.6	2	4	6	10
0.30	2.38	2.33	2.22	2.13	1.96	1.44	1.17	0.87
0.50	2.36	2.29	2.13	2.01	1.81	1.23	0.96	0.69
1.00	2.33	2.21	2.01	1.85	1.60	0.99	0.74	0.51
2.00	2.27	2.13	1.89	1.70	1.43	0.81	0.58	0.38
3.00	2.26	2.10	1.83	1.63	1.35	0.73	0.51	0.33
4.00	2.24	2.07	1.81	1.60	1.30	0.69	0.48	0.30
5.00	2.23	2.05	1.78	1.57	1.27	0.66	0.45	0.28
7.00	2.22	2.03	1.74	1.53	1.21	0.62	0.41	0.25
10.00	2.22	2.03	1.74	1.53	1.21	0.62	0.41	0.25
30.00	2.22	2.03	1.74	1.53	1.21	0.62	0.41	0.25

Table B.3 Electrical resistivity for various K and F and $\theta=0.5$

F \ K	1.1	1.2	1.4	1.6	2	4	6	10
0.30	3.04	3.00	2.83	2.72	2.52	1.85	1.49	1.09
0.50	3.03	2.91	2.73	2.59	2.32	1.58	1.22	0.86
1.00	2.97	2.83	2.59	2.38	2.05	1.26	0.93	0.63
2.00	2.92	2.74	2.44	2.21	1.85	1.05	0.74	0.49
3.00	2.90	2.70	2.37	2.12	1.75	0.95	0.67	0.43
4.00	2.88	2.68	2.33	2.07	1.69	0.90	0.63	0.39
5.00	2.87	2.65	2.30	2.03	1.65	0.86	0.59	0.37
9.00	2.84	2.61	2.24	1.96	1.58	0.79	0.53	0.32
10.00	2.85	2.61	2.24	1.96	1.56	0.79	0.52	0.31
30.00	2.85	2.61	2.24	1.96	1.56	0.79	0.52	0.31
50.00	2.85	2.61	2.24	1.96	1.56	0.79	0.52	0.31
80.00	2.85	2.61	2.24	1.96	1.56	0.79	0.52	0.31

Table B.4 Electrical resistivity for various *K* and *F* and θ=0.4

K F	1.1	1.2	1.4	1.6	2	4	6	10
0.30	4.05	3.96	3.79	3.63	3.37	2.46	1.96	1.43
0.50	4.00	3.85	3.70	3.45	3.13	2.11	1.62	1.13
1.00	3.95	3.75	3.45	3.19	2.75	1.69	1.23	0.83
2.00	3.90	3.65	3.25	2.94	2.48	1.39	0.99	0.64
3.00	3.85	3.59	3.16	2.83	2.33	1.27	0.88	0.56
4.00	3.86	3.57	3.12	2.77	2.27	1.21	0.83	0.52
5.00	3.82	3.53	3.08	2.72	2.22	1.17	0.80	0.50
7.00	3.80	3.50	3.01	2.67	2.16	1.11	0.75	0.46
10.00	3.80	3.49	3.00	2.63	2.13	1.07	0.72	0.44
11.00	3.80	3.49	2.99	2.62	2.10	1.06	0.71	0.43
12.80	3.80	3.49	2.99	2.60	2.08	1.06	0.69	0.42
20.00	3.80	3.49	2.99	2.60	2.08	1.06	0.69	0.42
50.00	3.80	3.49	2.99	2.60	2.08	1.06	0.69	0.42
80.00	3.80	3.49	2.99	2.60	2.08	1.06	0.69	0.42

Table B.5 Electrical resistivity for various K and F and θ=0.3

K / F	1.1	1.2	1.4	1.6	2	4	6	10
0.30	5.71	5.59	5.35	5.13	4.74	3.50	2.76	1.99
0.50	5.65	5.47	5.15	4.85	4.37	2.91	2.26	1.55
1.00	5.62	5.36	4.90	4.55	3.92	2.38	1.74	1.15
2.00	5.48	5.15	4.61	4.17	3.50	1.99	1.40	0.90
3.00	5.48	5.12	4.55	4.05	3.35	1.82	1.27	0.80
4.00	5.44	5.06	4.44	3.95	3.25	1.70	1.20	0.75
5.00	5.39	4.98	4.35	3.85	3.14	1.65	1.13	0.70
8.00	5.36	4.93	4.27	3.76	3.04	1.56	1.06	0.65
10.00	5.36	4.92	4.23	3.73	3.00	1.53	1.03	0.63
13.00	5.36	4.89	4.19	3.66	2.95	1.50	0.98	0.59
19.00	5.36	4.89	4.19	3.66	2.94	1.50	0.98	0.59
25.00	5.36	4.89	4.19	3.66	2.94	1.50	0.98	0.59
50.00	5.36	4.89	4.19	3.66	2.94	1.50	0.98	0.59
80.00	5.36	4.89	4.19	3.66	2.94	1.50	0.98	0.59

Table B.6 Electrical resistivity for various K and F and $\theta=0.2$

K F	1.1	1.2	1.4	1.6	2	4	6	10
0.30	8.96	8.75	8.38	8.04	7.50	5.43	4.30	3.07
0.50	8.85	8.57	8.11	7.69	6.98	4.62	3.53	2.42
1.00	8.80	8.40	7.71	7.14	6.20	3.80	2.78	1.81
2.00	8.52	8.00	7.14	6.52	5.45	3.05	2.14	1.36
3.00	8.55	7.96	7.01	6.26	5.17	2.78	1.92	1.20
4.00	8.47	7.87	6.91	6.15	5.06	2.69	1.85	1.15
5.00	8.45	7.85	6.85	6.07	4.96	2.61	1.78	1.10
7.00	8.40	7.77	6.76	5.99	4.86	2.53	1.71	1.05
10.00	8.38	7.73	6.68	5.88	4.75	2.44	1.64	1.00
20.00	8.33	7.67	6.59	5.78	4.62	2.34	1.57	0.95
25.00	8.33	7.65	6.57	5.76	4.62	2.33	1.55	0.94
32.50	8.31	7.61	6.52	5.70	4.57	2.33	1.52	0.91
40.00	8.31	7.61	6.52	5.70	4.57	2.33	1.52	0.91
80.00	8.31	7.61	6.52	5.70	4.57	2.33	1.52	0.91